Protocell development within evaporating lakes on the early Earth

Zachary R. Cohen

A dissertation
submitted in partial fulfillment of the
requirements for the degree of

Doctor of Philosophy in Chemistry and Astrobiology

University of Washington

2023

Reading Committee:

Sarah L. Keller, Chair
Matt F. Bush
David C. Catling

Program Authorized to Offer the Degree:

Department of Chemistry

University of Washington

Abstract

Protocell development within evaporating lakes on the early Earth

Zachary R. Cohen

Chair of the Supervisory Committee:
Sarah L. Keller
Department of Chemistry

My research addresses the problem of how the first cells assembled from non-living material in the early Earth environment by testing whether putative components of the first cells could have assembled within evaporating lakes on the early Earth. Evaporation concentrates dissolved solutes, potentially converting chemical precursors into the membranes and biopolymers of the earliest cells. The first cell membranes may have been composed of fatty acids, and I have characterized plausible sources of membrane-forming fatty acids on the early Earth. The first peptides may have been formed during evaporation and subsequent dehydration of lakes filled with environmentally available amino acids, and I have shown that fatty acid membranes do not inhibit peptide formation during dehydration. I have also shown that these fatty acid membranes retain their encapsulated contents in salty water following partial evaporation from the lake; however, complete dehydration disrupts encapsulation by the membranes. Additionally, I have shown that fatty acid membranes retain encapsulated contents when exposed to cold temperatures below the membrane melting transition; cold temperatures are beneficial during the synthesis of RNA genomes. All of the work above, which has been published in academic journals, appears in Chapters 1 through 4 of this dissertation. In Chapter 5, I describe unpublished findings about RNA assembly and membrane encapsulation in natural carbonate lakes, modern analogs for locations that may have enabled the origin of life on early Earth. I have also described unpublished observations using size-exclusion chromatography of fatty acid vesicles that I hope will facilitate future research in this area. Taken together, my dissertation research results support the hypothesis that membranes and biopolymers developed together into the first cells within evaporating lakes on the early Earth.

Table of contents

Acknowledgements

I thank my dissertation reading committee, Sarah Keller, Matt Bush, and David Catling, for their time and attention. I thank the remaining members of my dissertation committee, Jesse Zalatan and James Carothers, for their feedback. I am profoundly grateful to my research advisors, Sarah Keller, Roy Black, and David Catling, for their patient and thoughtful mentoring. Because of them, I feel prepared for the next steps in my research career. I have benefitted tremendously from my collaborators and friends in the Keller and Catling groups. Thank you to my friends and family for love and support.

Introduction

How did non-living components of the early Earth environment (e.g. water, minerals, organic molecules, and energy) assemble into the first life? Geological evidence from the Moon suggests that Earth formed during a sterilizing impact ~4.5 billion years ago, and terrestrial fossils suggest that Earth has been inhabited by microbial life since at least ~3.7 billion years ago (1). The origin of life on Earth marks the transition from sterile planet to living planet, and this process is one of the most glaring gaps in our understanding of the Earth's history. It is important that the scientific community fill this gap by demonstrating a plausible synthesis of life from environmentally-available components. Additionally, research into the origin of life on Earth informs our search for alien life elsewhere in the universe. By investigating the natural assembly of cellular life from non-living material, we could design synthetic cells that supply us with useful products or act as medical therapies. Finally, origin of life research boosts public engagement with science in a unique way. For all of these reasons, I have chosen to write my dissertation about the origin of life on Earth.

Because life on modern Earth consists mostly of cells, my research has focused on the synthesis of the earliest cells. Just like modern cells, the earliest cells may have consisted of biopolymers encapsulated within a membrane compartment. The membranes of the earliest cells may have been composed of fatty acids, which were likely available on the early Earth environment (Chapter 4). Meanwhile, formation of biopolymers such as RNA and peptides may have been restricted to specific Earth environments, such as evaporating lakes. I have investigated whether the presence of membranes allows biopolymer formation during dehydration (Chapter 1), and whether partial or full dehydration disrupts encapsulation by the membrane (Chapter 2). I have also tested whether membranes can function within cold environments that could have enabled the synthesis of RNA genomes (Chapter 3). Finally, I have shown that natural carbonate lakes provide compatible conditions for RNA assembly and membrane encapsulation. Taken together, my dissertation research is consistent with the hypothesis that membranes, peptides, and RNA could have assembled into the earliest cells within cold, evaporating lakes on the early Earth.

Reference:

1) Ohtomo Y, Kakegawa T, Ishida A, Nagase T, Rosing MT. 2014. Evidence for biogenic graphite in early Archaean Isua metasedimentary rocks. Nat. Geosci. 7: 25-8.

Chapter 1:

Prebiotic membranes and micelles do not inhibit peptide formation during dehydration

*This chapter was first published in *ChemBioChem* in 2021. It was written in collaboration with Brennan L. Kessenich, Avijit Hazra, Julia Nguyen, Richard S. Johnson, Michael J. MacCoss, Gojko Lalic, Roy. A. Black, and Sarah L. Keller.

Abstract

Cycles of dehydration and rehydration could have enabled formation of peptides and RNA in otherwise unfavorable conditions on the early Earth. Development of the first protocells would have hinged upon colocalization of these biopolymers with fatty acid membranes. Using atomic force microscopy, we find that a prebiotic fatty acid (decanoic acid) forms stacks of membranes after dehydration. Using LC-MS-MS (liquid chromatography-tandem mass spectrometry) with isotope internal standards, we measure the rate of formation of serine dipeptides. We find that dipeptides form during dehydration at moderate temperatures (55°C) at least as fast in the presence of decanoic acid membranes as in the absence of membranes. Our results are consistent with the hypothesis that protocells could have formed within evaporating environments on the early Earth.

Main text

Two requirements for the origin of life on Earth are 1) formation of biopolymers (e.g. RNA and proteins) from environmentally available precursors, and 2) co-localization of those polymers with membranes to form the first protocells[1,2]. At first glance, these requirements appear incompatible. At moderate temperatures below 100°C, condensation reactions (which convert amino acids into peptides) are thermodynamically unfavorable in water[3,4]. Above 100°C, these reactions occur (albeit at low yields ~1%)[5,6], but prebiotic membranes composed of short chain fatty acids become unstable[7].

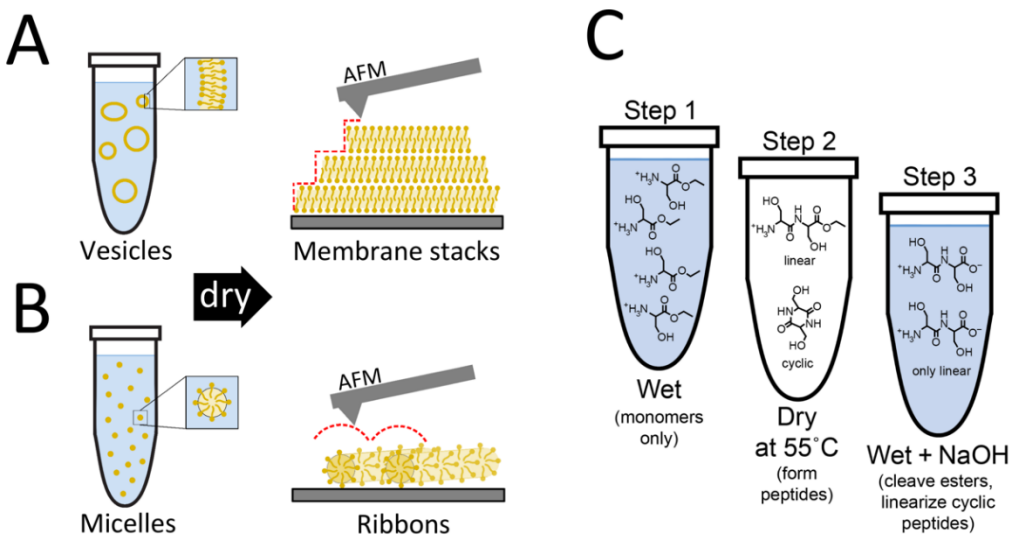

Figure 1: Schematics of the experiments described in this paper. We use atomic force microscopy to show that dried vesicles assemble into membrane stacks (A) whereas dried micelles assemble into ribbons (B). Separate experiments measure formation of dipeptides (C). In Step 1, monomers (10 mM serine-ethyl-ester) were mixed with fatty acids that either formed membranes (decanoic acid) or did not (heptanoic acid). In Step 2, the dispersions were dried and held at 55°C so that dimers formed. In Step 3, the dimers were rehydrated, and then treated with NaOH, which cleaved ethyl-esters and linearized cyclic dipeptides. Isotope-labeled internal standards were added prior to analysis by LC-MS-MS.

One way to resolve this problem is to alternate between wet and dry conditions (Fig 1), as might have occurred within evaporating lakes or ponds on the early Earth[8,9]. Dehydration at moderate temperatures has been shown to convert amino acids into peptides[10], and dehydrated membranes have been shown to re-assemble upon rehydration[11]. This raises an interesting question: if fatty acid molecules are added to amino acid solutions undergoing evaporative cycles, do the fatty acids act as spectator molecules or do they enhance (or hinder) biopolymer formation? Is the rate of dipeptide production from amino acids enhanced in the presence of fatty acid membranes? Similar questions have previously been asked for membranes of phospholipids, which are less likely to have been available on the early Earth (but are convenient to use in experiments). Previous researchers found that nucleotides adopt orientations that are favorable for polymerization[12] and that they oligomerize within stacks of dehydrated phospholipid membranes[13], but that amino acids polymerize into peptides more slowly in the presence of dry phospholipid membranes[14].

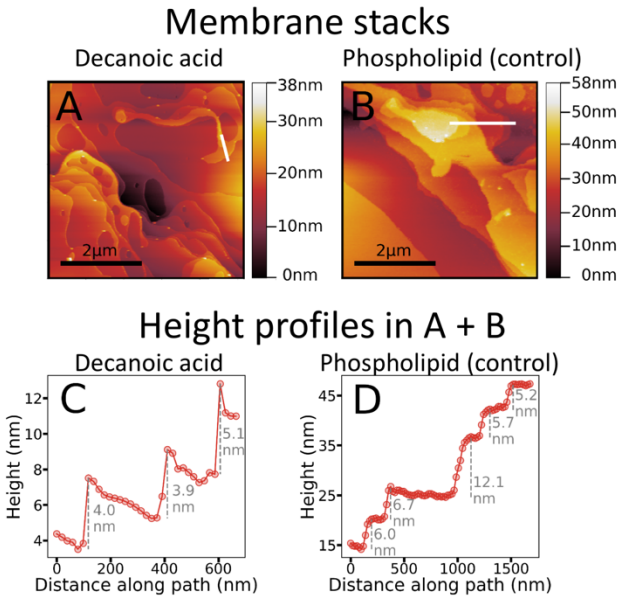

Figure 2. Atomic force micrographs show that dehydrated vesicles assemble into membrane stacks. When aqueous dispersions of 50 mM decanoic acid vesicles are dried on mica substrates at room temperature, membrane stacks appear (A), along with ribbons (Fig 3A). Control dispersions of 1 mM phospholipid (DOPC) vesicles produce only stacks (B). Height profiles of the stacks (C-D, measured along the white lines in A and B) show discrete steps, consistent with membrane stacks. The pH of decanoic acid and phospholipid dispersions before dehydration was 6.8 and 7.3 respectively.

Here, our focus is on fatty acid membranes at moderate temperatures. The membranes of the earliest protocells were likely composed of fatty acids[15] that were delivered to Earth via meteorites[16] or synthesized locally via Fischer-Tropsch[17] or sparking reactions[18]. First, we test whether dehydration of solutions containing fatty acid vesicles (dispersions) produces oriented stacks of membranes as in phospholipid systems. Our experiments incorporate two types of fatty acids: decanoic acid and heptanoic acid. Decanoic acid's longer chain of 10 carbons enables it to self-assemble into membranes (as well as wormlike micelles)[19], whereas the shorter, 7-carbon chain of heptanoic acid precludes membrane formation[20].

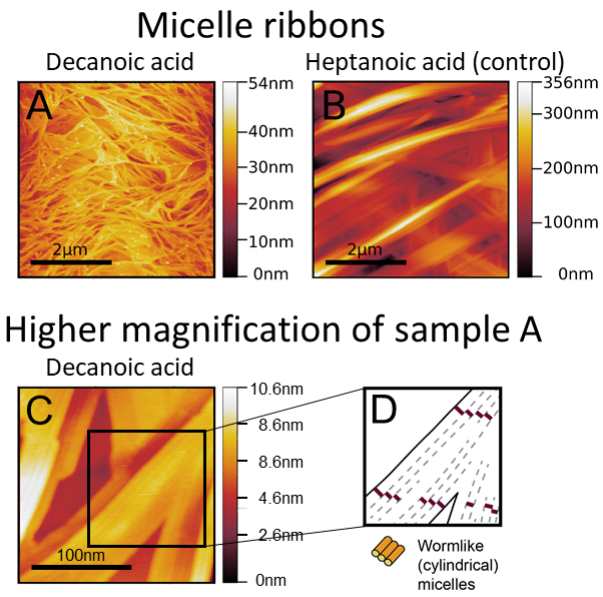

Figure 3. Atomic force micrographs show that dehydrated micelles assemble into ribbons. Decanoic acid vesicles are always in equilibrium with micelles[28], so dried dispersions of 50 mM decanoic acid vesicles produce ribbons (A) in addition to membrane stacks (Fig 2A). Control dispersions of 50 mM heptanoic acid, which form micelles and not vesicles, produce only ribbons (B). Magnification reveals that ribbons are bundles of wormlike micelles (C). The schematic highlights the boundaries for each wormlike micelle, which are typically ~6 nm in diameter (D). The pH of decanoic acid and heptanoic acid dispersions before dehydration was 6.8.

Our atomic force micrographs show that decanoic acid dispersions dry in two morphologies, membrane stacks (Fig 2A) and ribbons (Fig 3A). We find regions of either membrane stacks or ribbons within the same dehydrated sample. The membrane stacks are characterized by stepped mesas (Fig 2C). Similar mesas assemble in the positive control of dried phospholipid membranes (Fig 2B, 2D). Mesas have been observed previously in hydrated phospholipid membranes[21-25], and in dry layers of fatty acids that have been collected by dipping a mica substrate through a Langmuir-Blodgett monolayer[26]. Step heights in Fig 2 roughly correspond to heights of hydrated phospholipid membranes measured by atomic force microscopy[21-25]. We observed similar results with decanoic acid when serine-ethyl-ester (the monomer in our tests for dimerization) was included in the dispersion, as shown in Fig S14-15 of the Supporting Information (SI). Ribbons appear (Fig 3A) in addition to the membrane stacks (Fig 2A) in the dried samples of decanoic acid, and ribbons alone appear in a dried heptanoic acid sample (Fig 3B). The ribbons are composed of bundles of wormlike micelles (Fig 3C-D), consistent with other micellar systems[27].

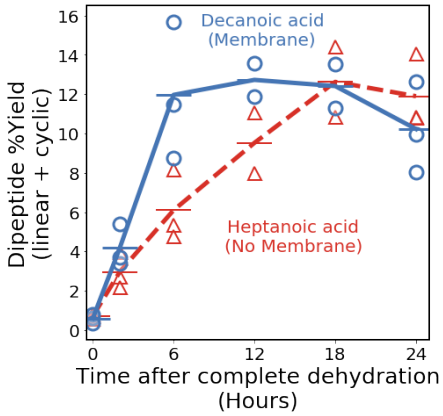

Figure 4. The rate of dipeptide formation after dehydration of 10 mM serine-ethyl-ester at 55°C is at least as high in the presence of decanoic acid (membrane) as in the presence of heptanoic acid (no membrane). The percent yield of serine dipeptide (sum of linear and cyclic forms) is shown as a function of time after complete dehydration, for periods of 0 to 24 hours. Horizontal lines indicate the average, and open symbols show all data points.

Our central question is whether dried fatty acid membranes affect the rate of dipeptide formation from serine-ethyl-ester. We find that the rate of dipeptide formation is at least as high in the presence of dried membranes as in the absence of membranes (Fig 4). Serine itself is prebiotically plausible because it could have been delivered to Earth by meteorites[29], or synthesized via sparking reactions[30]. Additionally, serine binds to fatty acid vesicles, resulting in membrane stabilization[31]. We modified serine with a C-terminal ethyl ester because it has been well-established that ethyl or adenylate esters enable room-temperature reaction with another amino acid to form a dipeptide[32], whereas unmodified amino acids require dehydration at high temperatures above 90°C for peptide formation[10]. This work with amino acid esters also provides further reason to focus on serine: amino acid esters react with the amine of serine to form dipeptides more efficiently than they react with 14 other amino acids[33]. Amino acid esters (i.e. aminoacyl-tRNAs) are used to form peptides and proteins in all modern organisms. Amino acids activated with esters are also prebiotically plausible because they form when hydroxy acids (which are found in meteorites[34]) are dried in the presence of amino acids[35].

We measured the production of dipeptides following dehydration of 10 mM serine-ethyl-ester with 50 mM decanoic acid or 50 mM heptanoic acid. We used liquid chromatography to deliver the products to a tandem mass spectrometer (Fig S1). Although we were not able to fully separate dipeptides from tripeptides and single amino acids (Fig S3), tandem mass spectrometry creates a "fingerprint" of fragments that uniquely identifies the dipeptides (Table S1). High-accuracy quantification by mass spectrometry requires calibration with isotope-labeled internal standards (Fig S4). We synthesized isotope-labeled dipeptides (SI section 1), and purchased isotope-labeled serine and

tripeptides (Fig S2). We could not procure standards for cyclic dipeptides, so we linearized any cyclic dipeptides by adding NaOH prior to analysis by LC-MS-MS. Our NaOH treatment simultaneously cleaved any remaining ethyl-esters (Fig S6-S7), while retaining linear dipeptides (instead of cleaving them into single amino acids, Fig S9). After the base treatment, we used the LC-MS-MS procedure to measure the total amount of linear dipeptide relative to the isotope internal standard.

We find that the rate of dipeptide formation is at least as high when the sample contains decanoic acid (which forms membranes) as when the sample contains heptanoic acid (which does not form membranes). The presence of fatty acids does not have a significant effect on the yield of dipeptide after 6 hours of dehydration: in the absence of fatty acids, we estimate 11.5% yield when the initial pH is 7 (Fig S12) compared to 12.0% and 6.1% in the presence of decanoic acid and heptanoic acid, respectively (Fig 4). Although our measurements do not distinguish linear and cyclic dipeptides, both compounds can elongate into growing peptide chains[36]. In our experiments, we detect very low yields (<1%) of serine tripeptides (Fig S11).

We minimized potential artifacts, such as variation in the rate of drying of decanoic acid dispersions versus heptanoic acid dispersions, by drying samples quickly under N2 gas. Under these conditions, no detectable dipeptide forms until samples are completely dehydrated. We found a slight difference in the pH of the rehydrated decanoic acid sample compared to the heptanoic acid sample, and we confirmed that the difference is too small to affect our results (Fig S12, Table S3). We observed a decrease in total serine residues, both with and without membranes (Fig S11).

Additional cycles of dehydration and rehydration have been shown to increase both the yield and maximum length of peptides[37]. Peptide formation is one of many reactions that proceed most effectively in dehydrated or partially dehydrated conditions[13, 38], so future work will determine whether membranes change the rates of these other reactions. It will also be interesting to determine whether formation of peptides by alternative mechanisms (such as activation with hydroxy acids[35], ligation of α-aminonitriles[39], or salt-induced ligation of amino acids[40]) will be affected by membranes.

In conclusion, we show that peptide formation from activated amino acids is fully compatible with the presence of fatty acids, whether as membranes or as wormlike micelles. Peptide formation in the presence of dried membranes would be expected to facilitate encapsulation of the peptides by vesicles upon rehydration, as has been shown for RNA oligomers[41]. Our results are consistent with the hypothesis that amino acids, peptides, and membranes could have co-localized into protocells within evaporating pools on the early Earth.

Experimental section

Materials

Serine-ethyl-ester hydrochloride and serine were purchased from Sigma-Aldrich (St. Louis, MO). Linear dipeptide, cyclic dipeptide, and the tripeptide were purchased from Bachem (Bubendorf, CH). Isotope-labeled serine (3C13 + N15) was from Cambridge Isotope Labs (Tewksbury, MA), isotope-labeled (2C13) tripeptide was from New England Peptide (Gardner, MA), fatty acids (heptanoic acid and decanoic acid) were from Nu-Chek Prep (Elysian, MN), and dioleoylphosphatidylcholine (DOPC) lipids were from Avanti Polar Lipids (Alabaster, AL). The procedure for synthesis of isotope-labeled linear dipeptide is presented in the SI (Section 1). 0.2 μm Nylon filters were purchased from Thermo Fisher Scientific (Hanover Park, IL). Stock solutions of serine-ethyl-ester were made by dissolving solid serine-ethyl-ester hydrochloride to 0.5 M in H2O. Stock dispersions of fatty acids were made by dissolving solid fatty acid to 0.18 M in 0.19 M NaOH, followed by gentle heating.

Conversion of serine-ethyl-ester into peptides after dehydration

Samples containing 10 mM serine-ethyl-ester, 20 mM PIPES buffer (pKa=6.8), and 50 mM fatty acid (either heptanoic acid or decanoic acid) were prepared by diluting the components from stock solutions. pH was adjusted to 7.00 (± 0.03) by the addition of concentrated HCl or NaOH. (Some experiments were run at pH 6.83, and similar results were obtained (Fig S13)). Sample dehydration was a multi-step process. In the first step, 200 μL aliquots of the sample were distributed to individual test tubes, which were maintained at 55°C under a stream of N2 for 1 hour. Next, the mass of each test tube and sample was measured, and the test tubes were returned to 55°C under a stream of N2 for an additional 0.5 hour. Final mass measurements of each test tube and sample confirmed that there were no detectable changes in mass (within ± 0.5 mg), so the samples were deemed dehydrated and the "clock" of the experimental time was set at 0 hours. Test tubes containing dehydrated samples were maintained in a heat block at 55°C for varying times, after which the sample was rehydrated with 200 μL H2O, allowed to sit at room temperature for 1 hour, then vortexed vigorously to resolubilize dried material. Independent experiments were performed on separate days.

Sample preparation for liquid chromatography-tandem mass spectrometry (Fig S5)

After rehydration and vortexing, 100 μL of each sample was immediately mixed with 4 μL of NaOH solution (final NaOH concentration 0.192 M) and held at 50°C for 2 hours. This base treatment cleaved any ethyl-esters to generate serine monomers, dipeptides, and tripeptides with free carboxyl termini. The base treatment simultaneously linearized any cyclic dipeptides so they could be quantified during tandem mass spectrometry via comparison to an isotope internal standard. Figs S6-S10 of the SI validate this procedure.

Base-treated samples were diluted 1:20 in a 0.1% (m/m H2O) heptafluorobutyric acid solution containing 250 μM isotope-labeled serine and 50 μM isotope-labeled linear dipeptide. For samples in which the tripeptide concentration was measured, 0.5 μM isotope-labeled tripeptide was included. The diluted sample was mixed with HCl solution (final HCl concentration 15 mM) to induce aggregation of fatty acids, and the fatty acid aggregates were removed by filtration with a 0.2 μm Nylon filter.

Procedure for liquid chromatography-tandem mass spectrometry

Samples were analyzed on a Vantage triple quad mass spectrometer (Thermo Fisher Scientific, Hanover Park, IL) using a Nanoaquity HPLC system (Waters Corporation, Milford, MA), and a Waters ACQUITY UPLC M-Class HSS T3 Column (100 Å, 1.8 μm, 300 μm X 100 mm) operated at 25°C. Solvent A was an aqueous solution of 0.1% acetic acid and 0.02% heptafluoro-butyric acid (HFBA). Solvent B was acetonitrile with 0.1% acetic acid and 0.02% HFBA. Samples were loaded at 5 μl/min for 2 min followed

by a gradient of 0-25% solvent B over 15 min, then 25-100% solvent B over 5 min. Collision energies and target fragment ions were chosen for serine, linear dipeptide, tripeptide, and the isotope-labeled internal standards (Table S1). Chromatograms for each ion were integrated in the program Skyline[42] (Seattle, WA), which created an output file that listed the normalized area (total ion count/total ion count for isotope standard) in a CSV format (Fig S1).

Conversion to concentration units via calibration curve

Each compound was dissolved in water to 10 mM, then serially diluted to desired concentrations. 100 µL solutions were mixed with NaOH solution (final NaOH concentration 0.192 M) and heated for 2 hours at 50°C. The base-treated sample was diluted 1:20 in a solution containing 0.1% (m/m H2O) heptafluorobutyric acid, 250 µM heavy isotope serine, and 50 µM heavy isotope dipeptide. For samples in which tripeptide concentrations were measured, 0.5 µM heavy isotope tripeptide was included. Finally, the diluted sample was mixed with HCl solution (final HCl concentration 15 mM). Independent experiments were performed on separate days.

Atomic Force Microscopy

Aqueous 50 mM heptanoic acid or decanoic acid samples were adjusted to pH 6.80 (±0.03) by addition of aqueous HCl or NaOH. Under these conditions, heptanoic acid self-assembles into micelles, and decanoic acid into both vesicles and micelles. Aqueous 1 mM DOPC dispersions were prepared by adding water to a dried lipid film, sonicating, then adjusting pH to 7.31 by addition of aqueous HCl or NaOH. Under these conditions, DOPC self-assembles into vesicles. A 3 µL droplet of sample was placed on a freshly-cleaved mica substrate and allowed to dry 1-2 hours before imaging. All AFM images were acquired in tapping mode in air on a Cypher ES (Asylum Research, Goleta, CA) with AC240TS cantilevers. Height profiles were measured with the software Gwyddion[43] (Brno, Czech Republic). No attempt was made to correct for edge overshoot due to hysteresis in the piezo, seen in Fig 3A[44].

Acknowledgements

We gratefully acknowledge Martin Sadilek, Matt Bush, and Frank Turecek for helpful discussions. This work was supported by grant NNX17AK86G (Exobiology) from NASA to S.L.K., by grant MCB 192573 from the National Science Foundation (NSF) to S.L.K., and by grant P41 GM103533 from the National Institutes of Health (NIH) to M.J.M. Z.R.C. and B.L.K. were funded by NSF fellowships (GRFP DGE 1762114). Support for AFM experiments was provided by the U.S. Department of Energy (DOE), Office of Basic Energy Sciences (BES) Chemical Sciences, Geosciences, and Biosciences Division at the Pacific Northwest National Laboratory (PNNL).

References

1. R. A. Black, M. C. Blosser, Life 2016, 6, 33.
2. G. F. Joyce, J. W. Szostak, Cold Spring Harbor Perspect. Biol. 2018, 10.
3. H. M. Huffman, J. Phys. Chem. 1942, 46, 885–891.
4. R. Wolfenden, Annu. Rev. Biochem. 2011, 80, 645–667.
5. E. Imai, H. Honda, K. Hatori, A. Brack, K. Matsuno, Science 1999, 283, 831–833.
6. W. Takahagi, K. Seo, T. Shibuya, Y. Takano, K. Fujishima, M. Saitoh, S. Shimamura, Y. Matsui, M. Tomita, K. Takai, ACS Earth Space Chem. 2019, 3, 2559–2568.
7. S. S. Mansy, J. W. Szostak, PNAS 2008, 105, 13351–13355.
8. B. Damer, D. Deamer, Astrobiology 2019, 20, 429–452.

9. D. D. Sasselov, J. P. Grotzinger, J. D. Sutherland, Sci. Adv. 2020, 6.
10. M. Rodriguez-Garcia, A. J. Surman, G. J. T. Cooper, I. Suárez-Marina, Z. Hosni, M. P. Lee, L. Cronin, Nat. Commun. 2015, 6.
11. D. W. Deamer, G. L. Barchfeld, J. Mol. Evol. 1982, 18, 203–206.
12. L. Toppozini, H. Dies, D. W. Deamer, M. C. Rheinstädter, PLOS ONE 2013, 8, e62810.
13. S. Rajamani, A. Vlassov, S. Benner, A. Coombs, F. Olasagasti, D. Deamer, Origins Life Evol. Biospheres 2008, 38, 57–74.
14. M. P. Joshi, A. A. Sawant, S. Rajamani, Chem. Sci. 2021, 12, 2970–2978.
15. D. Deamer, J. P. Dworkin, S. A. Sandford, M. P. Bernstein, L. J. Allamandola, Astrobiology 2002, 2, 371–381.
16. J. G. Lawless, G. U. Yuen, Nature 1979, 282, 396–398.
17. D. W. Nooner, J. Oro, in Hydrocarbon Synthesis from Carbon Monoxide and Hydrogen, American Chemical Society, 1979, pp. 159–171.
18. G. U. Yuen, J. G. Lawless, E. H. Edelson, J. Mol. Evol. 1981, 17, 43–47.
19. T. Namani, P. Walde, Langmuir 2005, 21, 6210–6219.
20. C. L. Apel, D. W. Deamer, M. N. Mautner, Biochim. Biophys. Acta, Biomembr. 2002, 1559, 1–9.
21. A. S. Muresan, K. Y. C. Lee, J. Phys. Chem. B 2001, 105, 852–855.
22. F. Tokumasu, A. J. Jin, G. W. Feigenson, J. A. Dvorak, Ultramicroscopy 2003, 97, 217–227.
23. J. V. Bleecker, P. A. Cox, R. N. Foster, J. P. Litz, M. C. Blosser, D. G. Castner, S. L. Keller, J. Phys. Chem. B 2016, 120, 2761–2770.
24. J. V. Bleecker, P. A. Cox, S. L. Keller, Biophys. J. 2016, 110, 2305–2308.
25. Z. Lv, S. Banerjee, K. Zagorski, Y. L. Lyubchenko, in Nanoscale Imaging: Methods and Protocols (Ed.: Y.L. Lyubchenko), Springer, New York, NY, 2018, pp. 129–143.
26. D. Y. Takamoto, E. Ter-Ovanesyan, D. K. Schwartz, R. Viswanathan, S. Chiruvolu, J. A. Zasadzinski, Acta Phys. Pol. A 1998, 93, 373–382.
27. F. Jiao, X. Wu, T. Jian, S. Zhang, H. Jin, P. He, C.-L. Chen, J. J. De Yoreo, Angew. Chem., Int. Ed. 2019, 58, 12223–12230.
28. B. Dejanović, K. Mirosavljević, V. Noethig-Laslo, S. Pečar, M. Šentjurc, P. Walde, Chem. Phys. Lipids 2008, 156, 17–25.
29. J. R. Cronin, C. B. Moore, Science 1971, 172, 1327–1329.
30. A. P. Johnson, H. J. Cleaves, J. P. Dworkin, D. P. Glavin, A. Lazcano, J. L. Bada, Science 2008, 322, 404–404.
31. C. E. Cornell, R. A. Black, M. Xue, H. E. Litz, A. Ramsay, M. Gordon, A. Mileant, Z. R. Cohen, J. A. Williams, K. K. Lee, G. P. Drobny, S. L. Keller, Proc. Natl. Acad. Sci. U.S.A. 2019, 116, 17239–17244.
32. A. L. Weber, L. E. Orgel, J. Mol. Evol. 1978, 189–198.
33. A. L. Weber, L. E. Orgel, J. Mol. Evol. 1979, 13, 185–191.
34. E. T. Peltzer, J. L. Bada, Nature 1978, 272, 443–444.
35. J. G. Forsythe, S.-S. Yu, I. Mamajanov, M. A. Grover, R. Krishnamurthy, F. M. Fernández, N. V. Hud, Angew. Chem., Int. Ed. 2015, 54, 9871–9875.
36. D. Barreiro-Lage, P. Bolognesi, J. Chiarinelli, R. Richter, H. Zettergren, M. H. Stockett, L. Carlini, S. Diaz-Tendero, L. Avaldi, J. Phys. Chem. Lett. 2021, 12, 7379–7386.
37. T. D. Campbell, R. Febrian, J. T. McCarthy, H. E. Kleinschmidt, J. G. Forsythe, P. J. Bracher, Nat. Commun. 2019, 10, 4508.
38. C. Gibard, S. Bhowmik, M. Karki, E.-K. Kim, R. Krishnamurthy, Nat. Chem. 2017, 10, 212–217.
39. P. Canavelli, S. Islam, M. W. Powner, Nature 2019, 571, 546–549.
40. B. M. Rode, Peptides 1999, 20, 773–786.
41. D. Milshteyn, B. Damer, J. Havig, D. Deamer, Life 2018, 8, 11.

42. B. MacLean, D. M. Tomazela, N. Shulman, M. Chambers, G. L. Finney, B. Frewen, R. Kern, D. L. Tabb, D. C. Liebler, M. J. MacCoss, Bioinformatics 2010, 26, 966–968.
43. D. Nečas, P. Klapetek, Open Phys. 2012, 10, 181–188.
44. M. Radmacher, J. P. Cleveland, M. Fritz, H. G. Hansma, P. K. Hansma, Biophys. J. 1994, 66, 2159–2165.

Supplementary information

Section I: Synthesis of isotope internal standard for the linear serine dipeptide

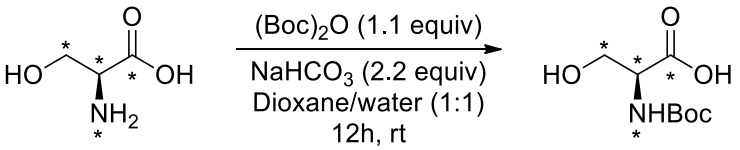

A 20 mL round bottom flask (RB) was charged with a stir bar, isotope serine (ser*), (0.5 mmol, 1.0 equiv, 54.5 mg), and sodium bicarbonate (1.1 mmol, 2.2 equiv, 9.2 mg). A 1:1 mixture of dioxane/water (1.5 mL) was added to the RB to make the concentration of ser* 0.3 M. Boc-anhydride (0.55 mmol, 1.1 equiv, 120.2 mg) was added slowly to the mixture. The mixture was allowed to stir for 12 h, after which the solvent was evaporated under a vacuum. The residue was dissolved in ethyl acetate (10 mL) and washed with water (10 mL, washed twice). The organic layer was collected and set aside. The aqueous layer (10 mL X 2) was collected and acidified with 5% HCl solution in water until the pH reached 3. The aqueous layer was extracted with ethyl acetate (20 mL, extracted twice) using a 100 mL separatory funnel. All the organic layers were combined, dried over anhydrous Na_2SO_4, filtered to get rid of the Na_2SO_4, and concentrated under vacuum to give 90.9 mg of the desired boc-ser* in 87% yield. The sticky, colorless semisolid was used in the next step without further purification.

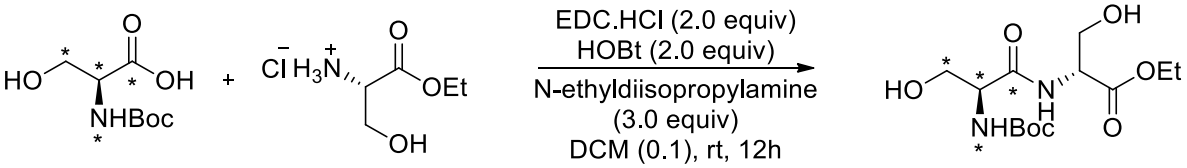

A 50 mL RB was charged with a stir bar, boc-ser* (0.43 mmol, 1.0 equiv, 90.9 mg), and ser-ethyl-ester.HCl (0.5 mmol, 1.1 equiv, 84.6 mg). Dry dichloromethane (DCM) was added to make the concentration of boc-ser* 0.1 M. The mixture was stirred at 0°C for 10 minutes in an ice bath. 1-Ethyl-3-(3'-dimethylaminopropyl)carbodiimide hydrochloride (EDC.HCl 0.86 mmol, 2.0 equiv, 167.2 mg), hydroxybenzotriazole (HOBt, 0.86 mmol, 2.0 equiv, 116.2 mg) and N-ethyldiisopropyl amine (1.29 mmol, 3.0 equiv, 166.8 mg) were added, in that order. The ice bath was taken off, and the mixture was stirred overnight at room temperature. After 12 hours, water (20 mL) was added to the reaction mixture, and the mixture was extracted with DCM (20 mL, extracted twice) using 100 mL separatory funnel. The organic layers were combined, dried over anhydrous Na_2SO_4, filtered to remove the Na_2SO_4, and concentrated under vacuum. Silica gel column (hexane/ethyl acetate were the eluent) chromatography provided the product boc-ser*-ser-ethyl-ester in 70% yield (96.4 mg).

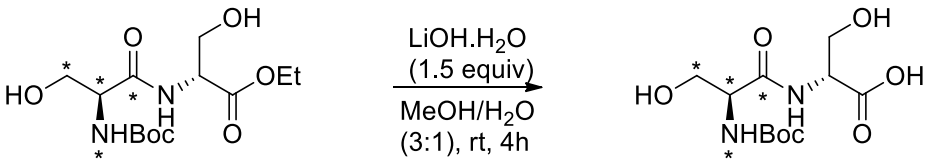

A 20 mL RB was charged with a stir bar and $LiOH.H_2O$ (0.45 mmol, 1.5 equiv, 18.9 mg). A mixture of solvents $MeOH/H_2O$ (3:1, 4 mL), and boc-ser*-ser-ethyl-ester (0.3 mmol, 1.0 equiv, 96.4 mg) were added to the to the RB and stirred for 4 hours at room temperature. After 4 hours, the solution was acidified to pH 2 with a saturated aqueous solution of citric acid. The mixture was extracted with ethyl acetate (20 mL, extracted thrice). The organic layers were combined and dried over Na_2SO_4, filtered to remove the Na_2SO_4 and concentrated under vacuum to give the desired product Boc-ser*-ser-OH as a highly viscous and hygroscopic oil in quantitative yields (88.2 mg). The product was used in the next step without further purification.

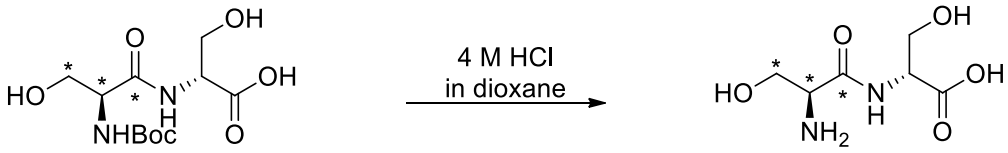

Boc-ser*-ser-OH (0.3 mmol, 1.0 equiv, 88.2 mg) was taken in a vial and stirred with 4 M HCl in dioxane (1 mL) for 4 hours. Following that, dioxane was evaporated and crashed with hexane. The product was purified with silica gel column chromatography using methanol as the eluent. The eluent was collected, evaporated under vacuum, and isolated as a viscous liquid in 95% yield (54.6 mg). The product was characterized by liquid chromatography and tandem mass spectrometry.

Section II: Quantitative liquid chromatography-tandem mass spectrometry (LC-MS-MS) with isotope internal standards

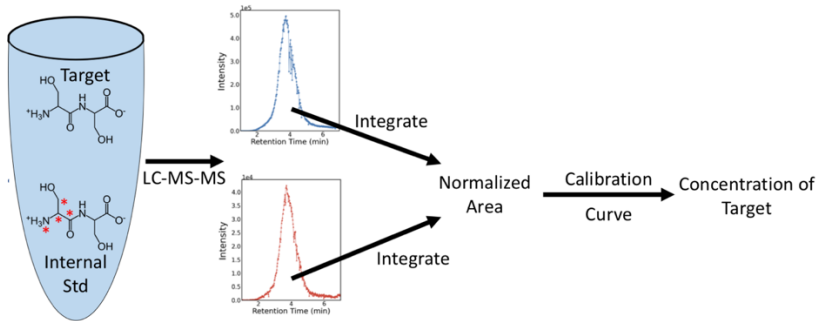

Figure S1: Procedure to measure the concentration of serine, linear serine dipeptides, and serine tripeptides. For simplicity, the scheme depicts analysis of only the linear serine dipeptide; all target compounds and internal standards (Fig S2) were analyzed in parallel during a single LC-MS-MS run. Calibration curves were generated as described in the experimental section of the main text.

Target Compound	Internal Standard
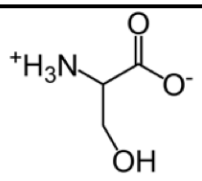 Serine ([M+H] m/z = 106)	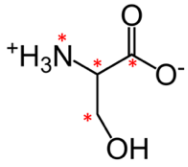 Isotope Serine ([M+H] m/z = 110)
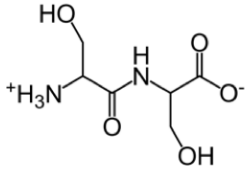 Dipeptide ([M+H] m/z = 193)	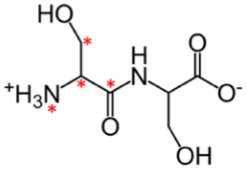 Isotope Dipeptide ([M+H] m/z = 197)
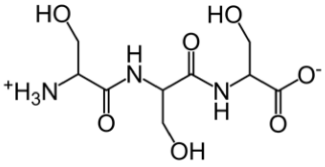 Tripeptide ([M+H] m/z = 280)	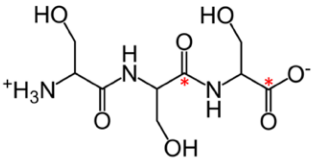 Isotope Tripeptide ([M+H] m/z = 282)

Figure S2: Molecular structures for the target compounds and internal standards that were analyzed by LC-MS-MS. Red asterisks indicate the position of heavy isotopes (either carbon-13 or nitrogen-15).

Table S1: Precursor and fragment m/z, and collision energies for target compounds and internal standards.

Target compound	Target compound			Internal standard		
	Precursor m/z	Fragment m/z	Collision energy (V)	Precursor m/z	Fragment m/z	Collision energy (V)
Serine	106.0	42.0	26	110.0	45.0	26
	106.0	60.0	13	110.0	63.0	13
Linear Serine dipeptide	193.1	60.0	18	197.0	63.0	18
	193.1	106.0	15	197.0	106.0	15
Serine tripeptide	280.0	60.0	34	282.0	60.0	34
	280.0	147.0	19	282.0	147.0	19
	280.0	175.0	13	282.0	176.0	13

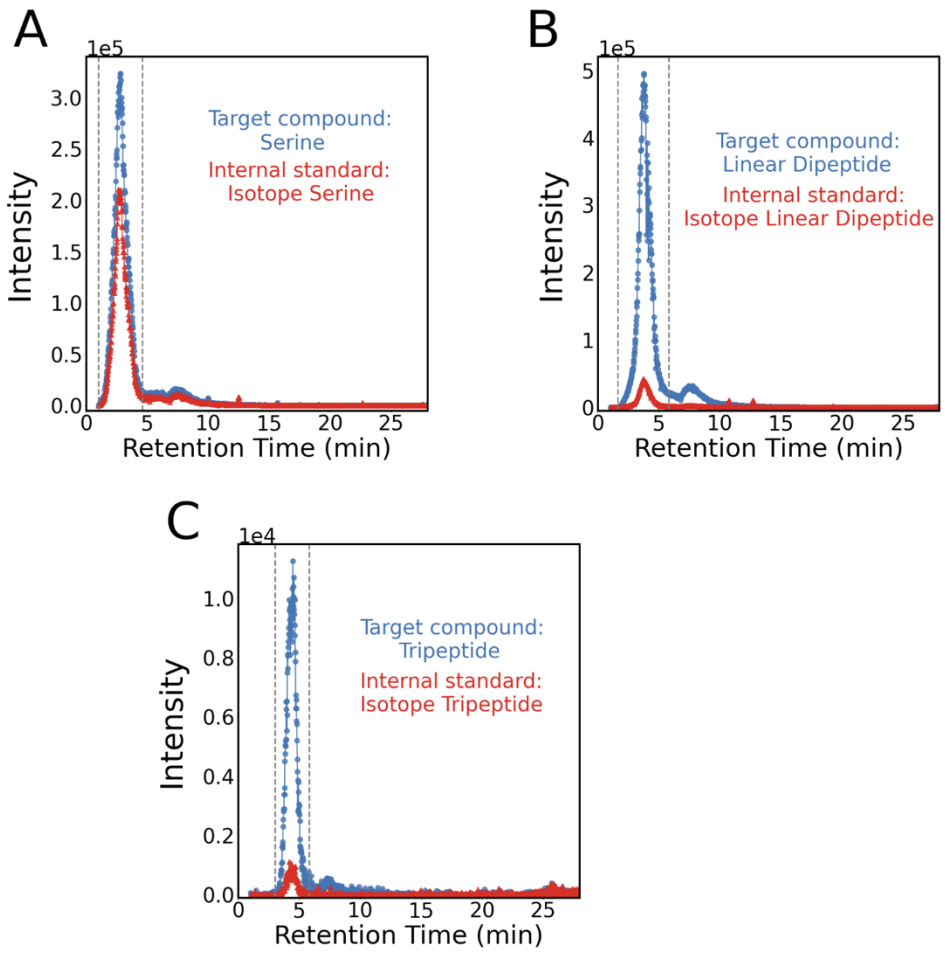

Figure S3: Representative LC-MS-MS chromatograms show that target compounds co-elute with their corresponding isotope internal standards. Samples contain the following target compounds: A) 10 mM serine, B) 5 mM linear serine dipeptide, C) 50 µM serine tripeptide. All samples contain the same mixture of internal standards: 5 mM isotope serine, 1 mM isotope linear serine dipeptide, and 10 µM isotope serine tripeptide. The total "intensity" is calculated by summing the intensities of all individual fragment ions. The normalized area is the ratio of the areas under the chromatogram for the target compound and internal standard. Dashed grey lines indicate the integration region for each pair of compounds.

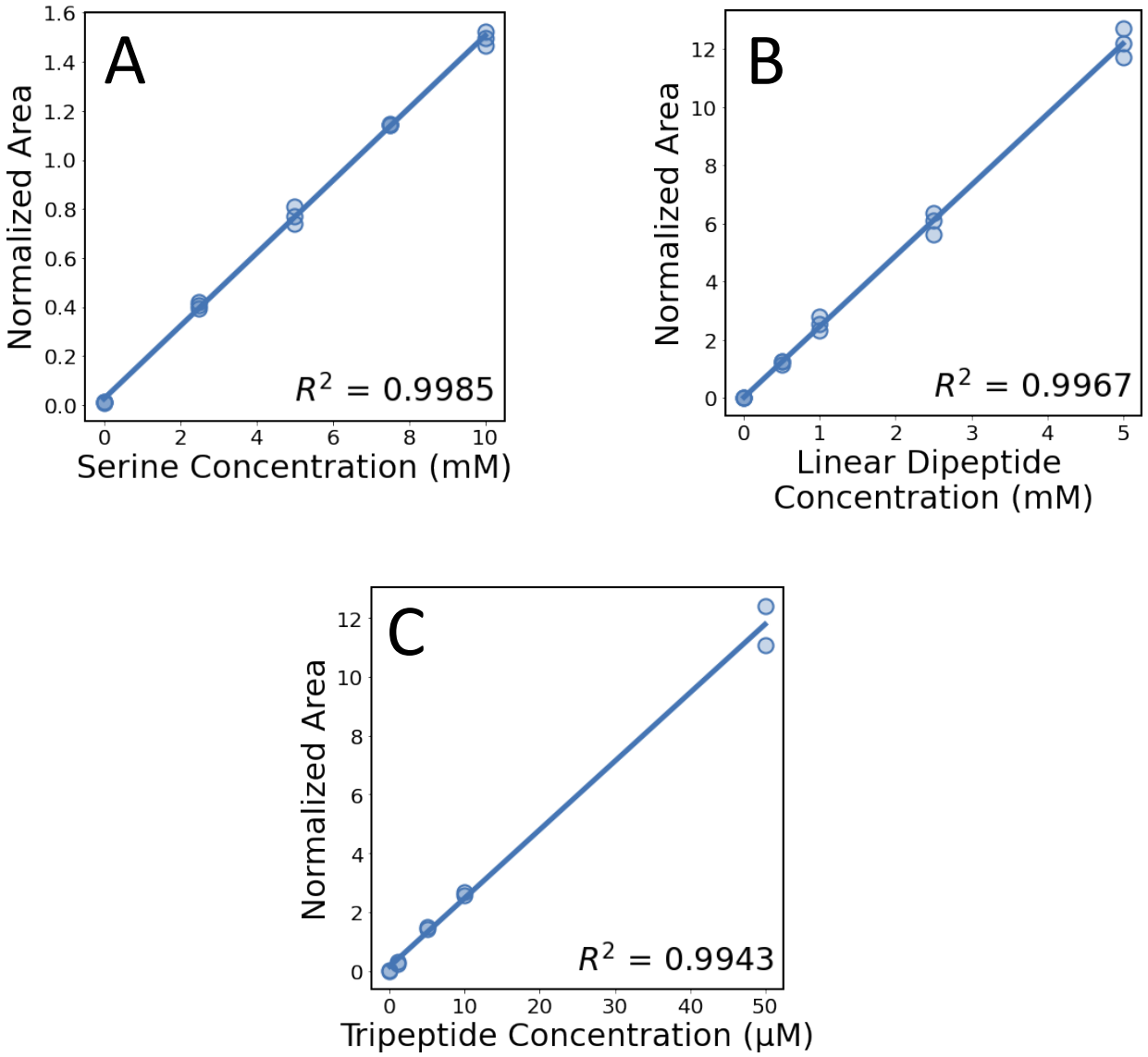

Figure S4: Calibration curves used to convert normalized areas into concentrations for the following target compounds: A) serine, B) linear serine dipeptide, C) serine tripeptide. These data were also used to validate the base treatment procedure (Fig S6 and S9).

Table S2: Estimated limits of detection for each target compound.

Target compound	Limit of detection (mM)
Serine	0.466
Linear Serine dipeptide	0
Serine tripeptide	0

Limits of detection for target compounds were found using the calibration data in Fig S4 and the following method:

1) For samples with 0 mM of the target compound, the mean ($mean_0$) and standard deviation (std_0) of the normalized areas were found.
2) For samples with 2.5 mM of the target compound, the standard deviation ($std_{2.5}$) of the normalized area was found.
3) The normalized area that corresponds to the limit of detection (T) is calculated by the method of Armbruster and Pry (1):
$$T = mean_0 + 1.645\ std_0 + 1.645\ std_{2.5}$$
4) The limit of detection in units of normalized area was converted to units of mM by looking up the corresponding value in Fig S4.

Section III: Validation of sample preparation procedure prior to LC-MS-MS

In order to validate the procedure for base treatment (Fig S5 Step1), we demonstrate three important results:

1) During base treatment, serine-ethyl-ester is converted into serine with nearly 100% yield (Fig S6-S7). Based on this result, we assume that peptide-ethyl-esters are converted into peptides with free C-termini in similarly high yield.

2) During base treatment, <1% of serine-ethyl-ester is converted into serine dipeptides. Based on this result, we assume that additional amide bonds are not formed during base treatment (Fig S8).

3) At maximum, 6.3% of serine dipeptides are cleaved into serine monomers during base treatment (Fig S9). This value is obtained by measuring the concentration of serine monomers in control standards of linear serine dipeptide after base treatment. The value of 6.3% is an upper estimate because the standard may have contained some serine monomer. A value of 6.3% does not change the conclusions in the main text. For example, in the experiments in Figure 4 of the main text, even if the total yield of dipeptides in the "No Membrane" sample is 6.3% higher before base treatment (6.5% yield instead of 6.1% yield six hours after dehydration), we still conclude that the rates of dipeptide formation are similar in the presence or absence of membranes.

4) During base treatment, cyclic dipeptides are converted into linear dipeptides with at least 78% yield (Fig S10). Because cyclic dipeptides are converted into linear dipeptides during base treatment, we cannot determine the ratio of the linear and cyclic dipeptides generated during dehydration. Instead, our measurements of linear dipeptide concentration correspond to the sum of the linear dipeptides generated during dehydration, and at least 78% of the cyclic dipeptides generated during dehydration (minus any dipeptide that is cleaved as in the previous paragraph).

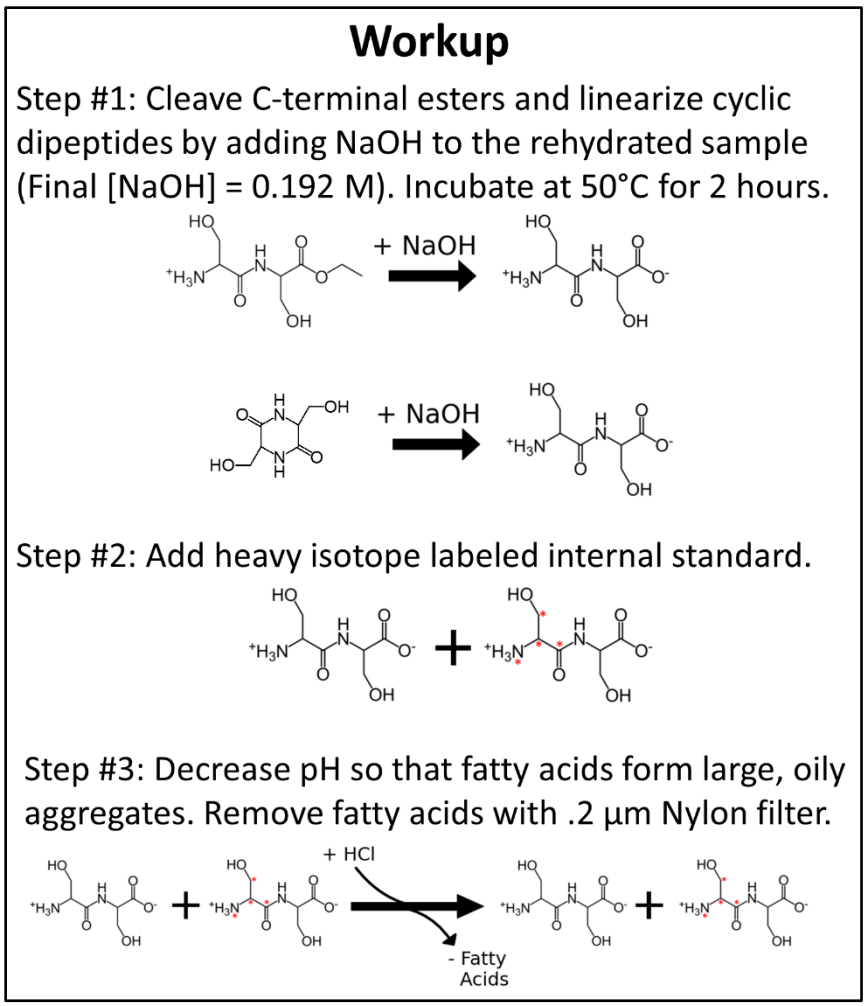

Figure S5: Procedure for preparation of samples prior to analysis by LC-MS-MS.

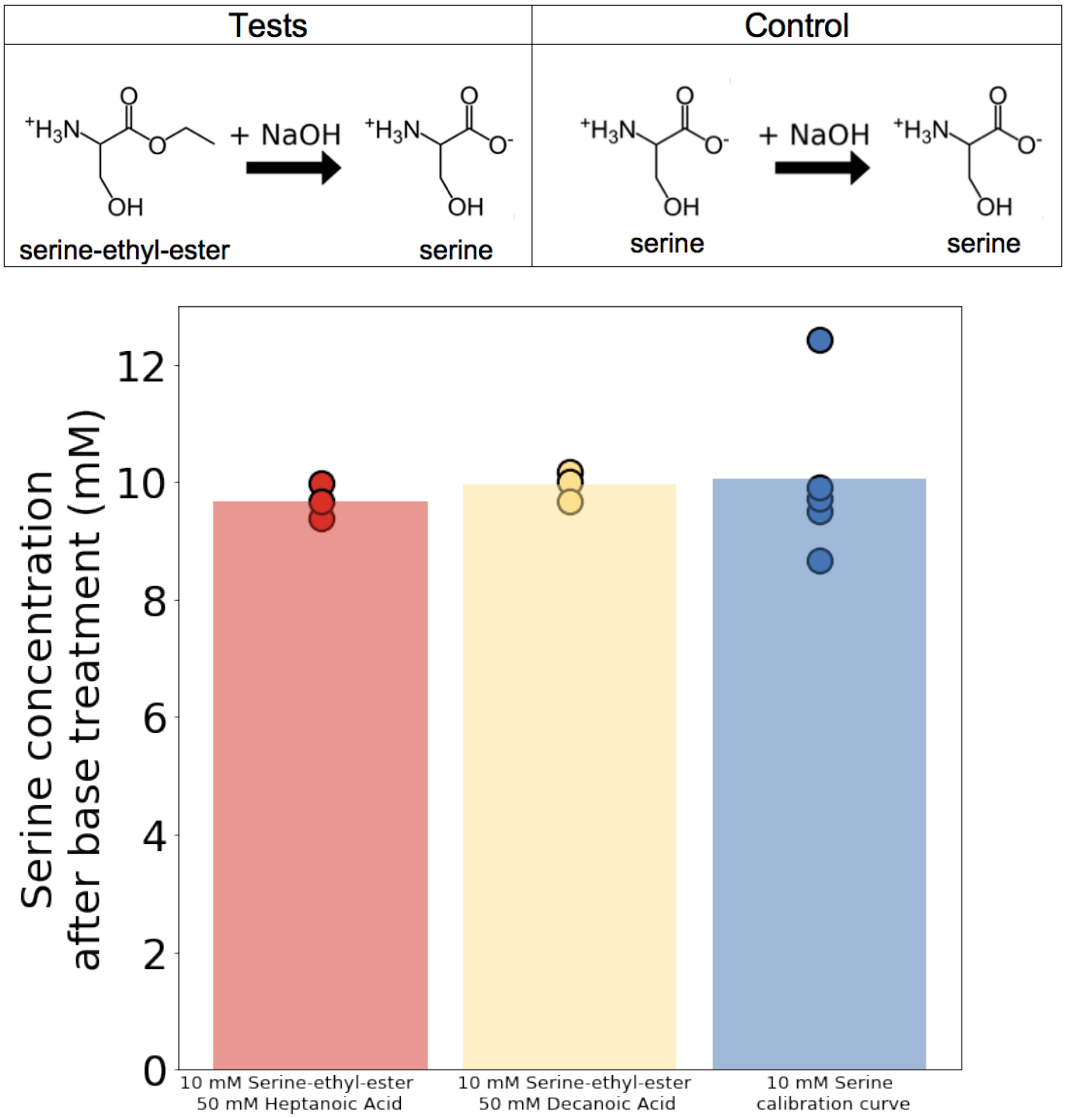

Figure S6: During treatment with base, all serine-ethyl-esters are converted into serine, as shown in the reaction. Two different tests were run. The first had initial concentrations of 10 mM serine-ethyl-ester and 50 mM heptanoic acid (left column). The second had initial concentrations of 10 mM serine-ethyl-ester and 50 mM decanoic acid (middle column). A control containing 10 mM serine was used for comparison (right column). All test samples and control samples were treated with base (with no dehydration). After the treatment, the concentration of serine cleaved from the ethyl ester was measured. The serine concentrations from both tests correspond to the control.

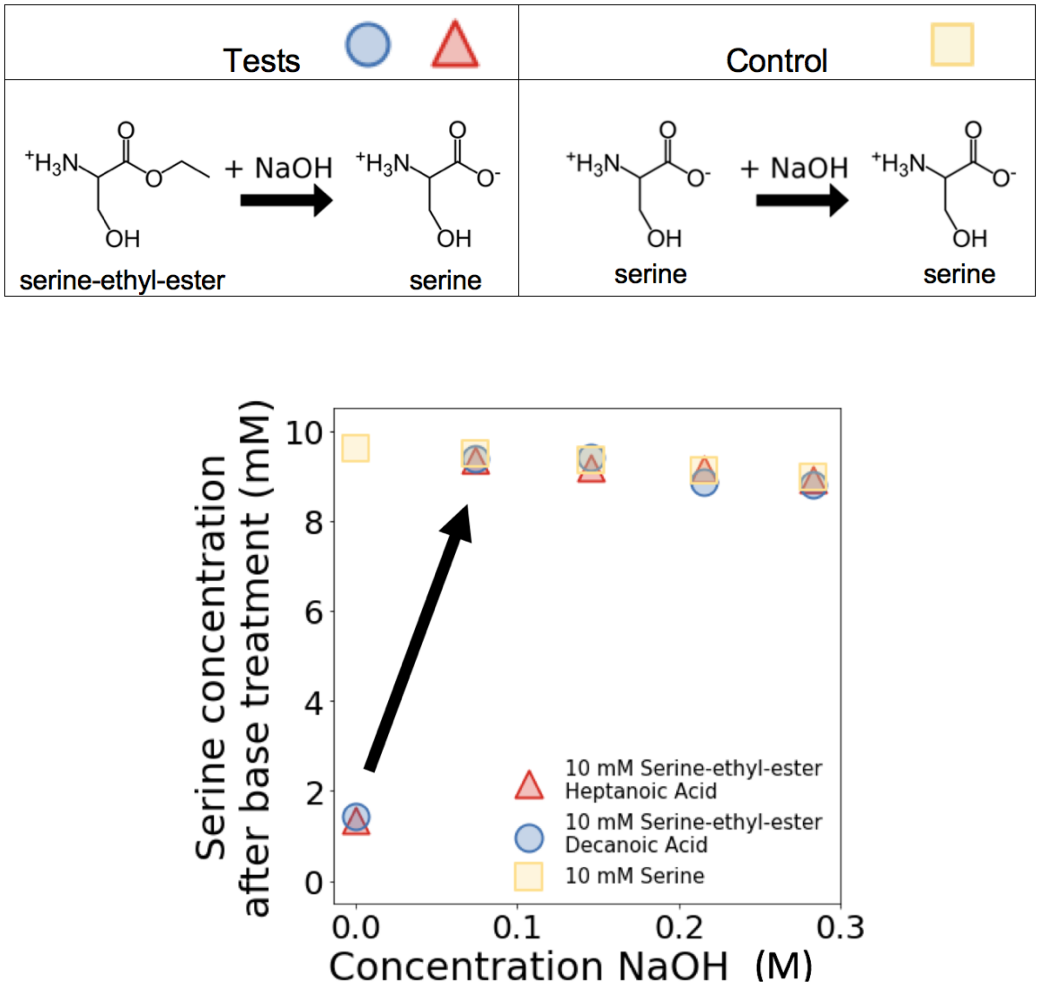

Figure S7: Verification that the concentration of NaOH used in the main text to cleave ethyl esters (0.192 M) is well above the minimum concentration required for complete conversion of serine-ethyl-ester into serine. Two different tests were run. The first had initial concentrations of 10 mM serine-ethyl-ester and 50 mM heptanoic acid (triangles). The second had initial concentrations of 10 mM serine-ethyl-ester and 50 mM decanoic acid (circles). A control containing 10mM serine was used for comparison (squares). After treatment with the base, the concentration of serine cleaved from the ethyl ester was measured. The concentrations of serine produced from mixtures of 10 mM serine-ethyl-ester and fatty acids match the measured concentration of 10 mM serine at all NaOH concentrations except 0 M.

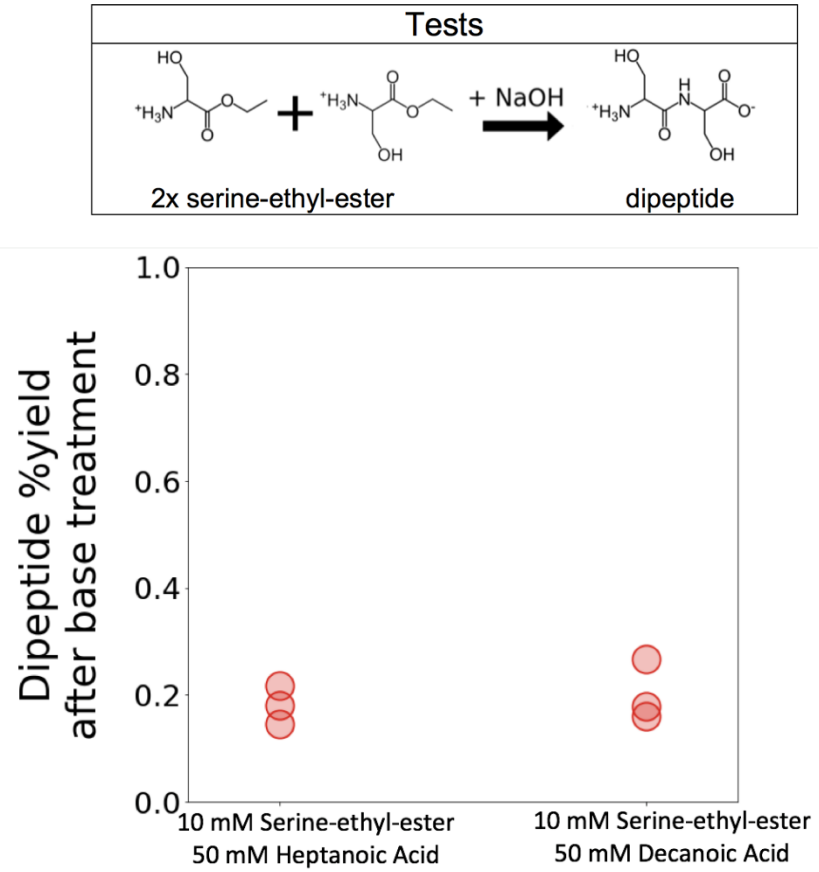

Figure S8: Without dehydration, conversion of serine-ethyl-esters to dipeptide (as in the reaction shown at the top) gives less than 1% yield of dipeptide. Two different tests were conducted. The first had initial concentrations of 10 mM serine-ethyl-ester and 50 mM heptanoic acid (1st column). The second had initial concentrations of 10 mM serine-ethyl-ester and 50 mM decanoic acid (2nd column).

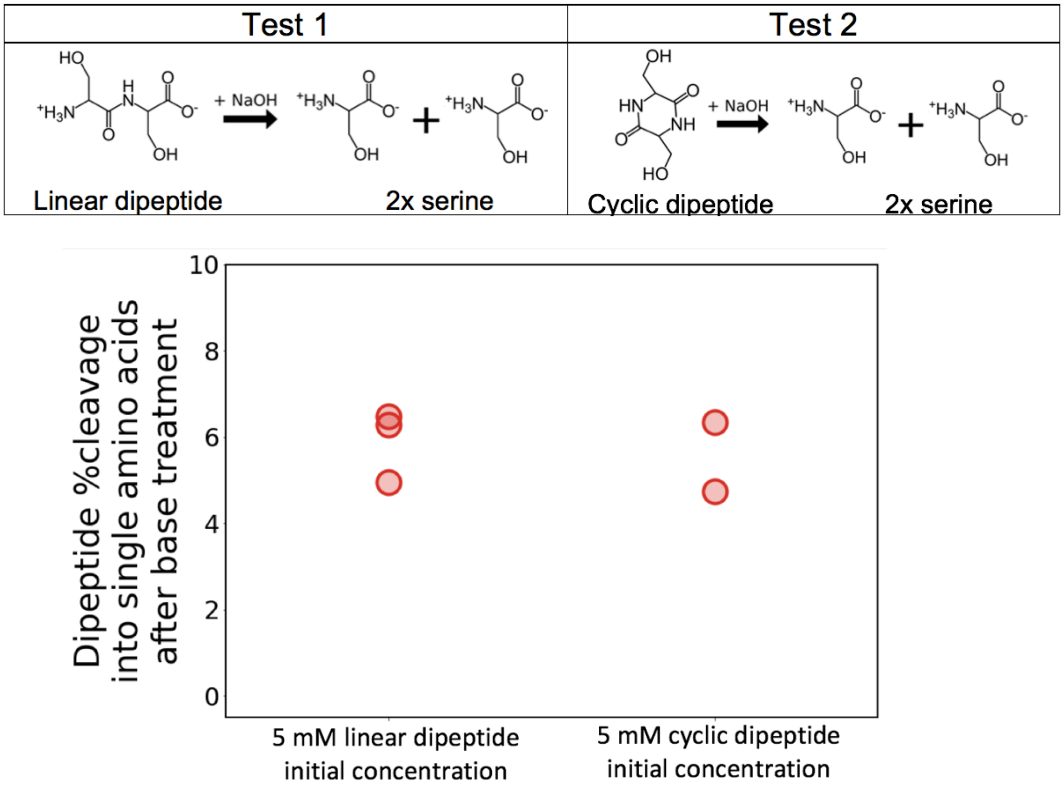

Figure S9: At maximum, only 6.3% of dipeptides are converted into serine amino acids when treated with NaOH. Two different tests were conducted. The first had initial concentration of 5 mM linear dipeptide (1st column). The second had initial concentration of 5 mM cyclic dipeptide (2nd column). The effect of converting 6.3% of dipeptides into amino acids is small in the context of our main results. For example, in the absence of dipeptide cleavage, we would detect a maximum 6.5% yield of dipeptides in the "No membrane" experiments 6 hours after dehydration (Figure 4), rather than the 6.1% yield that we report in the main text.

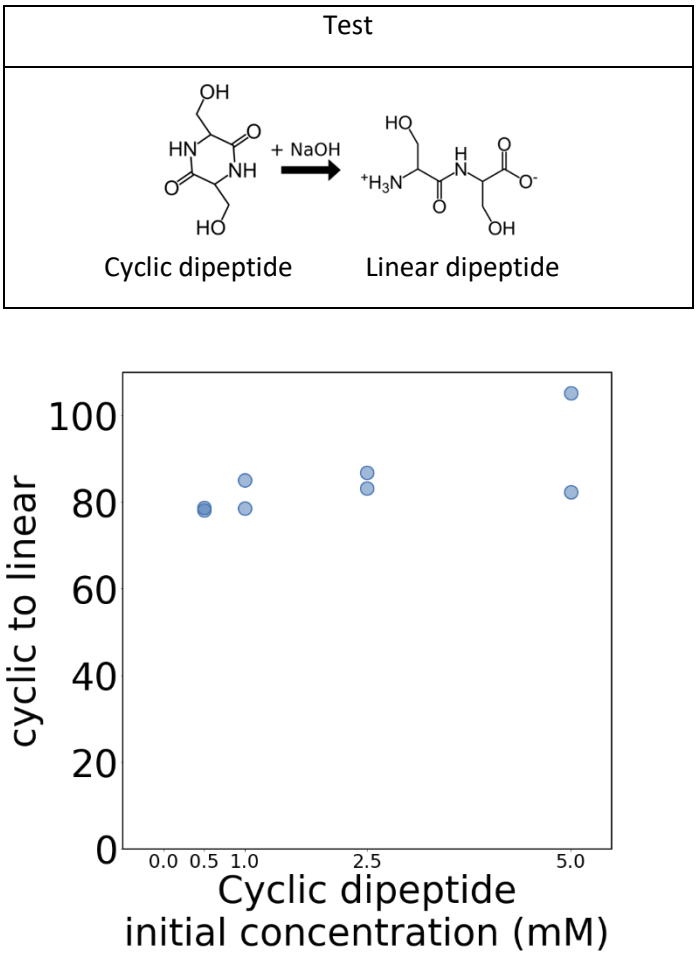

Figure S10: At minimum, 78% of cyclic dipeptides are converted to linear dipeptides during treatment with NaOH. These values do not vary strongly with the initial concentration of cyclic dipeptide. The remaining 22% of cyclic dipeptides are undetectable by LC-MS-MS, and create an upper bound for the experimental uncertainty in the percent yield of dipeptide. This uncertainty does not affect the central result that dipeptide formation is at least as fast in the presence of decanoic acid versus heptanoic acid.

Section IV: The total concentration of serine residues is not conserved throughout dehydration

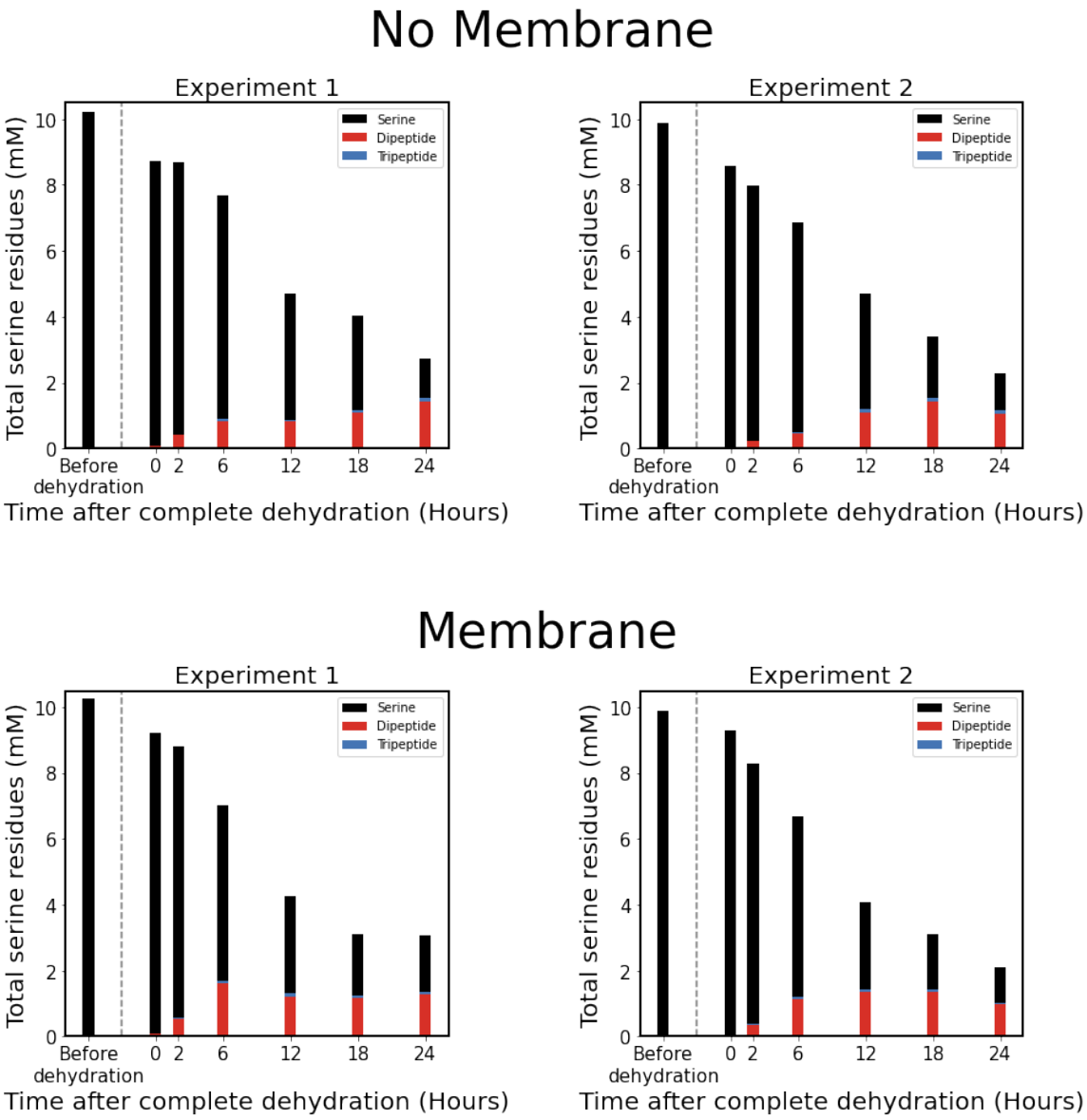

Figure S11: The total concentration of serine residues detected by LC-MS-MS decreases with time, following complete dehydration. The total concentration of serine residues = 1 x (the concentration of serine amino acids) + 2 x (the concentration of dipeptides) + 3 x (the concentration of tripeptides). The rate of decrease is similar for the "No Membrane" (heptanoic acid) and "Membrane" (decanoic acid) samples. Experiments 1 and 2 were independent. It is not known if the missing serine is consumed in an unknown side reaction or if it is irreversibly bound to the glass surface of the test tube.

Section V: Changes in pH are too small to affect rates of dipeptide formation

In order to confirm that pH did not change significantly upon dehydration, we measured the pH in both the "No Membrane" and "Membrane" samples under identical conditions: after dehydration at 55°C, 6 hours of incubation at 55°C in the dehydrated state, and then rehydration (Table S3).

Table S3: pH shifts slightly after a process of dehydration, incubation at 55°C for 6 hours, rehydration.

	Without membrane (50 mM heptanoic acid)	With membrane (50 mM decanoic acid)
pH before dehydration	6.95	6.99
pH after 6 h of dehydration (and subsequent rehydration)	7.09	6.85

In Table S3, the largest shift in pH is only 0.24 units. In order to determine if this shift could significantly affect the rate of dipeptide formation, we measured dipeptide yield over a large range of pH values, as shown in Fig S12 below. Fatty acids were not included in these experiments.

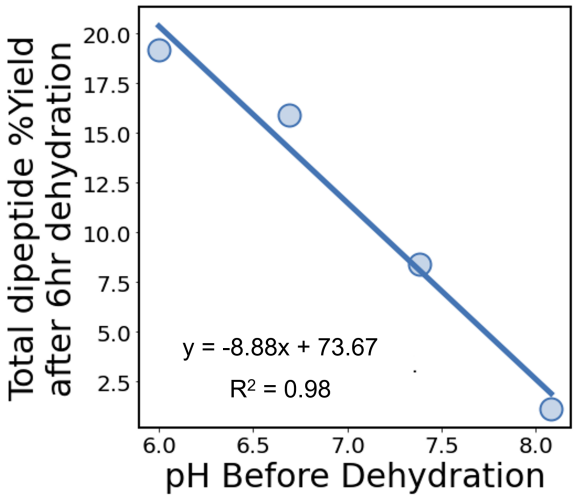

Figure S12: Percent yield of dipeptides from 10 mM serine-ethyl-ester following dehydration and 6 hours incubation at 55°C (in the absence of fatty acids), as a function of the solution's pH before dehydration.

Based on the linear fit to the data in Fig S12, the largest increase in pH in Table S3 (from pH 6.85 to 7.09) would correspond to a decrease in dipeptide yield of only 2.2% (from 12.8% to 10.6%). Thus, the rate of dipeptide formation in the presence of membranes is at least as fast as the rate without membranes, even when changes in pH are accounted for.

Section VI: Peptide formation at different initial pH values

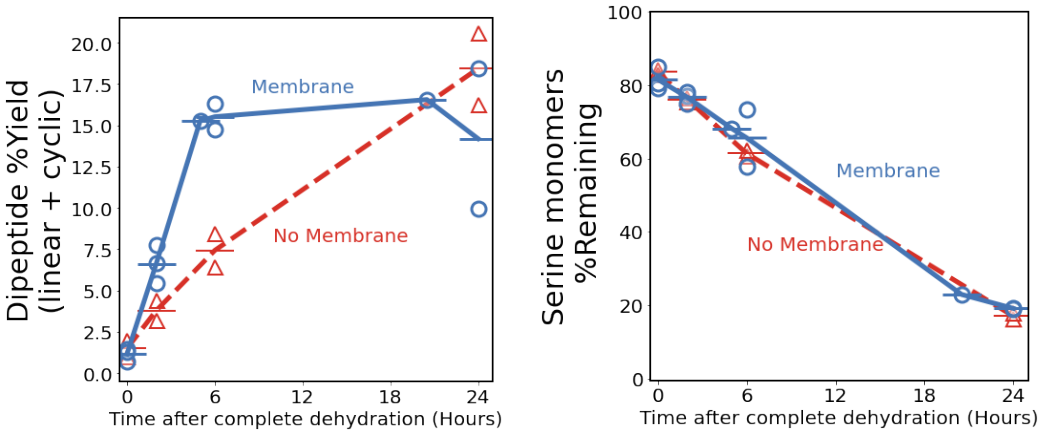

Figure S13: Measurements of dipeptide % yield (left) and the percent of initial serine monomers remaining (right) for experiments at an initial pH of 6.83. Similar trends are observed in the original experiments (Fig 4 of main text, and Fig S11) which differ in two specific ways: 1) originally the initial pH was 6.83 instead of 7.00, and 2) the concentration of NaOH used during the base treatment step was 0.146 M rather than 0.192 M. For the "Membrane" group, data are from three independent experiments. For the "No membrane" group, data are from two independent experiments. Lines indicate the average, and open symbols show all data points.

Section VII: Dehydrated decanoic acid vesicles form membrane stacks and ribbons in the presence of serine ethyl ester.

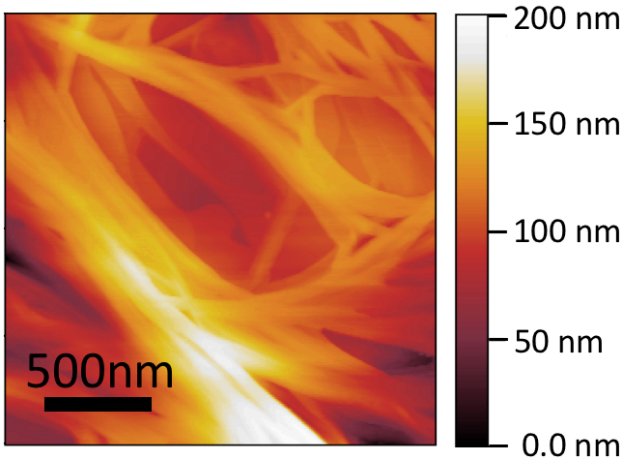

Figure S14: AFM image of ribbon morphology produced upon dehydration of a solution of 50 mM decanoic acid vesicles + 10mM Serine-ethyl-ester (pH 6.83).

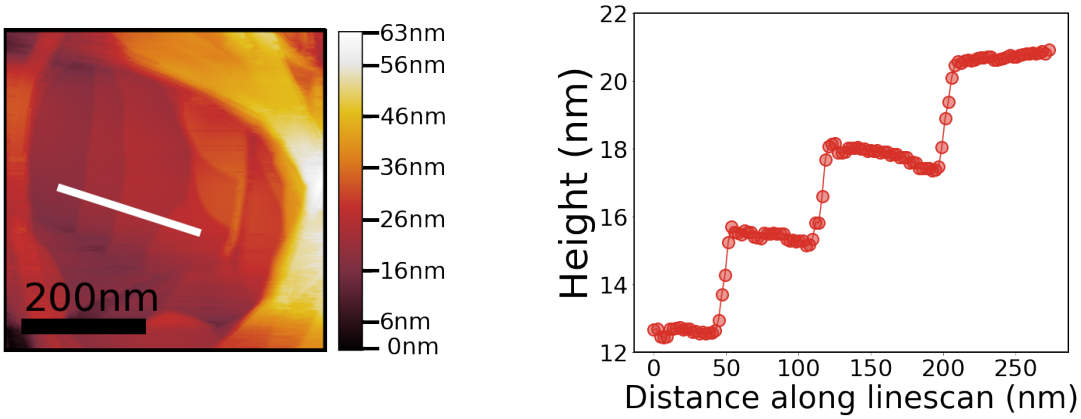

Figure S15: (Left) AFM image of stacks produced upon dehydration of a solution of 50 mM decanoic acid vesicles and 10 mM serine-ethyl-ester (pH 6.83). (Right) The height of the stacks (measured along the white line in the AFM image) changes in discrete steps. Unlike figures in the main text, the "facet levels" parameter was adjusted during analysis of this image to account for artifacts that arose because the AFM tip was constrained within a deep pit.

Section VIII: References

1. Armbruster, D. A. & Pry, T. Limit of Blank, Limit of Detection and Limit of Quantitation. *Clin Biochem Rev* **29**, S49–S52 (2008).

Chapter 2:

Prebiotic protocell membranes retain encapsulated contents during flocculation, and phospholipids preserve encapsulation during dehydration

*This chapter was first published in *Langmuir* in 2022. It was written in collaboration with Caitlin E. Cornell, David C. Catling, Roy. A. Black, and Sarah L. Keller.

Abstract

The first cell membranes were likely composed of single chain amphiphiles such as fatty acids. An open question is whether fatty acid membranes could have functioned within evaporative lakes on the early Earth, which have been hypothesized to concentrate prebiotic reactants. Evaporation also concentrates monovalent salts, which in turn cause fatty acid membrane vesicles to flocculate; significant loss of encapsulated contents during flocculation would have impeded early cell evolution. Here, we tested whether fatty acid vesicles retain encapsulated contents after flocculation and after drying. We found that vesicles composed of 2:1 decanoic acid: decanol encapsulate calcein dye throughout a process of flocculation in saturated salt solution and subsequent disaggregation of vesicles by dilution of the salt. However, 30-minutes of complete dehydration disrupted encapsulation by fatty acid vesicles. In contrast, phospholipid vesicles maintained encapsulation. Our results reveal a selective pressure for protocells to incorporate phospholipids: while fatty acid membranes can retain encapsulated contents during periods of dilute and saturating salt, phospholipids are necessary for encapsulation during dry periods. Our results are consistent with the hypothesis that evaporative lakes were productive sites for prebiotic chemistry and the origin of cells.

Main text

Compartmentalization is necessary for cells. It allows genetic material to be sequestered and metabolite concentrations to be regulated. The earliest protocells were likely separated from their environment by a membrane of fatty acids[1] that were delivered to Earth via meteorites[2] or synthesized locally via Fischer-Tropsch[3] or sparking reactions[4].

A protocell is typically depicted as a single vesicle enclosing an interior solution[5–7], as in Fig 1a. If the vesicle is made of fatty acids, it is stable over a limited range of solution pH values within about half a unit of the effective pKa of the fatty acids[8]. If too many fatty acids are charged, only micelles form. If no fatty acids are charged, an oil forms. Even if the pH is conducive to forming vesicles, those vesicles can aggregate into "flocs" (Fig 2a) if the solution has high salt concentration[9]. Flocculation occurs when monovalent cations from the salt screen the negative charges on fatty acids, eliminating electrostatic repulsion between vesicles[10].

Salty water would have been common on the early Earth, so flocculation of fatty acid vesicles has traditionally been viewed as an obstacle to protocell development[1,11]. Geological evidence suggests that the origin of life on Earth probably occurred before 3.7 Gya[12,13] and that exposed land would have been present at that time[14]. When lakes or ponds form in closed basins (i.e. with no outflow) on terrain made of volcanic rock (i.e. basalt, as expected on the early Earth[14,15]), the water becomes enriched in dissolved carbonate. The inorganic carbon is derived from atmospheric CO_2 that dissolves in rainwater and then in streams or groundwater to form carbonic acid, which is consumed by reacting with minerals in the catchment rocks, thereby raising the pH and releasing cations that are mainly charge-balanced by bicarbonate[16]. Closed-basin lakes transiently experience saturating salt concentrations during evaporative cycles[17–20]. Evaporative, carbonate-rich lakes are appealing sites for the origin of cells because they can concentrate phosphate and ferrocynanides[19,20], making them productive sites for prebiotic syntheses that require phosphate, nitriles, or dehydration[21–23]. Therefore, it is worth re-evaluating whether salt-induced flocculation is detrimental. Here we tested whether flocculation prevents vesicles from performing their central role of encapsulating soluble material.

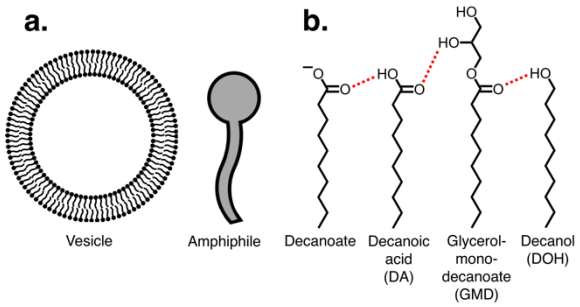

Figure 1. (a) Sketches of a vesicle and amphiphile, and (b) structures of prebiotic amphiphiles showing the hydrogen bonding (red dashes) required for bilayer formation.

We produced vesicles from plausibly prebiotic amphiphiles: decanoic acid (DA), decanol (DOH), and glycerol-mono-decanoate (GMD), shown in Fig 1b. Glycerol-monoesters like GMD reduce flocculation at moderate (< 0.6 M NaCl) but not high salt concentrations[11], as do nucleobases[24] and amino acids[25]. We flocculated vesicles with sodium bicarbonate ($NaHCO_3$) and sodium chloride (NaCl), which dissociate into monovalent ions. We did not include divalent cations in our experiments because divalent cations are kept to relatively low concentrations in natural carbonate-rich lakes due to precipitation of calcium, magnesium, or iron carbonates[26]. On the early Earth, such buffering by carbonate insolubility would keep divalent cations at low (< 2 mM) saturation concentrations[19,20]. Consequently, the relevant aqueous chemistry is dominated by sodium carbonate and chloride, which are highly soluble and can become concentrated during evaporation[19]. In the presence of low concentrations of divalent cations (< 3 mM), fatty acid vesicles maintain encapsulation of small molecules (nucleotides) over long time scales (> 24 hours)[27].

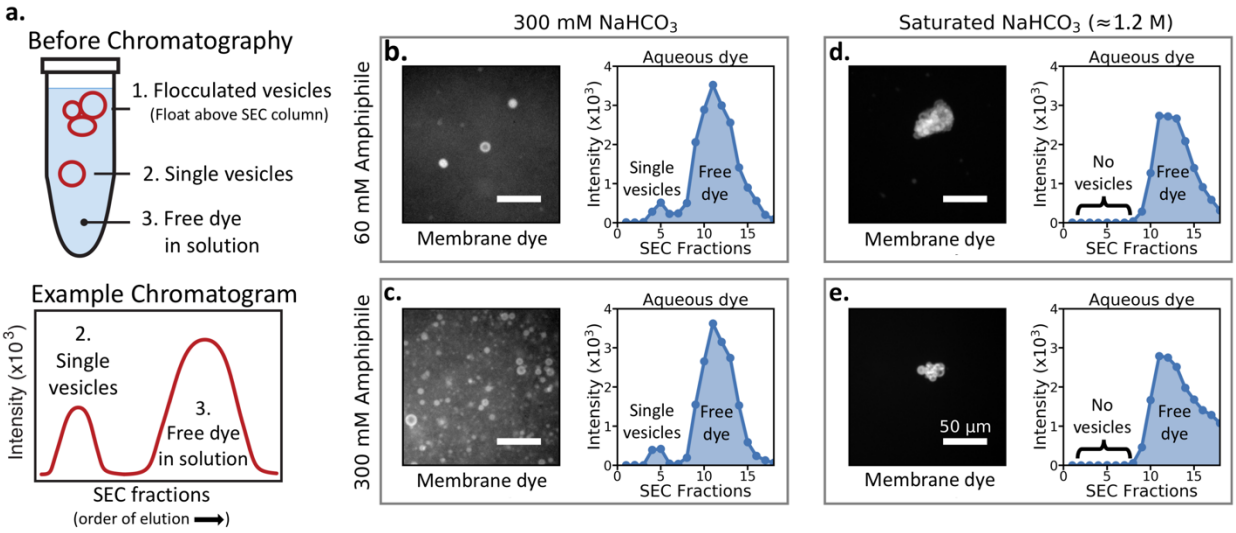

Figure 2. Increasing the concentration of amphiphile does not prevent vesicle flocculation in saturated $NaHCO_3$ solution. (a) Schematic: in a fatty acid solution, aqueous dye appears in the lumens of flocculated vesicles (1), in single vesicles (2), or free in solution (3). Flocculated vesicles cannot be detected by size-exclusion chromatography (SEC) because their low density prevents them from entering the SEC resin. Single fatty acid vesicles of 4:1:1 DA:DOH:GMD remained dispersed at low salt (b-c) and flocculated in saturated salt (d-e). Images show fluorescence micrographs taken before SEC with a hydrophobic dye that labels membranes (rhodamine 6G). Graphs show SEC chromatograms, which assay larger volumes than micrographs. At low salt concentration (b-c), images and SEC confirm that single vesicles remained dispersed throughout the solution. In saturated salt solution (d-e), only flocculated vesicles appeared in the images, and SEC confirmed that no single vesicles remained. Increasing the concentration of amphiphile did not prevent vesicle flocculation in saturated $NaHCO_3$ solution. To optimize imaging (which did not change the results) the sample in panel e was diluted 1:1 with SEC running buffer. Scale bars are 50 µm.

Vesicles flocculated in saturated salt solution, independent of whether they were made of fatty acids or phospholipids. For example, vesicles of 4:1:1 DA:DOH:GMD flocculated in saturated $NaHCO_3$, independent of the fatty acid concentration (Fig 2). Even when the concentration of amphiphile was increased (as would occur during dehydration), vesicles still flocculated when the $NaHCO_3$ became saturated (Fig 2e). No vesicles escaped flocculation, independent of whether the sample was evaluated by fluorescence microscopy or by size-exclusion chromatography (SEC). The composition 4:1:1 DA:DOH:GMD was chosen because those vesicles are more stable than vesicles of 2:1 DA:DOH[28]. Phospholipid vesicles of 95:5 DOPC:DOPG flocculated under the same salt conditions (Fig S1-S2).

Our central question is whether flocculation disrupts encapsulation of solutes by fatty acid vesicles. We prepared vesicles of 2:1 DA:DOH encapsulating calcein dye as a proxy for prebiotic molecules (Fig 3). We found that the dye remained in the vesicle lumens throughout a two-step cycle of flocculation in high salt and dispersal in low salt. This result held independent of whether flocculation was achieved with saturated $NaHCO_3$ or with saturated NaCl. Surprisingly in light of previous work, glycerol-mono-decanoate was not required for membrane stability[11]. Because calcein is a relatively small molecule, we can be confident that flocculated vesicles are also impermeable to larger molecules like ribozymes.

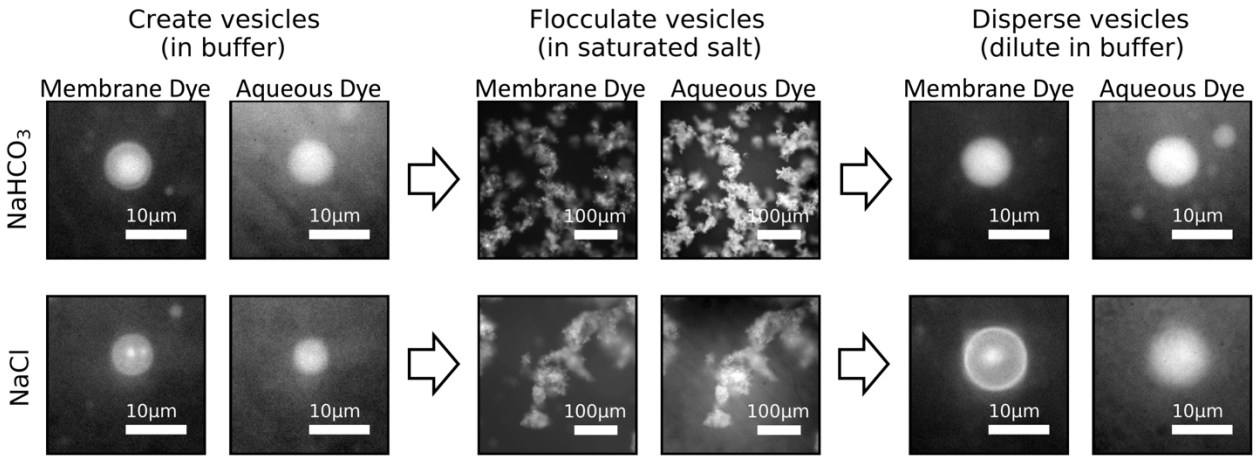

Figure 3. Fatty acid vesicles composed of 2:1 DA:DOH maintained encapsulation of an aqueous dye (calcein) throughout a process of salt-induced flocculation and subsequent dispersal. Immediately after adding salt, the vesicles flocculated; after 1 hr, the salt was diluted. Encapsulation was maintained independent of which saturated salt (~1.2 M $NaHCO_3$ or ~6.1 M NaCl) was used to induce flocculation. The dye that labeled vesicle membranes (rhodamine 6G) was added immediately prior to imaging. To optimize imaging (which did not change the results), we varied the preparation or treatment of samples in two ways. First, the samples shown in the left columns (the initial vesicles) and at the top right (after dilution from saturated $NaHCO_3$) were diluted 1:3 with SEC running buffer prior to imaging. Second, in the bottom row, flocculated vesicles in NaCl encapsulated a low (0.5 mM) initial calcein concentration to

prevent self-quenching, whereas vesicles before and after flocculation encapsulated 5 mM calcein initially. More discussion of this issue, and corresponding wide-field images are in the SI (Fig S3-S9).

In addition to our qualitative results from imaging, we verified quantitatively that the rate of dye leakage is not faster from flocculated vesicles than from dispersed vesicles (Fig 4). We encapsulated a self-quenching concentration of carboxyfluorescein in vesicles; an increase in fluorescence indicated leakage into the surrounding solution. We flocculated the vesicles with saturated $NaHCO_3$ or saturated NaCl. We did not observe leakage of the dye on the timescale (~ 3 h) of the experiment. As a positive control, we artificially achieved total leakage by disrupting the vesicles with Triton-X-100. We used microscopy to confirm that vesicles flocculated in these saturated salt conditions (Fig S12).

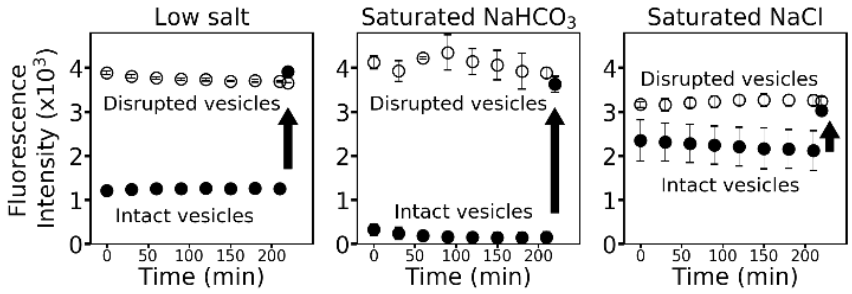

Figure 4. Single vesicles (low salt: 100mM $NaHCO_3$) and flocculated vesicles (saturated salt) encapsulated a dye on long time scales (>3 hours). Vesicles composed of 2:1 DA:DOH were formed in a solution with a self-quenching concentration (20 mM) of carboxyfluorescein dye. Unencapsulated dye was removed by SEC. Fluorescence intensity increased when the dye leaked out of vesicles and decreased when the dye photobleached. At each time point, the same two aliquots were assayed. In one, vesicles were intact (filled symbols). In the other, vesicles were disrupted with Triton-X-100, leading to total release of the dye (open symbols). At the last timepoint, the intact vesicles were also disrupted with Triton-X-100 (arrows). Triton-X-100 did not affect the fluorescence (Fig S10). We observed that carboxyfluorescein fluorescence varies with the type and concentration of salt (Fig S10-S11); calcein fluorescence is also known to be quenched by some divalent cations[29]. Error bars are standard deviations of two independent experiments. When error bars are not shown, they are smaller than the symbols.

The challenge of predicting whether flocculation of membranes will lead to leakage of vesicle contents underscores the importance of our measurements. Flocculation of vesicles will result in vesicle rupture if adhesion between vesicles generates tensions that exceed the lysis tension (~ 5-10 mN/m for phospholipid membranes)[30]. Tension also favors the formation of pores in membranes[31], which can lead to loss of vesicle contents. Previous work focused on vesicles of phospholipids, and showed that they remain intact during salt-induced flocculation[32]. Compared to phospholipid membranes, fatty acid

membranes might be expected to have higher densities of hydrophobic defects, which are a precursor to pore formation[31]. However, it is difficult to predict whether fatty acid membranes are uniformly more susceptible to pore formation than phospholipid membranes because the packing of fatty acids is sensitive to their charge, which may be different at the membrane surface than in solution[33]. Pore formation in a single membrane is stabilized when each leaflet of the membrane has a positive spontaneous curvature[31], as expected for fatty acid membranes near a micelle transition. On the other hand, at low pH, the addition of fatty acids to phospholipid membranes imparts a negative spontaneous curvature and a high bending rigidity[34].

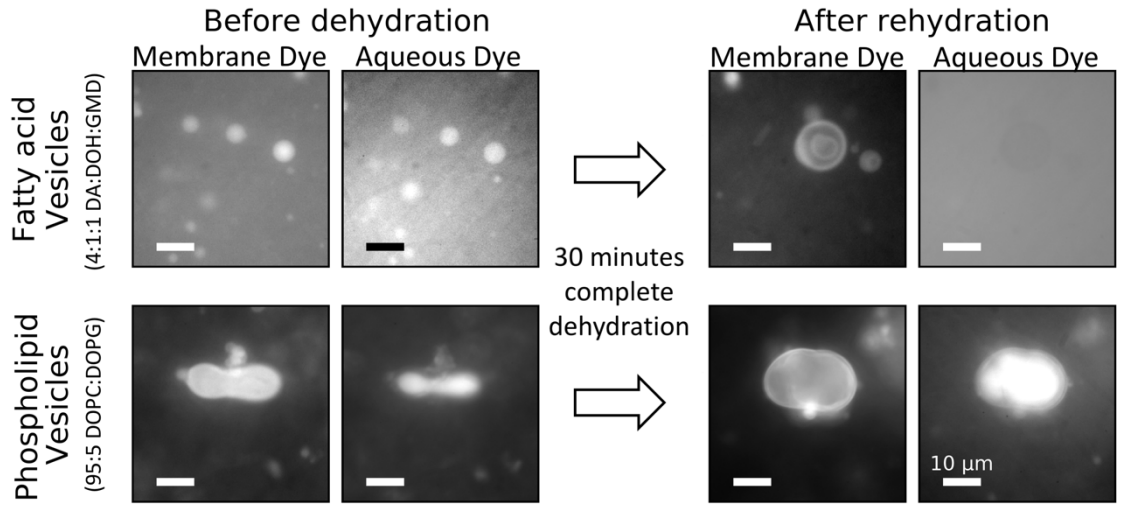

Figure 5. Vesicles of fatty acids (4:1:1 DA:DOH:GMD, top) and phospholipids (95:5 DOPC:DOPG, bottom) initially encapsulated an aqueous dye (calcein). After 30 minutes of dehydration and 60 minutes of rehydration, fatty acid vesicles were visible with a mem-brane dye, but they no longer encapsulated the aqueous dye (top right micrograph). In contrast, after the same dehydration cycle, phospholipid vesicles still encapsulated the aqueous dye (bottom right micrograph). In all samples, the dye that labeled vesicle membranes (rhodamine 6G) was added immediately prior to imaging. Corresponding wide-field images are in the SI (Fig S13-S19). Scale bars are 10 μm.

Our results above imply that fatty acid-based protocells could have survived salt-induced flocculation during an evaporative cycle, but what if the evaporation were complete? We found that fatty acid vesicles lost the ability to encapsulate calcein dye within 30 min of dehydration, even when glycerol-mono-decanoate was incorporated to provide additional stability (4:1:1 DA:DOH:GMD) (Fig 5). After rehydration, dried fatty acids reassembled into vesicles, and the encapsulated solution had a similar dye concentration to the exterior solution. After the dye was removed from the exterior solution by SEC, the encapsulated solution again appeared brighter (Fig S16). Our observations with decanoic acid vesicles are

consistent with a report that only about 1% of encapsulated calcein is retained during dehydration of oleic acid vesicles[35] (although oleic acid is unlikely to have been present on the prebiotic Earth because natural abiotic synthesis has not been observed). The presence of sugars in the prebiotic environment could have improved retention upon formation of a glassy precipitate[36].

In contrast to fatty acid vesicles, phospholipid vesicles retained encapsulated calcein after 30 min of dehydration and rehydration (Fig 5). Based on previous studies, the amount of retained dye may decrease as dry periods become longer[37]. The ability of dried phospholipid vesicles to re-encapsulate the bulk solution during rehydration had previously been demonstrated[38]. Before the emergence of phospholipids, cycles of dehydration and rehydration would have induced mixing between protocells, which may have been a primitive mechanism for exchanging genetic material. Incorporation of phospholipids could have provided an advantage to individual protocells by preserving their encapsulated contents.

When vesicles of fatty acids flocculate in saturated solutions of monovalent salts, they maintain encapsulation of dye molecules as well as dispersed vesicles do. In contrast, prebiotically plausible coacervates are disrupted in relatively dilute NaCl solutions (250 mM), although they can reassemble after complete dehydration and rehydration to sequester charged polymers[39]. Within dynamic lake environments that experience dehydration and rehydration on diurnal or seasonal timescales[40], fatty acid-based vesicles may have grown and divided during periods when the salt concentration was low, and then retained their contents despite flocculation during periods of high salt concentration.

While fatty acid vesicles do not retain encapsulated material through periods of complete dehydration, we show that phospholipid vesicles can. Taken together, our results are consistent with the hypothesis that evaporating pools on Earth's surface were conducive to protocell development, and not an obstacle as previously thought.

Experimental section

Materials

Decanoic acid was purchased from Nu-Chek Prep (Elysian, MN). Decanol and glycerol-mono-decanoate were purchased from Sigma-Aldrich (St. Louis, MO). DOPC and DOPG were purchased from Avanti Polar Lipids (Alabaster, Al). Bicine, calcein, rhodamine 6G, and carboxyfluorescein were purchased from Sigma-Aldrich (St. Louis, MO). Sepharose 4B was used as the resin for size-exclusion chromatography, and was purchased from Sigma-Aldrich (St. Louis, MO). Triton-X-100 was purchased from Supleco (Bellefonte, PA). Fisherbrand™ 96 - well polystyrene plates (Hanover Park, IL) were used for analyzing samples from size-exclusion chromatography.

Preparation of vesicle solutions

Stock solutions of decanoate were made by dissolving solid decanoic acid in equimolar NaOH solution, followed by gentle heating and rocking. Vesicle solutions were prepared by the following steps: 1) mix solutions of salt and fluorescent dye. 2) Add decanoate solution. 3) Add liquid decanol and mix to induce vesicle assembly. The resulting vesicles encapsulated the bulk solution of salts and dyes. 4) For samples that contained glycerol-mono-decanoate, solid glycerol mono-decanoate was added to the vesicle solution, then briefly heated at 55°C to incorporate into vesicles. 5) The pH was adjusted after the amphiphiles were added. The pH adjustments were performed at room temperature, and vesicle samples were occasionally kept warm in a hot metal block.

Size-exclusion chromatography (SEC)

SEC columns were prepared with 6.9 mL of Sepharose 4B resin. Before each SEC run, the column was flushed with at least two volume equivalents of running buffer. 500 µL of sample was added to the SEC column, and 400 µL fractions were collected by hand. After all fractions were collected, the column was flushed with at least 2 volume equivalents of 0.2 M bicine (pH 9) for storage. 100 µL aliquots of each fraction were deposited into 96 well plates. Calcein fluorescence was measured using a Thermo Labsystems (Gulph Mills, PA) Fluoroskan Ascent FL Fluorescence Microplate Reader with ex485/em520. For experiments using vesicle samples composed of decanoic acid and decanol (and glycerol-mono-decanoate, in some cases), the SEC running buffer contained any salts and buffers that were present in the original vesicle sample, to match ionic conditions. Regardless of the vesicle composition, the SEC running buffer contained decanoic acid at only 20 mM so that the total amphiphile concentration never dropped below the critical vesicle concentration. Higher concentrations caused the SEC resin to clog due to the large number of vesicles. Nonetheless, individual vesicles containing decanol (and glycerol-mono-decanoate, in some cases) were stable for hours after SEC despite dilution of the amphiphiles during SEC. For samples of phospholipid vesicles, the SEC running buffer contained only salts and buffers that were present in the sample to match ionic conditions. No additional phospholipid was included in the SEC running buffer.

Fluorescence microscopy

100 µL samples were prepared for imaging by mixing vesicle solutions with 2 mM rhodamine 6G stock (membrane dye). The rhodamine 6G concentration in final samples was between 20 µM and 40 µM. The edges of a cover slip were coated with vacuum grease and 80 µL of sample was placed in the resulting well. Another cover slip was placed on top. Images were collected on a Nikon (Melville, NY) Eclipse upright epifluorescence microscope (ME600L). A Chroma (Bellows Falls, VT) FITC/Alexa488 filter cube was used for calcein fluorescence images (aqueous dye), and a Chroma mCherry/Texas Red filter cube was used for rhodamine fluorescence images. In the rhodamine 6G channel, vesicles appear as a bright ring when they are much larger than the objective's depth of field and when the focus is at the vesicle midplane. When vesicles are relatively small and/or they are imaged above or below the midplane, the rhodamine 6G fluorescence appears as a bright circle rather than a ring. A Wavelength Electronics (Bozeman, MT) temperature controller was used to maintain the imaging stage at desired temperature.

Experiments on flocculation with different amphiphile concentrations (Fig 2)

For 60 mM amphiphile samples, vesicles were made from 40 mM decanoic acid, 10 mM decanol, 10 mM glycerol-mono-decanoate. For 300 mM amphiphile samples, vesicles were made from 200 mM decanoic acid, 50 mM decanol, 50 mM glycerol-mono-decanoate. In both cases, the solution inside and outside the vesicles contained 0.5 mM calcein and 300 mM $NaHCO_3$. For samples with saturated $NaHCO_3$, enough $NaHCO_3$ was added for 1.5 M if it were all soluble, but excess accumulated as

solid leaving a saturated $NaHCO_3$ (~1.2 M) solution. Regardless of $NaHCO_3$ concentration, final pH was adjusted to 8.7 (± 0.05). SEC was performed with running buffer that contained 20 mM decanoic acid and either 300 mM $NaHCO_3$ or saturated $NaHCO_3$. In both cases, the running buffer was adjusted to pH 8.7 (± 0.05). The entire experiment, including imaging, was performed at 40°C.

Experiments on calcein retention during flocculation by saturated $NaHCO_3$ (Fig 3)

Vesicles were made from 100 mM decanoic acid and 50 mM decanol. The solution inside and outside the vesicles contained 5 mM calcein and 375 mM $NaHCO_3$. pH was adjusted to 8.7 (± 0.05). Unencapsulated calcein was removed by SEC, where the running buffer contained 20 mM decanoic acid and 375 mM $NaHCO_3$ at pH 8.7 (± 0.05). SEC fractions corresponding to vesicles (early eluting) were combined, and the vesicles were mixed with a pH 8.7 (± 0.05) saturated $NaHCO_3$ solution. The final mixture was also saturated with ~1.2 M $NaHCO_3$ (enough $NaHCO_3$ was added for 1.5 M if it were all soluble, but excess accumulated as solid leaving a saturated $NaHCO_3$ solution). Vesicles were added to a saturated $NaHCO_3$ solution instead of solid $NaHCO_3$ to prevent changes to the pH upon mixing. After 1 hour, the $NaHCO_3$ was diluted to at most 375 mM in a solution of 50 mM decanoic acid and 25 mM decanol at pH 8.7 (± 0.05). Dilution into a 50 mM decanoic acid and 25 mM decanol solution prevented the amphiphile concentration from decreasing below the critical vesicle concentration. The entire experiment, including imaging, was performed at 40°C. To acquire images of vesicles, aliquots were diluted in SEC running buffer (1 vesicle aliquot: 3 SEC running buffer, by volume) to reduce the concentration of vesicles, and thus improve image quality by reducing out-of-focus light.

Experiments on calcein retention during flocculation by saturated NaCl (Fig 3)

Vesicles were made from 250 mM decanoic acid and 125 mM decanol. The solution inside and outside the vesicles contained 5 mM calcein, 100 mM NaCl, and 50 mM bicine. pH was adjusted to 8.7 (± 0.05). Unencapsulated calcein was removed by SEC, where the running buffer contained 20 mM decanoic acid, 100 mM NaCl, and 50 mM bicine at pH 8.7 (± 0.05). SEC fractions corresponding to vesicles (early eluting) were combined, and solid NaCl was added to the vesicles for a saturated ~6.1 M NaCl solution (enough NaCl was added for 7.2 M if it were all soluble, but excess accumulated as solid). After 1 hour, the NaCl was diluted to at most 400 mM in a solution of 30 mM decanoic acid and 50 mM bicine at pH 8.7 (± 0.05). Dilution into a 30 mM decanoic acid and 50 mM bicine solution prevented the amphiphile concentration from decreasing below the CVC. The entire experiment, including imaging, was performed at 40°C. To acquire images of vesicles before the addition of solid NaCl, an aliquot was diluted in SEC running buffer (1 vesicle aliquot: 3 SEC running buffer, by volume) to reduce the concentration of vesicles, and thus improve image quality by reducing out-of-focus light. During flocculation, the encapsulated calcein became further concentrated, resulting in self-quenching (Fig S7-S8). To improve image quality by reducing self-quenching, an identical experiment was performed using an initial calcein concentration of only 0.5 mM. Images from this flocculated sample are presented in Fig 3.

Experiments on carboxyfluorescein leakage (Fig 4)

Vesicles were made from 100 mM decanoic acid and 50 mM decanol. The initial solution inside and outside the vesicles contained 20 mM carboxyfluorescein and 100 mM $NaHCO_3$. pH was adjusted to 8.7 (± 0.05). Unencapsulated carboxyfluorescein was removed by SEC, where the running buffer contained only 20 mM decanoic acid and 100 mM $NaHCO_3$ at pH 8.7 (± 0.05). SEC fractions corresponding to vesicles (early eluting) were combined. For experiments on non-flocculated vesicles, the post-SEC sample was diluted 1:1 with additional running buffer, and then added to an empty well on a 96 well plate. For the saturated NaCl sample, the post-SEC sample was diluted 1:1 with additional running buffer, and then added to a well that contained enough solid NaCl for a saturated ~6.1 M NaCl

solution (enough NaCl was added for 7.2 M if it were all soluble, but excess accumulated as solid). Microscopy was used to confirm that the vesicles were flocculated (Fig S12). For the saturated $NaHCO_3$ sample, the post-SEC sample was diluted 1:1 with pH 8.7 (± 0.05) saturated $NaHCO_3$ solution inside of a well on a 96 well plate. The final mixture was also saturated with ~1.2 M $NaHCO_3$ (enough $NaHCO_3$ was added for 1.8 M if it were all soluble, but excess accumulated as solid leaving a saturated $NaHCO_3$ solution). Vesicles were added to a saturated $NaHCO_3$ solution instead of solid $NaHCO_3$ to prevent changes to the pH upon mixing. Microscopy was used to confirm that the vesicles were flocculated (Fig S12). In all cases, duplicate 100 µL aliquots were placed in 96 well plates, and carboxyfluorescein fluorescence (ex485/em520) was measured in triplicate. The same two duplicate aliquots were measured at each time point. In parallel duplicate aliquots, Triton-X-100 was added (t = 0) to induce complete disruption of encapsulation by vesicles or flocs. Enough Triton-X-100 was added for 0.32% (mass/mass), but addition of Triton-X-100 only changed the sample volume by 2%. Carboxyfluorescein fluorescence was measured every 0.5 hr. The 96 well plate was shaken before each measurement to evenly distribute the flocs across the well. For the samples without initial Triton-X-100, Triton-X-100 was added after the final timepoint, and fluorescence measured again.

Experiments on calcein retention during dehydration (Fig 5)

Vesicles were made from 100 mM decanoic acid, 25 mM decanol, and 25 mM glycerol-mono-decanoate. The initial solution inside and outside the vesicles contained 5 mM calcein, 100 mM NaCl, and 50 mM bicine. pH was adjusted to 8.7 (± 0.05). The SEC running buffer contained only 20 mM decanoic acid, 100 mM NaCl, and 50 mM bicine at pH 8.7 (± 0.05). For experiments on phospholipid vesicles, a film composed of 5 mg 95% DOPC and 5% DOPG was hydrated for about 72 hours with 1 mL of 5 mM calcein, 100 mM NaCl, and 50 mM bicine solution at pH 8.7 (± 0.05). After 72 hours of hydration, the vesicle solution was again adjusted to pH 8.7 (± 0.05). The SEC running buffer contained only 100 mM NaCl and 50 mM bicine at pH 8.7 (± 0.05). During experiments on either fatty acid vesicles or phospholipid vesicles, unencapsulated calcein was removed by SEC, and fractions corresponding to vesicles (early eluting) were combined. 200 µL aliquots of the combined fractions were distributed to separate test tubes, and each tube was dried at room temperature under a stream of N_2 for 1 hour. Next, the mass of each test tube and sample was measured, and the test tubes were again put under a stream of N_2 for an additional 0.5 hour. Final mass measurements of each test tube and sample confirmed that there were no detectable changes in mass (within ± 0.5 mg), so the samples were deemed dehydrated. The dry samples were immediately rehydrated with 200 µL H2O, allowed to sit at room temperature for 1 hour, then vortexed vigorously to resolubilize dried material.

Acknowledgements

This work was supported in part by a grant (NNX17AK86G, Exobiology) from NASA to S.L.K. and R.A.B, by a grant (MCB 1925731) from the NSF to S.L.K, and by a grant (511570FY20, DCC) from the Simons Foundation to D.C.C. ZRC was funded by an NSF fellowship (NSF GRFP DGE 1762114). We thank Dr. Zoe Todd for guidance with vesicle experiments.

References

(1) Deamer, D.; Dworkin, J. P.; Sandford, S. A.; Bernstein, M. P.; Allamandola, L. J. The First Cell Membranes. *Astrobiology* **2002**, *2* (4), 371–381.

(2) Lawless, J. G.; Yuen, G. U. Quantification of Monocarboxylic Acids in the Murchison Carbonaceous Meteorite. *Nature* **1979**, *282* (5737), 396–398.
(3) Nooner, D. W.; Oro, J. Synthesis of Fatty Acids by a Closed System Fischer-Tropsch Process. In *Hydrocarbon Synthesis from Carbon Monoxide and Hydrogen*; Advances in Chemistry; American Chemical Society, **1979**; Vol. 178, pp 159–171.
(4) Yuen, G. U.; Lawless, J. G.; Edelson, E. H. Quantification of Monocarboxylic Acids from a Spark Discharge Synthesis. *J Mol Evol* **1981**, *17* (1), 43–47.
(5) Black, R. A.; Blosser, M. C. A Self-Assembled Aggregate Composed of a Fatty Acid Membrane and the Building Blocks of Biological Polymers Provides a First Step in the Emergence of Protocells. *Life* **2016**, *6* (3), 33.
(6) Joyce, G. F.; Szostak, J. W. Protocells and RNA Self-Replication. *Cold Spring Harb Perspect Biol* **2018**, *10* (9), a034801.
(7) Lopez, A.; Fiore, M. Investigating Prebiotic Protocells for a Comprehensive Understanding of the Origins of Life: A Prebiotic Systems Chemistry Perspective. *Life* **2019**, *9* (2), 49.
(8) Apel, C. L.; Deamer, D. W.; Mautner, M. N. Self-Assembled Vesicles of Monocarboxylic Acids and Alcohols: Conditions for Stability and for the Encapsulation of Biopolymers. *Biochimica et Biophysica Acta (BBA) - Biomembranes* **2002**, *1559* (1), 1–9.
(9) Maurer, S. E.; Nguyen, G. Prebiotic Vesicle Formation and the Necessity of Salts. *Orig Life Evol Biosph* **2016**, *46* (2–3), 215–222.
(10) Weitz, D. A.; Lin, M. Y.; Lindsay, H. M. Universality Laws in Coagulation. *Chemometrics and Intelligent Laboratory Systems* **1991**, *10* (1), 133–140.
(11) Monnard, P.-A.; Apel, C. L.; Kanavarioti, A.; Deamer, D. W. Influence of Ionic Inorganic Solutes on Self-Assembly and Polymerization Processes Related to Early Forms of Life: Implications for a Prebiotic Aqueous Medium. *Astrobiology* **2002**, *2* (2), 139–152.
(12) Rosing, M. T. 13C-Depleted Carbon Microparticles in >3700-Ma Sea-Floor Sedimentary Rocks from West Greenland. *Science* **1999**, *283* (5402), 674–676.
(13) Ohtomo, Y.; Kakegawa, T.; Ishida, A.; Nagase, T.; Rosing, M. T. Evidence for Biogenic Graphite in Early Archaean Isua Metasedimentary Rocks. *Nature Geosci* **2014**, *7* (1), 25–28.
(14) Korenaga, J. Was There Land on the Early Earth? *Life* **2021**, *11* (11), 1142.
(15) Tang, M.; Chen, K.; Rudnick, R. L. Archean Upper Crust Transition from Mafic to Felsic Marks the Onset of Plate Tectonics. *Science* **2016**, *351* (6271), 372–375.
(16) Eugster, H. P.; Jones, B. F. Behavior of Major Solutes during Closed-Basin Brine Evolution. *American Journal of Science* **1979**, *279* (6), 609–631.
(17) Sasselov, D. D.; Grotzinger, J. P.; Sutherland, J. D. The Origin of Life as a Planetary Phenomenon. *Science Advances* **2020**, *6* (6), eaax3419.
(18) Damer, B.; Deamer, D. The Hot Spring Hypothesis for an Origin of Life. *Astrobiology* **2019**, *20* (4), 429–452.
(19) Toner, J. D.; Catling, D. C. Alkaline Lake Settings for Concentrated Prebiotic Cyanide and the Origin of Life. *Geochimica et Cosmochimica Acta* **2019**, *260*, 124–132.
(20) Toner, J. D.; Catling, D. C. A Carbonate-Rich Lake Solution to the Phosphate Problem of the Origin of Life. *Proc Natl Acad Sci USA* **2020**, *117* (2), 883–888.
(21) Patel, B. H.; Percivalle, C.; Ritson, D. J.; Duffy, C. D.; Sutherland, J. D. Common Origins of RNA, Protein and Lipid Precursors in a Cyanosulfidic Protometabolism. *Nature Chemistry* **2015**, *7* (4), 301–307.
(22) Rodriguez-Garcia, M.; Surman, A. J.; Cooper, G. J. T.; Suárez-Marina, I.; Hosni, Z.; Lee, M. P.; Cronin, L. Formation of Oligopeptides in High Yield under Simple Programmable Conditions. *Nat Commun* **2015**, *6* (1), 8385.

(23) Forsythe, J. G.; Yu, S.-S.; Mamajanov, I.; Grover, M. A.; Krishnamurthy, R.; Fernández, F. M.; Hud, N. V. Ester-Mediated Amide Bond Formation Driven by Wet–Dry Cycles: A Possible Path to Polypeptides on the Prebiotic Earth. *Angewandte Chemie International Edition* **2015**, *54* (34), 9871–9875.

(24) Black, R. A.; Blosser, M. C.; Stottrup, B. L.; Tavakley, R.; Deamer, D. W.; Keller, S. L. Nucleobases Bind to and Stabilize Aggregates of a Prebiotic Amphiphile, Providing a Viable Mechanism for the Emergence of Protocells. *Proceedings of the National Academy of Sciences* **2013**, *110* (33), 13272–13276.

(25) Cornell, C. E.; Black, R. A.; Xue, M.; Litz, H. E.; Ramsay, A.; Gordon, M.; Mileant, A.; Cohen, Z. R.; Williams, J. A.; Lee, K. K.; Drobny, G. P.; Keller, S. L. Prebiotic Amino Acids Bind to and Stabilize Prebiotic Fatty Acid Membranes. *Proc Natl Acad Sci USA* **2019**, *116* (35), 17239–17244.

(26) Zorz, J. K.; Sharp, C.; Kleiner, M.; Gordon, P. M. K.; Pon, R. T.; Dong, X.; Strous, M. A Shared Core Microbiome in Soda Lakes Separated by Large Distances. *Nat Commun* **2019**, *10* (1), 4230.

(27) Mansy, S. S.; Schrum, J. P.; Krishnamurthy, M.; Tobé, S.; Treco, D. A.; Szostak, J. W. Template-Directed Synthesis of a Genetic Polymer in a Model Protocell. *Nature* **2008**, *454* (7200), 122–125.

(28) Mansy, S. S.; Szostak, J. W. Thermostability of Model Protocell Membranes. *Proc Natl Acad Sci U S A* **2008**, *105* (36), 13351–13355.

(29) Breuer, W.; Epsztejn, S.; Millgram, P.; Cabantchik, I. Z. Transport of Iron and Other Transition Metals into Cells as Revealed by a Fluorescent Probe. *American Journal of Physiology-Cell Physiology* **1995**, *268* (6), C1354–C1361.

(30) Evans, E. A. Analysis of Adhesion of Large Vesicles to Surfaces. *Biophysical Journal* **1980**, *31* (3), 425–431.

(31) Akimov, S. A.; Volynsky, P. E.; Galimzyanov, T. R.; Kuzmin, P. I.; Pavlov, K. V.; Batishchev, O. V. Pore Formation in Lipid Membrane I: Continuous Reversible Trajectory from Intact Bilayer through Hydrophobic Defect to Transversal Pore. *Sci Rep* **2017**, *7* (1), 12152.

(32) Pigor, T.; Lawaczeck, R. On the Interaction of Phospholipid Vesicles with Chaotropic Ions. *Z. Naturforsch* **1983**, *38* (3–4), 307–312.

(33) Gilbile, D.; Docto, D.; Kingi, D. T.; Kurniawan, J.; Monahan, D.; Tang, A.; Kuhl, T. L. How Well Can You Tailor the Charge of Lipid Vesicles? *Langmuir* **2019**, *35* (48), 15960–15969.

(34) Tyler, A. I. I.; Greenfield, J. L.; Seddon, J. M.; Brooks, N. J.; Purushothaman, S. Coupling Phase Behavior of Fatty Acid Containing Membranes to Membrane Bio-Mechanics. *Frontiers in Cell and Developmental Biology* **2019**, *7*, 187.

(35) Sarkar, S.; Dagar, S.; Rajamani, S. Influence of Wet–Dry Cycling on the Self-Assembly and Physicochemical Properties of Model Protocellular Membrane Systems. *ChemSystemsChem* **2021**, *3* (5), e2100014.

(36) Sun, W. Q.; Leopold, A. C.; Crowe, L. M.; Crowe, J. H. Stability of Dry Liposomes in Sugar Glasses. *Biophysical Journal* **1996**, *70* (4), 1769–1776.

(37) Wolkers, W. F.; Oldenhof, H.; Tablin, F.; Crowe, J. H. Preservation of Dried Liposomes in the Presence of Sugar and Phosphate. *Biochimica et Biophysica Acta (BBA) - Biomembranes* **2004**, *1661* (2), 125–134.

(38) Deamer, D. W.; Barchfeld, G. L. Encapsulation of Macromolecules by Lipid Vesicles under Simulated Prebiotic Conditions. *J Mol Evol* **1982**, *18* (3), 203–206.

(39) Fares, H. M.; Marras, A. E.; Ting, J. M.; Tirrell, M. V.; Keating, C. D. Impact of Wet-Dry Cycling on the Phase Behavior and Compartmentalization Properties of Complex Coacervates. *Nat Commun* **2020**, *11* (1), 5423.

(40) Yechieli, Y.; Wood, W. W. Hydrogeologic Processes in Saline Systems: Playas, Sabkhas, and Saline Lakes. *Earth-Science Reviews* **2002**, *58* (3), 343–365.

Supplementary information

Section 1: Phospholipid vesicles flocculate in saturated $NaHCO_3$

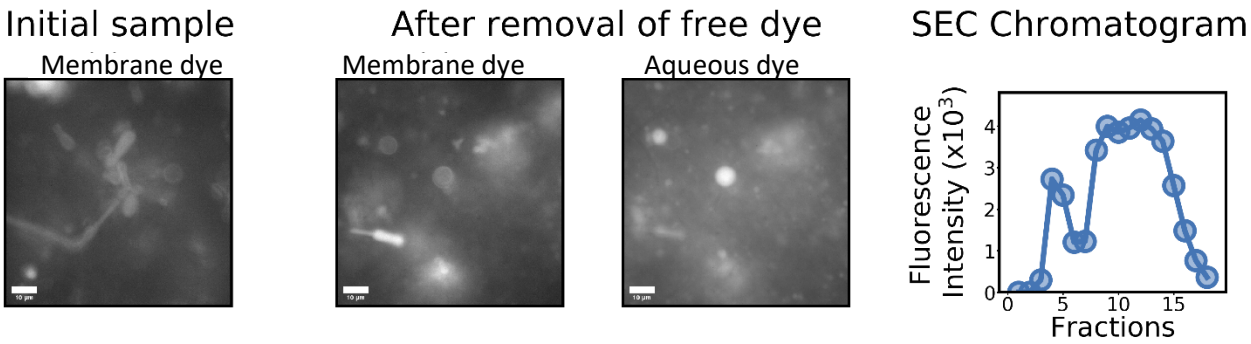

Figure S1: Phospholipid vesicles composed of 5 mg/mL 95 mol % DOPC + 5 mol % DOPG do not flocculate in the presence of 100 mM $NaHCO_3$. Vesicles were formed by hydrating a lipid film with 5 mM calcein and 100 mM $NaHCO_3$ for 48 hours. After 48 hours, the pH of the vesicle sample was adjusted to 8.7 (± 0.05), and size-exclusion chromatography was performed using a running buffer consisting of 100 mM $NaHCO_3$ at pH 8.7. Fluorescence micrographs show unaggregated vesicles before and after size-exclusion chromatography. The SEC chromatogram shows two peaks, which suggests a population of calcein-containing vesicles, in addition to unencapsulated calcein. Scale bars are 10 µm.

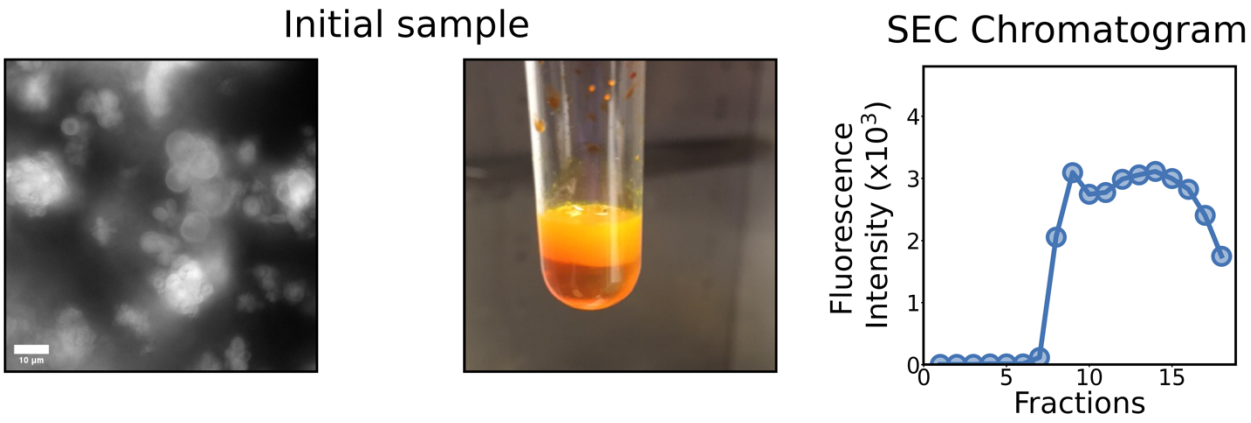

Figure S2: Phospholipid vesicles composed of 5 mg/mL 95 mol % DOPC + 5 mol % DOPG flocculate in the presence of saturated $NaHCO_3$. Vesicles were formed by hydrating a lipid film with 5 mM calcein and 100 mM $NaHCO_3$ for 48 hours. After 48 hours, enough $NaHCO_3$ was added for 1.8 M if it were all soluble, but excess accumulated as solid leaving a saturated ~1.2 M $NaHCO_3$ solution. The pH of the saturated solution was adjusted to 8.7 (± .05), and size-exclusion chromatography was performed using a running buffer consisting of saturated ~1.2 M $NaHCO_3$ (enough $NaHCO_3$ for 1.5 M if it were all soluble, but excess accumulated as solid) at pH 8.7. The fluorescence micrograph shows flocculated vesicles before size-exclusion chromatography. In the test tube, a floc layer floats above the unencapsulated calcein. At the very bottom of the test tube, a layer of undissolved $NaHCO_3$ is visible. Because the flocs are less dense than the surrounding solution, they do not flow into the SEC resin. The SEC chromatogram does not show an early-eluting peak, which suggests there are no unaggregated vesicles. Only a late eluting peak is seen in the chromatogram, corresponding to unencapsulated calcein. Scale bar is 10 µm.

Section 2: Additional images from flocculation experiments.

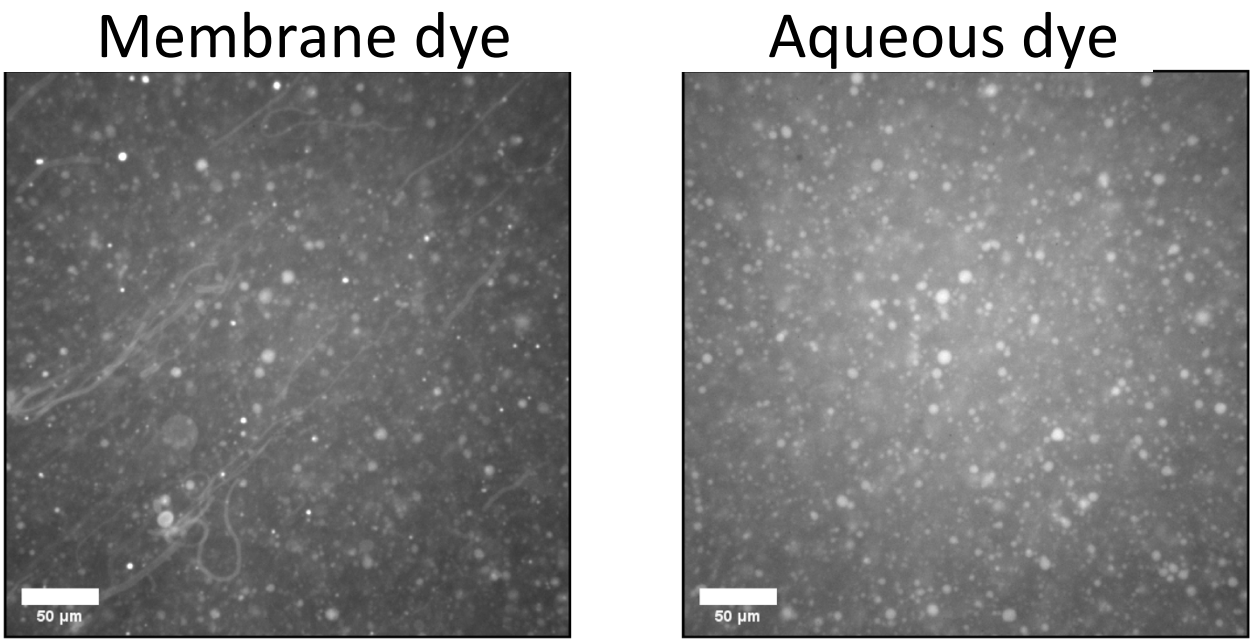

Figure S3: Additional images from the $NaHCO_3$ flocculation experiment shown in Fig 3 ("Create vesicles"). See "Experiments on calcein retention during flocculation by saturated $NaHCO_3$" in the methods section for full details. The vesicles were diluted 1:3 with SEC running buffer prior to imaging. Scale bars are 50 µm.

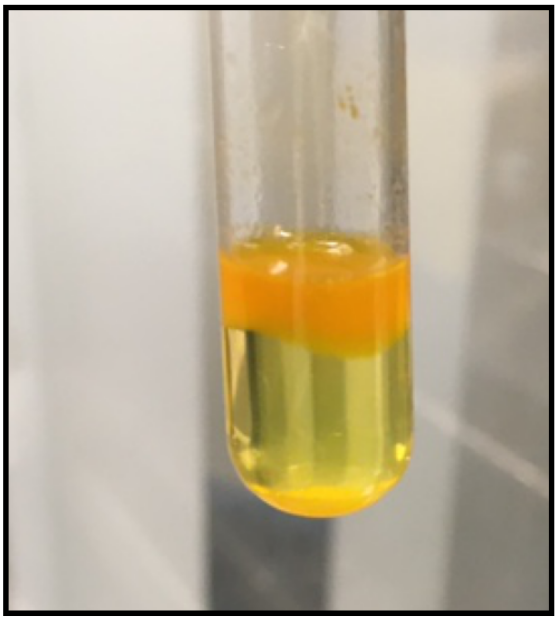

Figure S4: Additional image from the $NaHCO_3$ flocculation experiment shown in Fig 3 ("Flocculate vesicles"). Upon exposing the vesicles to saturated $NaHCO_3$, a thick layer of flocculated vesicles can be seen in the test tube. Importantly, this floc layer is still bright with calcein. Below the low-density floc layer is a layer of solution containing unencapsulated calcein, and at the very bottom of the tube is a layer of undissolved $NaHCO_3$. See "Experiments on calcein retention during flocculation by saturated $NaHCO_3$" in the methods section for full details.

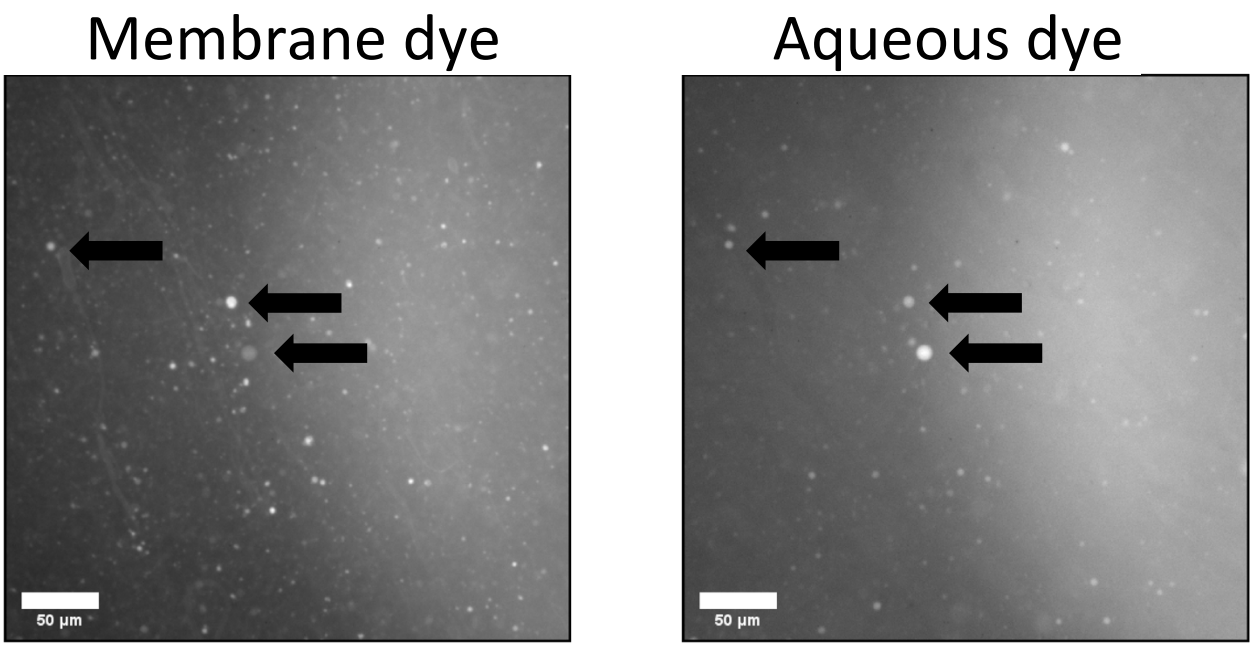

Figure S5: Additional images from the $NaHCO_3$ flocculation experiment shown in Fig 3 ("Disperse vesicles"). See "Experiments on calcein retention during flocculation by saturated $NaHCO_3$" in the methods section for full details. The vesicles were diluted 1:3 with SEC running buffer prior to imaging. Arrows indicate a few of the vesicles that have encapsulated calcein (bright in both membrane dye and aqueous dye). Scale bars are 50 µm.

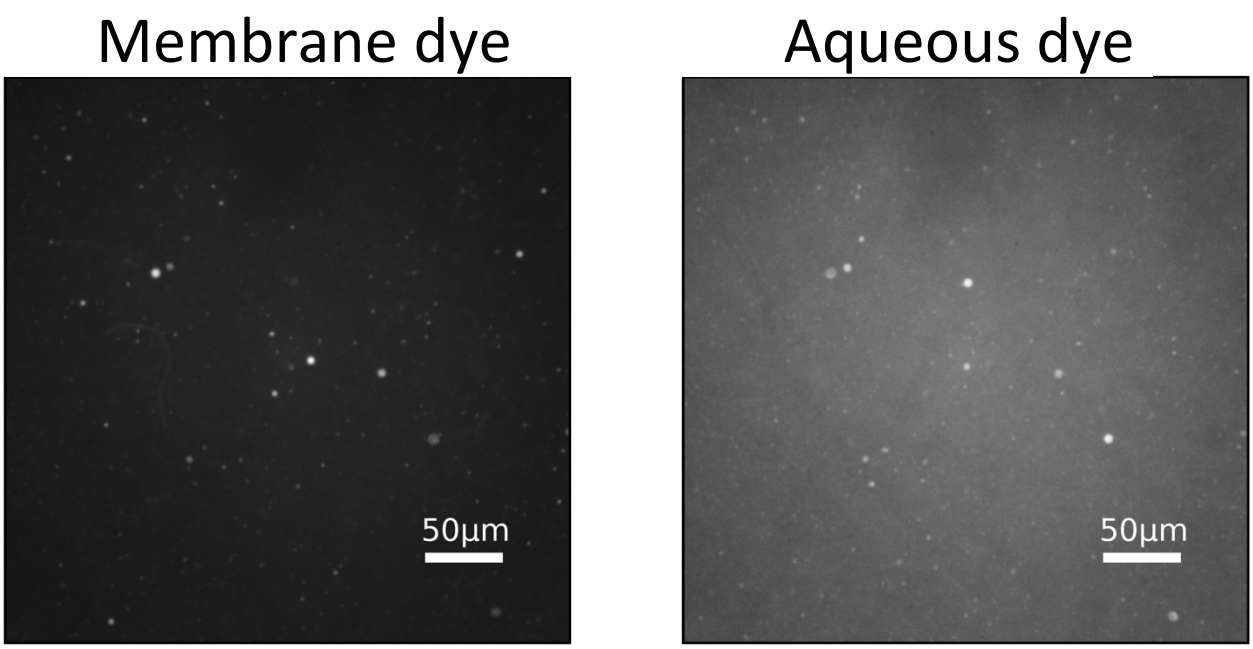

Figure S6: Additional images from the NaCl flocculation experiment shown in Fig 3 ("Create vesicles"). See "Experiments on calcein retention during flocculation by saturated NaCl" in the methods section for full details. The vesicles were diluted 1:3 with SEC running buffer prior to imaging. Scale bars are 50 µm.

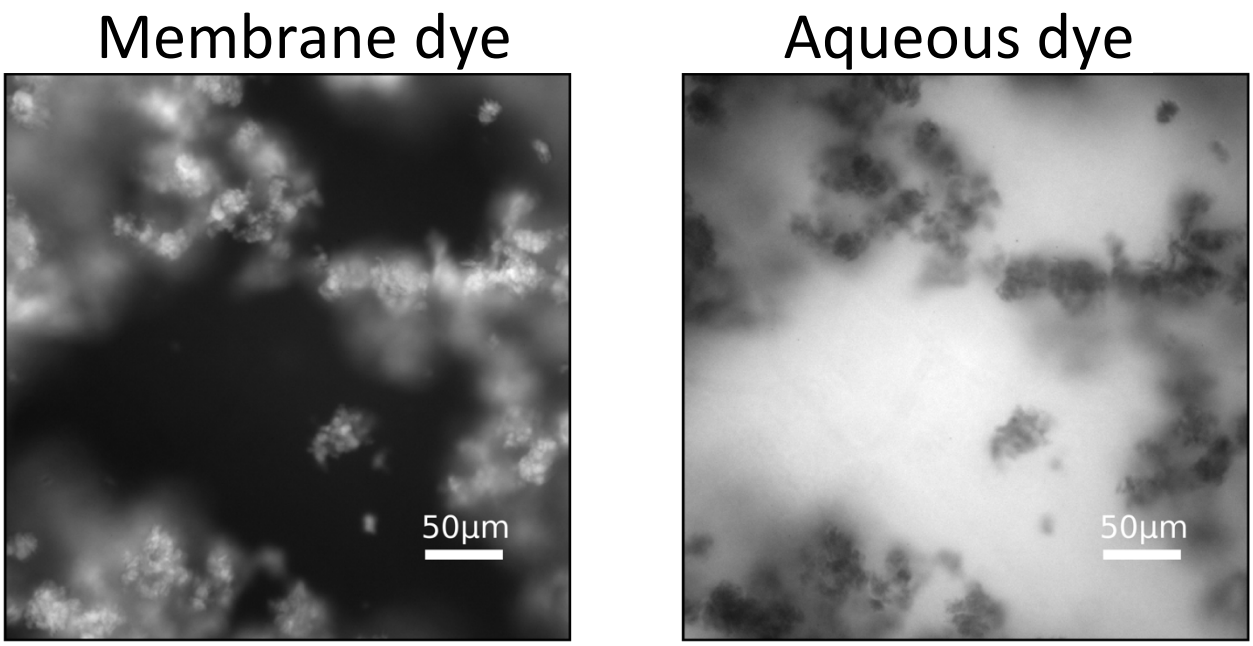

Figure S7: Alternative image from the NaCl flocculation experiment shown in Fig 3 ("Flocculate vesicles"). Unlike the image shown in Fig 3 where 0.5 mM calcein is encapsulated in flocculated vesicles, in this image the flocculated vesicles encapsulate 5 mM calcein. Upon inducing flocculation, the effective concentration of encapsulated calcein increases high enough to induce self-quenching. As a result, flocculated vesicles appear darker than the surrounding solution in the calcein channel. Prior to flocculation, this same sample is shown in Fig 3 "Create vesicles". When this sample is diluted so that the NaCl concentration is low enough to allow flocculated vesicles to disaggregate, the vesicles also appear to be bright with calcein (Fig 3 "Disperse vesicles"). See "Experiments on calcein retention during flocculation by saturated NaCl" in the methods section for full details. Scale bars are 50 µm.

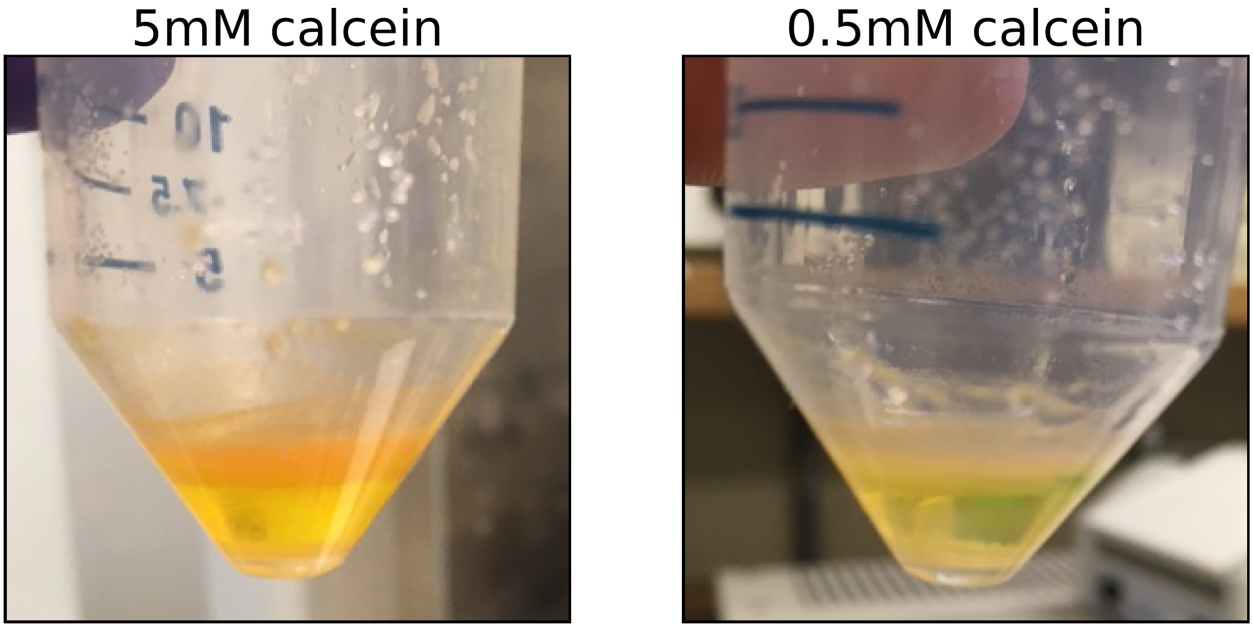

Figure S8: Additional images from the NaCl flocculation experiments shown in Fig 3 ("Flocculate vesicles"). Upon adding enough solid NaCl to saturate the solution, a thick layer of flocculated vesicles can be seen in both test tubes. With 5 mM calcein, the color of the floc layer appears redder than the surrounding solution, suggesting self-quenching of encapsulated calcein. With 0.5 mM calcein, the color of the floc layer appears more similar to the surrounding solution. In both cases, there is a layer of solution containing unencapsulated calcein below the low-density floc layer. At the very bottom of the tube is a layer of undissolved NaCl. See "Experiments on calcein retention during flocculation by saturated NaCl" in the methods section for full details.

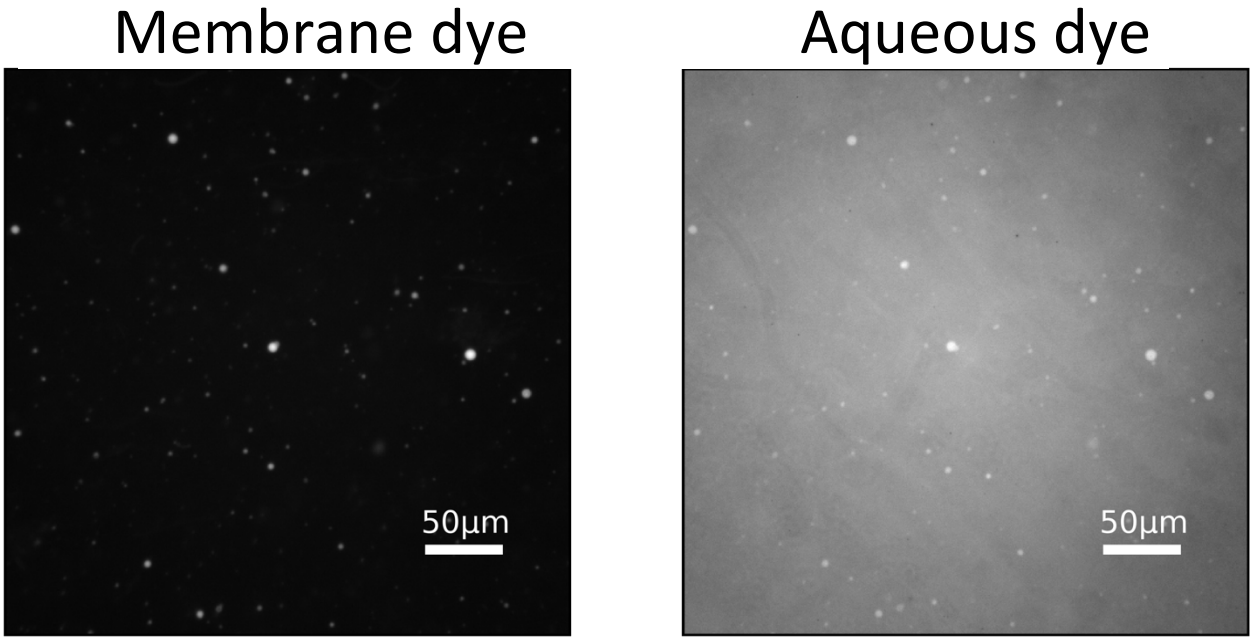

Figure S9: Additional images from the NaCl flocculation experiment shown in Fig 3 ("Disperse vesicles"). See "Experiments on calcein retention during flocculation by saturated NaCl" in the methods section for full details. Scale bars are 50 µm.

Section 3: Additional data from carboxyfluorescein leakage experiments.

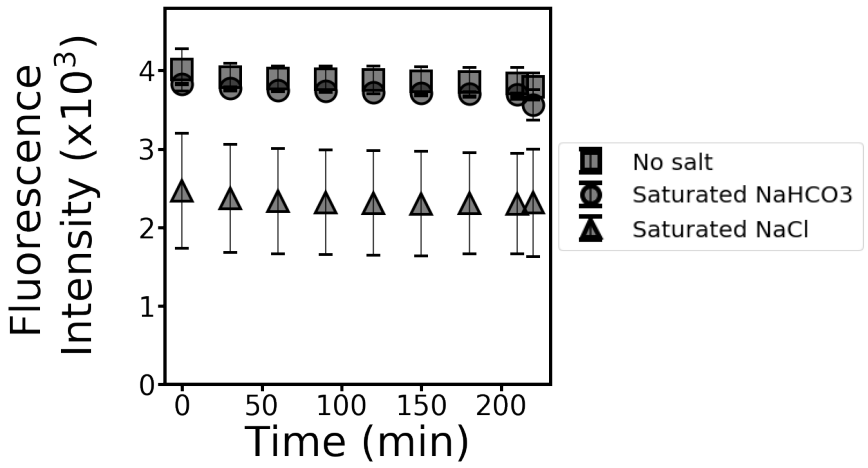

Figure S10: In the absence of vesicles, the fluorescence intensity from 1 mM carboxyfluorescein slightly decreases with time due to photobleaching. Saturated NaCl seems to quench carboxyfluorescein fluorescence. Triton-X-100 is added before the final timepoint, and the result demonstrates that the fluorescence intensity does not change upon addition of Triton-X-100. Error bars represent the standard deviation from two independent experiments.

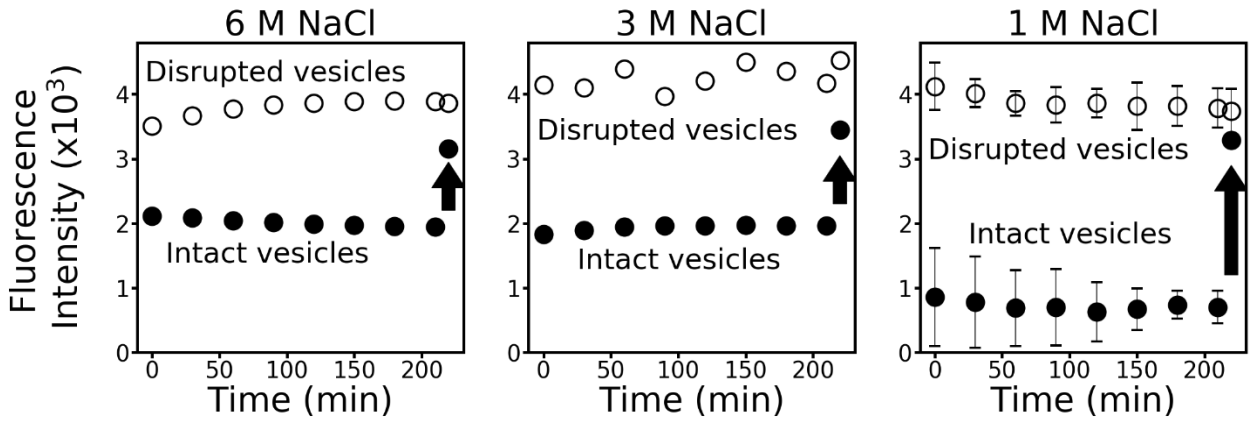

Figure S11: As the concentration of NaCl decreases, the ratio of fluorescence intensities in the disrupted vesicles to the intact vesicles increases. Leakage was monitored through time for flocculated vesicles (filled symbols), and total dye release was induced by Triton-X-100 at the final timepoint (upward arrow). For comparison, total dye release was induced by Triton-X-100 in parallel samples (open symbols). Flocculated vesicles were composed of 2:1 DA: DOH. For the 6 M and 3 M NaCl experiments, the results are for only one experiment each. For the 1 M NaCl experiment, error bars represent the standard deviation from two independent experiments.

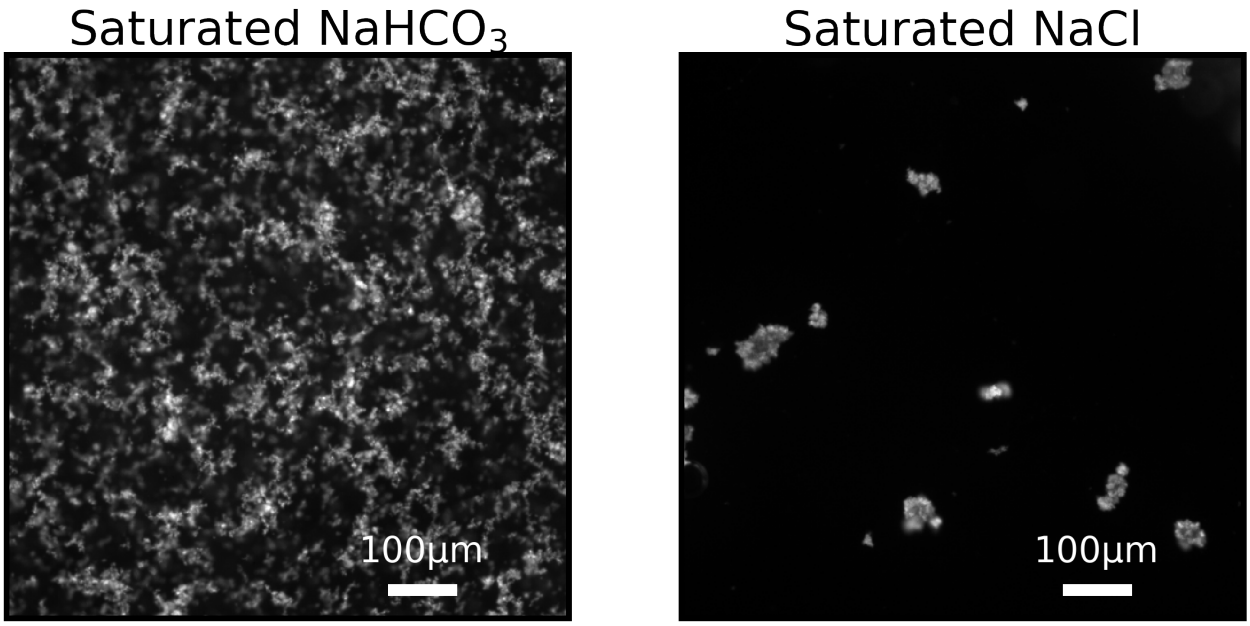

Figure S12: Microscopy confirms that vesicles in saturated salt solution flocculate under the conditions used during Figure 4 experiments. Flocculated vesicles were prepared in the same way as the Figure 4 experiments (see "Experiments on carboxyfluorescein leakage" in the methods section for more details), except that a larger volume of saturated solution was prepared in a test tube, rather than within a 96 well plate. Scale bars are 100 µm.

Section 4: Additional images from dehydration experiments.

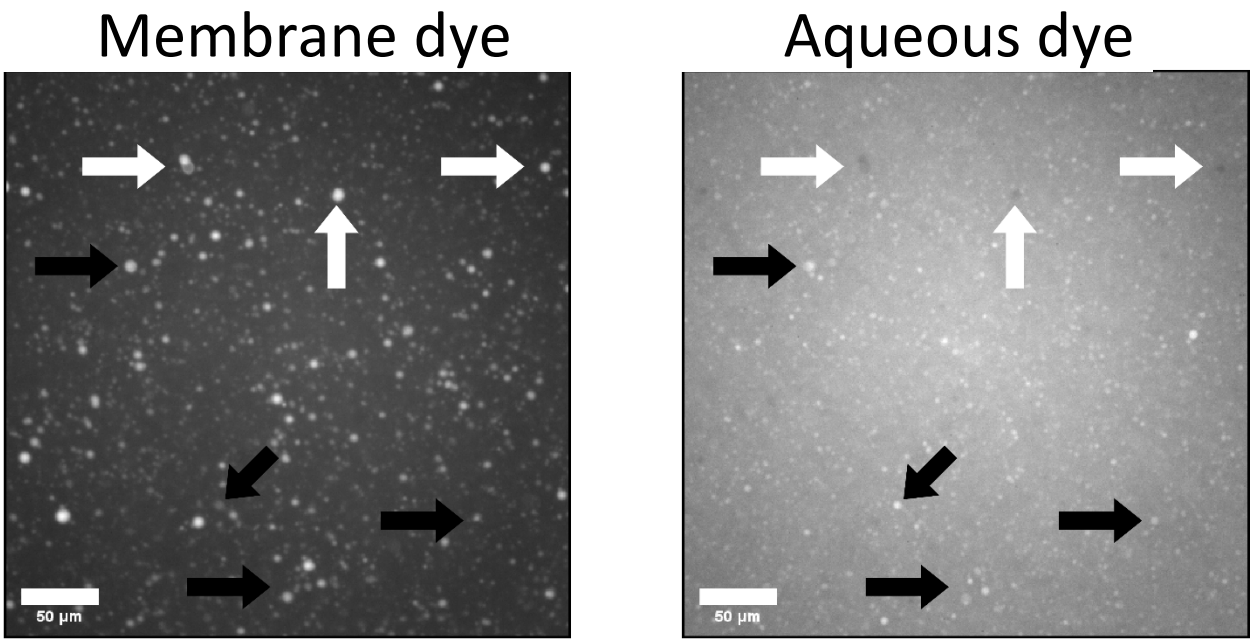

Figure S13: Additional images from the dehydration experiment with fatty acid vesicles composed of 4DA: 1DOH: 1GMD shown in Fig 5 ("Before dehydration"). See "Experiments on calcein retention during dehydration" in the methods section for full details. Black arrows indicate vesicles that are labeled by both the vesicle and aqueous dyes. White arrows indicate vesicles whose calcein florescence is quenched by rhodamine 6G. See Figure S15 for a thorough explanation of this topic. Scale bars are 50 µm.

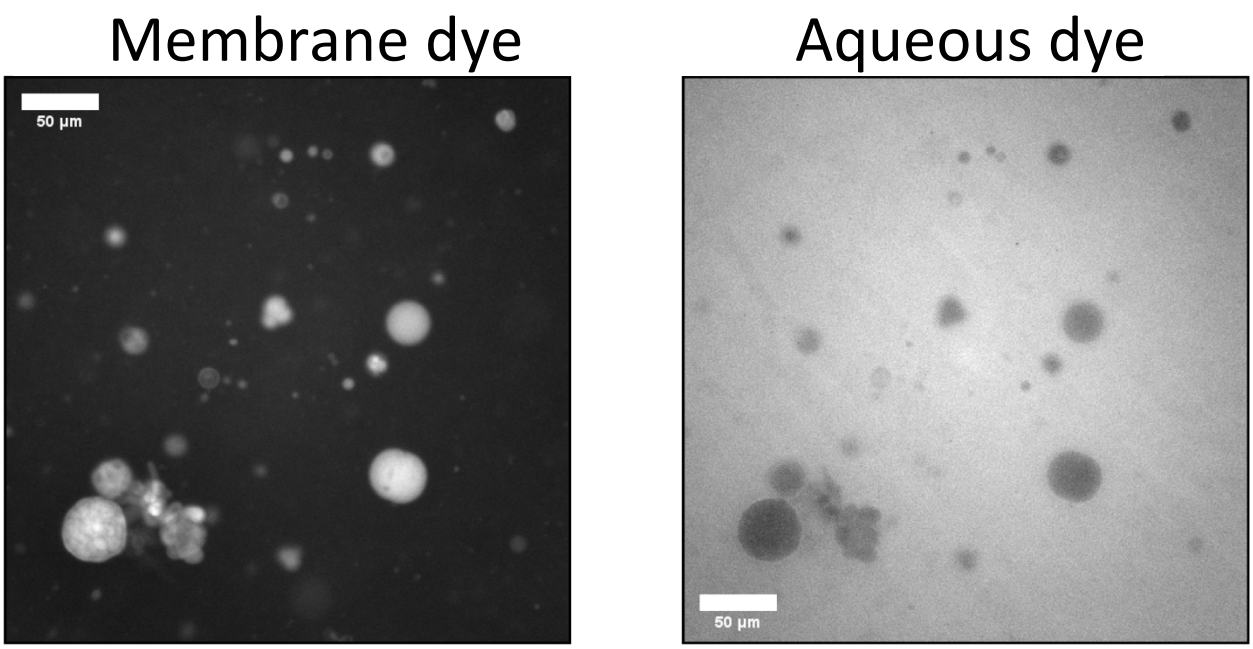

Figure S14: Additional images from the dehydration experiment with fatty acid vesicles composed of 4DA: 1DOH: 1GMD shown in Fig 5 ("After rehydration"). See "Experiments on calcein retention during dehydration" in the methods section for full details. Distinct dark regions in the aqueous dye channel are caused by quenching of calcein fluorescence by rhodamine6G. See Figure S15 for a thorough explanation of this topic. Scale bars are 50 µm.

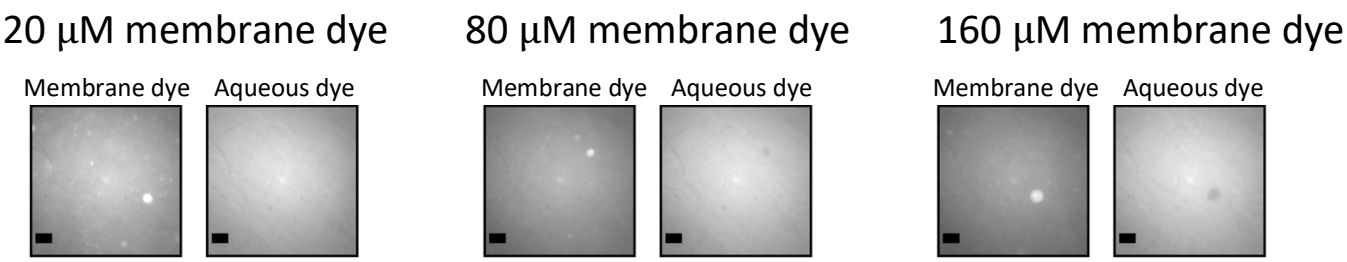

Figure S15: The fluorescence from calcein within vesicles was quenched when the concentration of rhodamine 6G was high. Vesicles were made from 50 mM decanoic acid and 25 mM decanol. The solution inside and outside the vesicles contained 100 mM NaCl, 490 μM calcein, and 50 mM bicine. Vesicle aliquots were mixed with different concentrations of rhodamine 6G. At the highest rhodamine 6G concentrations, calcein fluorescence inside the vesicle was quenched. Scale bars are 20 μm.

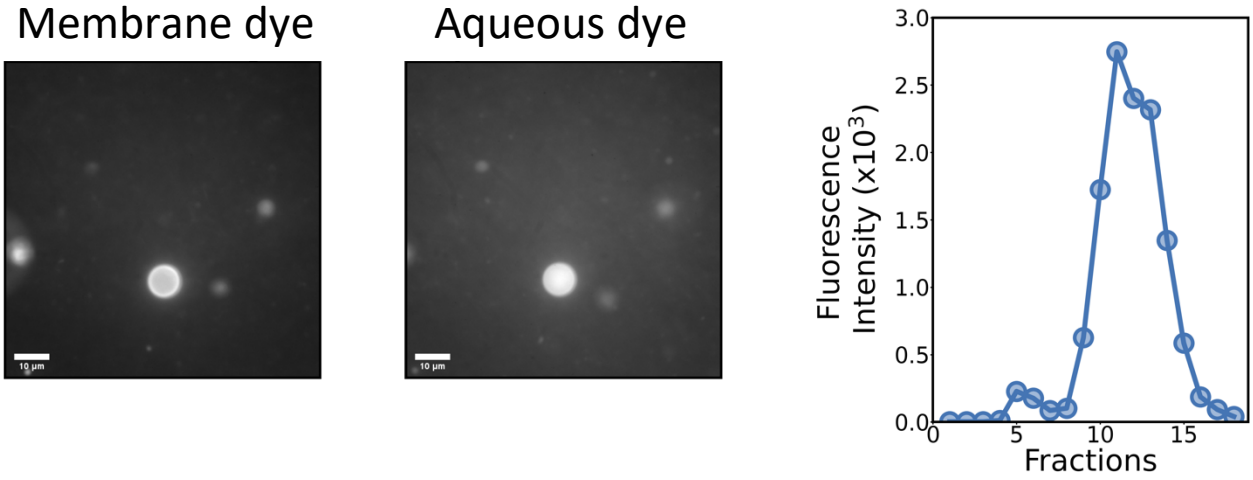

Figure S16: Additional data from the dehydration experiment with fatty acid vesicles composed of 4DA: 1DOH: 1GMD shown in Fig 5. After rehydration, the vesicles were subjected to another round of SEC to confirm that they had indeed re-encapsulated the bulk calcein solution. The SEC chromatogram did show an early-eluting peak corresponding to calcein-containing vesicles, and images of these vesicles confirmed that calcein was encapsulated. See "Experiments on calcein retention during dehydration" in the methods section for full details. Scale bars are 10 µm.

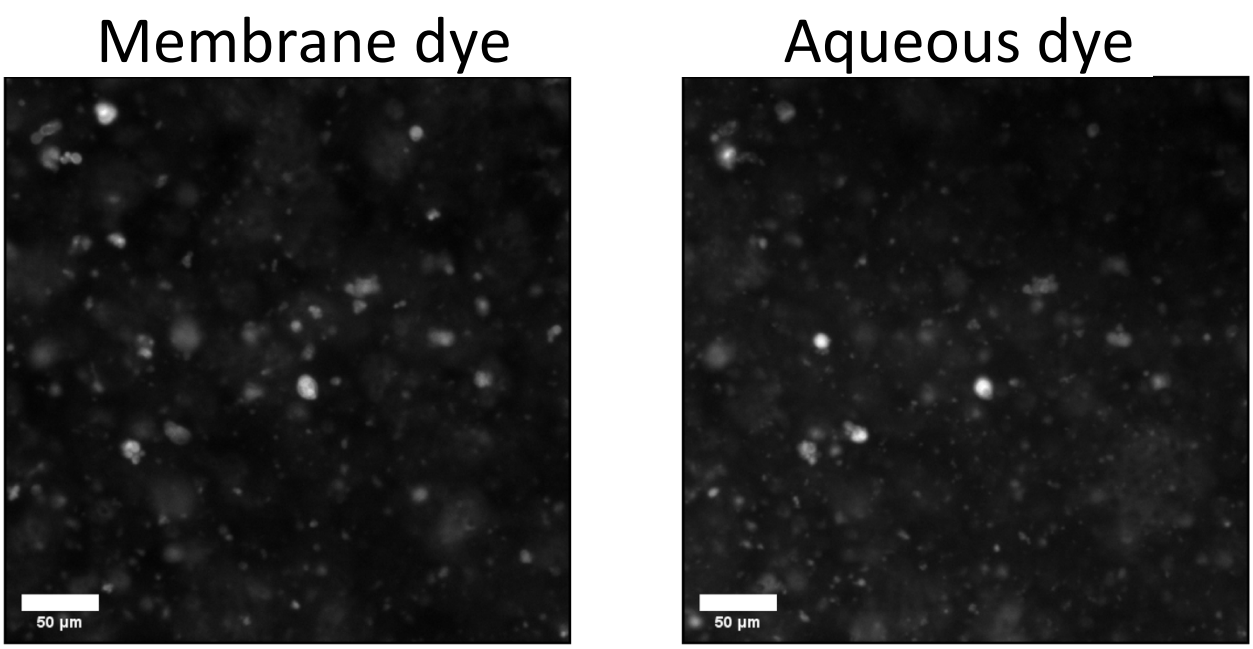

Figure S17: Additional images from the dehydration experiment with phospholipid vesicles composed of 95 mol % DOPC and 5 mol % DOPG shown in Fig 5 ("Before dehydration"). See "Experiments on calcein retention during dehydration" in the methods section for full details. Scale bars are 50 µm.

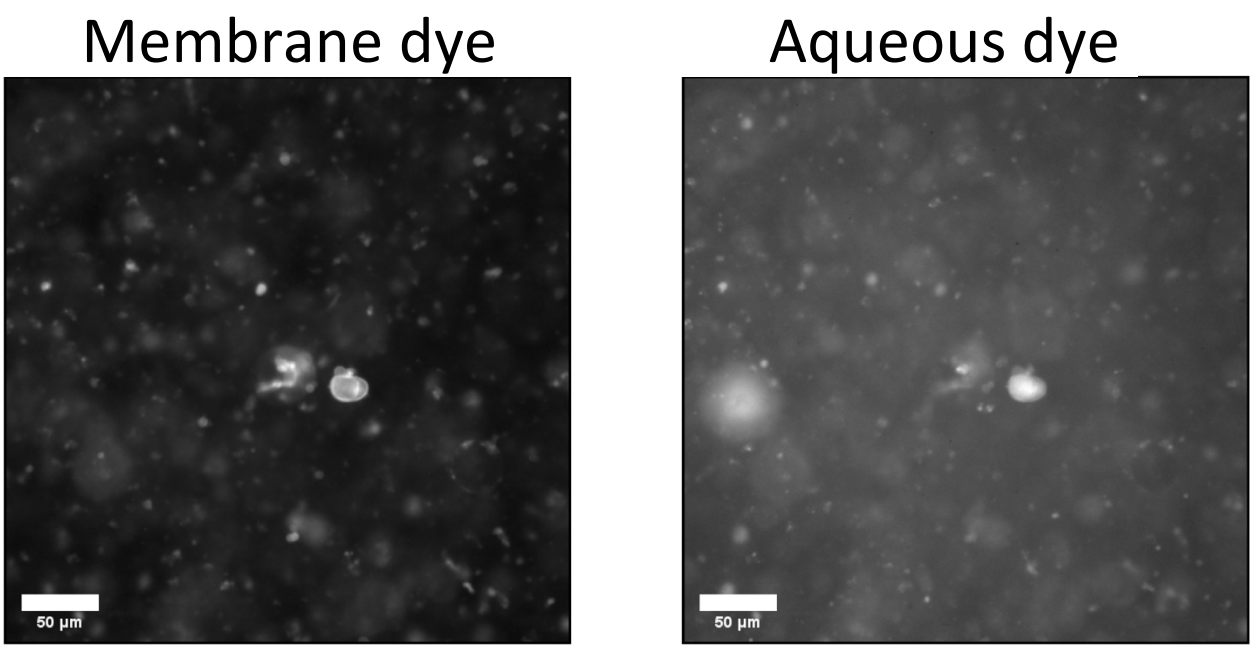

Figure S18: Additional images from the dehydration experiment with phospholipid vesicles composed of 95 mol % DOPC and 5 mol % DOPG shown in Fig 5 ("After rehydration"). See "Experiments on calcein retention during dehydration" in the methods section for full details. Scale bars are 50 µm.

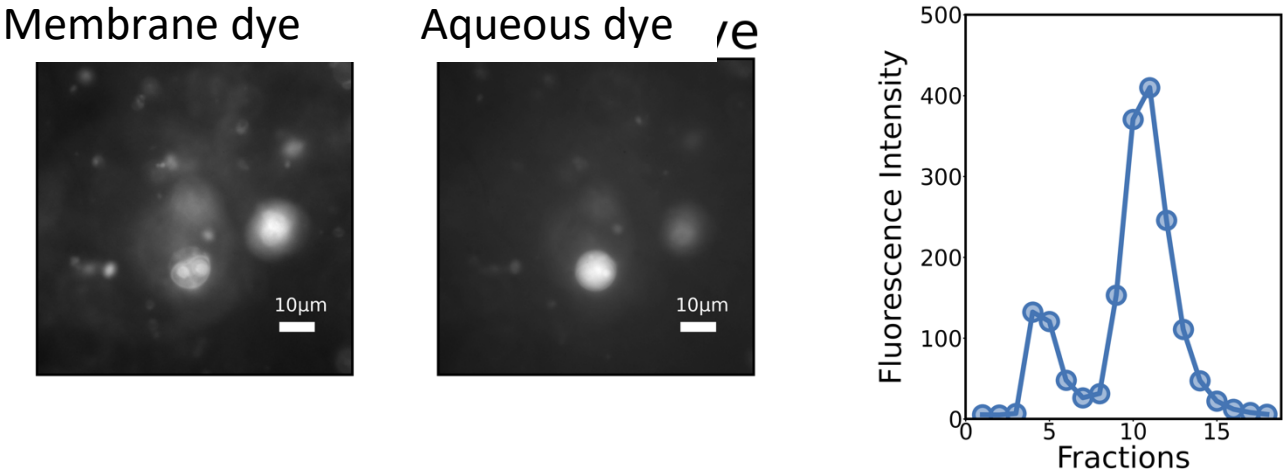

Figure S19: Additional data from the dehydration experiment with phospholipid vesicles composed of 95 mol % DOPC and 5 mol % DOPG shown in Fig 5. After rehydration, the vesicles were subjected to another round of SEC. The SEC chromatogram did show an early-eluting peak corresponding to calcein-containing vesicles, and images of these vesicles confirmed that calcein was encapsulated. See "Experiments on calcein retention during dehydration" in the methods section for full details. Scale bars are 10 µm.

Chapter 3:

Prebiotic Vesicles Retain Solutes and Grow by Micelle Addition after Brief Cooling below the Membrane Melting Temperature

*This chapter was first published in *Langmuir* in 2022. It was written in collaboration with Zoe R. Todd, David C. Catling, Roy. A. Black, and Sarah L. Keller.

Abstract

Replication of RNA genomes within membrane vesicles may have been a critical step in the development of protocells on the early Earth. Cold temperatures near 0°C improve the stability of RNA and allow efficient copying, while climate models suggest a cold early Earth, so the first protocells may have arisen in cold-temperature environments. However, at cold temperatures, saturated fatty acids, which would have been available on the early Earth, form gel phase membranes that are rigid and restrict mobility within the bilayer. Two primary roles of protocell membranes are to encapsulate solutes and to grow by incorporating additional fatty acids from the environment. We test here whether fatty acid membranes in the gel phase accomplish these roles. We find that gel-phase membranes of 10-carbon amphiphiles near 0°C encapsulate aqueous dye molecules as efficiently as fluid-phase membranes do, but the contents are released if the aqueous solution is frozen at -20°C. Gel-phase membranes do not grow measurably by micelle addition, but growth resumes when membranes are warmed above the gel-liquid transition temperature. We find that longer, 12 carbon amphiphiles do not retain encapsulated contents near 0°C. Together, our results suggest that protocells could have developed within environments that experience temporary cooling below the membrane melting temperature, and that membranes composed of relatively short chain fatty acids would encapsulate solutes more efficiently as temperatures approached 0°C.

Main text

Many models for the formation of protocells on the early Earth involve encapsulation of RNA by a membrane[1]. However, it remains unclear whether environmental conditions that enhance the stability and function of RNA were beneficial, neutral, or detrimental to the stability and function of membranes.

We have previously explored aspects of this question in the context of evaporating lakes that concentrate salts[2]. Here, we explore the effect of temperature.

Cold temperatures could have enabled development of RNA genomes[3]. In particular, nucleobases[4] and RNA[5,6] are more stable at temperatures near 0°C. Partially frozen water-ice eutectic mixtures and freeze-thaw cycles allow synthesis of nucleobases[7,8], oligomerization of nucleotides[9–13], and catalysis by ribozymes[14–17]. Coupled global carbon cycle and climate simulations show that the average surface temperature of the Earth may have been near 0°C from about 4.4 to 4.0 billion years ago when life likely originated[18].

How would membranes have fared in low temperature environments? Although the permeability and gel-liquid transitions of modern, phospholipid membranes are well-studied[19,20], corresponding data for prebiotic, fatty acid membranes are sparser. Fatty acids assemble into membranes when the solution pH is within about half a unit of the fatty acid pKa in the bilayer[21]. Fatty acids were delivered to the early Earth via meteorites[22], but they also could have been synthesized by the Fischer-Tropsch mechanism[23] or sparking reactions[24].

Historically, experiments with fatty acids have focused on membranes that are above their melting temperature[25], where the fatty acids are in a fluid phase characterized by high lateral mobility and mobile acyl chains (Fig. 1). A fluid, fatty acid membrane would have conferred many advantages to a protocell. Fluid vesicles have been shown to grow by incorporating additional fatty acids from micelles[26–28] or other vesicles[29]. Because these vesicles accumulate excess surface area as they grow, gentle shear forces can induce vesicle division[27], providing a simple, environmentally-driven mechanism for reproduction. Fluid membranes are permeable to small molecules while retaining larger ones, enabling synthesis of genetic polymers inside vesicles[30]. In addition, the building blocks of RNA and protein polymers bind to fluid-phase fatty acid vesicles, which could concentrate these molecules from dilute solutions in the early Earth environment[31–34].

Below their melting temperatures, fatty acid membranes are in a gel phase[35–37], characterized by amphiphiles with low lateral mobility and rigid acyl chains. It was previously unknown whether rigid, gel-phase fatty acid vesicles can retain encapsulated contents and whether they can grow via micelle addition. Here, we test permeability and growth in membranes of prebiotic single-chain amphiphiles with intermediate (10-carbon and 12-carbon) chain lengths.

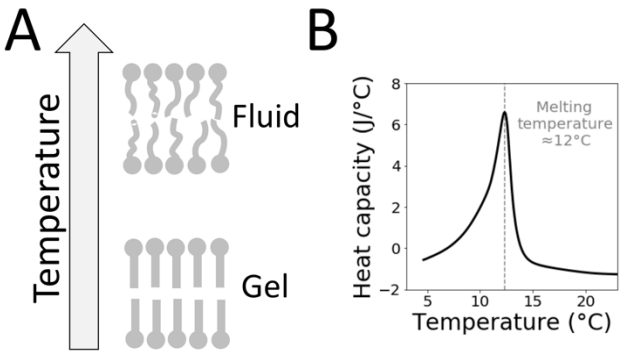

Figure 1: (A) The melting temperature of a fatty acid membrane is the transition from the gel to fluid phase. (B) For membranes composed of 1:1 decanoic acid:decanol at pH 8.7 (± 0.05), we measured a melting temperature of ~12°C using differential scanning calorimetry (see methods and results), which is consistent with previous results[36].

Our goal is to determine whether cold conditions, which enhance the stability of RNA, would have been detrimental to membranes of protocells, either by causing leakage of aqueous contents or by preventing growth. Specifically, we investigated conditions in which fatty acid membranes were in a gel phase rather than a fluid phase.

Our focus is on prebiotic fatty acids, which include decanoic acid (10-carbons), and, to a lesser extent, dodecanoic acid (12-carbons) [22–24]. We added a prebiotic long-chain alcohol (decanol or dodecanol) to the vesicles in order to improve retention of encapsulated dye after size-exclusion chromatography (SEC). Unless otherwise specified, vesicles were multilamellar with a heterogenous distribution of sizes up to ~10 µm. Because the melting temperature of fatty acid membranes is not necessarily the same as for pure fatty acids [35–37], we measured membrane transitions, which vary from < 4°C to 51°C (Table 1, Fig. S1-S6).

To quantify leakage across membranes, we filled fatty acid vesicles with high (60 mM) concentrations of self-quenched carboxyfluorescein dye. Subsequent leakage of the dye from the self-quenched interior of the vesicle to the dilute exterior produced a robust fluorescence signal. We held vesicles at temperatures above or below their membrane melting transition and found that dye leaks from the interior of gel-phase vesicles at a similar, slow rate as from fluid-phase vesicles (Fig. 2A). Moreover, gel-phase vesicles maintain encapsulation of dye over long periods (24 hours) near 0°C (Fig. S12). Dye retention is similarly high when fatty acid vesicles are quickly cycled across the gel-liquid transition (Fig. 2B-C). For example, when vesicles of 1:1 decanoic acid:decanol (with a melting temperature of ~12°C as in Fig. S1) were cycled three times between ~25°C and 0.0°C ± 2.7°C, the

leakage of encapsulated carboxyfluorescein dye was indistinguishable from leakage from vesicles that were maintained in only fluid or gel phases (Fig. 2B). The ability of gel-phase membranes to retain encapsulated solutes suggests that protocells composed of fatty acid membranes could have survived within cold, unfrozen environments.

Our results in Fig. 2B are surprising in the context of phospholipid membranes. Although the permeability of phospholipid membranes is similar in the fluid and gel phases, it spikes near the phospholipid's melting temperature [19,38]. In contrast, fatty acid membranes do not appear to experience higher permeability as they repeatedly pass through their melting temperature. Overall, vesicles of fatty acids are regarded as more permeable than vesicles of modern phospholipids [39]. In some scenarios, permeability is an advantage: replication of RNA in protocells may have been enabled by the movement of small molecules across the membrane while larger molecules were retained in the protocell's lumen[30]. It is difficult to place our results on gel-phase vesicles in the context of other fatty acid membranes because we are unaware of any other tests of membrane permeability (or growth) for gel-phase fatty acid membranes.

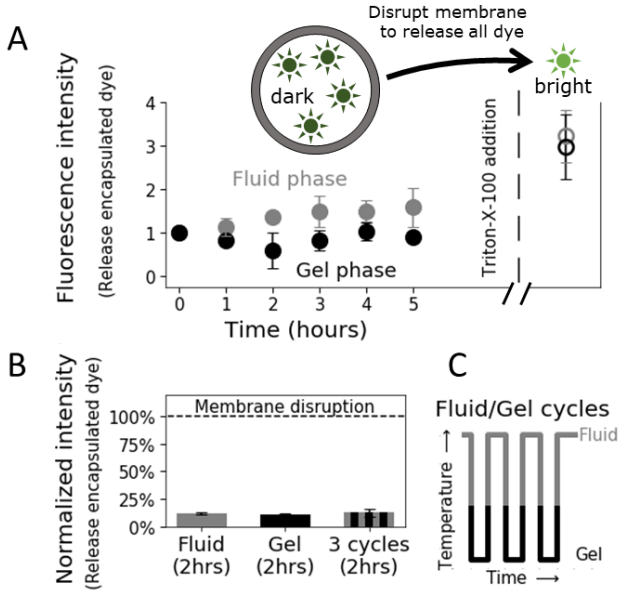

Figure 2: Gel phase fatty acid vesicles encapsulate dye as efficiently as fluid phase vesicles do. (A) Complete disruption of vesicle membranes with Triton X-100 releases all encapsulated dye and increases fluorescence. In contrast, leakage of dye is slow across fluid- and gel-phase membranes. In Panel A, vesicles of 2:1 decanoic acid:decanol (melting temperature ~9°C, Fig. S2) were held in the gel (5.0 ± 0.9°C) or fluid phase (25.0°C ± 1.2°C) up to 5 hours, and fluorescence was measured in a fluorimeter. (B-C) Cycling temperature three times between the fluid (25.0°C) and gel phases (0.0 ± 2.7°C) does not increase leakage relative to holding vesicles at a constant temperature. Vesicles of 1:1 decanoic acid:decanol (melting temperature ~12°C, Fig. S1) were held at constant temperature or cycled for 2 hours. Fluorescence was measured in a plate-reader before and after disruption of membranes with

Triton X-100. Fluorescence intensity data are normalized as a percent after disruption. Normalized intensities are related to (but not necessarily proportional to) the number of dye molecules that leak from vesicles. Error bars are standard deviations from 3-4 independent experiments.

Having established that gel-phase vesicles can retain their contents, we next examined if they grow upon addition of micelles. In short, we did not observe convincing signs of growth after the addition of micelles to gel phase vesicles. However, subsequent heating of vesicles above their melting temperature allows them to grow again (Fig. 3). We conducted our experiments by adding decanoic acid micelles to fluid (25.0 ± 1.4°C) or gel (1.0 ± 0.5°C) vesicles with melting temperatures of ~17°C (Fig. S3), then monitoring vesicle growth over times ranging from 0-40 min. Specifically, we measured Förster resonance energy transfer (FRET) between two dyes in the membrane, and we converted fluorescence intensities to membrane surface areas, as described in the Methods.

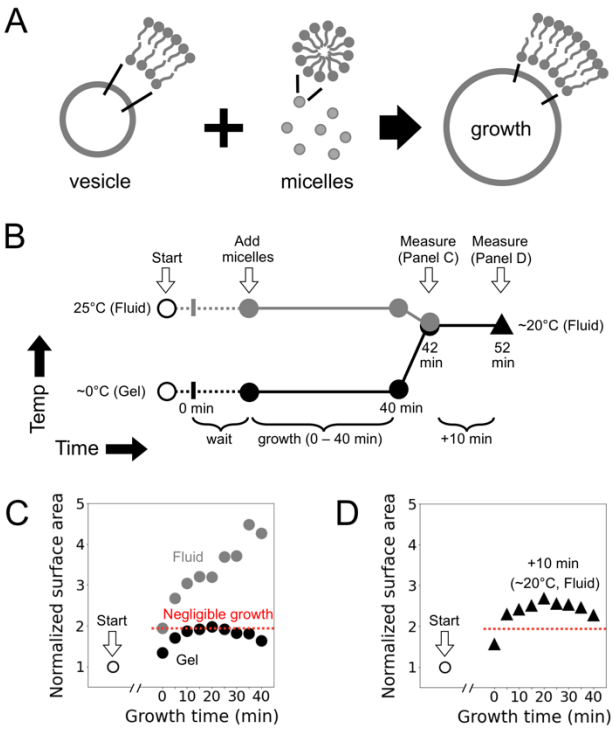

Figure 3: In the presence of micelles, the surface area of fluid-phase (but not gel-phase) vesicles increases with time. (A) Vesicles grow by incorporating fatty acids from micelles. (B) Protocol for introducing micelles to 100-nm diameter decanoic acid vesicles (melting temperature ~17°C) in the fluid (25.0 ± 1.4°C) or gel (1.0 ± 0.5°C) phase. Growth times ranged from 0-40 min, and the sum of the growth time and wait time was always 40 min. Over the next 2 min, all samples were brought into the fluid phase (25.0°C), and FRET was measured at ~20°C (data in Panel C). After an additional 10 min at ~20°C, FRET was measured again for the samples that had been in the gel phase (data in Panel D). Gel-phase vesicles showed negligible growth during the timecourse, relative to fluid-phase vesicles at zero growth time. However,

the vesicles in these samples did grow during an additional 10 min in the fluid phase (~20°C). Data in panels C and D are from a single experiment, and are consistent with other independent trials (Fig. S9-S10).

In detail, our vesicle growth results were as follows. First, we generated unilamellar, 100 nm vesicles by extrusion. When micelles were added to fluid-phase vesicles, the membrane area increased with time (Fig. 3C), consistent with previous observations[26–28]. In controls without micelles, membrane area remained constant, as expected (Fig. S11). When micelles were added to gel-phase vesicles, membrane area showed negligible growth – it did not exceed the area of fluid-phase vesicles at zero time (Fig. 3C and Fig. S9). When micelles were added to gel-phase vesicles (at each point in the timecourse) and subsequently the set of samples was held in the fluid phase (~20°C for 10 min), vesicle surface area increased (Fig. 3D and S10). These results were reproducible over multiple independent experiments (Fig. S9-S10).

In addition to decanoic acid, which was used in the experiments above, saturated fatty acids with longer carbon chains were likely present on early Earth as well[22–24]. Could these longer-chain fatty acids assemble into the membranes of protocells if the Earth was cold? Longer-chain fatty acids are often used in model protocells because they have lower critical vesicle concentrations[35], and because they encapsulate aqueous solutes at higher temperatures[40]. We next asked: if temperature is much lower (near 0°C), do longer-chain fatty acids encapsulate solutes more (or less) effectively than decanoic acid?

We produced vesicles of longer chain 12-carbon amphiphiles (1:1 dodecanoic acid:dodecanol) with a gel-liquid transition at ~31°C (Fig. S4). This transition temperature is higher than for membranes composed of 1:1 decanoic acid:decanol (~12°C), and the solubility of 12-carbon amphiphiles is lower than for 10-carbon amphiphiles. When the vesicles of 12-carbon amphiphiles are held in the gel phase close to the gel-liquid transition (25°C), they retain encapsulated dye (Fig. 4) like the vesicles of 10-carbon amphiphiles. However, at lower temperatures (~0°C, on ice), they completely release the dye, unlike the 10-carbon vesicles at ~0°C (Fig. 2). It is unclear if this difference is due to the larger, 30°C offset between the membrane's melting temperature and the sample temperature or due to the low solubility of 12-carbon chains at 0°C. We observe similar behavior with vesicles of 14-carbon amphiphiles (1:1 tetradecanoic acid: tetradecanol, Fig. S13-14), whereas short-chain 9-carbon amphiphiles (1:1 nonanoic acid: nonanol) retain encapsulated dye at 0°C (Fig. S15). Our results imply

that membranes composed of relatively short-chain fatty acids would have had an advantage as temperatures approached 0°C.

Our results above report on the behavior of model protocell membranes in the gel phase, when the vesicles are in unfrozen solution near 0°C. But what if the early Earth experienced even colder temperatures such that the bulk solution froze completely? To investigate this, we examined if fatty acid vesicles retain encapsulated solutes after freezing and thawing of the surrounding solution.

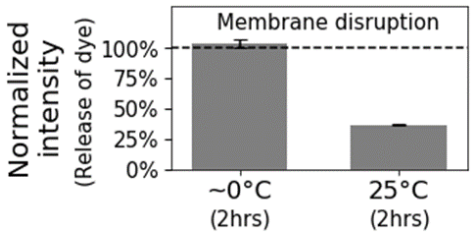

Figure 4: Vesicles of 12-carbon amphiphiles (1:1 dodecanoic acid:dodecanol) release encapsulated dye after 2 hrs at ~0°C, but retain dye after 2 hrs at 25°C. Fluorescence intensity is normalized by the fluorescence intensity after membrane disruption by Triton X-100, and expressed as a percent. Error bars are standard deviations from three independent experiments.

We froze solutions of vesicles composed of 2:1 decanoic acid: decanol at -20°C, and we observed that all encapsulated dye leaked from the vesicles upon thawing (Fig. 5). We observed similar behavior for vesicles of 1:1 nonanoic acid: nonanol (Fig. S16). This is in contrast to modern, phospholipid membranes, which retain some of their encapsulated contents after complete freezing[41]. Our vesicles of 2:1 decanoic acid:decanol have a membrane transition temperature of ~9°C, so there is ~30°C offset between the membrane transition temperature and the sample temperature. This may be analogous to our experiments with 12-carbon amphiphiles because we create a similar ~30°C offset, and we observe release of encapsulated dye in both experiments.

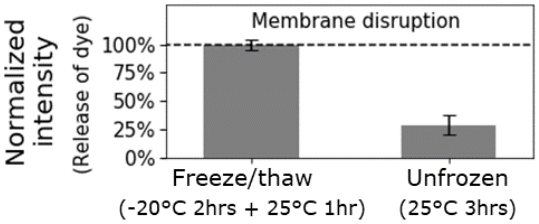

Figure 5: Vesicles of 10-carbon amphiphiles (2:1 decanoic acid:decanol) release encapsulated dye after 2 hrs of freezing at -20°C and 1 hr of thawing at 25°C. A unfrozen sample of the vesicles retains dye after 3 hrs at 25°C. Fluorescence intensity is normalized by the fluorescence intensity after membrane

disruption by Triton X-100, and expressed as a percent. Error bars are standard deviations from three independent experiments.

Temperatures near 0°C enable synthesis of RNA genomes[3–12,14–17], making cold brines an attractive environment for the development of protocells on the early Earth. Here, we have shown that vesicles composed of 10-carbon amphiphiles (decanoic acid and decanol) retain encapsulated solutes when they are transiently cooled to temperatures near 0°C, even though the vesicle membranes are in a gel phase at these cold temperatures. Gel-phase membranes of decanoic acid do not grow by micelle addition, but membrane growth ensues when the temperature is increased above the melting transition. Suppressing the melting temperature could enable the growth of fatty acid membranes near 0°C. Sugars, nucleobases, amino acids, and peptides in the prebiotic environment could bind to fatty acid vesicles[31,32,34] and decrease the membrane melting temperature, as membrane proteins do in cell-derived phospholipid membranes[42]. Similarly, polyaromatic hydrocarbons incorporate into fatty acid membranes[43] and could behave analogously to sterols by fluidizing the membrane.

We have shown that vesicles of 12-carbon amphiphiles (dodecanoic acid and dodecanol) do not encapsulate solutes after cooling near 0°C, which suggests that protocells composed of relatively short-chain amphiphiles may have had an advantage in cold conditions on the early Earth. Additionally, complete freezing disrupts encapsulation by fatty acid vesicles, which may have constrained protocell development to unfrozen solutions. Our results imply that fatty acid vesicles could have contributed to the formation of the earliest protocells within cold, unfrozen environments on the early Earth

Experimental section

Materials

Decanol, dodecanoic acid, dodecanol, and carboxyfluorescein were purchased from Sigma-Aldrich (St. Louis, MO). Decanoic acid was from Nu-Chek Prep (Elysian, MN) and $NaHCO_3$ was from EMD Chemicals (Darmstadt, Germany). Sepharose 4B was used for size-exclusion chromatography (Sigma-Aldrich, St. Louis, MO). Triton X-100 was from Supleco (Bellefonte, PA). Rhodamine B dihexadecanoyl-phosphoethanolamine (rhodamine-DHPE), N-(7-nitrobenz-2-oxa-1,3-diazol-4-yl)-dihexadecanoyl-phosphoethanolamine (NBD-PE), and 96-well polystyrene plates were from ThermoFisher (Waltham, MA). A 300-µL quartz cuvette #23-3.45-Q-3 was from Starna Cells (Atascadero, CA).

Preparation of vesicle solutions

1.0 M stock solutions of decanoate and dodecanoate were made by dissolving solid decanoic or dodecanoic acid in an equimolar NaOH solution, followed by gentle heating to 60°C and rocking for 1.25 hr. Vesicle solutions were prepared in the following order: (1) Stock solutions of 1.0 M $NaHCO_3$ and 0.10 M carboxyfluorescein were diluted into ~18 mΩ-cm water. (2) 1.0 M decanoate (or 1.0 M dodecanoate) stock solution was added. (3) Liquid decanol (or dodecanol) was added, which induced vesicles to form. At this step, the solution contained 0.10 M $NaHCO_3$ and 60 mM carboxyfluorescein, both inside and outside the vesicles. The pH was adjusted to 8.70 ± 0.05 by adding small volumes of concentrated HCl or NaOH solutions**.** To avoid insolubility of dodecanoate and dodecanol at low temperatures, their stock solutions were heated at 60°C for 1 hr before mixing. The resulting solution was maintained at 60°C, and the solution was housed in a test tube held in an aluminum block at 60°C during pH adjustment.

Determining membrane melting temperature using calorimetry

Heat capacities of vesicle solutions were measured using a Malvern Panalytical (Malvern, UK) MicroCal VP-capillary differential scanning calorimeter. 0.10 M $NaHCO_3$ at pH 8.7 (± 0.05) was used as a reference solution. Temperature sweeps were conducted at 60°C/hr.

Size-exclusion chromatography (SEC)

To encapsulate concentrated dye in vesicles, we allowed vesicles to self-assemble in a self-quenched (60 mM) carboxyfluorescein solution as described above, eluted the resulting solution through a SEC column, and collected aliquots enriched in vesicles and depleted of free dye. SEC columns were prepared with 6.9 mL Sepharose 4B resin. Before each SEC run, the column was flushed with at least two volume equivalents of running buffer. 500 µL vesicle solutions in the concentrations listed in Table 1 were added to the SEC column, and 400 µL fractions were collected by hand. After all fractions were collected, the column was flushed with at least 2 volume equivalents of 0.2 M bicine (pH 9) for storage. The SEC running buffer contained 0.10 M $NaHCO_3$ to match ionic conditions in the vesicle sample and 20 mM fatty acid (either decanoic acid or dodecanoic acid, corresponding to the vesicles) so that the total amphiphile concentration remained above the critical vesicle concentration[2]. The pH of the running buffer was adjusted to 8.70 (± 0.05) by adding small volumes of concentrated HCl or NaOH solutions. The fractions containing vesicles were combined and further diluted in SEC running buffer for analysis.

Table 1:

Expt.	**Vesicles**	**Carbons**	**Ratio**	**Conc. before SEC**	**Conc. after SEC + dilution**	**Melting Temp**	**T_{melt} Data**
Fig. 1	decanoic acid / decanol	10	1:1	37.5 mM / 37.5 mM	–	~12°C	Fig. S1
Fig. 2A, Fig. 5	decanoic acid / decanol	10	2:1	250 mM / 125 mM	~50 mM / ~25 mM	~9°C	Fig. S2

Fig. 2B	decanoic acid / decanol	10	1:1	112.5 mM / 112.5 mM	~37.5 mM / ~37.5 mM	~12°C	Fig. S1
Fig. 3	decanoic acid	10	–	60 mM	–	~17°C	Fig. S3
Fig. 4	dodecanoic acid / dodecanol	12	1:1	112.5 mM / 112.5 mM	~37.5 mM / ~37.5 mM	~31°C	Fig. S4
Fig. S13, S14	tetradecanoic acid / tetradecanol	14	1:1	112.5 mM / 112.5 mM	~37.5 mM / ~37.5 mM	~51°C	Fig. S5
Fig. S15, S16	nonanoic acid / nonanol	9	1:1	112.5 mM / 112.5 mM	~37.5 mM / ~37.5 mM	< 4°C	Fig. S6

Release of encapsulated dye at constant temperature

After SEC, vesicle solutions contained ~50 mM decanoic acid and ~25 mM decanol, and the vesicles encapsulated self-quenched carboxyfluorescein at ~60 mM. Vesicle solutions were held in a glass cuvette at 23.8-25.6°C (for fluid-phase membranes) and 4.5-5.9°C (for gel-phase membranes), including during measurement. Carboxyfluorescein fluorescence (ex475/em520) was measured every hour for 5 hours using a Horiba Fluorolog (Kyoto, Japan). After 5 hours, Triton X-100 was added (final concentration 0.3% by weight) to disrupt vesicles, leading to complete release of encapsulated carboxyfluorescein and corresponding increase in the fluorescence signal.

Release of encapsulated dye during temperature cycling

After SEC, vesicle solutions contained ~37.5 mM decanoic acid and ~37.5 mM decanol, and the vesicles encapsulated self-quenched carboxyfluorescein at ~60 mM. 350-µL aliquots of vesicle solution were distributed to 1.5 mL Eppendorf tubes, and three types of experiments were performed. In Experiment 1, samples were maintained in an oven at 25°C (fluid phase) for 120 min. In Experiment 2, samples were maintained at –2.7 to 1.8°C (gel-phase fatty acid membranes in a fluid-phase solution) for 120 min using either a refrigerator or an ice bath. In Experiment 3, temperature was cycled three times, starting with 20 min at the cold temperature (–2.7 to 1.8°C, either in a refrigerator or ice bath), then 20 min in an oven at 25°C, for a total of 120 min. The 20-min equilibration times were verified to be long enough for completion of the gel-liquid transition of all vesicles. Triplicate 100 µL aliquots from each vesicle sample were then transferred into a 96-well plate. Carboxyfluorescein fluoresence was measured at room temperature using a Thermo Labsystems (Gulph Mills, PA) Fluoroskan Ascent FL Fluorescence Microplate Reader with ex485/em520. At the end of the experiment, Triton X-100 (final concentration 0.3% by weight) was added to disrupt vesicles and release all encapsulated carboxyfluorescein.

Vesicle surface area assay

Hydrophobic dyes were added to solutions of nominally 100-nm vesicles as follows. First, vesicles self-assembled in solutions of 60 mM decanoic acid and 200 mM HEPES, with pH adjusted to 7.60 (+/- 0.05) by the addition of small volumes of concentrated NaOH solution. Next, stock solutions of

dye in chloroform (10 mM NBD-PE and 5 mM rhodamine-DHPE) were dried in glass vials under N_2 followed by 30 min under vacuum. The vesicle solution was added to the vials corresponding to a final concentration of dye of 60 μM. The vials were rocked for 2 days to incorporate dye into the vesicles. The vesicles were extruded 9 times through 100-nm filters. 90 μL aliquots of vesicle solution were distributed to wells in a 96-well plate, which was then placed on a metal heating block (Fig. S7). Temperature was maintained at 24.7-26.4°C for fluid-phase vesicles and at 0.9-1.5°C for gel-phase vesicles.

Vesicles grew in the presence of micelles for 0-40 min. The protocol for adding micelles to vesicle solutions (Fig. 3B) was designed so that all Förster resonance energy transfer (FRET) data were collected simultaneously at room temperature (~20°C) because membrane FRET is inefficient at ~0°C. 1) We prepared parallel samples of vesicles in the fluid or the gel phase in a 96-well plate. 2) The 96-well plate was equilibrated to the temperature of fluid or gel-phase vesicles, along with a solution of decanoic acid micelles (1.0 M decanoic acid in 1.0 M NaOH). 3) In 5 min intervals, 10 μL of micelle solution (~2 equivalents of decanoic acid) was added to a different vesicle sample in the 96-well plate to achieve growth times of 0-40 min (the time prior to addition of the micelle solution is referred to as the "wait time" in Figure 3). The total time elapsed from the start of the experiment was the same for each vesicle sample, 40 min. One 100-μL aliquot of vesicles without micelles was reserved as a control. 4) Over an additional 2 min, the plate was brought to 25°C, then room temperature (~20°C), and 5) FRET was measured in all wells simultaneously (ex485/em538 and ex485/em589). Thus, micelle addition and vesicle growth occurred in either gel or fluid phase, and surface area was always measured on fluid-phase vesicles. 6) Vesicles that had been in the gel phase were then held at room temperature for an additional 10 min, and FRET was measured again. Using a phenomenological relationship between the FRET intensity (*I*, taken as em538/em589) and the concentration of dye molecules in the membrane (Fig. S8), the vesicle surface area (*A*) was calculated as:

$$A = 4\pi r^2 \frac{C_0}{C_t} \quad (1)$$

In the equation, *r* is the initial radius of the vesicles (taken as 50 nm), C_0 is the initial concentration of FRET-pairs in the membrane (0.1%), and C_t is the concentration of those FRET-pairs at time *t* (determined from Fig. S8). Surface area was normalized by the value from a control without added micelles.

Release of dye from vesicles of 12-carbon amphiphiles

After SEC, vesicle solutions contained ~37.5 mM dodecanoic acid and ~37.5 mM dodecanol, and the vesicles encapsulated self-quenched carboxyfluorescein at ~60 mM. Two 350-μL volumes of vesicle solution were distributed to 1.5-mL Eppendorf tubes. One was maintained at 25°C for 120 min; the other was maintained on ice for 120 min. The membranes were in the gel phase at both temperatures. Triplicate 100-μL aliquots from each volume were transferred into a 96-well plate. Carboxyfluorescein fluorescence was measured at room temperature using a Thermo Labsystems (Gulph Mills, PA) Fluoroskan Ascent FL Fluorescence Microplate Reader with ex485/em520. At the end of the experiment, Triton X-100 (final concentration 0.3% by weight) was added to disrupt vesicles, which released all encapsulated carboxyfluorescein.

Release of dye from vesicles during complete freezing

After SEC, vesicle solutions contained ~50 mM decanoic acid and ~25 mM dodecanol, and the vesicles encapsulated self-quenched carboxyfluorescein at ~60 mM. Two 500-µL samples of vesicle solution were distributed to glass tubes. One sample was maintained at 25°C for 180 min; the other sample was frozen at -20°C for 120 min, and then maintained at 25°C for 60 min to thaw. Both samples were incubated for a total time of 180 min. Triplicate 100-µL aliquots from each vesicle sample were transferred to a 96-well plate. Carboxyfluorescein fluorescence was measured at room temperature using a Thermo Labsystems (Gulph Mills, PA) Fluoroskan Ascent FL Fluorescence Microplate Reader with ex485/em520. At the end of the experiment, Triton X-100 (final concentration 0.3% by weight) was added to disrupt vesicles, which released all encapsulated carboxyfluorescein.

ACKNOWLEDGEMENTS

We thank Dr. Tim Pollock for assistance with calorimetry experiments. This research was supported in part by grant NNX17AK86G (Exobiology) from NASA to S.L.K., by grant MCB 1925731 from the National Science Foundation to S.L.K, and by grant 511570FY20, DCC from the Simons Foundation to D.C.C. ZRC was funded by an NSF GRFP fellowship (DGE 1762114), and by grant 511570FY20. Z.R.T. is an NHFP postdoc (grant HST-HF2-51471).

REFERENCES

(1) Joyce, G. F.; Szostak, J. W. Protocells and RNA Self-Replication. *Cold Spring Harb Perspect Biol* **2018**, *10* (9), a034801.
(2) Cohen, Z. R.; Cornell, Caitlin. E.; Catling, D. C.; Black, R. A.; Keller, S. L. Prebiotic Protocell Membranes Retain Encapsulated Contents during Flocculation, and Phospholipids Preserve Encapsulation during Dehydration. *Langmuir* **2022**, *38* (3), 1304–1310.
(3) Bada, J. L.; Lazcano, A. Some Like It Hot, But Not the First Biomolecules. *Science* **2002**, *296* (5575), 1982–1983.
(4) Levy, M.; Miller, S. L. The Stability of the RNA Bases: Implications for the Origin of Life. *Proc. Natl. Acad. Sci USA* **1998**, *95* (14), 7933–7938.
(5) Li, Y.; Breaker, R. R. Kinetics of RNA Degradation by Specific Base Catalysis of Transesterification Involving the 2'-Hydroxyl Group. *J. Am. Chem. Soc.* **1999**, *121* (23), 5364–5372.
(6) Moulton, V.; Gardner, P. P.; Pointon, R. F.; Creamer, L. K.; Jameson, G. B.; Penny, D. RNA Folding Argues Against a Hot-Start Origin of Life. *J Mol Evol* **2000**, *51* (4), 416–421.
(7) Levy, M.; Miller, S. L.; Brinton, K.; Bada, J. L. Prebiotic Synthesis of Adenine and Amino Acids Under Europa-like Conditions. *Icarus* **2000**, *145* (2), 609–613.
(8) Menor-Salván, C.; Ruiz-Bermejo, Dra. M.; Guzmán, M. I.; Osuna-Esteban, S.; Veintemillas-Verdaguer, S. Synthesis of Pyrimidines and Triazines in Ice: Implications for the Prebiotic Chemistry of Nucleobases. *Chemistry – A European Journal* **2009**, *15* (17), 4411–4418.
(9) Kanavarioti, A.; Monnard, P.-A.; Deamer, D. W. Eutectic Phases in Ice Facilitate Nonenzymatic Nucleic Acid Synthesis. *Astrobiology* **2001**, *1* (3), 271–281.
(10) Monnard, P.-A.; Kanavarioti, A.; Deamer, D. W. Eutectic Phase Polymerization of Activated Ribonucleotide Mixtures Yields Quasi-Equimolar Incorporation of Purine and Pyrimidine Nucleobases. *J. Am. Chem. Soc.* **2003**, *125* (45), 13734–13740.
(11) Trinks, H.; Schröder, W.; Biebricher, C. K. Ice And The Origin Of Life. *Orig Life Evol Biosph* **2005**, *35* (5), 429–445.

(12) Monnard, P.-A.; Szostak, J. W. Metal-Ion Catalyzed Polymerization in the Eutectic Phase in Water–Ice: A Possible Approach to Template-Directed RNA Polymerization. *Journal of Inorganic Biochemistry* **2008**, *102* (5), 1104–1111.
(13) Zhang, S. J.; Duzdevich, D.; Ding, D.; Szostak, J. W. Freeze-Thaw Cycles Enable a Prebiotically Plausible and Continuous Pathway from Nucleotide Activation to Nonenzymatic RNA Copying. *Proc. Natl. Acad. Sci USA* **2022**, *119* (17), e2116429119.
(14) Vlassov, A. V.; Johnston, B. H.; Landweber, L. F.; Kazakov, S. A. Ligation Activity of Fragmented Ribozymes in Frozen Solution: Implications for the RNA World. *Nucleic Acids Research* **2004**, *32* (9), 2966–2974.
(15) Kazakov, S. A.; Balatskaya, S. V.; Johnston, B. H. Ligation of the Hairpin Ribozyme in *Cis* Induced by Freezing and Dehydration. *RNA* **2006**, *12* (3), 446–456.
(16) Attwater, J.; Wochner, A.; Pinheiro, V. B.; Coulson, A.; Holliger, P. Ice as a Protocellular Medium for RNA Replication. *Nat Commun* **2010**, *1* (1), 76.
(17) Attwater, J.; Wochner, A.; Holliger, P. In-Ice Evolution of RNA Polymerase Ribozyme Activity. *Nature Chem* **2013**, *5* (12), 1011–1018.
(18) Kadoya, S.; Krissansen-Totton, J.; Catling, D. C. Probable Cold and Alkaline Surface Environment of the Hadean Earth Caused by Impact Ejecta Weathering. *Geochemistry, Geophysics, Geosystems* **2020**, *21* (1), e2019GC008734.
(19) Blicher, A.; Wodzinska, K.; Fidorra, M.; Winterhalter, M.; Heimburg, T. The Temperature Dependence of Lipid Membrane Permeability, Its Quantized Nature, and the Influence of Anesthetics. *Biophys J* **2009**, *96* (11), 4581–4591.
(20) Marsh, D. *Handbook of Lipid Bilayers*, 2nd ed.; CRC Press: Boca Raton, 2013.
(21) Apel, C. L.; Deamer, D. W.; Mautner, M. N. Self-Assembled Vesicles of Monocarboxylic Acids and Alcohols: Conditions for Stability and for the Encapsulation of Biopolymers. *Biochimica et Biophysica Acta (BBA) - Biomembranes* **2002**, *1559* (1), 1–9.
(22) Lawless, J. G.; Yuen, G. U. Quantification of Monocarboxylic Acids in the Murchison Carbonaceous Meteorite. *Nature* **1979**, *282* (5737), 396–398.
(23) Nooner, D. W.; Oro, J. Synthesis of Fatty Acids by a Closed System Fischer-Tropsch Process. In *Hydrocarbon Synthesis from Carbon Monoxide and Hydrogen*; Advances in Chemistry; American Chemical Society, 1979; Vol. 178, pp 159–171.
(24) Yuen, G. U.; Lawless, J. G.; Edelson, E. H. Quantification of Monocarboxylic Acids from a Spark Discharge Synthesis. *J Mol Evol* **1981**, *17* (1), 43–47.
(25) Mansy, S. S.; Szostak, J. W. Thermostability of Model Protocell Membranes. *Proc. Natl. Acad. Sci USA* **2008**, *105* (36), 13351–13355.
(26) Chen, I. A.; Szostak, J. W. A Kinetic Study of the Growth of Fatty Acid Vesicles. *Biophysical Journal* **2004**, *87* (2), 988–998.
(27) Zhu, T. F.; Szostak, J. W. Coupled Growth and Division of Model Protocell Membranes. *J. Am. Chem. Soc.* **2009**, *131* (15), 5705–5713.
(28) Todd, Z. R.; Cohen, Z. R.; Black, R. A.; Keller, S. L.; Catling, D. C. Growth of Prebiotically Plausible Fatty Acid Vesicles Proceeds in the Presence of Prebiotic Building Blocks. *In prep.* **2022**.
(29) Toparlak, Ö. D.; Wang, A.; Mansy, S. S. Population-Level Membrane Diversity Triggers Growth and Division of Protocells. *JACS Au* **2021**, *1* (5), 560–568.
(30) Mansy, S. S.; Schrum, J. P.; Krishnamurthy, M.; Tobé, S.; Treco, D. A.; Szostak, J. W. Template-Directed Synthesis of a Genetic Polymer in a Model Protocell. *Nature* **2008**, *454* (7200), 122–125.
(31) Black, R. A.; Blosser, M. C.; Stottrup, B. L.; Tavakley, R.; Deamer, D. W.; Keller, S. L. Nucleobases Bind to and Stabilize Aggregates of a Prebiotic Amphiphile, Providing a Viable Mechanism for the Emergence of Protocells. *Proc. Natl. Acad. Sci USA* **2013**, *110* (33), 13272.

(32) Cornell, C. E.; Black, R. A.; Xue, M.; Litz, H. E.; Ramsay, A.; Gordon, M.; Mileant, A.; Cohen, Z. R.; Williams, J. A.; Lee, K. K.; Drobny, G. P.; Keller, S. L. Prebiotic Amino Acids Bind to and Stabilize Prebiotic Fatty Acid Membranes. *Proc. Natl. Acad. Sci USA* **2019**, *116* (35), 17239–17244.
(33) Xue, M.; Black, R. A.; Cornell, C. E.; Drobny, G. P.; Keller, S. L. A Step toward Molecular Evolution of RNA: Ribose Binds to Prebiotic Fatty Acid Membranes, and Nucleosides Bind Better than Individual Bases Do. *ChemBioChem* **2020**, *21* (19), 2764–2767.
(34) Xue, M.; Black, R. A.; Cohen, Z. R.; Roehrich, A.; Drobny, G. P.; Keller, S. L. Binding of Dipeptides to Fatty Acid Membranes Explains Their Colocalization in Protocells but Does Not Select for Them Relative to Unjoined Amino Acids. *J. Phys. Chem. B* **2021**, *125* (29), 7933–7939.
(35) Hargreaves, W. R.; Deamer, D. W. Liposomes from Ionic, Single-Chain Amphiphiles. *Biochemistry* **1978**, *17* (18), 3759–3768.
(36) Kapoor, S.; Berghaus, M.; Suladze, S.; Prumbaum, D.; Grobelny, S.; Degen, P.; Raunser, S.; Winter, R. Prebiotic Cell Membranes That Survive Extreme Environmental Pressure Conditions. *Angewandte Chemie International Edition* **2014**, *53* (32), 8397–8401.
(37) Misuraca, L.; Caliò, A.; Grillo, I.; Grélard, A.; Oger, P. M.; Peters, J.; Demé, B. High-Temperature Behavior of Early Life Membrane Models. *Langmuir* **2020**, *36* (45), 13516–13526.
(38) Chakrabarti, A. C.; Breaker, R. R.; Joyce, G. F.; Deamer, D. W. Production of RNA by a Polymerase Protein Encapsulated within Phospholipid Vesicles. *J Mol Evol* **1994**, *39* (6), 555–559.
(39) Chen, I. A.; Salehi-Ashtiani, K.; Szostak, J. W. RNA Catalysis in Model Protocell Vesicles. *J. Am. Chem. Soc.* **2005**, *127* (38), 13213–13219.
(40) Jordan, S. F.; Rammu, H.; Zheludev, I. N.; Hartley, A. M.; Maréchal, A.; Lane, N. Promotion of Protocell Self-Assembly from Mixed Amphiphiles at the Origin of Life. *Nat Ecol Evol* **2019**, 3, 1705–1714.
(41) Litschel, T.; Ganzinger, K. A.; Movinkel, T.; Heymann, M.; Robinson, T.; Mutschler, H.; Schwille, P. Freeze-Thaw Cycles Induce Content Exchange between Cell-Sized Lipid Vesicles. *New J. Phys.* **2018**, *20* (5), 055008.
(42) Mužić, T.; Tounsi, F.; Madsen, S. B.; Pollakowski, D.; Konrad, M.; Heimburg, T. Melting Transitions in Biomembranes. *Biochimica et Biophysica Acta (BBA) - Biomembranes* **2019**, *1861* (11), 183026.
(43) Groen, J.; Deamer, D. W.; Kros, A.; Ehrenfreund, P. Polycyclic Aromatic Hydrocarbons as Plausible Prebiotic Membrane Components. *Orig Life Evol Biosph* **2012**, *42* (4), 295–306.

Supplementary information

Section 1: Determining membrane melting temperature using calorimetry

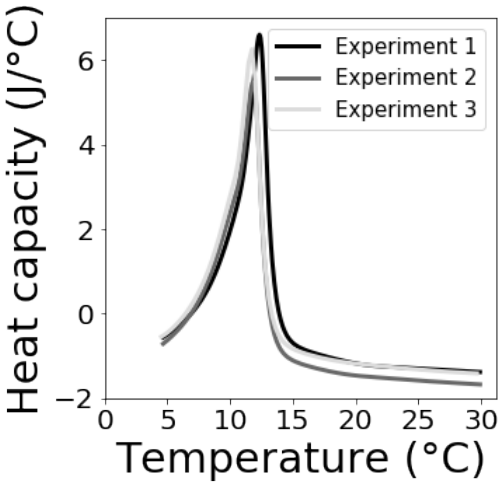

Figure S1: The melting temperature of membranes composed of 1:1 decanoic acid: decanol is roughly 12°C, consistent with previous results[1]. In three independent measurements, vesicles composed of 187.5 mM decanoic acid and 187.5 mM decanol were prepared so that the interior and exterior solution was 100 mM $NaHCO_3$ at pH 8.7 (± 0.05). Vesicle samples were diluted into a solution of 100 mM $NaHCO_3$ at pH 8.7 (± 0.05) so that the final amphiphile concentration was 37.5 mM decanoic acid and 37.5 mM decanol.

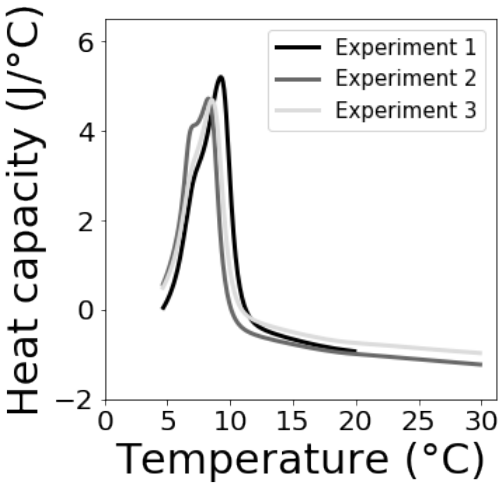

Figure S2: The melting temperature for membranes composed of 2:1 decanoic acid: decanol is ~9°C. In three independent experiments, vesicles composed of 250 mM decanoic acid and 125 mM decanol were prepared so that the interior and exterior solution was 100 mM $NaHCO_3$ at pH 8.7 (± 0.05). Vesicle samples were diluted into a solution of 100 mM $NaHCO_3$ at pH 8.7 (± 0.05) so that the final amphiphile concentration was 50 mM decanoic acid and 25 mM decanol. Some experiments in the main text (Fig 2B) with membranes of the same composition were conducted between 4.5°C and 5.9°C, which we characterize as the gel phase. An advantage of conducting experiments near the melting temperature is that membrane permeability is expected to be highest at the gel-liquid transition, based on previous experiments with phospholipids[2]. Because we observe that fluorescent dyes leak at similar rates across fatty acid membranes at 4.5 - 5.9°C, (slightly below the melting temperature) and at 25°C (well above the melting temperature), we can conclude that gel phase vesicles effectively encapsulate the dye.

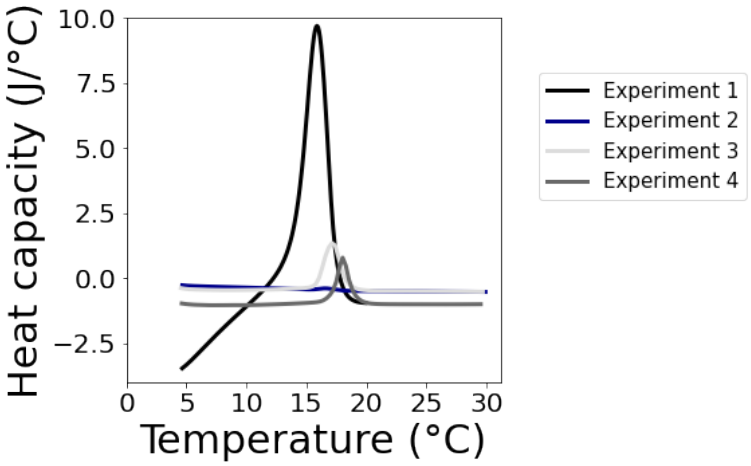

Figure S3: The melting temperature for membranes composed of decanoic acid is ~17°C. In four independent experiments, vesicles composed of 50 mM decanoic acid were prepared so that the interior and exterior solutions both contained 100 mM NaCl and 30 mM monosodium phosphate at pH 7.0 (± 0.05). Unlike other calorimetry experiments in our paper, a solution of 100 mM NaCl and 30 mM monosodium phosphate at pH 7.0 (+/- 0.05) was used as a reference solution, to match the ionic composition in the vesicle sample. The temperature sweep was conducted at 60°C/hr. For completeness, all data are shown, including Experiment 2, in which the instrument failed to register a change in heat capacity. Experiments spanned 7 months.

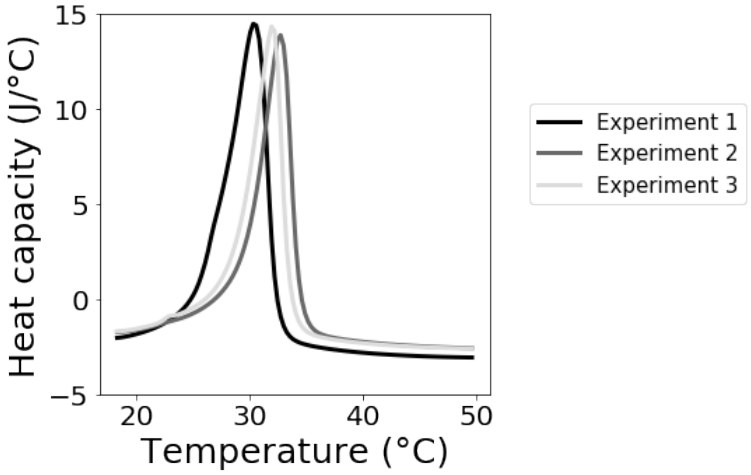

Figure S4: The melting temperature for membranes composed of 1:1 dodecanoic acid: dodecanol is ~31°C. In three independent experiments, vesicles composed of 37.5 mM dodecanoic acid and 37.5 mM dodecanol were prepared at 60°C so that the interior and exterior solution was 100 mM $NaHCO_3$ at pH 8.7 (± 0.05).

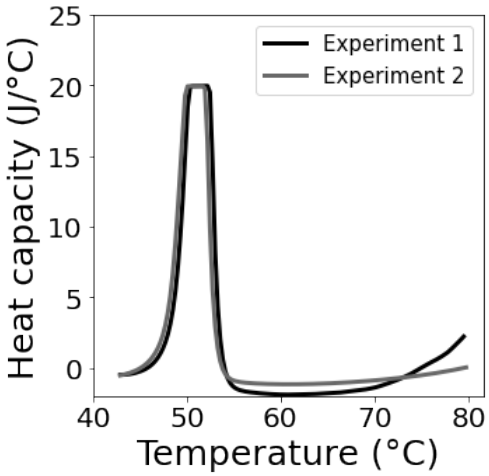

Figure S5: The melting temperature for membranes composed of 1:1 tetradecanoic acid: tetradecanol (14 carbons) is ~51°C. In two independent experiments, vesicles composed of 37.5 mM tetradecanoic acid and 37.5 mM tetradecanol were prepared at 60°C so that the interior and exterior solution was 100 mM $NaHCO_3$ at pH 8.7 (± 0.05).

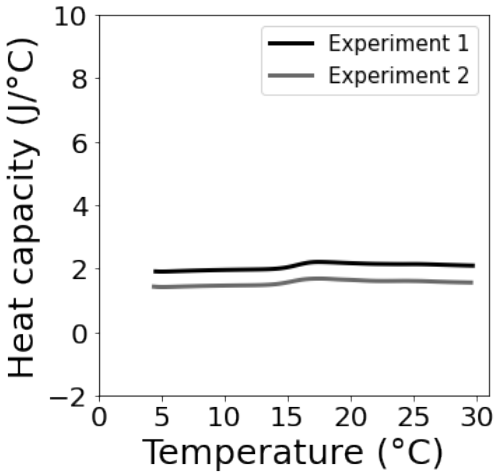

Figure S6: We do not observe a melting transition for membranes composed of 1:1 nonanoic acid: nonanol (9 carbons) above 4°C, the lowest temperature that our instrument is capable of measuring. In two independent experiments, vesicles composed of 37.5 mM nonanoic acid and 37.5 mM nonanol were prepared so that the interior and exterior solution was 100 mM $NaHCO_3$ at pH 8.7 (± 0.05).

Section 2: Förster resonance energy transfer (FRET) to determine vesicle surface area

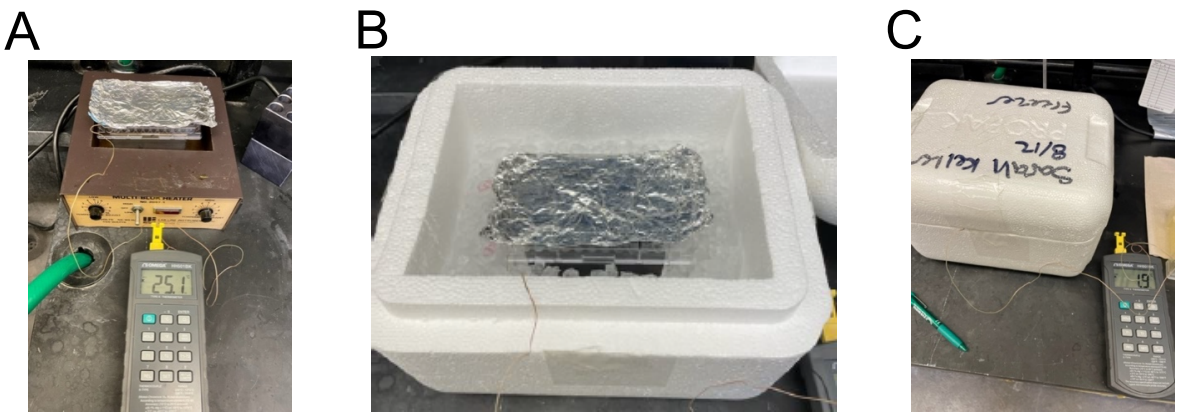

Figure S7: A 96-well plate filled with vesicle aliquots was maintained at constant temperature during the FRET assay, outlined in Figure 3 of the main text. The plate was placed on a metal block, and a digital thermometer was rested in an unused well filled with 100 µL H_2O. (A) To maintain vesicles in the fluid phase, the metal block was heated to 25.0 ± 1.4°C. (B) To maintain vesicles in the gel phase, the metal block was placed in a styrofoam ice bath. The 96-well plate did not contact the ice directly. (C) After a styrofoam lid was affixed, the temperature at the sample was 1.0 ± 0.5°C. After the last aliquot of micelles was added to gel phase vesicles, the plate was removed from the ice bath and set on a 60°C metal block for ~1.5 min until the plate reached 25°C. Fluorescence was measured at room temperature 2 min after the block was removed from the ice bath. For a third replicate experiment (Fig S9), temperature was varied in an Eppendorf MasterCycler Gradient Thermal Cycler in which the 96-well plate sat directly on a metal stage that enabled rapid temperature equilibration.

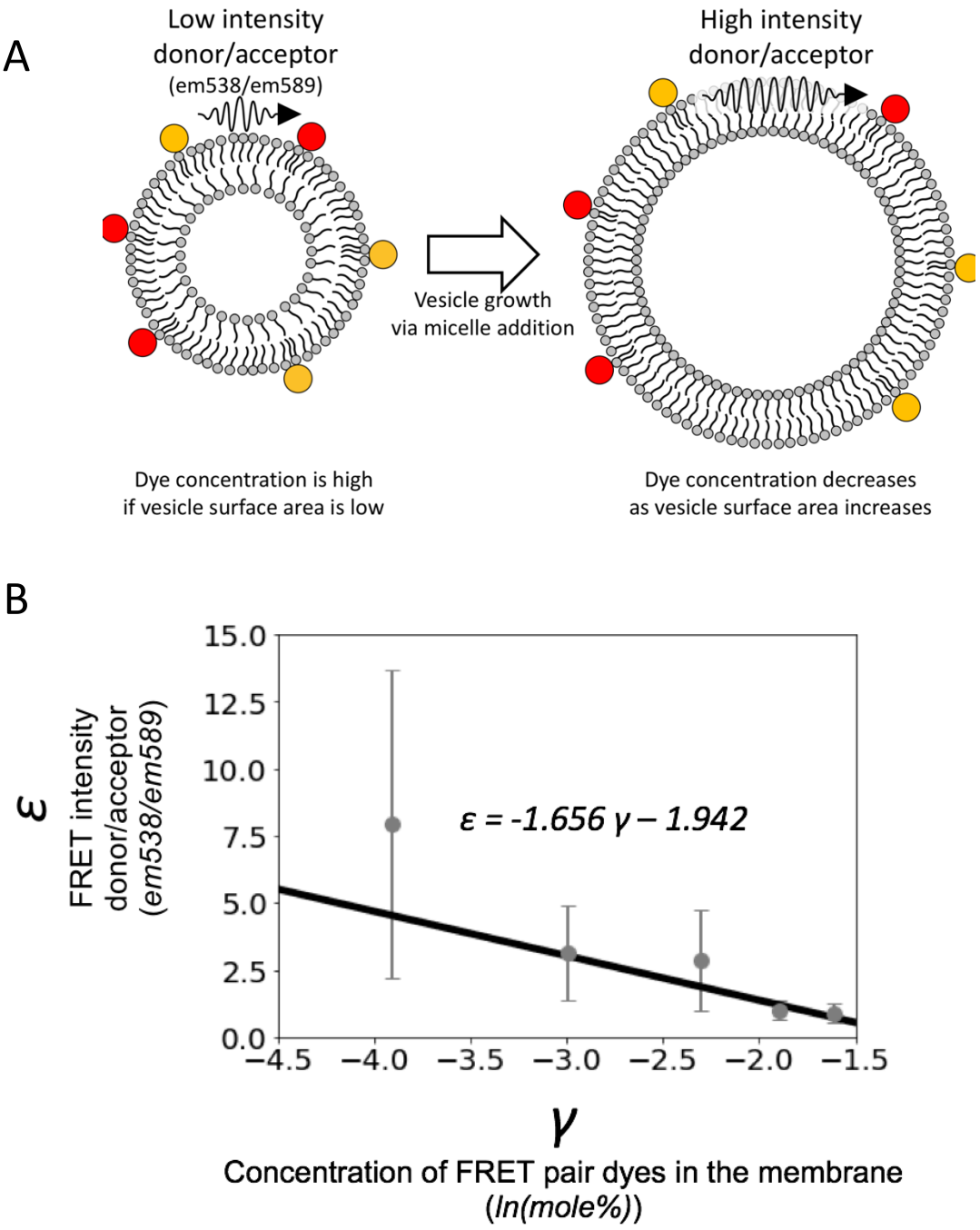

Figure S8: Ratio of donor/acceptor intensities (called the FRET intensity) decreases as the concentration of FRET dyes in the membrane increases. (A) Schematic representation of FRET within a membrane. (B) Phenomenological relationship between the FRET intensity ε (expressed as the ratio of donor fluorescence to acceptor fluorescence) and the concentration of dyes in the membrane γ (expressed as the natural logarithm of the mole ratio of dyes to amphiphiles[3]). We used this relationship together with equation 1 in the main text to calculate the surface area of vesicles. Error bars correspond to standard deviations from 2 independent measurements. This plot is reproduced from Todd et al. 2022 with permission of the authors[3].

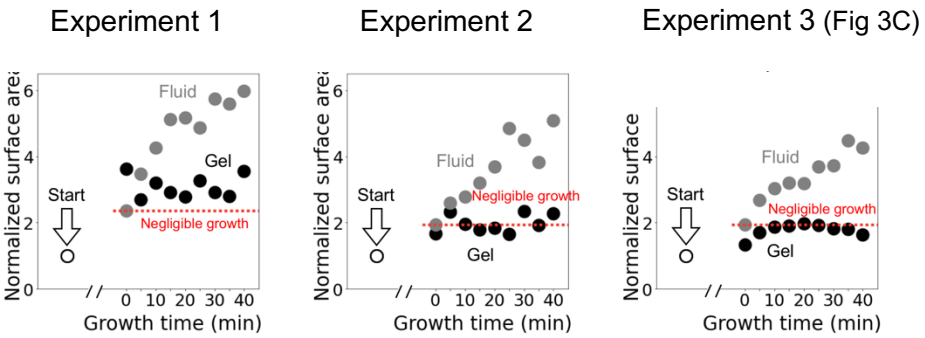

Figure S9: Replicate experiments 1 and 2 support the conclusion in Fig. 3C that the surface area of gel phase vesicles does not grow after additions of micelles. Experiment 1 was performed using an Eppendorf MasterCycler Gradient Thermal Cycler; fluid phase vesicles were maintained between 24.9°C and 25.1°C, and gel phase vesicles were maintained between 7.2°C and 7.7°C. Experiment 2 was performed as described in Fig S5; fluid phase vesicles were maintained between 23.6°C and 26.4°C, and gel phase vesicles were maintained between 0.9°C and 2.5°C.

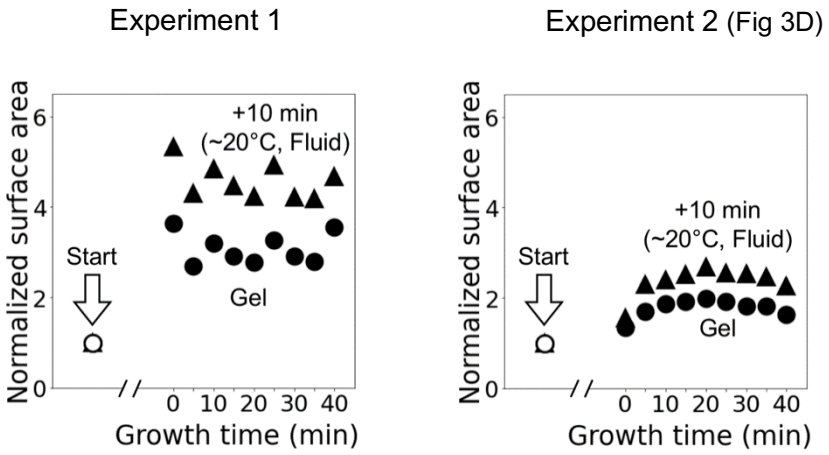

Figure S10: A repeat of the experiment reported in Fig. 3D of the main text confirms that vesicles grow after their membranes become fluid, even if micelles were added when the membranes were in the gel phase.

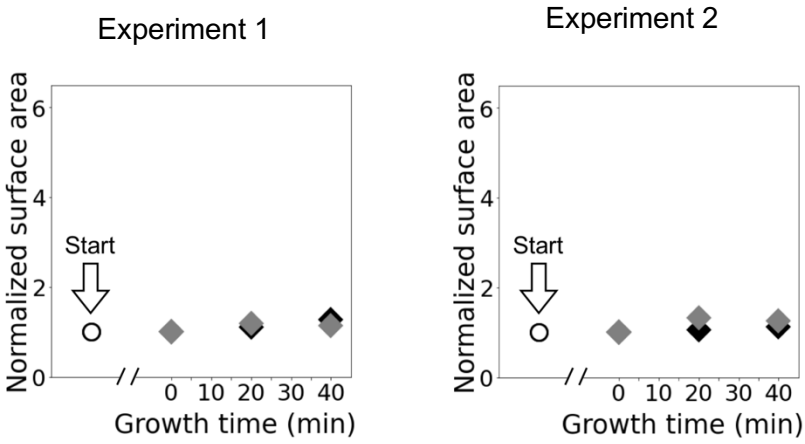

Figure S11: The two independent control experiments in this figure show that the surface area of fatty acid vesicles does not change when micelles are not added. Unlike the experiment reported in Fig 3, in which 10 µL of micelles (1M decanoic acid in 1 M NaOH) were added to 90 µL of vesicles, here 10 µL of 1M NaOH was added to 90 µL of vesicles. Gray points correspond to fluid phase vesicles, and black points correspond to gel phase vesicles.

Section 3: Additional encapsulation data

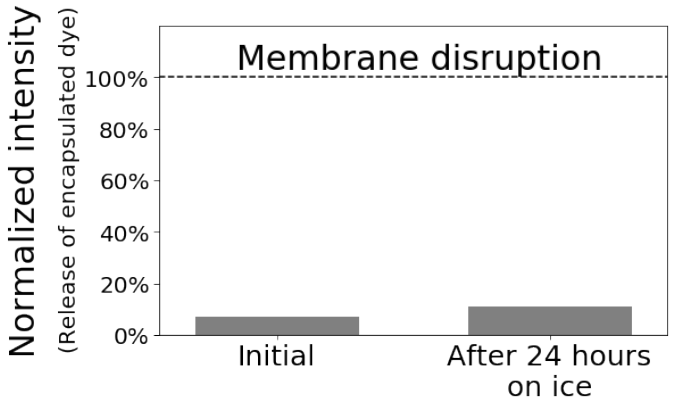

Figure S12: Vesicles composed of 1:1 decanoic acid: decanol retain encapsulated dye when the vesicles are kept on ice (~0°C) for 24 hours. The dotted line indicates the fluorescence intensity following disruption of the membrane by Triton X-100. Data are from a single experiment.

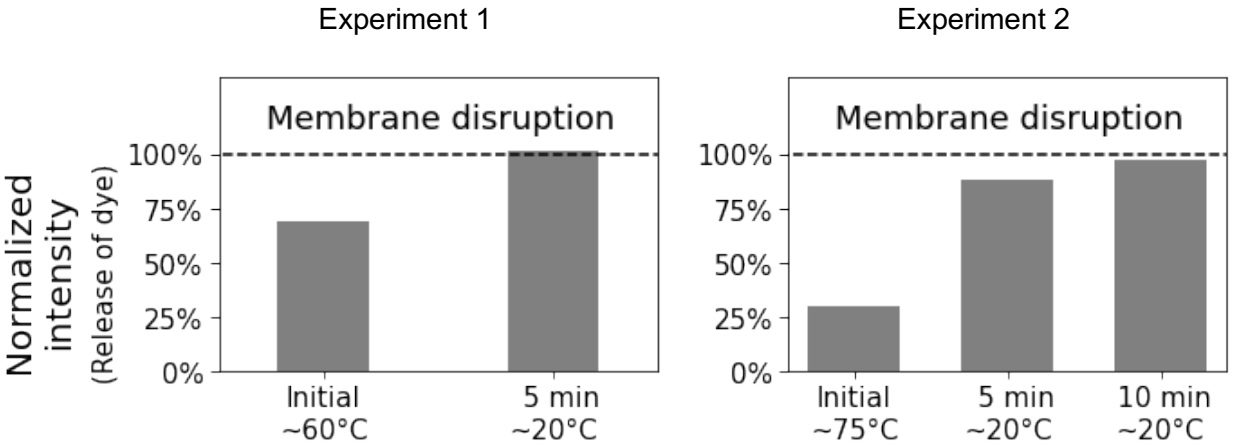

Figure S13: Vesicles composed of 1:1 tetradecanoic acid: tetradecanol release encapsulated dye after brief incubation at room temperature (~20°C). In experiment 1, vesicles were prepared as described for 12-carbon amphiphiles. In experiment 2, the temperature was raised to 75°C to improve the solubility of the amphiphiles during size-exclusion chromatography. In both experiments, fluorescence was measured either as close as possible to the initial temperature (60°C or 75°C), or at room temperature (~20°C). The dotted line indicates the fluorescence intensity following disruption of the membrane by Triton X-100.

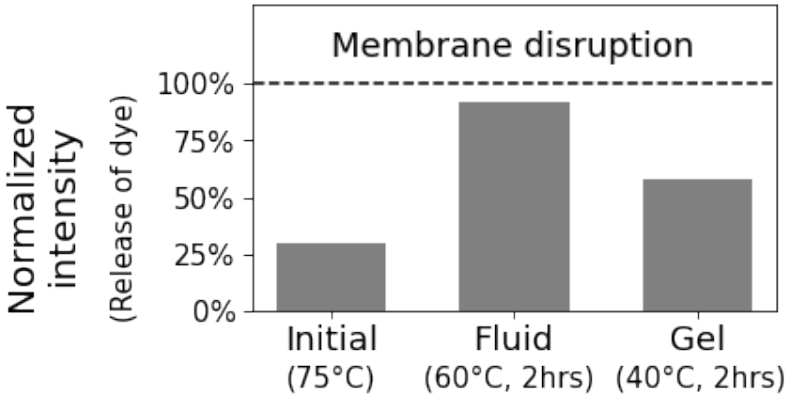

Figure S14: Vesicles composed of 1:1 tetradecanoic acid: tetradecanol retain encapsulated dye after 2 hrs in the gel phase (40°C). Vesicles were prepared as described for 12-carbon amphiphiles, except that the temperature was raised to 75°C to improve the solubility of the amphiphiles during size-exclusion chromatography. At 75°C, the sample contains vesicles that encapsulate dye. Fluorescence was measured either as close as possible to the initial temperature (75°C), or to the fluid temperature (60°C). The dotted line indicates the fluorescence intensity following disruption of the membrane by Triton X-100. Data are from a single experiment.

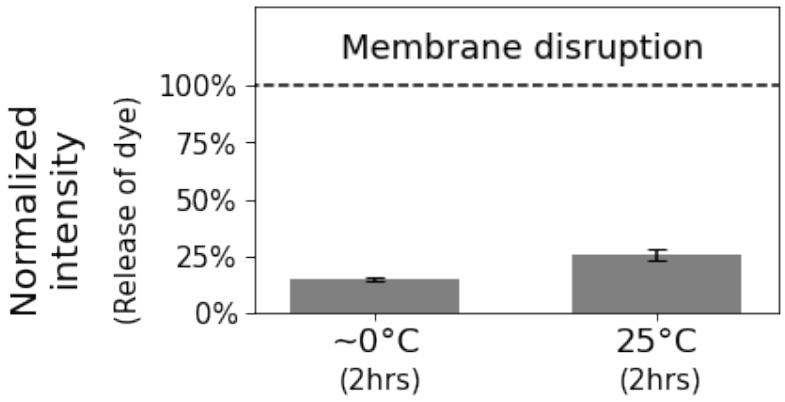

Figure S15: Vesicles composed of 1:1 nonanoic acid: nonanol retain encapsulated dye after 2 hrs at 0°C. Vesicles were prepared as described for 1:1 decanoic acid: decanol. The dotted line indicates the fluorescence intensity following disruption of the membrane by Triton X-100. Error bars are standard deviations from two independent experiments.

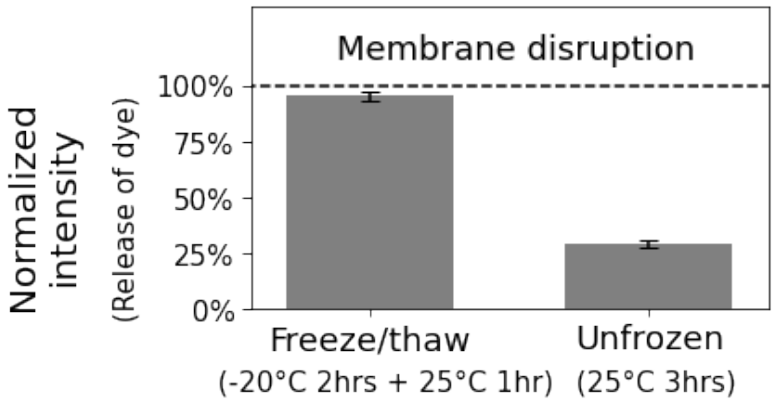

Figure S16: Vesicles composed of 1:1 nonanoic acid: nonanol release encapsulated dye after complete freezing at -20°C and thawing at 25°C. Vesicles were prepared as described for 1:1 decanoic acid: decanol. The dotted line indicates the fluorescence intensity following disruption of the membrane by Triton X-100. Error bars are standard deviations from two independent experiments.

Section 4: Supplementary references

(1) Kapoor, S.; Berghaus, M.; Suladze, S.; Prumbaum, D.; Grobelny, S.; Degen, P.; Raunser, S.; Winter, R. Prebiotic Cell Membranes That Survive Extreme Environmental Pressure Conditions. *Angewandte Chemie International Edition* **2014**, *53* (32), 8397–8401.

(2) Blicher, A.; Wodzinska, K.; Fidorra, M.; Winterhalter, M.; Heimburg, T. The Temperature Dependence of Lipid Membrane Permeability, Its Quantized Nature, and the Influence of Anesthetics. *Biophys J* **2009**, *96* (11), 4581–4591.

(3) Todd, Z. R.; Cohen, Z. R.; Black, R. A.; Keller, S. L.; Catling, D. C. Growth of Prebiotically Plausible Fatty Acid Vesicles Proceeds in the Presence of Prebiotic Building Blocks. *In prep.* **2022**.

Chapter 4:

Plausible Sources of Membrane-Forming Fatty Acids on the Early Earth: A Review of the Literature and an Estimation of Amounts

*This chapter was first published in *ACS Earth and Space Chemistry* in 2023. It was written in collaboration with Zoe R. Todd, Nicholas Wogan, Roy. A. Black, Sarah L. Keller, and David C. Catling.

Abstract

The first cells were plausibly bounded by membranes that assembled from fatty acids with at least 8 carbons. Although the presence of fatty acids on the early Earth is widely assumed within the astrobiology community, there is no consensus regarding their origin and abundance. In this review, we highlight three possible sources of fatty acids: (1) delivery by carbonaceous meteorites, (2) synthesis on metals delivered by impactors, and (3) electrochemical synthesis by spark discharges. We also discuss fatty acid synthesis by UV or particle irradiation, gas-phase ion-molecule reactions, and aqueous redox reactions. We compare estimates for the total mass of fatty acids supplied to Earth by each source during the Hadean eon, after an extremely massive asteroid impact that would have reset Earth's fatty acid inventory. We find that synthesis on iron-rich surfaces derived from the massive impactor, in contact with an impact-generated reducing atmosphere, could have contributed ~10^2 times more total mass of fatty acids than either subsequent delivery by carbonaceous meteorites or electrochemical synthesis. Additionally, we estimate that a single carbonaceous meteorite would not deliver a high enough concentration of fatty acids (~15 mM for decanoic acid) into an existing body of water on the Earth's surface to spontaneously form membranes unless the fatty acids were further concentrated by another mechanism, such as subsequent evaporation of the water. Our estimates rely heavily on various assumptions, leading to significant uncertainties; nevertheless, these estimates provide rough order-of-magnitude comparisons of various sources of fatty acids on the early Earth. We also suggest specific experiments to improve future estimates. Our calculations support the view that fatty acids would have been available on the early Earth. Further investigation is needed to assess the mechanisms by which fatty acids could have been concentrated sufficiently to assemble into membranes during the origin of life.

Main text

Cells use bilayer membranes to separate themselves from their environment. In modern cells, these membranes are composed of phospholipids. During the origin of cells on Earth, more primitive membranes likely played a similar role,[1] sequestering cellular building blocks[2,3] and polymers[4]. The hydrocarbons in modern phospholipids are tails of fatty acids connected by an ester linkage to the glycerol backbone. Fatty acids themselves can assemble into membranes. Fatty acids were likely more abundant than phospholipids on the early Earth, leading to a common hypothesis that the membranes of the first cells were composed of fatty acids[1].

Fatty acids consist of a hydrocarbon tail and a carboxylic acid headgroup (Fig 1). Saturated fatty acids with eight or more carbons in a linear chain can assemble into membranes[5]. Fatty acids with unsaturated[6] or branched[7] chains can also assemble into membranes, although in these cases it is unknown whether the minimum number of carbons for membrane assembly is greater or less than eight. Fatty acids with carboxylic acids at both ends of a carbon chain do not assemble into membranes on their own, although these dicarboxylic acids can incorporate into membranes when additional types of amphiphiles are present[8].

To form membranes, the solution pH must be within about half a unit of the effective pK_a of the fatty acid in a bilayer[5] (where $pK_a = -\log_{10}$ of the equilibrium constant, K_a, for the dissociation of the fatty acid into a proton and the negatively-charged amphiphile). If the solution pH is high enough such that the vast majority of headgroups are charged, or if the fatty acids have fewer than eight carbons, then fatty acids assemble into nanoscale micelles that cannot encapsulate aqueous solutes (Fig 1). On the other hand, if the solution pH is low enough that the vast majority of headgroups are uncharged, then fatty acids separate into an oil phase[9].

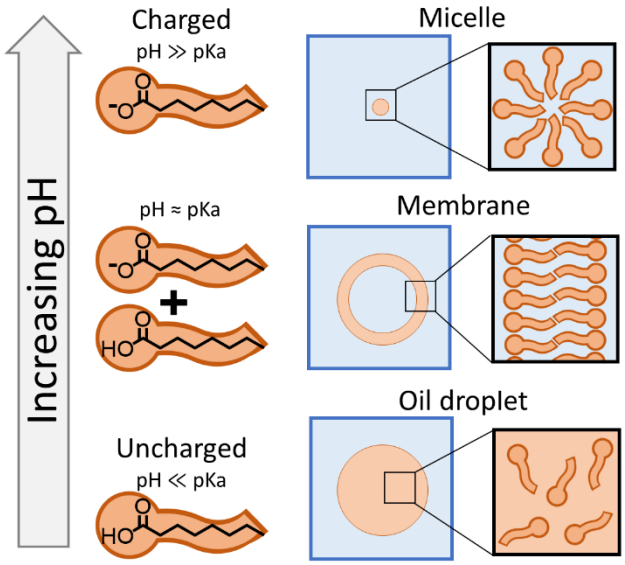

Figure 1: Fatty acid assembly depends on the pH of the surrounding solution. When the pH is below the effective pK_a of the fatty acids in a bilayer, fatty acids form an oil that is immiscible with the surrounding aqueous solution (bottom). When the pH is near the effective pK_a, fatty acids assemble into bilayers in a membrane (middle). Vesicles, spherical shells of these membranes, may have served as the membrane compartments for the first cells on Earth. When the pH is above the pK_a of the fatty acids in a bilayer, the fatty acids assemble into micelles, which cannot encapsulate aqueous solutes (top).

Fatty acid membranes provide some advantages for early cell replication compared to modern phospholipid membranes[9]. For example, fatty acid membranes are moderately permeable to salts and small organic molecules such as nucleotides, allowing internal replication of nucleic acids, which would have been critical for developing cells[10]. The surface area of these vesicles increases when they incorporate additional fatty acids from the environment into the membrane[11,12]. A growing vesicle can be supplied with fatty acids from micelles[11,13], or from other vesicles[14]. Vesicles that retain fatty acids grow while others shrink, which could have enabled competition between primitive cells for a limited supply of fatty acids[12]. After acquiring excess membrane surface area, primitive cells could have divided when exposed to modest shear stress[13,15]. Vesicles of phospholipids do not grow or divide as readily because aqueous solubility of a phospholipid with two hydrophobic tails is much lower than the solubility of a single-tailed fatty acid, so transfer through aqueous solution is slower[16,17].

Here, we review how membrane-forming fatty acids could have been supplied on the early Earth. We identify three relatively well-characterized sources of abiotic fatty acids: delivery by meteorites, synthesis on the surface of metal catalysts, and synthesis by electrochemistry (Fig 2). There are also reports of fatty acid syntheses that fall outside these categories, but these have been less

robustly investigated. We summarize the important details of the experiments that have been carried out and discuss whether similar reactions could have plausibly occurred on the early Earth. Finally, we estimate the total mass of fatty acids produced from each of the three relatively well-characterized sources during the Hadean eon, when the first cells are hypothesized to have formed[18].

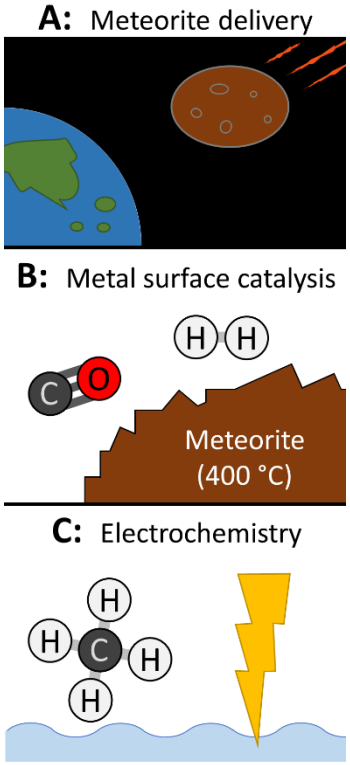

Figure 2: There are three well-characterized sources that could have provided fatty acids to the early Earth. A) Carbonaceous meteorites can deliver fatty acids[19–22]. B) Metal surfaces can catalyze fatty acid synthesis. As one example, Nooner and Oro (1979) mixed filings of the Canyon Diablo meteorite (containing iron and nickel) with deuterium and carbon monoxide gasses and heated to 400 °C to produce fatty acids[23]. Similar experiments have used pure Fe, Ni, or Fe- and Ni-containing minerals as catalysts, and a variety of carbon and hydrogen sources to synthesize fatty acids (Table 1). C) Fatty acids can also be synthesized during electrical sparking (Table 2). As one example, Yuen et al. (1981) used an electric discharge to synthesize fatty acids from methane[24].

CARBONACEOUS METEORITES DELIVER FATTY ACIDS TO EARTH

Fatty acids have been detected in a variety of carbonaceous meteorites that have landed on Earth[19–22], and molecules extracted from at least one such meteorite assemble into membranes[25]. At least 18 different carbonaceous meteorites have been analyzed, and both linear-chain and branched-chain fatty acids have been identified[26]. Depending on the type of carbonaceous meteorite, the

abundance of membrane-forming fatty acids can range from 1 ppb to 100 ppm by mass[26]. Recent reviews provide detailed analyses of meteoritic fatty acids[26,27]. Importantly, it remains unclear which types of reactions are responsible for synthesizing meteoritic fatty acids in space[26].

Could fatty acids delivered by carbonaceous meteorites have dissolved into water and assembled into membranes? Meteorites can fragment in airbursts during passage through the atmosphere, allowing some fatty acids to remain intact[28,29]. Meteorites with radius less than 100 m tend to fragment when differential pressure across the small body exceeds the material strength[28]. The Chelyabinsk ordinary chondrite meteorite (radius ~ 10 m) that fell in Russia in 2013 fragmented at an altitude above 25 km, and fragments were spread into an area 250 – 300 km^2 around the trajectory[30]. The largest fragment was ~ 0.7 m mean diameter and fell into a a lake. Fatty acids in carbonaceous chondrites would likely be similarly dispersed over a wide spatial area.

When meteorite fragments disperse into water on Earth's surface, fatty acids can dissolve. Numerical models suggest that nucleobases leach out of 20 cm meteorite fragments and mix into surrounding water within about three years[29]. At moderately alkaline pH, fatty acids can be even more soluble because of their charged headgroup. However, in order for fatty acids to assemble into membranes, the fatty acids must accumulate in solution above the critical vesicle concentration (~15 mM for decanoic acid[3]). If fatty acids are present at concentrations below the critical vesicle concentration, membrane assembly does not occur.

Here, we use the measured abundance of decanoic acid (a 10-carbon fatty acid) in carbonaceous meteorites[26] to calculate the volume of a meteorite fragment that would be required to deliver enough decanoic acid into water so that the concentration of decanoic acid equals the critical vesicle concentration. Although it is not known precisely how meteorite size, initial velocity, or impact angle influences the fraction of fatty acids that survive impact, we note that a large portion of the meteorite's initial mass (and thus a large portion of its fatty acids) may be destroyed by ablation and heating during travel through the atmosphere[31–33]. Given that our estimates rely on the average mass fraction of decanoic acid that has been recovered from natural carbonaceous meteorites, and that we do not know a priori the mass, velocity, and impact angle of each meteorite, we assume the measured fatty acid abundances represent the average survival over the entire population of possible impacts. Although this assumption introduces potential errors, a more precise calculation is beyond the scope of this study.

The volume of a meteorite fragment (V_{meteor}, expressed in m^3) that would be required to deliver enough decanoic acid to reach the critical vesicle concentration as a function of water volume (V_{water}, expressed in m^3) is given by equation 1:

$$V_{meteor} = \frac{C_{cvc}\, V_{water}\, w}{a\, \rho} \quad (1)$$

where C_{cvc} is the critical vesicle concentration for decanoic acid (1.5×10^{-5} moles/m^3 of water, equivalent to 15 mM), w is the molar mass of decanoic acid (0.1723 kg/mole), a is the dimensionless fraction of the meteorite's mass that is decanoic acid (2×10^{-5} for CM2 type meteorites), and ρ is the meteorite density (2100 kg/m^3 for CM type meteorites).

The result of our estimate is shown in Fig. 3. To deliver enough decanoic acid to form membranes, the volume of the meteorite fragment would have to exceed the volume of the waterbody. If a meteorite fragment were to land in a large enough waterbody to submerge the fragment, the decanoic acid that subsequently dissolved in the water would be too dilute to form membranes. However, this does not rule out membrane formation. The concentration of fatty acids could increase during dry periods, accompanied by a net loss of water due to evaporation[34]. Although we limited our calculation to decanoic acid because the critical vesicle concentration has been measured, a range of fatty acids from 8 to 12 carbons can be delivered simultaneously during a meteorite impact. The presence of these additional fatty acids could enable membrane formation at lower concentrations of decanoic acid[35,36]. We do not consider that CM type meteorites can contain significant water (up to ~9% by mass[37]). If all meteoritic fatty acids were to somehow dissolve in only this meteoritic water, the concentration of decanoic acid could exceed the critical vesicle concentration; this can be interpreted as an upper limit for the concentration of fatty acids delivered by a meteorite.

To conclude our section on carbonaceous meteorites, we find that meteorite delivery was unlikely to directly yield high enough aqueous concentrations of fatty acids to form membranes on the early Earth. Additional processes would have been necessary to further concentrate fatty acids above the critical vesicle concentration, which we cannot rule out.

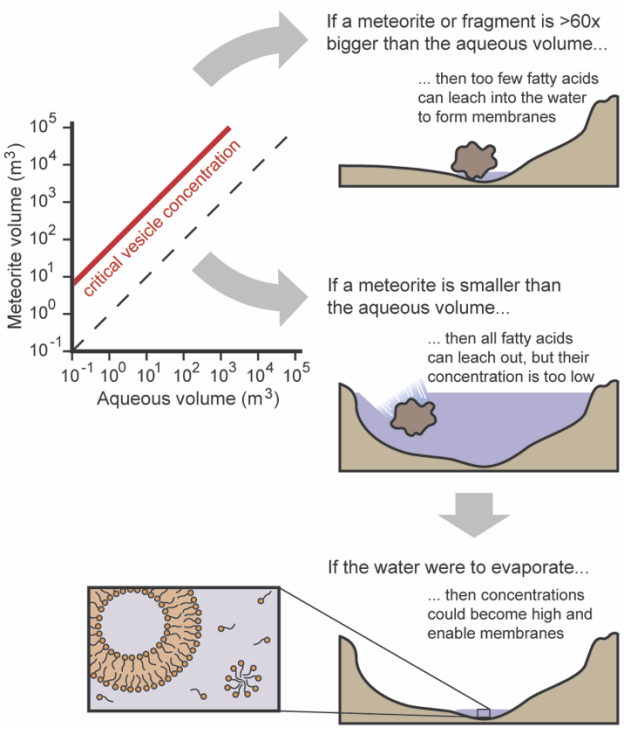

Figure 3: A single fragment of a carbonaceous meteorite cannot directly deliver enough decanoic acid to a body of water to form membranes. To exceed the critical vesicle concentration (~15 mM)[3], the volume of the meteorite would exceed the volume of the water. However, subsequent evaporation of the water could concentrate decanoic acid and enable membrane formation. A CM2 type meteorite is assumed because it contains the most decanoic acid on average (20 ppm by mass[26]). The density of CM-type meteorites is 2100 kg/m^3 [38]. Only meteorites with radii less than 100 m (~10^6 m^3 for a spherical meteorite) can fragment and impact the Earth's surface with low enough energy to preserve fatty acids[28,29]. See equation 1 for details of the calculation.

CATALYSIS OF FATTY ACID SYNTHESIS BY METAL SURFACES

The most commonly reported abiotic synthesis of fatty acids involves catalytic metal surfaces. Within this class of syntheses, Fischer-Tropsch reactions are the most thoroughly investigated. Fischer-Tropsch reactions occur when H_2 and either CO or CO_2 adsorb onto a metal surface[39,40]. Surfaces of solid iron or nickel are most commonly tested, although FeS, NiS, and Fe_3O_4 minerals have also been used to produce fatty acids[41–44]. In most experiments, metal surfaces must be heated above 150 °C to produce fatty acids. Catalysts contain metals in their reduced form; synthesis of membrane-forming fatty acids (at least 8 carbons) has not been demonstrated on oxidized metal surfaces[23,45–48]. Synthesis of fatty acids seems to occur at the gas-solid interface (Figure 4). Even in experiments designed to eliminate gaseous headspace, reactions are suggested to proceed in gaseous bubbles within the aqueous solution[48]. Whether or not an explicit gaseous headspace is present, the carbon-containing precursors are generally

supplied as gases. However, for experimental convenience in hydrothermal experiments, both formic acid and oxalic acid have been used as aqueous starting materials for fatty acid synthesis because both compounds decompose into H_2 and CO_2 at temperatures above 150°C[49].

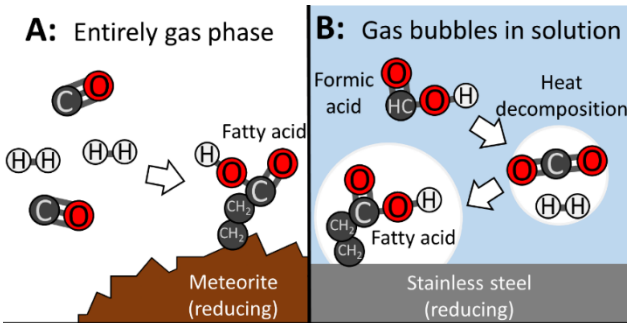

Figure 4: Fatty acid synthesis occurs at the interfaces between reducing metal surfaces and a gaseous headspace. A) Nooner and Oro (1976, 1979) showed that deuterium and carbon monoxide gases react together on the surface of hot (400°C) meteorite filings to produce membrane-forming fatty acids[23,50]. When the meteorite filings were artificially oxidized, fatty acid synthesis was not observed[23]. B) In hydrothermal experiments, McCollum et al. (1999) report that synthesis of membrane-forming fatty acids occurs within gaseous bubbles adsorbed onto oxidation-resistant stainless steel surfaces[49]. When oxidized metal surfaces are present instead of stainless steel, only short chain (< 5 carbons) fatty acids are formed[23,45–48]. In these hydrothermal experiments, aqueous formic acid or oxalic acid is used for experimental convenience as a source of H_2 and CO_2.

Metal-catalyzed reactions generally create a diverse mixture of product types, including hydrocarbons and fatty alcohols in addition to fatty acids[48,49,51–54]. For each type of product, molecules with more carbons are less abundant[40]. Many experiments have produced only short chain carboxylic acids, containing fewer than the 8 carbons required for membrane assembly[5] (Figure 5). The carbon chain of a fatty acid could be elongated upon further reaction with a metal catalyst[40], although additional experiments are required to validate this hypothesis. Table 1 summarizes experiments in the literature that have produced fatty acids using metal catalysts.

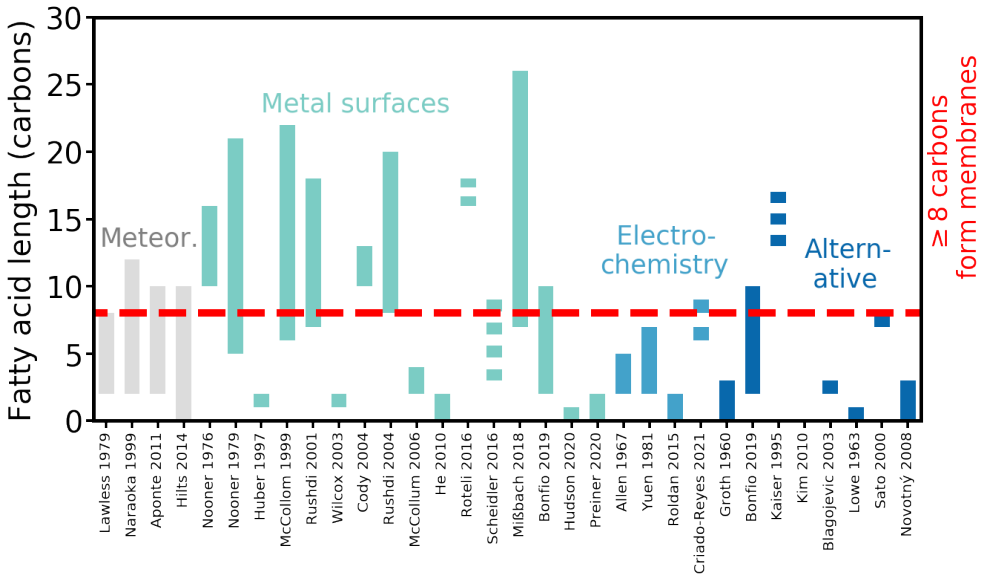

Figure 5: Length of fatty acids delivered by meteorites (labeled "Meteor.") or produced in abiotic synthesis experiments. Fatty acids with at least eight carbons, indicated by the dashed red line, can assemble into membranes. All the fatty acids produced are saturated and unbranched (except in Scheidler et al. 2016, where experiments also produced unsaturated fatty acids). Note that detection of a fatty acid with a certain length may not have been attempted during every experiment.

Metal-catalyzed reactions could have occurred on the early Earth after meteorite impacts, which delivered iron, nickel, and heat. Meteoritic metals could have been exposed to atmospheric H_2, CO_2, and CO, enabling surface-catalyzed synthesis of fatty acids. Extremely large impactors, about the size of the asteroid Vesta (~10^{20} kg), could have transformed the Earth into a global Fischer-Tropsch reactor with surface temperatures >100°C and high partial pressures of H_2, CO_2, and CO for thousands of years[55]. Catalytic metal surfaces would be required to produce fatty acids, so future research in this area will be especially valuable if it constrains the location and quantity of reduced metals after such impacts[56]. Although a large impact would have been catastrophic for any life that was already present on Earth, it could have potentially seeded Earth's post-impact surface with fatty acids and other necessary biomolecules, enabling life to emerge subsequently[57].

Ground-breaking experiments by Nooner and Oro (1976, 1979) modeled a post-impact scenario for fatty acid synthesis[23,50]. It remains uncertain how the yield of fatty acids depends on experimental

parameters such as partial pressure and temperature. Kinetic models for the Fischer-Tropsch process have been developed in industrial settings, which generally do not mimic plausible early Earth conditions, and the quantitative form of the models depends on the design of the reactor[58]. Until experiments are conducted to understand how fatty acid production depends on reaction parameters more relevant to the early Earth, there will be substantial uncertainty in estimates of production of fatty acids by metal catalysts on the early Earth.

Another natural setting in which metal catalyzed synthesis of fatty acids might occur are hydrothermal environments, where conversion of CO_2 and H_2 into fatty acids is thermodynamically favorable[59]. Fatty acids have been detected in natural hydrothermal systems; however, it is unclear what fraction of those fatty acids were produced by modern cells[60]. Ultramafic rocks (relatively Fe and Mg-rich, and Si-poor) are common at some deep sea hydrothermal vents[61]. Could metal-rich minerals within these rocks serve as catalysts for fatty acid synthesis? To address this question, we consider the oxidation state of the mineral surface. Ultramafic mineral surfaces become oxidized by reacting with seawater and generating H_2 in serpentinization reactions[62]. As noted above, to date there have been no reports of synthesis of membrane-forming fatty acids (at least 8 carbons) on oxidized metal surfaces[23,45–48]. Laboratory experiments failed to produce fatty acids with more than 2 carbons when oxidized olivine (ultramafic mineral with general composition $(Fe, Mg)SiO_4$) was the sole catalyst[45]. In these experiments, the olivine was heated in water for 96 days to allow ample time for oxidation by serpentinization, and formic acid was included as an additional source of H_2[45]. It is unknown whether olivine surfaces could catalyze fatty acid synthesis before becoming oxidized during serpentinization.

Hydrothermal experiments with oxidation-resistant stainless steel surfaces – clearly not natural settings – do produce fatty acids from formic acid up to 22 carbons[49]. However, these experiments also permitted vapor-phase reactions, which may have enabled production of longer fatty acids regardless of

the oxidation state of the surface. Thus, in natural hydrothermal settings, it remains unclear if catalytically active, reduced mineral surfaces could persist or be replenished quickly enough to catalyze fatty acid synthesis. Without a suitable catalyst, fatty acid synthesis would likely be slow or nonexistent in hydrothermal environments[62]. In conclusion, additional experiments are necessary to determine whether fatty acids could be synthesized in natural hydrothermal settings.

Table 1: Summary of experiments that used metal surfaces to catalyze synthesis of fatty acids. Unless otherwise specified, fatty acids were saturated and unbranched.

Year and Ref. #	Explicit gas phase?	Explicit aqueous phase?	H_2 source	Carbon source	Solid surface	Reaction conditions	Number of carbons per fatty acid
1976[50]	Yes	No	D_2 (g)	CO (g)	Meteorite filings and K_2CO_3	50 hrs at 370°C	10 - 16
1979[23]	Yes	No	D_2 (g)	CO (g)	Meteorite filings (containing iron and nickel) and carbonate salts	48 hrs at 400°C	5 - 21
1997[41]	Yes	Yes	N/A	CO (g) and CH_3SH (aq)	NiS - FeS	1 week at 100°C	2
1999[49]	Yes	Yes	Formic acid or oxalic acid (aq)	Formic acid or oxalic acid (aq)	Stainless steel	> 48 hrs at 175°C	6 - 22
2001[51]	No	Yes	Oxalic acid (aq)	Oxalic acid (aq)	Stainless steel	48 hrs at 100°C	7 – 18
2003[63]	Yes	No	N/A	CH_4 and CO_2	5% Pt/alumina	2 hrs with temperature increasing from 200 to 400°C	2
2004[64]	No	Yes	Formic acid (aq)	Nonane-thiol	Ni^0 *	6 hrs at 250°C and 200 Mpa	10 - 13
2004[52]	No	Yes	Oxalic acid (aq)	Oxalic acid (aq)	Stainless steel	18 hrs at 300°C	8 - 20
2006[48]	No	Yes	Formic acid (aq)	Formic acid (aq)	Powdered iron	86 hrs at 250°C and 325 bar	2 - 4
2010[65]	Yes	Yes	Water (l) **	CO_2 (aq)	Iron nanoparticles	25-200 hrs at fixed temp from 80-200°C	1 - 2
2016[66]	Yes	Yes	N/A	Formamide	Meteorite powder	24 hrs at 140°C	16, 18
2016[42]	Yes	Yes	N/A	CO (g) and acetylene (g)	NiS	1 week at 105°C and 2.5 bar	Saturated: 3, 5 Unsaturated: 3, 5, 7, 9
2018[53]	No	Yes	Oxalic acid (g)	Oxalic acid (g)	Stainless steel	> 66 hrs at 175°C	7 - 26
2018[67]	Yes	Yes	N/A	CO_2 (g)	Fe^0, Ni^0, Co^0	16 hrs at fixed temp from 30-150°C	1 – 2
2019[54]	Yes	Yes	N/A	HCN, Na_2CO_2, formaldehyde	Macroporous Ni	Multi-step reaction	2 - 10
2020[43]	No	Yes	Water (l)	CO_2 (aqueous)	NiS - FeS	50 min at room temperature	1
2020[44]	Yes	Yes	H_2 (g)	CO_2 (g)	Fe_3S_4, Fe_3O_4, Ni_3Fe	0-24 hrs at fixed temp from 60-100°C	1 -2

Note: The minimum and maximum length fatty acids may have been synthesized during separate experiments that were reported in the same reference.

* Other minerals were tested as well, although reactions with Ni^0 produced linear fatty acids with the greatest number of carbons.

** H_2 is generated when water oxidizes the Fe

ELECTROCHEMICAL SYNTHESIS OF FATTY ACIDS

Electrochemical reactions can generate diverse organic compounds, including amino acids[68,69], nucleobases[70], and fatty acids. For example, spark discharges between an electrode in the gaseous headspace and another electrode in either the same headspace[71] or in solution[24,72] can produce fatty acids. In the experiments summarized in Table 2, CH_4 in the gaseous headspace served as the source of carbon in three of the four experiments generating linear fatty acids of varying lengths, with only one experiment reporting chains long enough (at least 8 carbons) to form membranes[71]. An additional electric discharge experiment produced carbon chains of 2 - 6 carbons with carboxylic acids on both ends[73].

The goal of most electrochemical experiments is to simulate lightning strikes through a methane-rich atmosphere on the early Earth. However, attributes of natural lightning strikes are challenging to reproduce in the laboratory. Criado-Reyes et al. (2021) used a Tesla coil that generated a $3x10^4$ Volt potential for 7 days at room temperature[71]. In contrast, a natural lightning strike generates a potential of about 10^8 V for < 1 second[74], and temperatures of the air surrounding a lightning strike can reach 30,000°C[75]. Unfortunately, experimental evidence is lacking to describe how fatty acid yields depend on the voltage, duration, or total energy dissipated by laboratory sparking. Chyba and Sagan (1991) assumed that electrochemical production of organic molecules on early Earth should depend on the total amount of electrical energy dissipated by lightning strikes and coronal discharges[76]. Additional experiments are needed to validate this assumption.

Only slightly more is known about the role of the atmosphere and solid surfaces during electrochemical synthesis. Experiments by Schlesinger and Miller (1983) have shown that the yield of amino acids during sparking increases with partial pressure of CH_4[77]; similar experiments with fatty acids are still needed. Borosilicate glass as a substrate has also been shown to increase the yields of electrochemical fatty acid synthesis[71]. Although borosilicate does not occur naturally, silicates would have been ubiquitous on the early Earth because they are common rock-forming minerals. Additional experiments are necessary to better understand how the yields of electrochemical fatty acid production depend on the gaseous, solid, aqueous, and electrical environments. Nevertheless, the available experimental data suggest that fatty acid synthesis is possible under certain electrochemical conditions.

Table 2: Summary of electrochemical experiments that have synthesized fatty acids. All fatty acids were saturated and unbranched.

Year and Ref. #	Electric discharge description	Carbon source	Reaction conditions	Number of carbons per fatty acid
1967[72]	1 electrode in solution, 1 electrode in headspace	CH_4 (g)	96 hrs of discharge	2 – 5
1981[24]	1 electrode in solution, 1 electrode in headspace	CH_4 (g)	24 hrs of discharge; pH = 8	2 - 7
2015[78]	Both electrodes in solution	CO_2 (aq)	150 hrs with electric potential cycling from -0.8 V to 0.2 V	1 – 2
2021[71]	Both electrodes in headspace	CH_4 (g)	Discharge alternating on/off for 14 days. pH = 8.7. Room temperature.	6, 9

ALTERNATIVE TYPES OF FATTY ACID SYNTHESIS

In addition to the three main sources reviewed above, there are references in the literature to four alternative types of fatty acid synthesis (Figure 6, Table 3). These include photochemical reactions[54,79], irradiation by massive particles[80,81], gas-phase ion-molecule reactions[82], and redox reactions in aqueous solution[83–85].

There have been two reports of fatty acid synthesis by UV photochemistry. By irradiating a gaseous mixture of ethane and ammonia above boiling water (Figure 6A) at 185 nm and 254 nm, Groth and Weyssenhoff (1960) generated fatty acids 1-5 carbons long[79]. Bonfio et al. (2019) used a multi-step procedure to synthesize longer-chain fatty acids capable of membrane assembly[54]. UV irradiation at 254 nm was used in one step, and catalysis by a nickel surface was used in a subsequent step. Photochemistry could provide a plausible explanation for the presence of fatty acids on the surface of the early Earth because UV radiation down to ~200 nm could have penetrated prebiotic atmospheres[86]. The experiments by Groth and Weyssenhoff (1960) did not generate fatty acids when methane was used instead of ethane[79]; further investigation is needed to determine whether radiation from realistic early Earth solar spectra could have enabled photochemical conversion of methane into fatty acids. In contrast, Bonfio et al. (2019) used starting materials that are more plausibly prebiotic such as formaldehyde, HCN, NaH_2PO_4, Na_2CO_3, and NaSH[54], but these reagents impose a constraint on the geochemical scenario for the early Earth. In a separate experiment by Dworkin et al. (2001), membrane-forming amphiphiles were synthesized by irradiating ultra-cold ices composed of 100:50:1:1

H_2O:CH_3OH:NH_3:CO with 121.6 nm and ~160 nm UV photons, although the identity of these amphiphiles was not determined[87].

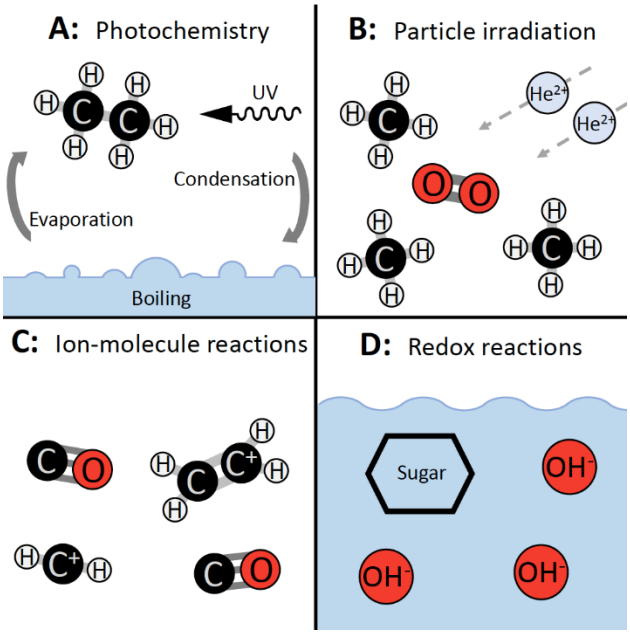

Figure 6: Alternative reaction types that have demonstrated fatty acid synthesis. A) Groth and Weyssenhoff (1960) used UV photochemistry to convert ethane into fatty acids[79]. B) Kaiser et al. (1995) irradiated an ultra-cold (10K) mixture of ~99% CH_4 and ~1% O_2 with 9 MeV alpha particles to produce fatty acids[80]. C) Blagojevic et al. (2003) report reactions between gas phase ions (CH_2^+ and $C_2H_4^+$) and CO to produce in fatty acids[82]. D) Novotny et al. (2008) report decomposition of monosaccharides into fatty acids under mild alkaline conditions (50 mM NaOH)[84].

The second type of "alternative" fatty acid synthesis is irradiation by particles. Experiments of this type were designed to simulate chemistry in the outer solar system, rather than the early Earth. By irradiating an ultra-cold (10 K) mixture of ~99% CH_4 and ~1% O_2 with 9 MeV alpha particles, Kaiser et al. (1995) produced linear fatty acids with either 13, 15, or 17 carbons[80] (Figure 6B). In a subsequent experiment by Kim et al. (2010), an ultra-cold (10 K) mixture of CO_2 and hydrocarbons (1 – 6 carbons) was irradiated with 5 keV electrons. The presence of carboxylic acids was confirmed by Fourier-transform infrared spectroscopy, but specific fatty acids were not identified[81].

A third alternative fatty acid synthesis is discussed by Blagojevic et al. (2003). In their experiments, reactions between gas phase ions (CH_2^+ and $C_2H_4^+$) and molecules (CO) resulted in carboxylic acids with 2 or 3 carbons (Figure 6C). Additional gas-phase ion-molecule reactions to produce formic acid (e.g. $CH_4 + O_2^+ \rightarrow HCOOH_2^+ + H$) have been suggested but not validated experimentally[88]. These reactions were suggested to occur in the interstellar medium, and the relevance to early Earth conditions has not been explored.

The fourth group of lesser studied fatty acid syntheses are redox reactions. Three sets of redox reactions have been shown to produce fatty acids in solution. The first experiments from Sato et al. (2000) use hydrogen peroxide to oxidize fatty aldehydes (7 - 8 carbons) to produce fatty acids with the same carbon chain length[85]. It is unlikely that sufficient hydrogen peroxide would have been present on the early Earth[89]. In the second set of experiments, Novotny et al. (2008) report decomposition of monosaccharides (3 - 6 carbons) into linear carboxylic acids (1 – 3 carbons) under mild alkaline conditions (50 mM NaOH, Figure 6D)[84]. Diverse monosaccharides are obtained in low yield during the formose reaction[90], and alkaline lakes on early Earth could have been sites for decomposition into short chain fatty acids[91,92]. Finally, Lowe et al. (1963) report production of formic acid and potentially other carboxylic acids by heating a mixture of ammonia and hydrogen cyanide to 90°C[83]. Hydrogen cyanide is considered a prebiotic reagent that can be sequestered and concentrated as ferrocyanide within early Earth environments[91,93].

There are numerous additional pathways for synthesis of short-chain (1 – 3 carbons) linear fatty acids[94], but because membrane assembly requires fatty acids with at least 8 carbons, we have generally omitted them. We are unaware of any abiotic mechanisms by which carbon chains of existing fatty acids are elongated. Modern cells synthesize fatty acids from acetyl-CoA using the sophisticated enzyme complex fatty acid synthetase[95]. Because the intermediate compounds that are produced during this

process are unstable, it is believed that fatty acid synthesis via these reactions would have occurred at a negligible rate on the early Earth before the emergence of enzyme catalysts[96]. Finally, thermodynamic calculations suggest that fatty acids can be synthesized from polyaromatic hydrocarbons[97], but, to our knowledge, this synthesis has never been demonstrated experimentally.

Table 3: Summary of experiments that have synthesized fatty acids by the mechanisms illustrated in Fig. 6. All fatty acids were saturated and unbranched.

Year and Ref. #	Reactants	Reaction conditions	Number of carbons per fatty acid
Photochemistry			
1960[79]	Ethane, NH_3, H_2O	1 week of UV irradiation (185 and 254 nm)	1 - 3
2019[54]	HCN, Formaldehyde, Na_2CO_2	Multi-step reaction (254 nm UV irradiation and catalysis by Ni surface)	2 - 10
Irradiation by massive particles			
1995[80]	CH_4, O_2	Irradiation with 9 MeV alpha particles at 10°K	13, 15, 17
2010[81]	CO_2, hydrocarbons (1 – 6 carbons)	Irradiation with 5 keV electrons at 10°K	Undetermined
Gas-phase ion-molecule reactions			
2003[82]	CO and either CH_2^+ or $C_2H_4^+$	CH_4 and C_2H_4 are ionized and reacted together in the presence of He and trace H_2O at 0.35 torr and room temperature.*	2 - 3
Redox reactions in solution			
1963[83]	HCN, NH_3	90°C for 18 hrs	1
2000[85]	Fatty aldehydes (either 7 or 8 carbons)	30% H_2O_2 solution at 90°C for 2 hrs	7 or 8
2008[84]	Either Glucose, fructose, arabinose, glyceraldehyde, or dihydroxyacetone	50 mM NaOH for 1 hr	1 - 3

* The authors suggest that their synthesis models low temperature, low pressure environments.

CRITICAL ANALYSIS OF ANALYTICAL TECHNIQUES

Many of the reactions discussed above produce a wide variety of fatty acids and other products. Uniquely identifying products can be challenging, and determining the concentration of each product is

even more difficult. In Table 4, we summarize the reported concentrations of fatty acids from each experiment, and comment on potential limitations of the analyses. In general, the papers in Table 4 convincingly identify fatty acids of various lengths, but do not provide substantial evidence for the fatty acid concentrations that they report. Moreover, many papers report only relative concentrations of fatty acids (e.g., X% of all products, by mass or moles) instead of absolute concentrations (e.g., X moles or X grams), so it is difficult to compare product yields between experiment types. An ideal strategy for characterization and absolute quantitation of fatty acids was employed by Yuen et al. (1981), which involved chromatography and tandem mass spectrometry with isotope-labelled internal standards to eliminate matrix effects[24]. Additional synthesis experiments that determine the absolute concentration of fatty acids would be valuable.

ESTIMATING THE CONTRIBUTION OF EACH SOURCE TO THE EARLY EARTH FATTY ACID INVENTORY

To gauge the relative importance of each fatty acid source for the origin of cells, we go beyond purely reviewing the literature, with a goal to estimate how much fatty acid could be supplied to the early Earth from three sources: delivery by carbonaceous chondrites, catalysis by metal surfaces, and electrochemistry. Many relevant parameters for these estimates lack experimental constraints, so assumptions are needed. Our first assumption is that cells formed during the latter part of the Hadean eon; the full eon is ~4.6 to 4.0 billion years ago (Gya)[18]. During the early Hadean, Earth was potentially hit by impactors that were large enough to sterilize the planet's surface and reset the fatty acid inventory, so life must have originated after the last such event[98]. The median age of estimates for the last ocean-vaporizing impact is ~4.3 Gya[99], and we assume that life had originated by 4.0 Gya[18]. In the subsections below, we construct back-of-the-envelope estimates for the total mass of fatty acids supplied to Earth during this interval. Our estimates are based on empirical data from the literature, and

we indicate when existing models from the literature are applied. We articulate our assumptions and suggest experiments that will help to refine these estimates. Our estimates cannot distinguish fatty acids that form membranes (more than 8 carbons) from those that do not (less than 8 carbons) because the empirical data that one of our estimates relies on does not do so.

Meteorite delivery

We estimate the total mass of 2-12 carbon fatty acids delivered to Earth by carbonaceous meteorites, M_s, using the following equation:

$$M_S = M \sum_{L=2}^{12} f_L \quad (2)$$

In equation 2, f_L is the dimensionless fraction of a meteorite's mass that comprises fatty acids of length L, where length denotes the number of carbons in the fatty acid chain. Values for f_L depend on the type of carbonaceous meteorite, and average values can range from 10^{-9} for 10-carbon fatty acids to 10^{-3} for 2-carbon fatty acids[26]. Parameter M is the time-integrated total mass of carbonaceous meteorites with radius 1-100 m that would impact Earth from 4.3 Gya to 4.0. To estimate M, we integrate the following equation for the mass flux (kg/year) at time t (years) in the past from 4.3 Gya to 4.0 Gya:

$$\dot{m} = 8.9C(1 + 1.6 \times 10^{-10} e^{t/\tau}) \left({m_{\max}}^{0.46} - {m_{\min}}^{0.46}\right) q \quad (3)$$

This equation is adapted from Chyba and Sagan (1992)[100]. In equation 3, $\dot{m}$ is the mass flux (mass/year) of the total mass of carbonaceous meteorites with mass from m_{min} to m_{max} that would impact Earth per year; C is the frequency of carbonaceous meteorites relative to all types of meteorites (~4%) observed in the meteorite fall record[101]; τ is a decay constant of 144 million years for the impactor population; m_{min} is taken as the mass of a meteorite with 1 m radius; m_{max} is taken as the mass of a meteorite with 100 m

radius; and q is 1 $kg^{0.54}$/year. We assume that all meteorites are spherical with a uniform density (2.1 g/cm^3 for CM-type meteorites[38] or 3.2 g/cm^3 for C2-type meteorites [102]), so we can calculate the mass of a meteorite in kilograms from its radius in meters. Meteorites with radius less than 100 m can fragment into pieces that impact the Earth's surface with low enough energy that fatty acids are preserved[28,29]. Using equation 3, we estimate that ~10^{15} kg of carbonaceous meteorites with radii between 1-100 m would impact Earth from 4.3 Gya to 4.0 Gya.

Assuming that all carbonaceous meteorites are either CM1-type or C2-type, we use equations 2 and 3 to calculate bounds for the total mass of fatty acids of length 2-12 carbons that could have been delivered to Earth from 4.3 Gya to 4.0 Gya. We find that 10^{10} - 10^{13} kg of fatty acids of length 2-12 carbons could have been delivered to Earth from 4.3 Gya to 4.0 Gya by carbonaceous meteorites. Our estimate varies over three orders of magnitude because the abundance of fatty acids on each type of meteorite (f_L) varies considerably between different meteorite types. We consider only carbonaceous chondrites because they are the most well-characterized type of meteorite that can deliver fatty acids. We do not quantify additional uncertainties in the meteorite flux, nor do we quantify the influence of meteorite size, impact velocity, and impact angle on the fraction of fatty acids that survive impact[103].

Catalysis by metal surfaces after Vesta-sized impact

Next, we consider fatty acid synthesis on metal surfaces in the wake of a large Vesta-sized (~10^{20} kg) asteroid impact on the early Earth. Such an impact would deliver iron to Earth's surface which could both act as a catalyst for fatty acid synthesis and generate a H_2-rich atmosphere by reactions with steam from the vaporized ocean[57], as in equation 4:

$$H_2O + Fe \rightarrow H_2 + FeO \quad (4)$$

An H_2-rich atmosphere appears to be required for fatty acid synthesis by metal catalysts (Table 1). Such a massive asteroid impact would generate a high enough surface temperature to destroy most organic molecules on Earth; then as the Earth cooled, synthesis of fatty acids could occur in the H_2-rich atmosphere. We consider only the last impactor that would reset Earth's fatty acid inventory, which most likely hit Earth between 4.4 – 4.1 Gya[99]. Significantly smaller meteorite impacts would not generate high partial pressures of H_2 in the atmosphere because H_2 escapes to space on timescales of ~ 10^6 – 10^7 years. Additionally, small impactors would not generate global surface temperatures above 200°C, which we assume is the minimum temperature required for fatty acid synthesis. Therefore, smaller impactors would not produce many fatty acids, and we do not consider their contribution here.

To estimate the total mass of fatty acids synthesized by metal catalysts after such an impact, M_c, we assume that the rate of fatty acid synthesis depends linearly on gas pressures according to the following equation:

$$M_c = \int_{t_{400}}^{t_{200}} k_c \, m_{cat} \, P_{H2}(t_c) \, P_{CO}(t_c) \, dt_c \qquad (5)$$

Here, k_c is an empirical rate constant for fatty acid synthesis, calculated from the results of experiments at 400°C by Nooner and Oro (1979). Nooner and Oro (1979) provide the only measurement to date of the absolute concentration of fatty acids produced on a metal catalyst in the absence of an aqueous phase. The value of k_c is 7.4×10^{-6} kilograms of 6-18 carbon fatty acids (excluding 12-carbon fatty acids, for which data are not available) per bar of H_2, per bar of CO, per hour of reaction time, per kilogram of catalytic surface available[23]. Only the summed mass of all fatty acids is reported in Nooner and Oro (1979); there is no information given about the number of moles of individual fatty acids. Here, m_{cat} is the mass of available metal catalyst, in kilograms. P_{H2} and P_{CO} are the atmospheric partial pressures of hydrogen and carbon monoxide, respectively, in bar; both are functions of time, t_c. The product is integrated over time from t_{400} to t_{200}. t_{400} is the number of hours after the impact until the surface

temperature reaches 400°C, and t_{200} is the number of hours after the impact until the surface temperature cools to 200°C. We assume that fatty acid synthesis occurs at a constant rate k_c when the temperature is within this range, and that the reaction does not occur when the temperature is outside this range.

We assume that 33% of the asteroid's mass is iron, and that 7% of this iron (i.e. 2.3% of the total asteroid mass) remains available on Earth's surface to catalyze fatty acid synthesis (giving m_{cat} = 2.3×10^{18} kg) based on a linear extrapolation of the impact simulation performed by Citron and Stewart (2022)[56]. The assumption of ~33% mass iron follows Zahnle et al. (2020)[55], which is the total iron in high iron enstatite (EH-type) meteorites[104] and also the fraction of Earth's mass in its iron core[105]. Bodies with enstatite composition are candidates for impactors that hit the Earth after the Moon-forming impact and Earth's core formation, although the contribution of carbonaceous versus enstatite compositions is debated[106–108]. In EH enstatites, which are highly reduced, most of the iron is metallic with a smaller fraction of iron sulfide[109]. In a post-impact vapor plume, the iron is vaporized into atoms, which condensation sequences show condenses to form metallic iron with subsequent cooling[110].

We assume that another fraction of the asteroid's iron (between 1% and 90%) is used to generate H_2 from excess H_2O according to equation 4. We adapted a thermochemical model previously developed by Zahnle et al. (2020) to compute P_{H2}, P_{CO}, and temperature as a function of time after the impact[55]. Depending on the fraction of the asteroid's iron that reacts with water to produce H_2 gas, we find that P_{H2} ranges from 10^{-3} bar to 10^{-1} bar, and P_{CO} ranges from 10^{-3} bar to 10^{-7} bar. We calculate that the Earth's post-impact temperature would be between 200˚C and 400˚C for ~1000 years, and we assume that fatty acid synthesis occurs at a constant rate during this time. Equation 5 estimates that between 10^{11} kg and 10^{15} kg of fatty acids of length 6-18 carbons (excluding 12 carbons, for which data are not available) would be synthesized using metal catalysts in the wake of a Vesta-size impactor.

Our estimate for the total mass of fatty acids synthesized by metal catalysts is uncertain because many factors in our analysis are poorly constrained. First, it is not known whether reduced metals would remain exposed to the atmosphere on Earth's surface after an extremely massive impact[56]. Additionally, it is unclear how an H_2O steam atmosphere would influence the rate of fatty acid synthesis; steam can affect the yield of Fischer-Tropsch reactions in different ways, depending on the type of catalyst and the type of reaction product[111]. Even without steam in the atmosphere, it is uncertain whether the rate of fatty acid synthesis depends linearly on gas partial pressures. Kinetic models for the Fischer-Tropsch process have been developed in industrial settings, which generally do not mimic plausible early Earth conditions; functions for each partial pressure depend on the engineered design of the catalyst[58]. Additionally, the effect of temperature on the final product distribution also appears to depend on the catalyst design[51,112]. Separate experiments indicate that the yield of fatty acids depends linearly on the amount of catalyst surface area that is available[64]. In general, further experiments are necessary to constrain these reaction parameters and the precise functional form for fatty acid production in plausible conditions on the early Earth.

Electrochemical synthesis

We also construct an estimate for the total mass of fatty acids that could be synthesized by electrochemistry from 4.3 Gya to 4.0 Gya,

$$M_E = R\, P_{CH4}\, B\, t_E \quad (6)$$

where *R* is an empirical rate constant for synthesis of 2 – 7 carbon fatty acids, calculated from electrochemical experiments by Yuen et al. (1981). The value of *R* is 1.1×10^{-17} kilograms of 2-7 carbon fatty acids per bar of CH_4, per joule of electrical energy dissipated by sparking, per hour of reaction time[24]. Although there are no electrochemical experiments that provide absolute concentrations for

membrane-forming (longer than 8 carbons) fatty acids, Yuen et al. (1981) provide absolute concentrations for the largest number of fatty acids. P_{CH4} is the partial pressure of methane on the early Earth, which we estimate to be between 10^{-15} bar to 10^{-1} bar after the last Vesta-sized (~10^{20} kg) asteroid impact. This value depends on the initial pre-impact abundance of atmospheric CO_2, the fraction of the impactor's iron that becomes oxidized (1 – 100%), and the importance of methane-forming catalysts, which may reduce the quench temperature of methane, thereby increasing its abundance[55]. B is the amount of electrical energy dissipated by lightning and corona discharges on the Hadean Earth during a year. We assume that B is 1.5x10^{18} joules per year, which is the electrical energy dissipated per year on the modern Earth[76]. t_E is the reaction time in years. We assume t_E is 10^5 years, which is an estimate for the lifetime of a methane-rich atmosphere after a Vesta-sized (~10^{20} kg) asteroid impact[55].

By applying these assumptions, we calculate that 10^{-4} kg to 10^{10} kg of fatty acids of length 2-7 carbons could be synthesized on Earth from 4.3 Gya to 4.0 Gya by electrochemical reactions. Although separate experiments have shown that electrochemical production of membrane forming fatty acids with more than 8 carbons is possible[71], membrane-forming fatty acids were not detected in the experiments by Yuen et al. (1981), so our estimate is not directly informative about membrane formation on early Earth. More data are needed about the absolute concentration of membrane-forming fatty acids produced during electrochemical experiments.

There are uncertainties in our electrochemistry estimate. First, there is insufficient information available to estimate the total energy dissipated by the Tesla coil during the experiments by Yuen et al. (1981)[24]. If we assume that their tesla coil used 30,000 V potential[71] and 15 amps, we can estimate that ~4x10^{10} joules of energy were dissipated during their 24 hour experiment. Even if we had perfect information about the Tesla coil voltage and current, it might not be straightforward to estimate the amount of energy that is usable for chemical synthesis[113]. Furthermore, we assumed that the yield of

fatty acids depends only linearly on the amount of available electrical energy[76]. Further experiments are necessary to validate this assumption. Experiments by Schlesinger and Miller (1983) suggest that the yield of amino acids during sparking does increase linearly with increasing CH_4 partial pressure (below ~ 0.06 bar)[77], but further experiments are needed to validate this assumption for fatty acids.

Summary of estimates

We have compared the total mass of fatty acids produced by 3 different sources during the Hadean eon, following the last extremely massive impactor that would have reset Earth's fatty acid inventory. We estimate that 10^{11} kg to 10^{15} kg of 6-18 carbon fatty acids could have been synthesized by metal catalysts derived from the massive impactor. The total mass of fatty acids that could have been delivered by carbonaceous meteorites is 10^{10} kg to 10^{13} kg of 2-12 carbon fatty acids. The yield of 2-7 carbon fatty acids from electrochemical processes is potentially smaller, between 10^{-4} kg to 10^{10} kg. Consequently, an integrated supply of fatty acids to the Earth's surface from all sources (dominated by metal surface production) between ~10^{-4} kg/m^2 to ~10^{0} kg/m^2 is possible, given the Earth's surface area of 5.1x10^{14} m^2.

Ultimately, the local concentration of fatty acids determines whether or not membranes form, so the possible sources should be evaluated by this criterion. Although meteorites could have delivered a significant mass of fatty acids across the Earth's surface, the aqueous concentration of fatty acids in a single waterbody would not have been high enough to form membranes without evaporating a significant volume of water (Fig 3). In contrast, a local stockpile of fatty acids could have been produced on atmosphere-exposed metal surfaces after an extremely massive impact, and subsequent dissolution into water could have allowed membrane formation. Although little is known about the electrochemical synthesis rate for membrane-forming fatty acids, repeated lightning strikes into the same small waterbody seem unlikely, so it is unclear whether a high enough local concentration of membrane-

forming fatty acids could have formed via electrochemistry. Fatty acids in aqueous solution can be degraded via photochemistry[114], so fatty acids that are slowly synthesized by electrochemistry may not have attained high enough concentrations to form membranes, whereas a large stockpile of fatty acids dissolving off metal surfaces may have been less sensitive to photochemical degradation.

Although the estimates above have many uncertainties, they are valuable as a first attempt to quantitatively compare fatty acid sources on the early Earth. We hope that future experiments can further constrain these estimates.

ALTERNATIVE AMPHIPHILES

In addition to fatty acids, alternative types of amphiphiles may have been synthesized on the early Earth[115–117], and these amphiphiles might have incorporated into the membranes of the earliest cells. For example, alcohols are commonly produced along with fatty acids in many experiments[48,49,51–54], and long-chain fatty alcohols are known to stabilize fatty acid membranes[5,118]. An excess of long-chain fatty alcohols form oil droplets, and the oil may disrupt membranes. In addition, phase-separated coacervates could have served as another type of prebiotic compartment[119,120], and fatty acid membranes may have even assembled around such coacervate compartments[121].

CONCLUSIONS

Fatty acids can assemble into membranes and could have formed the boundaries for the first cells. Our review highlights multiple potential sources of fatty acids on the early Earth. The three most well-characterized sources are meteorite delivery, synthesis on metal surfaces, and synthesis by

electrochemistry. Other reactions involving photochemistry, irradiation by massive particles, ion-molecule reactions, and diverse redox reactions in aqueous solution may have also produced fatty acids in natural environments. To refine quantitative estimates for the relative importance of each fatty acid source, more detailed constraints are needed. We highlight the following questions to help any future experiments have the widest possible impact:

- How do the yields of fatty acids from metal-catalyzed reactions depend on the temperature and the partial pressures of gasses such as H_2, CO_2, and H_2O? Data would help to constrain estimates for fatty acid production following ocean-vaporizing impacts.
- Can membrane-forming fatty acids (> 8 carbons) form in hydrothermal experiments with non-oxidized, ultramafic minerals as the sole catalyst? Data would elucidate the potential for fatty acid production at hydrothermal vents.
- How do the yields of fatty acids depend on the voltage, duration, or total energy dissipated during electrical sparking? Data would help to constrain estimates for fatty acid production during lightning strikes.
- What are the absolute concentrations of fatty acids in these types of experiments?

In summary, our analysis suggests that fatty acids could have been available on the early Earth. We have not assessed whether those fatty acids would have been sufficiently concentrated to assemble into membranes except in the limited case of small meteorite fragments delivered into aqueous environments. For fatty acids supplied via alternative sources, further data are required to assess the potential for membrane formation. By investigating possible sources of fatty acids on the early Earth, we hope to constrain the environmental setting for the origin of cells.

Table 4: Summary of analytical techniques in each report. Unless otherwise specified, fatty acids are saturated and unbranched.

Year and Ref. #	Carbons per fatty acid	Yield information	Analytical techniques	Identification of products	Quantitation of product concentrations

Method 1: Metal surface catalysis					
1976[50]	10 - 16	None	GC-MS	Unambiguous identification by comparing fragmentation spectra from (derivatized) products with fragmentation spectra from authentic standards.	N/A
1979[23]	5 - 21	≤ 0.08 % yield of normal fatty acids (by mass, relative to initial CO)	GC-MS GC-FID	Unclear how products were identified. Comparisons with authentic standards were not shown.	No data were shown to validate the FID procedure for quantifying product concentrations.
1997[41]	2	≤ 40% yield (by moles, relative to initial CH_3SH)	GC-MS	Unclear how products were identified. Comparisons with authentic standards were not shown.	No data were shown to validate the GC-MS procedure for quantifying product concentrations.
1999[49]	6 - 22	≤ 20.8% of all products are fatty acids (by moles)	GC-MS GC-FID	Unambiguous identification of select products by comparing fragmentation spectra and retention times with authentic standards.	No data were shown to validate the procedure for quantifying product concentrations.
2001[51]	7 - 18	≤ 20% yield of fatty acids (by mass, relative to total mass of reaction extract)	GC-MS	Unambiguous identification by comparing fragmentation spectra and retention times with authentic standards.	No data were shown to validate the GC-MS procedure for quantifying product concentrations.
2003[63]	2	None	Diffuse reflectance infrared Fourier transform spectroscopy	Using diffuse reflectance infrared Fourier transform spectroscopy, experimental spectra were compared to authentic standards.	N/A
2004[64]	10 - 13	C10: 53.7% yield.	GC-MS	Unambiguous identification by comparing fragmentation spectra with authentic standards.	Calibration curves were described in the text to validate the procedure for quantifying product concentrations. Pentadecane was used as an internal standard for all compounds.
2004[52]	8 - 20	2.8% of all products are fatty acids (unclear whether by mass or moles)	GC-MS	Unambiguous identification by comparing fragmentation spectra and retention times with authentic standards.	No data were shown to validate the MS procedure for quantifying product concentrations.
2006[48]	2 - 4	C2: 1% yield C3: 0.06% yield C4: <0.02 % yield (by moles, relative to initial formic acid)	GC-MS GC-FID	Unclear how products were identified. Comparisons with authentic standards were not shown.	No data were shown to validate the FID procedure for quantifying product concentrations.
2010[65]	1 - 2	C2: 9.0 mM C3: 3.5 mM	GC-MS	Unambiguous identification by comparing fragmentation spectra with authentic standards.	Calibration curves were shown to validate the procedure for quantifying product concentrations. Internal standards were not used.

2016[66]	16, 18	C16: 0.011% yield C18: 0.02% yield (by moles, relative to initial NH_2CHO)	GC-MS	Unambiguous identification by comparing fragmentation spectra with authentic standards and literature references.	No data were shown to validate the MS procedure for quantifying product concentrations. Betulinic acid was mentioned as the internal standard for all products.
2016[42]	Saturated: 3, 5 Unsaturated: 3, 5, 7, 9	C3: 7.1 mM C5: 0.3 mM C3 unsaturated: 3.9 mM C5 unsaturated: 7.9 mM C7 unsaturated: 0.44 mM C9 unsaturated: 0.011 mM	GC-MS	For most products, unambiguous identification by comparing fragmentation spectra with authentic standards. For select products, identification was inferred based on mass spectra and relative retention times.	Calibration curves were mentioned (but not shown) to validate the procedure for quantifying product concentrations. For some products, calibration curves were made with authentic standards. For other products, related compounds were used for calibration. Internal standards were not used.
2018[53]	7 - 26	7.8% of all products are fatty acids (unclear whether by mass or moles)	GC-MS	Unambiguous identification by comparing fragmentation spectra with authentic standards.	No data were shown to validate the GC-MS procedure for quantifying product concentrations. N-eicosane d42 was mentioned as the internal standard for all experiments.
2018[67]	1 – 2	Formic acid: ≤ 0.21% yield Acetic acid: ≤ 0.053% yield (by moles, relative to initial CO_2)	GC-MS ^{1}H-NMR	Unambiguous identification by comparing GC-MS fragmentation spectra and retention times with authentic standards. In addition, H-NMR spectra were compared with authentic standards.	H-NMR calibration curves were shown to validate the procedure for quantifying product concentrations. Authentic standards were used, and DSS-Na was used as an internal standard.
2019[54]	2 - 10	36% of all 8-carbon products are fatty acids (by moles)	^{1}H-NMR	Unambiguous identification by comparing H-NMR spectra with authentic standards.	Data from H-NMR spectra were used to determine relative abundance of fatty acids. Internal standards were not discussed.
2020[43]	1	C1: 1.5 μM	^{1}H-NMR 13C-NMR	Unambiguous identification by comparing H-NMR spectra with authentic standards.	H-NMR spectra with an internal standard (acetone) were used to quantitate formate concentration. To validate the quantitation, additional formate was spiked in and a corresponding increase in H-NMR signal was observed.
2020[44]	1 -2	C1: ~20% yield C2: ~ 0.4% yield (by moles, relative to CO_2)	LC-MS LC-UV ^{1}H-NMR	Unambiguous identification by comparing H-NMR spectra with authentic standards.	H-NMR calibration curves were mentioned (not shown) to validate the procedure for quantifying product concentrations. Authentic standards were used, and DSS-Na was used as an internal standard.
Method 2: Electrochemistry					
1967[72]	2 – 5	C2: 1.2% yield C3: 0.86% yield C4: 0.088% yield	GC-MS	Unambiguous identification by comparing fragmentation spectra and retention times with authentic standards.	No data were shown to validate the MS procedure for quantifying product concentrations.

		C5: 0.066% yield (by moles, relative to initial CH_4)			
1981[24]	2 - 7	C2: 0.10% yield C3: 0.68% yield C4: 0.014% yield C5: 0.0050% yield C6: 0.00073% yield C7: 0.00025% yield (by moles, relative to initial CH_4)	GC-MS	Unambiguous identification by comparing fragmentation spectra and retention times with authentic standards.	Calibration curves were shown to validate the procedure for quantifying product concentrations. Singly deuterated internal standards were used for each product.
2015[78]	1 – 2	C1: ~ 1 μmoles C2: ~ 0.5 μmoles	^{1}H-NMR	Unambiguous identification by comparing H-NMR spectra with authentic standards.	H-NMR calibration curves were shown (for formic acid) to validate the procedure for quantifying product concentrations. Authentic standards were used and Me_4Si was used as an internal standard.
2021[71]	6, 9	C6: ≤ 0.0078% yield C9: ≤ 0.016% yield (by mass, relative to total mass of reaction extract)	GC-MS	Unambiguous identification by comparing fragmentation spectra and retention times with authentic standards.	No data were shown to validate the GC-MS procedure for quantifying product concentrations.
Method 3: Photochemistry					
1960[79]	1 – 3	C1: 82 μmoles C2: 234 μmoles C3: 15 μmoles	Silica gel chroma-tography Acid-base titration	Identification of products by comparison of retention times with authentic standards.	Silica gel chromatography was used to separate C1, C2, and C3 products. Each putatively pure product was titered with NaOH to find the equivalence point.
2019[54]	2 - 10	36% of all 8-carbon products are fatty acids (by moles)	^{1}H-NMR	Unambiguous identification by comparing H-NMR spectra with authentic standards.	Data from H-NMR spectra were shown and used to determine relative abundance of fatty acids. Internal standards were not mentioned.
Method 4: Irradiation by massive particles					
1995[80]	13, 15, 17	C13: maximum 18.6 picograms C15: maximum 83.9 picograms C17: maximum 57.0 picograms	GC-MS	Unclear how products were identified. Comparison with authentic standards were not mentioned.	No data were shown to validate the MS procedure for quantifying product concentrations.
2010[81]	Undeter-mined	10^{16} molecules /cm^2	FTIR	Regions of the FTIR spectra were considered diagnostic for carboxylic acids: ν(O–H) stretching = 3500–2500 cm^{-1}.	The intensity of the FTIR spectra at 1720 cm^{-1} was used to provide an upper limit on carboxylic acid concentration.

				v(C=O) = 1720 cm^{-1} v(C–O) = 1282 cm^{-1}	
Method 5: Gas-phase ion-molecule reactions					
2003[82]	2 - 3	No data were shown	GC-MS	Unambiguous identification by comparing fragmentation spectra with authentic standards.	N/A
Method 6: Redox reactions in solution					
1963[83]	1	No quantitative data were shown	Paper chromat-ography	The presence of formic acid was inferred based on comparison of paper chromatography mobility to an authentic standard, and based on reaction with ammoniacal silver nitrate.	N/A
2000[85]	7 or 8	C7: 73 - 85% yield C8: 65% yield (unclear whether by mass or moles)	GC-MS	Unambiguous identification by comparing fragmentation spectra with authentic standards.	No data were shown to validate the GC-MS procedure for quantifying product concentrations.
2008[84]	1 - 3	C1: 7-20% yield C2: 0.7-12% yield C3: < 0.01 – 0.2% yield (by moles)	GC-MS	Unambiguous identification by comparing fragmentation spectra with publicly available data and by comparing retention times with authentic standards.	Calibration curves were mentioned (but not shown) to validate the procedure for quantifying product concentrations. An internal standard (heptadecane) was used.

ACKNOWLEDGMENTS

We thank Milomir Suvira for helpful discussions of electrochemical sparking, Dr. Martin Sadilek for helpful discussion of analytical methods, Dr. Kevin Zahnle for helpful comments on all portions of the manuscript, and Dr. Ben K.D. Pearce for sharing raw data on meteoritic fatty acid abundances that he and his colleagues compiled[26]. This work was supported in part by grant NNX17AK86G (Exobiology) from NASA to S.L.K, by a grant (MCB 1925731) from the NSF to S.L.K, and by a grant (511570FY20, DCC) from the Simons Foundation to D.C.C. ZRC was funded by an NSF fellowship (NSF GRFP DGE 1762114).

REFERENCES

(1) Deamer, D.; Dworkin, J. P.; Sandford, S. A.; Bernstein, M. P.; Allamandola, L. J. The First Cell Membranes. *Astrobiology* **2002**, *2* (4), 371–381.

(2) Black, R. A.; Blosser, M. C.; Stottrup, B. L.; Tavakley, R.; Deamer, D. W.; Keller, S. L. Nucleobases Bind to and Stabilize Aggregates of a Prebiotic Amphiphile, Providing a Viable Mechanism for the Emergence of Protocells. *Proc. Natl. Acad. Sci USA* **2013**, *110* (33), 13272.

(3) Cornell, C. E.; Black, R. A.; Xue, M.; Litz, H. E.; Ramsay, A.; Gordon, M.; Mileant, A.; Cohen, Z. R.; Williams, J. A.; Lee, K. K.; Drobny, G. P.; Keller, S. L. Prebiotic Amino Acids Bind to and Stabilize Prebiotic Fatty Acid Membranes. *Proc. Natl. Acad. Sci USA* **2019**, *116* (35), 17239–17244.
(4) Xue, M.; Black, R. A.; Cohen, Z. R.; Roehrich, A.; Drobny, G. P.; Keller, S. L. Binding of Dipeptides to Fatty Acid Membranes Explains Their Colocalization in Protocells but Does Not Select for Them Relative to Unjoined Amino Acids. *J. Phys. Chem. B* **2021**, *125* (29), 7933–7939.
(5) Apel, C. L.; Deamer, D. W.; Mautner, M. N. Self-Assembled Vesicles of Monocarboxylic Acids and Alcohols: Conditions for Stability and for the Encapsulation of Biopolymers. *Biochimica et Biophysica Acta (BBA) - Biomembranes* **2002**, *1559* (1), 1–9.
(6) Cistola, D. P.; Hamilton, J. A.; Jackson, D.; Small, D. M. Ionization and Phase Behavior of Fatty Acids in Water: Application of the Gibbs Phase Rule. *Biochemistry* **1988**, *27* (6), 1881–1888.
(7) Jordan, S. F.; Rammu, H.; Zheludev, I. N.; Hartley, A. M.; Maréchal, A.; Lane, N. Promotion of Protocell Self-Assembly from Mixed Amphiphiles at the Origin of Life. *Nat Ecol Evol* **2019**.
(8) Caschera, F.; de la Serna, J. B.; Löffler, P. M. G.; Rasmussen, T. E.; Hanczyc, M. M.; Bagatolli, L. A.; Monnard, P.-A. Stable Vesicles Composed of Monocarboxylic or Dicarboxylic Fatty Acids and Trimethylammonium Amphiphiles. *Langmuir* **2011**, *27* (23), 14078–14090.
(9) Chen, I. A.; Walde, P. From Self-Assembled Vesicles to Protocells. *Cold Spring Harb Perspect Biol* **2010**, *2* (7), a002170.
(10) Mansy, S. S.; Schrum, J. P.; Krishnamurthy, M.; Tobé, S.; Treco, D. A.; Szostak, J. W. Template-Directed Synthesis of a Genetic Polymer in a Model Protocell. *Nature* **2008**, *454* (7200), 122–125.
(11) Chen, I. A.; Szostak, J. W. A Kinetic Study of the Growth of Fatty Acid Vesicles. *Biophysical Journal* **2004**, *87* (2), 988–998.
(12) Chen, I. A. The Emergence of Competition Between Model Protocells. *Science* **2004**, *305* (5689), 1474–1476.
(13) Zhu, T. F.; Szostak, J. W. Coupled Growth and Division of Model Protocell Membranes. *J. Am. Chem. Soc.* **2009**, *131* (15), 5705–5713.
(14) Toparlak, Ö. D.; Wang, A.; Mansy, S. S. Population-Level Membrane Diversity Triggers Growth and Division of Protocells. *JACS Au* **2021**, *1* (5), 560–568.
(15) Hanczyc, M. M.; Fujikawa, S. M.; Szostak, J. W. Experimental Models of Primitive Cellular Compartments: Encapsulation, Growth, and Division. *Science* **2003**, *302* (5645), 618–622.
(16) Coreta-Gomes, F. M.; Vaz, W. L. C.; Moreno, M. J. Effect of Acyl Chain Length on the Rate of Phospholipid Flip-Flop and Intermembrane Transfer. *J Membrane Biol* **2018**, *251* (3), 431–442.
(17) Budin, I.; Szostak, J. W. Physical Effects Underlying the Transition from Primitive to Modern Cell Membranes. *Proc. Natl. Acad. Sci USA* **2011**, *108* (13), 5249–5254.
(18) Bell, E. A.; Boehnke, P.; Harrison, T. M.; Mao, W. L. Potentially Biogenic Carbon Preserved in a 4.1 Billion-Year-Old Zircon. *Proc. Natl. Acad. Sci USA* **2015**, *112* (47), 14518.
(19) Lawless, J. G.; Yuen, G. U. Quantification of Monocarboxylic Acids in the Murchison Carbonaceous Meteorite. *Nature* **1979**, *282* (5737), 396–398.
(20) Naraoka, H.; Shimoyama, A.; Harada, K. Molecular Distribution of Monocarboxylic Acids in Asuka Carbonaceous Chondrites from Antarctica. *Orig Life Evol Biosph* **1999**, *29* (2), 187–201.
(21) Aponte, J. C.; Alexandre, M. R.; Wang, Y.; Brearley, A. J.; Alexander, C. M. O.; Huang, Y. Effects of Secondary Alteration on the Composition of Free and IOM-Derived Monocarboxylic Acids in Carbonaceous Chondrites. *Geochimica et Cosmochimica Acta* **2011**, *75* (9), 2309–2323.
(22) Hilts, R. W.; Herd, C. D. K.; Simkus, D. N.; Slater, G. F. Soluble Organic Compounds in the Tagish Lake Meteorite. *Meteoritics & Planetary Science* **2014**, *49* (4), 526–549.
(23) Nooner, D. W.; Oro, J. Synthesis of Fatty Acids by a Closed System Fischer-Tropsch Process. In *Hydrocarbon Synthesis from Carbon Monoxide and Hydrogen*; Advances in Chemistry; American Chemical Society, 1979; Vol. 178, pp 159–171.

(24) Yuen, G. U.; Lawless, J. G.; Edelson, E. H. Quantification of Monocarboxylic Acids from a Spark Discharge Synthesis. *J Mol Evol* **1981**, *17* (1), 43–47.
(25) Deamer, D. W. Boundary Structures Are Formed by Organic Components of the Murchison Carbonaceous Chondrite. *Nature* **1985**, *317* (6040), 792–794.
(26) Lai, J. C.-Y.; Pearce, B. K. D.; Pudritz, R. E.; Lee, D. Meteoritic Abundances of Fatty Acids and Potential Reaction Pathways in Planetesimals. *Icarus* **2019**, *319*, 685–700.
(27) Sephton, M. A. Organic Compounds in Carbonaceous Meteorites. *Nat. Prod. Rep.* **2002**, *19* (3), 292–311.
(28) Chyba, C. F.; Thomas, P. J.; Brookshaw, L.; Sagan, C. Cometary Delivery of Organic Molecules to the Early Earth. *Science* **1990**, *249* (4967), 366–373.
(29) Pearce, B. K. D.; Pudritz, R. E.; Semenov, D. A.; Henning, T. K. Origin of the RNA World: The Fate of Nucleobases in Warm Little Ponds. *Proc. Natl. Acad. Sci USA* **2017**, *114* (43), 11327–11332.
(30) Zamozdra, S. N.; Kocherov, A. V. Underwater Excavations and Welcoming the Big Meteorite. In *Chelyabinsk Superbolide*; Gorkavyi, N., Dudorov, A., Taskaev, S., Eds.; Springer Praxis Books; Springer International Publishing: Cham, 2019; pp 122–147.
(31) Popova, O. P.; Jenniskens, P.; Emel'yanenko, V.; Kartashova, A.; Biryukov, E.; Khaibrakhmanov, S.; Shuvalov, V.; Rybnov, Y.; Dudorov, A.; Grokhovsky, V. I.; Badyukov, D. D.; Yin, Q.-Z.; Gural, P. S.; Albers, J.; Granvik, M.; Evers, L. G.; Kuiper, J.; Kharlamov, V.; Solovyov, A.; Rusakov, Y. S.; Korotkiy, S.; Serdyuk, I.; Korochantsev, A. V.; Larionov, M. Yu.; Glazachev, D.; Mayer, A. E.; Gisler, G.; Gladkovsky, S. V.; Wimpenny, J.; Sanborn, M. E.; Yamakawa, A.; Verosub, K. L.; Rowland, D. J.; Roeske, S.; Botto, N. W.; Friedrich, J. M.; Zolensky, M. E.; Le, L.; Ross, D.; Ziegler, K.; Nakamura, T.; Ahn, I.; Lee, J. I.; Zhou, Q.; Li, X.-H.; Li, Q.-L.; Liu, Y.; Tang, G.-Q.; Hiroi, T.; Sears, D.; Weinstein, I. A.; Vokhmintsev, A. S.; Ishchenko, A. V.; Schmitt-Kopplin, P.; Hertkorn, N.; Nagao, K.; Haba, M. K.; Komatsu, M.; Mikouchi, T.; (THE CHELYABINSK AIRBURST CONSORTIUM). Chelyabinsk Airburst, Damage Assessment, Meteorite Recovery, and Characterization. *Science* **2013**, *342* (6162), 1069–1073.
(32) Artemieva, N. A.; Shuvalov, V. V. From Tunguska to Chelyabinsk via Jupiter. *Annual Review of Earth and Planetary Sciences* **2016**, *44* (1), 37–56.
(33) Mehta, C.; Perez, A.; Thompson, G.; Pasek, M. A. Caveats to Exogenous Organic Delivery from Ablation, Dilution, and Thermal Degradation. *Life* **2018**, *8* (2), 13.
(34) Clark, B. C.; Kolb, V. M. Comet Pond II: Synergistic Intersection of Concentrated Extraterrestrial Materials and Planetary Environments to Form Procreative Darwinian Ponds. *Life* **2018**, *8* (2), 12.
(35) Cape, J. L.; Monnard, P.-A.; Boncella, J. M. Prebiotically Relevant Mixed Fatty Acid Vesicles Support Anionic Solute Encapsulation and Photochemically Catalyzed Trans-Membrane Charge Transport. *Chem. Sci.* **2011**, *2* (4), 661–671.
(36) Budin, I.; Prywes, N.; Zhang, N.; Szostak, J. W. Chain-Length Heterogeneity Allows for the Assembly of Fatty Acid Vesicles in Dilute Solutions. *Biophysical Journal* **2014**, *107* (7), 1582–1590.
(37) Trigo-Rodríguez, J. M.; Rimola, A.; Tanbakouei, S.; Soto, V. C.; Lee, M. Accretion of Water in Carbonaceous Chondrites: Current Evidence and Implications for the Delivery of Water to Early Earth. *Space Sci Rev* **2019**, *215* (1), 18.
(38) Britt, D. T.; Consolmagno, G. J. S. J. Stony Meteorite Porosities and Densities: A Review of the Data through 2001. *Meteoritics & Planetary Science* **2003**, *38* (8), 1161–1180.
(39) de Klerk, A. Fischer–Tropsch Synthesis. In *Fischer-Tropsch Refining*; John Wiley & Sons, Ltd: Hoboken, NJ; pp 73–103.
(40) Schulz, H.; Beck, K.; Erich, E. Mechanism of the Fischer Tropsch Process. In *Studies in Surface Science and Catalysis*; Bibby, D. M., Chang, C. D., Howe, R. F., Yurchak, S., Eds.; Methane Conversion; Elsevier, 1988; Vol. 36, pp 457–471.
(41) Huber, C.; Wächtershäuser, G. Activated Acetic Acid by Carbon Fixation on (Fe,Ni)S Under Primordial Conditions. *Science* **1997**, *276* (5310), 245–247.

(42) Scheidler, C.; Sobotta, J.; Eisenreich, W.; Wächtershäuser, G.; Huber, C. Unsaturated C 3,5,7,9 - Monocarboxylic Acids by Aqueous, One-Pot Carbon Fixation: Possible Relevance for the Origin of Life. *Scientific Reports* **2016**, *6* (1), 1–7.
(43) Hudson, R.; Graaf, R. de; Rodin, M. S.; Ohno, A.; Lane, N.; McGlynn, S. E.; Yamada, Y. M. A.; Nakamura, R.; Barge, L. M.; Braun, D.; Sojo, V. CO2 Reduction Driven by a PH Gradient. *Proc. Natl. Acad. Sci USA* **2020**, *117* (37), 22873–22879.
(44) Preiner, M.; Igarashi, K.; Muchowska, K. B.; Yu, M.; Varma, S. J.; Kleinermanns, K.; Nobu, M. K.; Kamagata, Y.; Tüysüz, H.; Moran, J.; Martin, W. F. A Hydrogen-Dependent Geochemical Analogue of Primordial Carbon and Energy Metabolism. *Nat Ecol Evol* **2020**, *4* (4), 534–542.
(45) McCollom, T. M.; Seewald, J. S. A Reassessment of the Potential for Reduction of Dissolved CO2 to Hydrocarbons during Serpentinization of Olivine. *Geochimica et Cosmochimica Acta* **2001**, *65* (21), 3769–3778.
(46) McCollom, T. M.; Seewald, J. S. Experimental Constraints on the Hydrothermal Reactivity of Organic Acids and Acid Anions: I. Formic Acid and Formate. *Geochimica et Cosmochimica Acta* **2003**, *67* (19), 3625–3644.
(47) McCollom, T. M.; Seewald, J. S. Experimental Study of the Hydrothermal Reactivity of Organic Acids and Acid Anions: II. Acetic Acid, Acetate, and Valeric Acid. *Geochimica et Cosmochimica Acta* **2003**, *67* (19), 3645–3664.
(48) McCollom, T. M.; Seewald, J. S. Carbon Isotope Composition of Organic Compounds Produced by Abiotic Synthesis under Hydrothermal Conditions. *Earth and Planetary Science Letters* **2006**, *243* (1), 74–84.
(49) McCollom, T. M.; Ritter, G.; Simoneit, B. R. T. Lipid Synthesis Under Hydrothermal Conditions by Fischer- Tropsch-Type Reactions. *Orig Life Evol Biosph* **1999**, *29* (2), 153–166.
(50) Nooner, D. W.; Gibert, J. M.; Gelpi, E.; Oró, J. Closed System Fischer-Tropsch Synthesis over Meteoritic Iron, Iron Ore and Nickel-Iron Alloy. *Geochimica et Cosmochimica Acta* **1976**, *40* (8), 915–924.
(51) Rushdi, A. I.; Simoneit, B. R. T. Lipid Formation by Aqueous Fischer-Tropsch-Type Synthesis over a Temperature Range of 100 to 400 °C. *Orig Life Evol Biosph* **2001**, *31* (1), 103–118.
(52) Rushdi, A. I.; Simoneit, B. R. T. Condensation Reactions and Formation of Amides, Esters, and Nitriles Under Hydrothermal Conditions. *Astrobiology* **2004**, *4* (2), 211–224.
(53) Mißbach, H.; Schmidt, B. C.; Duda, J.-P.; Lünsdorf, N. K.; Goetz, W.; Thiel, V. Assessing the Diversity of Lipids Formed via Fischer-Tropsch-Type Reactions. *Organic Geochemistry* **2018**, *119*, 110–121.
(54) Bonfio, C.; Caumes, C.; Duffy, C. D.; Patel, B. H.; Percivalle, C.; Tsanakopoulou, M.; Sutherland, J. D. Length-Selective Synthesis of Acylglycerol-Phosphates through Energy-Dissipative Cycling. *J. Am. Chem. Soc.* **2019**, *141* (9), 3934–3939.
(55) Zahnle, K. J.; Lupu, R.; Catling, D. C.; Wogan, N. Creation and Evolution of Impact-Generated Reduced Atmospheres of Early Earth. *Planet. Sci. J.* **2020**, *1* (1), 11.
(56) Citron, R. I.; Stewart, S. T. Large Impacts onto the Early Earth: Planetary Sterilization and Iron Delivery. **2022**.
(57) Benner, S. A.; Bell, E. A.; Biondi, E.; Brasser, R.; Carell, T.; Kim, H.-J.; Mojzsis, S. J.; Omran, A.; Pasek, M. A.; Trail, D. When Did Life Likely Emerge on Earth in an RNA-First Process? *ChemSystemsChem* **2020**, *2* (2), e1900035.
(58) Zhou, L.-P.; Hao, X.; Gao, J.-H.; Yang, Y.; Wu, B.-S.; Xu, J.; Xu, Y.-Y.; Li, Y.-W. Studies and Discriminations of the Kinetic Models for the Iron-Based Fischer−Tropsch Catalytic Reaction in a Recycle Slurry Reactor. *Energy Fuels* **2011**, *25* (1), 52–59.
(59) Shock, E.; Canovas, P. The Potential for Abiotic Organic Synthesis and Biosynthesis at Seafloor Hydrothermal Systems. *Geofluids* **2010**, *10* (1–2), 161–192.

(60) Konn, C.; Charlou, J. L.; Donval, J. P.; Holm, N. G.; Dehairs, F.; Bouillon, S. Hydrocarbons and Oxidized Organic Compounds in Hydrothermal Fluids from Rainbow and Lost City Ultramafic-Hosted Vents. *Chemical Geology* **2009**, *258* (3), 299–314.
(61) Bach, W.; Banerjee, N. R.; Dick, H. J. B.; Baker, E. T. Discovery of Ancient and Active Hydrothermal Systems along the Ultra-Slow Spreading Southwest Indian Ridge 10°–16°E. *Geochemistry, Geophysics, Geosystems* **2002**, *3* (7), 1–14.
(62) McCollom, T. M.; Seewald, J. S. Abiotic Synthesis of Organic Compounds in Deep-Sea Hydrothermal Environments. *Chem. Rev.* **2007**, *107* (2), 382–401.
(63) Wilcox, E. M.; Roberts, G. W.; Spivey, J. J. Direct Catalytic Formation of Acetic Acid from CO2 and Methane. *Catalysis Today* **2003**, *88* (1), 83–90.
(64) Cody, G. D.; Boctor, N. Z.; Brandes, J. A.; Filley, T. R.; Hazen, R. M.; Yoder, H. S. Assaying the Catalytic Potential of Transition Metal Sulfides for Abiotic Carbon Fixation 1 1Associate Editor: P. A. O'Day. *Geochimica et Cosmochimica Acta* **2004**, *68* (10), 2185–2196.
(65) He, C.; Tian, G.; Liu, Z.; Feng, S. A Mild Hydrothermal Route to Fix Carbon Dioxide to Simple Carboxylic Acids. *Org. Lett.* **2010**, *12* (4), 649–651.
(66) Rotelli, L.; Trigo-Rodríguez, J. M.; Moyano-Cambero, C. E.; Carota, E.; Botta, L.; Di Mauro, E.; Saladino, R. The Key Role of Meteorites in the Formation of Relevant Prebiotic Molecules in a Formamide/Water Environment. *Sci Rep* **2016**, *6* (1), 38888.
(67) Varma, S. J.; Muchowska, K. B.; Chatelain, P.; Moran, J. Native Iron Reduces CO2 to Intermediates and End-Products of the Acetyl-CoA Pathway. *Nat Ecol Evol* **2018**, *2* (6), 1019–1024.
(68) Miller, S. L. A Production of Amino Acids Under Possible Primitive Earth Conditions. *Science* **1953**, *117* (3046), 528–529.
(69) Johnson, A. P.; Cleaves, H. J.; Dworkin, J. P.; Glavin, D. P.; Lazcano, A.; Bada, J. L. The Miller Volcanic Spark Discharge Experiment. *Science* **2008**, *322* (5900), 404–404.
(70) Ferus, M.; Pietrucci, F.; Saitta, A. M.; Knížek, A.; Kubelík, P.; Ivanek, O.; Shestivska, V.; Civiš, S. Formation of Nucleobases in a Miller–Urey Reducing Atmosphere. *Proc. Natl. Acad. Sci USA* **2017**, *114* (17), 4306–4311.
(71) Criado-Reyes, J.; Bizzarri, B. M.; García-Ruiz, J. M.; Saladino, R.; Di Mauro, E. The Role of Borosilicate Glass in Miller–Urey Experiment. *Sci Rep* **2021**, *11* (1), 21009.
(72) Allen, W. V.; Ponnamperuma, C. A Possible Prebiotic Synthesis of Monocarboxylic Acids. *Biosystems* **1967**, *1* (1), 24–28.
(73) Zeitman, B.; Chang, S.; Lawless, J. G. Dicarboxylic Acids from Electric Discharge. *Nature* **1974**, *251* (5470), 42–43.
(74) Williams, E. R. The Electrification of Thunderstorms. *SCIENTIFIC AMERICAN* **1988**, 13.
(75) Orville, R. E. A High-Speed Time-Resolved Spectroscopic Study of the Lightning Return Stroke: Part II. A Quantitative Analysis. *Journal of the Atmospheric Sciences* **1968**, *25* (5), 839–851.
(76) Chyba, C.; Sagan, C. Electrical Energy Sources for Organic Synthesis on the Early Earth. *Origins Life Evol Biosphere* **1991**, *21* (1), 3–17.
(77) Schlesinger, G.; Miller, S. L. Prebiotic Synthesis in Atmospheres Containing CH4, CO, and CO2. *J Mol Evol* **1983**, *19* (5), 376–382.
(78) Roldan, A.; Hollingsworth, N.; Roffey, A.; Islam, H.-U.; Goodall, J. B. M.; Catlow, C. R. A.; Darr, J. A.; Bras, W.; Sankar, G.; Holt, K. B.; Hogarth, G.; Leeuw, N. H. de. Bio-Inspired CO2 Conversion by Iron Sulfide Catalysts under Sustainable Conditions. *Chem. Commun.* **2015**, *51* (35), 7501–7504.
(79) Groth, W. E.; Weyssenhoff, H. v. Photochemical Formation of Organic Compounds from Mixtures of Simple Gases. *Planetary and Space Science* **1960**, *2* (2), 79–85.
(80) Kaiser, R. I.; Gabrysch, A.; Roessler, K. Cosmic Ray Simulator: A Versatile Apparatus for Quantitative Studies on the Interaction of Cosmic Rays with Frozen Solids by on Line and in Situ

Quadrupole Mass Spectrometry and Fourier Transform Infrared Spectroscopy. *Review of Scientific Instruments* **1995**, *66* (4), 3058–3066.
(81) Kim, Y. S.; Kaiser, R. I. Abiotic Formation of Carboxylic Acids (RCOOH) in Interstellar and Solar System Model Ices. *ApJ* **2010**, *725* (1), 1002–1010.
(82) Blagojevic, V.; Petrie, S.; Bohme, D. K. Gas-Phase Syntheses for Interstellar Carboxylic and Amino Acids. *Monthly Notices of the Royal Astronomical Society* **2003**, *339* (1), L7–L11.
(83) Lowe, C. U.; Rees, M. W.; Markham, R. Synthesis of Complex Organic Compounds from Simple Precursors: Formation of Amino-Acids, Amino-Acid Polymers, Fatty Acids and Purines from Ammonium Cyanide. *Nature* **1963**, *199* (4890), 219–222.
(84) Novotný, O.; Cejpek, K.; Velíšek, J. Formation of Carboxylic Acids during Degradation of Monosaccharides. *Czech J. Food Sci.* **2008**, *26* (No. 2), 113–131.
(85) Sato, K.; Hyodo, M.; Takagi, J.; Aoki, M.; Noyori, R. Hydrogen Peroxide Oxidation of Aldehydes to Carboxylic Acids: An Organic Solvent-, Halide- and Metal-Free Procedure. *Tetrahedron Letters* **2000**, *41* (9), 1439–1442.
(86) Ranjan, S.; Sasselov, D. D. Constraints on the Early Terrestrial Surface UV Environment Relevant to Prebiotic Chemistry. *Astrobiology* **2017**, *17* (3), 169–204.
(87) Dworkin, J. P.; Deamer, D. W.; Sandford, S. A.; Allamandola, L. J. Self-Assembling Amphiphilic Molecules: Synthesis in Simulated Interstellar/Precometary Ices. *Proc. Natl. Acad. Sci USA* **2001**, *98* (3), 815–819.
(88) Ehrenfreund, P.; d'Hendecourt, L.; Charnley, S.; Ruiterkamp, R. Energetic and Thermal Processing of Interstellar Ices. *Journal of Geophysical Research: Planets* **2001**, *106* (E12), 33291–33301.
(89) Pecoits, E.; Smith, M. L.; Catling, D. C.; Philippot, P.; Kappler, A.; Konhauser, K. O. Atmospheric Hydrogen Peroxide and Eoarchean Iron Formations. *Geobiology* **2015**, *13* (1), 1–14.
(90) Omran, A.; Menor-Salvan, C.; Springsteen, G.; Pasek, M. The Messy Alkaline Formose Reaction and Its Link to Metabolism. *Life* **2020**, *10* (8), 125.
(91) Toner, J. D.; Catling, D. C. Alkaline Lake Settings for Concentrated Prebiotic Cyanide and the Origin of Life. *Geochimica et Cosmochimica Acta* **2019**, *260*, 124–132.
(92) Toner, J. D.; Catling, D. C. A Carbonate-Rich Lake Solution to the Phosphate Problem of the Origin of Life. *Proc. Natl. Acad. Sci USA* **2020**, *117* (2), 883–888.
(93) Sasselov, D. D.; Grotzinger, J. P.; Sutherland, J. D. The Origin of Life as a Planetary Phenomenon. *Sci. Adv.* **2020**, *6* (6), eaax3419.
(94) Yoneda, N.; Kusano, S.; Yasui, M.; Pujado, P.; Wilcher, S. Recent Advances in Processes and Catalysts for the Production of Acetic Acid. *Applied Catalysis A: General* **2001**, *221* (1), 253–265.
(95) Berg, J. M.; Tymoczko, J. L.; Stryer, L. *Biochemistry*, 5th ed.; W. H. Freeman: New York, NY, 2002.
(96) Weber, A. L. Origin of Fatty Acid Synthesis: Thermodynamics and Kinetics of Reaction Pathways. *J Mol Evol* **1991**, *32* (2), 93–100.
(97) Shock, E. L.; Schulte, M. D. Amino-Acid Synthesis in Carbonaceous Meteorites by Aqueous Alteration of Polycyclic Aromatic Hydrocarbons. *Nature* **1990**, *343* (6260), 728–731.
(98) Sleep, N. H.; Zahnle, K. J.; Kasting, J. F.; Morowitz, H. J. Annihilation of Ecosystems by Large Asteroid Impacts on the Early Earth. *Nature* **1989**, *342* (6246), 139–142.
(99) Marchi, S.; Bottke, W. F.; Elkins-Tanton, L. T.; Bierhaus, M.; Wuennemann, K.; Morbidelli, A.; Kring, D. A. Widespread Mixing and Burial of Earth's Hadean Crust by Asteroid Impacts. *Nature* **2014**, *511* (7511), 578–582.
(100) Chyba, C.; Sagan, C. Endogenous Production, Exogenous Delivery and Impact-Shock Synthesis of Organic Molecules: An Inventory for the Origins of Life. *Nature* **1992**, *355* (6356), 125–132.

(101) Bevan, A. W. R.; Bland, P. A.; Jull, A. J. T. Meteorite Flux on the Nullarbor Region, Australia. In *Meteorites: Flux with Time and Impact Effects.*; Geological Society, London, Special Publications, 1998; Vol. 140, pp 59–73.
(102) Macke, R. J.; Consolmagno, G. J.; Britt, D. T. Density, Porosity, and Magnetic Susceptibility of Carbonaceous Chondrites. *Meteoritics & Planetary Science* **2011**, *46* (12), 1842–1862.
(103) Pierazzo, E.; Chyba, C. F. Impact Delivery of Prebiotic Organic Matter to Planetary Surfaces. In *Comets and the Origin and Evolution of Life*; Thomas, P. J., Hicks, R. D., Chyba, C. F., McKay, C. P., Eds.; Advances in Astrobiology and Biogeophysics; Springer: Berlin, Heidelberg, 2006; pp 137–168.
(104) Keil, K. Mineralogical and Chemical Relationships among Enstatite Chondrites. *Journal of Geophysical Research (1896-1977)* **1968**, *73* (22), 6945–6976.
(105) McDonough, W. F. Compositional Model for the Earth's Core. *Treatise on Geochemistry* **2003**, *2*, 568.
(106) Dauphas, N. The Isotopic Nature of the Earth's Accreting Material through Time. *Nature* **2017**, *541* (7638), 521–524.
(107) Bermingham, K. R.; Worsham, E. A.; Walker, R. J. New Insights into Mo and Ru Isotope Variation in the Nebula and Terrestrial Planet Accretionary Genetics. *Earth Planet Sci Lett* **2018**, *487*, 221–229.
(108) Hellmann, J. L.; Hopp, T.; Burkhardt, C.; Becker, H.; Fischer-Gödde, M.; Kleine, T. Tellurium Isotope Cosmochemistry: Implications for Volatile Fractionation in Chondrite Parent Bodies and Origin of the Late Veneer. *Geochimica et Cosmochimica Acta* **2021**, *309*, 313–328.
(109) Macke, R. J.; Consolmagno, G. J.; Britt, D. T.; Hutson, M. L. Enstatite Chondrite Density, Magnetic Susceptibility, and Porosity. *Meteoritics & Planetary Science* **2010**, *45* (9), 1513–1526.
(110) Lewis, J. S.; Prinn, R. G. Planets and Their Atmospheres : Origin and Evolution. *Orlando FL Academic Press Inc International Geophysics Series* **1984**, *33*.
(111) Wang, Z.; Mai, K.; Kumar, N.; Elder, T.; Groom, L. H.; Spivey, J. J. Effect of Steam During Fischer–Tropsch Synthesis Using Biomass-Derived Syngas. *Catal Lett* **2017**, *147* (1), 62–70.
(112) Pendyala, V. R. R.; Shafer, W. D.; Jacobs, G.; Davis, B. H. Fischer–Tropsch Synthesis: Effect of Reaction Temperature for Aqueous-Phase Synthesis Over a Platinum Promoted Co/Alumina Catalyst. *Catal Lett* **2014**, *144* (6), 1088–1095.
(113) Navarro-González, R.; Romero, A.; Honda, Y. Power Measurements of Spark Discharge Experiments. *Orig Life Evol Biosph* **1998**, *28* (2), 131–153.
(114) Chiu, R.; Tinel, L.; Gonzalez, L.; Ciuraru, R.; Bernard, F.; George, C.; Volkamer, R. UV Photochemistry of Carboxylic Acids at the Air-Sea Boundary: A Relevant Source of Glyoxal and Other Oxygenated VOC in the Marine Atmosphere. *Geophysical Research Letters* **2017**, *44* (2), 1079–1087.
(115) Simoneit, B. R. T.; Rushdi, A. I.; Deamer, D. W. Abiotic Formation of Acylglycerols under Simulated Hydrothermal Conditions and Self-Assembly Properties of Such Lipid Products. *Advances in Space Research* **2007**, *40* (11), 1649–1656.
(116) Rapf, R. J.; Perkins, R. J.; Dooley, M. R.; Kroll, J. A.; Carpenter, B. K.; Vaida, V. Environmental Processing of Lipids Driven by Aqueous Photochemistry of α-Keto Acids. *ACS Cent. Sci.* **2018**, *4* (5), 624–630.
(117) Gibard, C.; Bhowmik, S.; Karki, M.; Kim, E.-K.; Krishnamurthy, R. Phosphorylation, Oligomerization and Self-Assembly in Water under Potential Prebiotic Conditions. *Nature Chemistry* **2017**, *10* (2), 212–217.
(118) Sarkar, S.; Dagar, S.; Verma, A.; Rajamani, S. Compositional Heterogeneity Confers Selective Advantage to Model Protocellular Membranes during the Origins of Cellular Life. *Sci Rep* **2020**, *10* (1), 4483.
(119) Jia, T. Z.; Chandru, K.; Hongo, Y.; Afrin, R.; Usui, T.; Myojo, K.; Cleaves, H. J. Membraneless Polyester Microdroplets as Primordial Compartments at the Origins of Life. *Proc. Natl. Acad. Sci USA* **2019**, *116* (32), 15830–15835.

(120) Fares, H. M.; Marras, A. E.; Ting, J. M.; Tirrell, M. V.; Keating, C. D. Impact of Wet-Dry Cycling on the Phase Behavior and Compartmentalization Properties of Complex Coacervates. *Nat Commun* **2020**, *11* (1), 5423.

(121) Tang, T.-Y. D.; Rohaida Che Hak, C.; Thompson, A. J.; Kuimova, M. K.; Williams, D. S.; Perriman, A. W.; Mann, S. Fatty Acid Membrane Assembly on Coacervate Microdroplets as a Step towards a Hybrid Protocell Model. *Nature Chemistry* **2014**, *6* (6), 527–533.

Chapter 5:

Natural carbonate lakes provide compatible conditions for RNA and membrane function that could have enabled the origin of life on Earth

*This chapter was written in collaboration with Zoe R. Todd, Dian Ding, Lijun Zhou, Saurja DasGupta, Sebastian Haas, Kimberly Sinclair, Sarah L. Keller, Roy A. Black, Jack W. Szostak, and David C. Catling.

Abstract

The origin of life on Earth likely occurred within an environment that concentrated cellular precursors and enabled their co-assembly into cells. Carbonate lakes can concentrate RNA precursors such as aqueous phosphate, and membrane precursors such as fatty acids. Subsequent assembly of RNA and membranes into cells is a long-standing problem because RNA function requires divalent cations (e.g. Mg^{2+}), whereas fatty acid membranes are disrupted by Mg^{2+}. Because carbonate lakes contain at most ~1 mM Mg^{2+}, we investigated whether RNAs and membranes function within natural carbonate lake water. We collected water from Last Chance Lake and Goodenough Lake in British Columbia, Canada. Because we sampled after seasonal evaporation, the lake water contained ~1 M Na^{+} and ~1 mM Mg^{2+} at pH 10. In the lab, we found that nonenzymatic, RNA-templated polymerization of 2-aminoimidazole activated ribonucleotides occurs at comparable rates in lake water and standard laboratory conditions (50 mM $MgCl_2$, pH 8). Additionally, we found that a ligase ribozyme that uses a 2-aminoimidazole activated oligonucleotide substrate is active in lake water after adjustment from pH ~10 to pH 9. We also observed that decanoic acid and decanol assembled into vesicles in dilute solution that resembles the lake water after seasonal rains, and that those vesicles retained encapsulated solutes despite salt-induced flocculation when the external solution is replaced with dry-season lake water. By identifying compatible conditions for nonenzymatic and ribozyme-catalyzed RNA assembly, and for encapsulation by membranes, our results suggest that carbonate lakes could have enabled the emergence of cellular life on Earth.

Significance Statement

In which environment did cells originate on the early Earth? The first cells (protocells) are thought to have consisted of informational and catalytic RNAs inside membrane vesicles. However, RNA function requires divalent cations (e.g. Mg^{2+}), whereas membranes of environmentally available amphiphiles (e.g. fatty acids) are disrupted by divalent cations. Here we report that natural carbonate lake water, which contains at most ~1 mM divalent cations, could provide compatible conditions for three processes thought to be important for the origin of cellular life: nonenzymatic RNA assembly, ribozyme activity, and encapsulation by prebiotic membranes. Our results suggest that carbonate lakes are uniquely suited to enable the formation of the first cells.

Main text

Protocells composed of genetic molecules and a lipid vesicle may have constituted an early stage of life on Earth (1). RNA may have been an important component of protocells because of its ability to store and transmit genetic information and to catalyze reactions (2). Protocell membranes may have been composed of fatty acids, which enable exchange of small metabolites with the external environment while encapsulating large polymers (3). However, divalent cations (e.g. Mg^{2+}) that are essential for nonenzymatic RNA copying (4) and ribozyme activity (5) disrupt fatty acid membranes, leading to release of encapsulated solutes (6). Chelation of divalent cations by excess citrate preserves fatty acid vesicles and enables internal RNA reactions (7), but high concentrations of citrate on the early Earth are unlikely. Serine and glycine maintain the integrity of fatty acid vesicles in 10 mM Mg^{2+} by increasing lamellarity (8), but RNA reactions have not been investigated under these conditions. Interestingly, nonenzymatic synthesis of a genetic polymer similar to RNA (NP-DNA, (3)) and ribozyme activity (9) have both been observed within fatty acid vesicles when the concentration of divalent cations is below 4 mM.

Carbonate lakes, otherwise known as soda lakes, are promising sites for the co-assembly of RNA and fatty acids into protocells. Carbonate lakes contain between 0.1 - 1 M of bicarbonate and carbonate anions (10). Because salts of divalent cations and carbonate anions have poor solubility, the concentration of divalent cations in carbonate lakes does not exceed ~1 mM (11). Additionally, carbonate lakes on the early Earth may have concentrated phosphate (12), ferrocyanide (13), and sulfur species (14), potentially enabling the synthesis of ribonucleotides during photochemically-driven reductive homologation of hydrogen cyanide (15, 16). Fatty acids could have been delivered to Earth by meteorites (17), synthesized endogenously on metal surfaces (18), or synthesized during electrochemical sparking (19), and those fatty acids could have been subsequently concentrated in carbonate lakes via evaporation to enable membrane formation (20).

Because carbonate lakes provide unique opportunities for the prebiotic formation of RNA and fatty acid vesicles, and because relatively low concentrations of divalent cations have been shown to enable RNA reactions within fatty acid vesicles, we investigated key components of protocell assembly within natural carbonate lake water. We collected water samples from Last Chance Lake and Goodenough Lake on the Cariboo Plateau in British Columbia, Canada. These carbonate lakes have some of the highest phosphate concentrations of lakes on Earth (21). We collected after seasonal evaporation when these lakes contain ~1 M Na^{+} and ~1 mM Mg^{2+} at pH 10 (Tables S1-S3). We tested for nonenzymatic, RNA-templated synthesis of RNA in water from both carbonate lakes. Additionally, we determined the activity of a ligase ribozyme in natural lake water, and we tested whether membranes composed of fatty acids and fatty alcohols can encapsulate aqueous solutes in natural lake water. Our findings directly inform the search for natural environments that could have supported the origin of cellular life on Earth.

Nonenzymatic, RNA-templated synthesis of RNA

Before the emergence of enzymes on the early Earth, short RNAs that formed during wet-dry cycling (22) or on mineral surfaces (23) may have been replicated by successive addition of chemically-activated ribonucleotides. For example, after pairing between a short RNA primer and the template,

2-aminoimidazole activated nucleotides can base pair with the template and react nonenzymatically with the primer to form a 3’-5’ phosphodiester linkage (Fig. 1A). Unlike polymerization of triphosphate nucleotides, 2-aminoimidazole activated nucleotides spontaneously form 5’-5’ bridged dinucleotide intermediates that enable rapid, nonenzymatic extension of RNA primers (24). Separation of the strands enables a new cycle of polymerization to generate a copy of the original template. Nonenzymatic primer extension may have been a necessary step in the formation of the first ribozymes, so we investigated whether this process can proceed in carbonate lake water.

We found that the rates of primer extension in lake water were comparable to the rates in standard laboratory conditions (Fig. 1). We prepared reactions in 90% natural water from Last Chance Lake (LC) or Goodenough Lake (GE), and we also prepared the reaction in artificial lake water that approximated the cation composition, anion composition, and pH of the natural lakes (0.5 M Na_2CO_3, 1 mM $MgCl_2$, and 200 mM bis-tris-propane at pH 10). Standard laboratory conditions were 50 mM $MgCl_2$ and 200 mM bis-tris-propane at pH 8. We measured the relative abundance of fluorescently labeled primers through time and calculated pseudo first-order rate constants for +1 nucleotide extension in each set of conditions (Fig. S1).

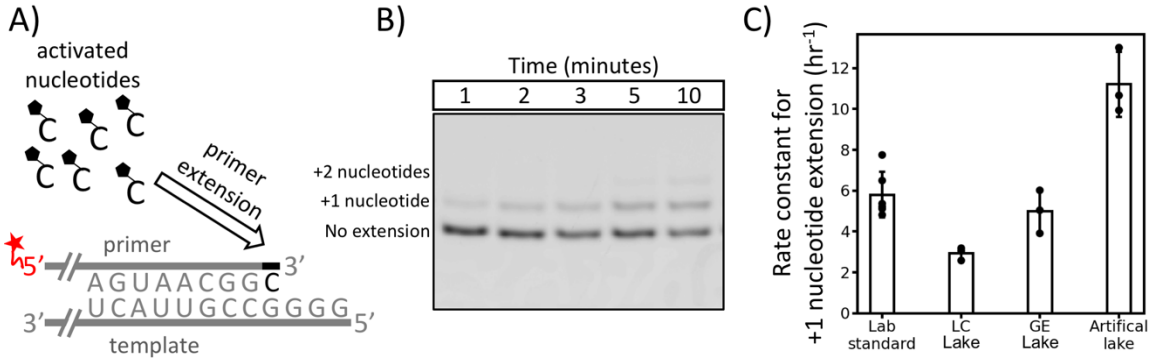

Figure 1. RNA primers on RNA templates are extended at comparable rates in carbonate lake water and in standard lab conditions. A) Schematic of RNA primer extension by 2-aminoimidazole activated ribonucleotides. Our data suggest that primer extension in lake water proceeds through a bridged dinucleotide intermediate (Fig. S2), consistent with previous results (24). The primer is fluorescently labeled at the 5’ end. B) Gel image showing RNA-templated extension of an RNA primer in Last Chance Lake water. RNAs smaller than the primer were not detected, suggesting that the RNA primer is not hydrolyzed. C) First-order rate constants for extension of an RNA primer by one nucleotide. Standard lab conditions are 50 mM $MgCl_2$ and 0.2 M bis-tris-propane at pH 8, and artificial lake water is 0.5 M Na_2CO_3, 1 mM $MgCl_2$, and 0.2 M bis-tris-propane at pH 10. Error bars correspond to the standard deviation from 3 independent experiments in lake waters, and 6 independent experiments in standard lab conditions. LC is Last Chance Lake and GE is Goodenough Lake.

The surprisingly fast initial rate of primer extension may be explained by the relatively high pH of the lake water. In artificial solutions that approximate the cation composition of natural lakes, the rate of primer extension increases rapidly with pH (Fig. S2). The primer 3’ hydroxyl group should tend to deprotonate as pH increases, which enables nucleophilic attack on the phosphate of an incoming nucleotide (25). Rapid primer extension in natural lake water also relies on formation of a bridged

dinucleotide intermediate, the same mechanism for primer extension in laboratory conditions (24). When we prevented formation of the bridged dinucleotide by supplying an excess of 2-aminoimidazole, the yield of extended primers in lake water was greatly reduced (Fig. S3). However, in the absence of primer and template RNAs, we did not observe formation of the bridged dinucleotide in natural lake water by ^{31}P NMR (Fig. S4). We suspect that bridged dinucleotide formation occurs on the template prior to primer extension.

We observed remarkably long lifetimes for RNA primers in lake water. After 72 hours, we did not observe hydrolysis of the primer in natural or artificial lake water (Fig. S5). The relatively low concentration of divalent cations may compensate for the high pH in lake water to keep the hydrolysis rate low (26). However, we also observed that few primers had been extended by at least 3 nucleotides after 72 hours in lake water, relative to standard laboratory conditions (Fig. 2). Why are fewer primers extended after 72 hours in lake water than in laboratory conditions despite comparable initial rates of extension? Carbonate anions in the lake water seem to play a role; artificial lake solutions that approximate the cation composition and pH of natural lakes showed lower yields of extended primers after 72 hours – but comparable initial rates of primer extension – when carbonate is the most abundant anion (Fig. S6). We also suspected that primer extension in lake water might be limited by poor binding of nucleotides to the template due to deprotonation of the nucleobases at high pH.

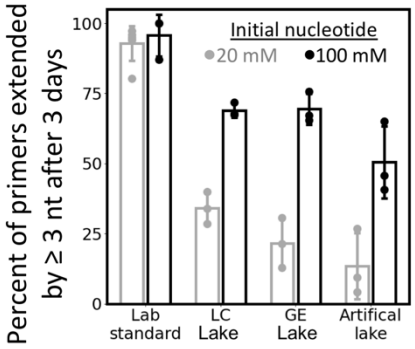

Figure 2. The yield of extended RNA primers is lower in carbonate lake water than standard lab conditions, although the yield in lake water increases by supplying a larger initial concentration of activated nucleotides (nt). A) The fraction of RNA primers that were extended by at least 3 nucleotides in natural and artificial lake water after 3 days, when either 20 mM (gray) or 100 mM (black) activated nucleotide is supplied. We did not observe any hydrolysis of the primer after 3 days (Fig. S8). Standard lab conditions are 50 mM $MgCl_2$ and 200 mM bis-tris-propane at pH 8, and artificial lake water is 0.5 M Na_2CO_3, 1 mM $MgCl_2$, and 200 mM bis-tris-propane at pH 10. Error bars correspond to the standard deviation from 3 independent experiments, except for the error bars for the 20 mM initial nucleotide in lab standard conditions sample which correspond to 6 independent experiments. LC is Last Chance Lake and GE is Goodenough Lake.

After increasing the initial concentration of activated nucleotides from 20 mM to 100 mM, we observed much more primer extension after 72 hours in lake water (Fig. 2). The percentage of primers that had been extended by 3 nucleotides nearly doubled in all lake samples due to the higher initial concentration of nucleotides. Although fewer primers were extended in lake water than in laboratory

conditions per activated nucleotide that was supplied, our observations show that considerable primer extension is possible in natural carbonate lakes when the concentration of activated nucleotides is relatively high. High concentrations of activated nucleotides could have been present after evaporation from shallow carbonate lakes on the early Earth.

We note that full extension of the primer on the template (i.e. +4 nucleotides) is exceedingly slow (Fig. S7). This problem of "last nucleotide addition" has previously been observed in laboratory conditions because dinucleotide intermediates can only form one base-pair with the template's terminal nucleotide (27). However, protocells may not have needed to synthesize the full complementary strand for a given template. Unlike modern cells composed of linear genomes, protocells may have been composed of virtual circular genomes where RNA synthesis can be transiently templated by multiple oligomers at different positions (28). Additionally, we recognize that 72 hours is not an endpoint for nonenzymatic primer extension in lake water. We observed sustained primer extension beyond 72 hours, which would further improve the yield of extended primers (Fig. S8). However, we did observe partial hydrolysis of the primer after 6 days (Fig. S5). Taken together, our findings suggest that nonenzymatic primer extension can proceed robustly in natural carbonate lake water.

Activity of a ligase ribozyme

Sustained nonenzymatic replication could enable the evolution of ribozymes, which could then catalyze RNA replication. Specifically, ligase ribozymes could enable RNA replication by joining RNAs on the same template. We previously identified by *in vitro* selection a 70 nucleotide ribozyme that catalyzes ligation between its 3' end and a substrate RNA activated by 2-aminoimidazole (29). Because the ribozyme's substrate is activated with 2-aminoimidazole rather than triphosphate, it is reasonable to imagine a continuous path from nonenzymatic to ribozyme-catalyzed RNA replication. Although our ribozyme was selected under moderate concentrations of divalent cations (5-20 mM Mg^{2+}), we have shown that it also functions when the concentration of Mg^{2+} is reduced to 1 mM (30). Therefore, we conducted experiments to determine whether this ligase ribozyme functions in natural carbonate lake water.

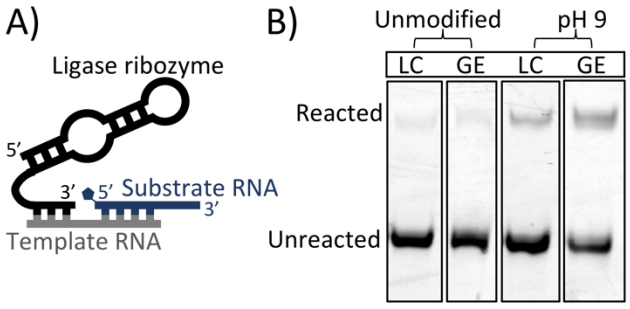

Figure 3. A ligase ribozyme is active in carbonate lake water after decreasing pH from ~10 to 9. A) The ribozyme and substrate base pair to the same RNA template. The 5' end of the substrate is activated with 2-aminoimidazole, and the ribozyme ligates the substrate onto its 3' end. B) In unmodified water (pH ~10) from either Last Chance Lake (LC) or Goodenough Lake (GE), the ribozyme activity is low. After adjusting the lake water to pH 9 by bubbling in carbon dioxide, the ribozyme activity increases substantially. Data are from a single experiment that is consistent with replicates (Fig. S9).

We observed low activity of the ligase ribozyme in 70% natural water from Last Chance Lake and Goodenough Lake; however, the ribozyme became active when the lake water was modified by decreasing the pH from ~10 to 9 by bubbling in carbon dioxide (Fig. 3). This pH sensitivity is not surprising; the ribozyme was selected at pH 8, so it is reasonable to expect higher activity as the solution becomes more similar to the selection conditions. 32 ± 3% of the ribozyme reacted after 20 hours in pH 9-adjusted water from Goodenough Lake, and 11 ± 1% of the ribozyme reacted after 20 hours in pH 9-adjusted water from Last Chance Lake. The ribozyme activity in lake water was lower than the activity in laboratory conditions (0.362 M NaCl, 1.2 mM $MgCl_2$, and 242 mM bis-tris-propane at pH 8) where 60 ± 6% of the ribozyme reacted after 20 hours (Fig. S9). When the ribozyme was replaced with an inactive RNA, we did not observe nonenzymatic ligation under any conditions (Fig. S10).

We performed experiments with artificial solutions to validate our results from the natural lake water. We consistently observed that decreasing the pH below 10 leads to higher ribozyme activity, whether the ionic composition mimics the natural lake (~0.5 M Na_2CO_3 and ~1 mM $MgCl_2$) or laboratory conditions (Fig. S11). Additionally, we observed that a high concentration of monovalent cations, which are present in the natural lake water, leads to lower yields of ribozyme-catalyzed ligation (30). In general, our data demonstrate that ribozymes can function in carbonate lake water, though it is clear that our chosen ribozyme is not particularly well adapted to carbonate lake water. We expect that selection in carbonate lake water will yield ribozymes with much higher activity under these conditions, and that natural selection in carbonate lake water could have generated diverse ribozymes during the origin of life.

Encapsulation by prebiotic membranes

To determine whether prebiotically plausible amphiphiles can assemble into vesicles in water from carbonate lakes during the dry season (i.e. after seasonal evaporation), we prepared a solution of 89% Last Chance Lake water containing 112.5 mM decanoic acid and 112.5 mM decanol with 0.1 mM carboxyfluorescein. The amphiphiles immediately floated to the surface, which is consistent with the behavior of flocculated vesicles in saturated solutions of monovalent cations (31). We replaced the exterior solution around the amphiphiles with 100% water from Last Chance Lake in order to remove unencapsulated carboxyflorescein (Fig. S12). However, we did not observe retention of internal carboxyflorescein, suggesting that the amphiphiles did not encapsulate solution (Fig S13). We subsequently diluted the salt concentration, and we did not observe separated vesicles with encapsulated carboxyflorescein (Fig S13). We conclude that the formation of vesicles capable of encapsulating solution is inefficient in natural water from Last Chance Lake's dry season.

Given that our water sample is from Last Chance Lake's dry season, we wondered whether amphiphiles might encapsulate solutes if they assemble into vesicles in dilute solution during the lake's wet season, and if those vesicles could retain encapsulated solutes as the exterior solution becomes saltier during evaporation in the dry season. We assembled vesicles of 1:1 decanoic acid: decanol in a relatively dilute salt solution of 0.1 M $NaHCO_3$ at pH 10 with 0.1 mM carboxyfluorescein. These conditions mimic dilute lake water during the wet season. We replaced the exterior solution around the vesicles with Last Chance Lake water from the dry season containing ~1 M Na^+ and ~1 mM Mg^{2+} at pH 10, and we imaged the vesicles with fluorescence microscopy (Fig. 4). We observed flocculated vesicles that retain encapsulated carboxyfluorescein despite the millimolar concentration of divalent

cations in the natural lake water. We are confident that the flocculated vesicles are surrounded by Last Chance Lake water because there is excellent contrast between encapsulated carboxyfluorescein and the exterior solution. We subsequently diluted the salt concentration in the exterior solution and found that separated vesicles still retained the dye. Full field images (Fig. S14) and a size-exclusion chromatogram (Fig. S13) show that many vesicles retain dye after dilution of the salt. We also found that vesicles retained encapsulated dye when the exterior solution is artificial lake water of 0.75 M Na_2CO_3 and 1 mM $MgCl_2$ at pH 10, or artificial lake water of 1 M NaCl, 1 mM $MgCl_2$, and 0.1 M $NaHCO_3$ at pH 10 (Fig. S15). However, because our method of exchanging the exterior solution around vesicles requires an extremely high concentration of unchelated monovalent cations, we were unable to determine whether vesicles retain encapsulated dye in water from Goodenough Lake, or in artificial lake water of 0.5M Na_2CO_3 and 1 mM $MgCl_2$ at pH 10 (Fig. S16). In summary, our results show that vesicles can encapsulate solutes in carbonate lake water after seasonal evaporation if the vesicles are allowed to assemble in dilute solution during the wet season.

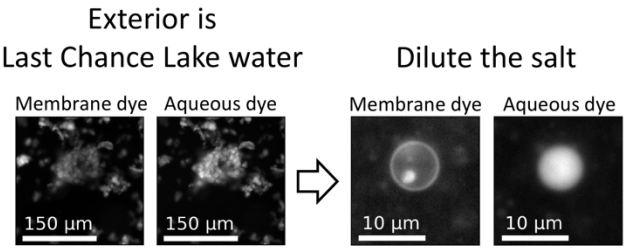

Figure 4. Vesicles of 1:1 decanoic acid: decanol encapsulate aqueous carboxyflorescein dye for more than 1 hour when the exterior solution is water from Last Chance Lake. Monovalent salts induce flocculation of vesicles into large aggregates. Vesicles were initially assembled in a dilute salt solution of 0.1 M $NaHCO_3$ at pH 10 with 0.1 mM carboxyflorescein dye before the exterior solution was replaced with Last Chance Lake water (Fig. S12). Subsequent dilution into a 56 mM decanoic acid and 0.1 M $NaHCO_3$, pH 10 solution causes vesicles to separate from each other, and separated vesicles still retain encapsulated dye. Similar results were obtained for vesicles in artificial lake water; however, we could not determine whether vesicles retain encapsulated dye in water from Goodenough Lake (Fig. S16). Rhodamine 6G membrane dye was added immediately prior to imaging. Full field images are in the SI (Fig. S13).

Conclusions

Our results suggest that carbonate lakes on the early Earth could have supported key features of protocell development. The nonenzymatic synthesis of RNA proceeds on RNA templates at a comparable rate in carbonate lake water as under standard laboratory conditions. We find that the yield of nonenzymatically extended RNAs increases with the concentration of activated nucleotides. Activated nucleotides could have reached high concentrations during evaporation from natural lakes, although continued nucleotide synthesis may become limited by the availability of phosphate (~40 mM in Last Chance Lake (21)). 2-aminoimidazole could be produced from nucleotide precursors (32), and nucleotide activation with 2-aminoimidazole could occur in the eutectic brines of partially frozen lakes (33). While nonenzymatic copying of sequence-general RNA templates remains challenging (34), our results show

that carbonate lakes are capable of supporting nonenzymatic RNA synthesis in a comparable manner to optimized laboratory conditions.

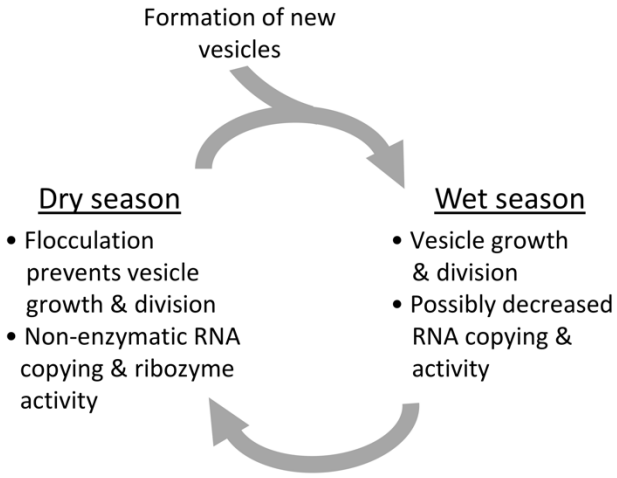

Figure 5. A hypothetical development cycle for protocells based on seasonal fluctuations in the water content of carbonate lakes.

Sustained nonenzymatic replication could have enabled the evolution of ribozymes which could then catalyze RNA replication, a key step during the origin of cells. Ligase ribozymes enable RNA-catalyzed RNA replication, and the use of a 2-aminoimidazole activated substrate could have enabled a continuous path from nonenzymatic to ribozyme-catalyzed RNA replication. We find that our *in vitro* selected ligase ribozyme retains activity in carbonate lake water when the pH is adjusted to be more similar to the selection conditions. Ribozymes that evolved in natural lakes would be optimized to function under such conditions, and these ribozymes could be isolated in the laboratory by performing *in vitro* selection experiments in natural lake water. Additionally, carbonate lakes on the early Earth may have had lower pH (between pH 6.5 and 9) due to a high concentration of CO_2 in the atmosphere (12).

Additionally, we show that prebiotic membranes can encapsulate solutes despite flocculation in carbonate lake water. It is likely that nonenzymatic RNA synthesis (35) and ribozyme-catalyzed ligation (30) can proceed inside flocculated vesicles whose exterior solution is carbonate lake water. However, future work is needed to identify conditions where 2-aminoimidazole activated mononucleotides or oligonucleotides can permeate into flocculated vesicles without releasing larger RNAs. We envision that RNA-membrane interactions could modulate both the extent of flocculation and permeability of the flocculated vesicles (36).

In conclusion, we propose a seasonal model for protocell development in carbonate lakes on the early Earth (Fig. 5). Vesicle formation could occur during seasonally wet periods when the monovalent cation concentration is decreased by dilution, and those vesicles could retain encapsulated contents during transient flocculation in the dry season. Formation of vesicles *de novo* seems to be inefficient in water from carbonate lakes in the dry season, and flocculation in water from the dry season may prevent membrane growth and division. Formation of new vesicles, growth, and division of existing vesicles (37) could occur during the wet season, or in dilute streams that feed into closed-basin lakes. Biopolymer building blocks such as nucleobases (38) and amino acids (8) enable vesicles to resist

flocculation in moderate concentrations of monovalent cations, which could prolong the seasonal duration of dispersed vesicles. Moreover, saturated solutions containing 1 mM Mg^{2+} (which are present during the dry season) are sufficient to enable nonenzymatic RNA copying and ribozyme activity. Taken together, our results suggest that natural carbonate lakes could have supported the formation of the earliest cellular life on Earth.

Experimental section

Materials

RNAs and DNA were from Integrated DNA technologies (Coralville, IA). NaCl, Na_2CO_3, bis-tris-propane, formamide, decanol, and carboxyflorescein were from Sigma-Aldrich (St. Louis, MO). 1 M $MgCl_2$ stock solution was from Ambion (Austin, TX). Ultrapure water, 0.5 M ethylenediaminetetraacetic acid, and SYBR Gold gel stain were from Invitrogen (Waltham, MA). 220 nm nylon syringe filters were from RESTEK (Bellefonte, PA). Decanoic acid was from Nu-Chek Prep (Elysian, MN), and $NaHCO_3$ was from EMD Chemicals (Darmstadt, Germany). Sepharose 4B was used for size exclusion chromatography (Sigma-Aldrich, St. Louis, MO).

Sampling from Last Chance Lake and Goodenough Lake

Autoclaved glass bottles were filled with water from either Last Chance Lake or Goodenough Lake during November 2021 (21). The water was kept on ice for ~6 hours during the return to the lab, at which point it was immediately frozen at -20°C. Subsequently, the water was thawed and filtered to 220 nm to remove contaminants such as sediment and microbes. The filtered water was again frozen at -20°C or -30°C. Aliquots of the lake water were kept refrigerated at 4°C for up to a few weeks until used in experiments.

Synthesis of 2-aminoimidazole activated cytidine monophosphate nucleotides

As previously described (39), 1 equivalent of cytidine monophosphate was mixed with 0.42 equivalents of 2-aminoimidazole hydrochloride, 8 equivalents of triphenylphosphine, and 1 equivalent of 1-hydroxy-7-azabenzotriazole in dry dimethyl sulfoxide. Then 10 equivalents of triethylamine and 7.3 equivalents of dipyridyl-disulfide were added. The mixture was incubated for 30 minutes, then the product was precipitated in acetone with sodium perchlorate. The precipitant was washed twice in 1:1 acetone: diethyl ether (v/v) and dried under vacuum. The dry pellet was resuspended in 0.1 M triethylamine-bicarbonate at pH 8, and purified by reverse-phase flash chromatography, with a 50 g C18Aq column. The desired product was separated from other compounds over 12 column volumes of 0–10% acetonitrile in 2 mM triethylamine-bicarbonate at pH 8. The purified product was lyophilized and stored at -30°C.

Nonenzymatic, RNA-templated extension of RNA primers

RNA primer-template duplexes were prepared by mixing primer and template stocks with lake water or artificial salt solutions. The RNA primer was labeled with 6-FAM at its 5' end, and the sequence of the primer was 5'-AGU GAG UAA CGG-3'. The sequence of the RNA template was 5'-GGGG CCG UUA CUC ACU AAA-3'. Cytidine monophosphate nucleotides activated by 2-aminoimidazole were resuspended in ultrapure water to 400 mM and kept on ice. Nucleotide solution was added to the primer-template duplex solution to initiate the reaction. The final solution volume was 10 µL, and the solution contained 1 µM primer, 1.5 µM template, and 20 mM nucleotide. Reactions in lake water contained 90% natural water from either Last Chance Lake or Goodenough Lake. Reactions in lab standard conditions contained 50 mM $MgCl_2$ and 0.2 M bis-tris-propane at pH8, and reactions in artificial lake water contained 0.5 M Na_2CO_3, 1 mM $MgCl_2$, and 0.2 M bis-tris-propane at pH 10. Aliquots of each reaction were quenched at various times into a solution containing 4 µM of RNA that is complementary to the template (5'-UUU AGU GAG UAA CGG CCCC-3') as well as 83.5% formamide (v), 25 mM ethylenediaminetetraacetic acid (EDTA), and 1x TBE (0.1 M EDTA, 89 mM Tris, and 89 mM boric acid at pH 8.3). Primer extension products in the quenched reaction samples were resolved by 20% polyacrylamide gel electrophoresis in 1x TBE gel running buffer. The gels were scanned with an Amersham Typhoon RGB Biomolecular Imager (GE Healthcare Life Sciences). The fluorescently labeled primer and extended primer bands were visualized, and then quantified using ImageQuant TL software to obtain relative band intensities.

Preparation of the ligase ribozyme

The ligase ribozyme with sequence 5'-GGA CAG CGA GCC ACU GCG GAA GAC CUU AAG AGG UGU AAU UGC UCA CCC CGC UGU CCU UUU UUG GCU AAGG-3' has been described previously (29, 30). The ribozyme was prepared by in vitro transcription of dsDNA templates with 2'-O-methyl modifications on the last two nucleotides (40). Transcription reactions were carried out in the presence of 40 mM Tris-HCl, 2 mM spermidine, 10 mM NaCl, 25 mM $MgCl_2$, 10 mM dithiothreitol (DTT), 30 U/mL RNase inhibitor murine (New England Biolabs), 2.5 U/mL thermostable inorganic pyrophosphatase (TIPPase, from New England Biolabs), 4 mM of each nucleotide triphosphate, 30 pmol/mL DNA template, and 1 U/µL T7 RNA Polymerase (New England Biolabs) at pH 8 for 3 h at 37°C. The reaction was quenched with DNase I (New England Biolabs) and RNA was extracted with phenol-chloroform-isoamyl alcohol (PCI), ethanol precipitated, and purified by denaturing polyacrylamide gel electrophoresis. The purified product was stored at -30°C.

Preparation of 2-aminoimidazole activated RNA substrate for ligation reaction

The 2-aminoimidazole activated RNA substrate was generated from a 5'-monophosphorylated oligonucleotide (5'-ACC ACC GCA UUC CGCA-3') by incubating it with 0.2 M 1-ethyl-3-(3 dimethylaminopropyl) carbodiimide (HCl salt) and 0.6 M 2-aminoimidazole (HCl salt, pH adjusted to 6) for 2 hours at room temperature. The product was washed five times with water in Amicon Ultra spin columns (3 kDa cutoff, 200 µL milli-Q water per wash) and purified by reverse phase analytical HPLC using a gradient of 98% to 75% 20 mM TEAB (triethylamine bicarbonate, pH 8) versus acetonitrile over 40 min (29). The purified product was stored at -30°C.

Ribozyme-catalyzed ligation reactions

Ribozyme and template RNA (5'-GCG GUG GUC CUU AGCC-3') were mixed with lake water or artificial salt solutions. The 2-aminoimidazole activated substrate RNA was added to the ribozyme-template solution to initiate the reaction. The final solution volume was 5 µL, and the solution contained 1 µM ribozyme, 1.2 µM template, and 2 µM substrate. Reactions contained 70% water from either Last Chance Lake or Goodenough Lake. For reactions with pH modified lake water, CO_2 was bubbled through 1 mL of water from either Last Chance Lake or Goodenough Lake for ~ 1 minute. The modified lake water remained stable near pH 9 for at least 1 week, and aliquots of the same 1 mL modified lake water were used for all replicate experiments. Ribozyme reactions were quenched immediately and after 20 hours by adding 1 µL of reaction into 5 µL of 8M urea, 0.1 M Tris-HCl, 0.1 M boric acid, and 0.1M EDTA. Reaction products in the quenched samples were resolved by denaturing polyacrylamide gel electrophoresis in 1x TBE gel running buffer. Gels were stained using SYBR Gold then scanned with an Amersham Typhoon RGB Biomolecular Imager (GE Healthcare Life Sciences).

Preparation of vesicles with carbonate lake water in the exterior solution

A stock solution of decanoate was made by dissolving solid decanoic acid in an equimolar NaOH solution, followed by gentle heating and rocking. Vesicle solutions were prepared by the following steps: (1) solutions of $NaHCO_3$ and carboxyfluorescein dye were mixed. (2) Decanoate solution was added. (3) Liquid decanol was added and mixed to induce vesicle assembly. The resulting vesicles of 112.5 mM decanoic acid and 112.5 mM decanol encapsulated the bulk solution of 0.1 M $NaHCO_3$ and 0.1 mM carboxyfluorescein. (4) The pH was adjusted to 10 after the amphiphiles were added. (5) The exterior solution around the vesicles was replaced with lake water (Fig. S12). By adding two volume equivalents of lake water to the initial vesicle sample, a layer of flocculated vesicles formed after gentle spinning for 10 – 30 seconds. The solution below this vesicle layer was removed. This replacement process was repeated 5 times. We are confident that this process produces vesicles that are surrounded by lake water because there is excellent contrast between encapsulated carboxyfluorescein and the exterior solution.

Fluorescence microscopy

Samples were prepared for imaging by mixing 100 µL of vesicle solution with 1 µL of 1 mM rhodamine 6G stock (membrane dye). The edges of a cover slip were coated with vacuum grease and 90 µL of sample was placed in the resulting well. Another cover slip was placed on top. Images were collected on a Nikon (Melville, NY) Eclipse upright epifluorescence microscope (ME600L). A Chroma (Bellows Falls, VT) FITC/Alexa488 filter cube was used for carboxyfluorescein fluorescence images (aqueous dye), and a Chroma mCherry/Texas Red filter cube was used for rhodamine fluorescence images.

Acknowledgments

This research was supported in part by Grant NNX17AK86G (Exobiology) from NASA to S.L.K., by Grant MCB 1925731 from the National Science Foundation to S.L.K., by Grants 511570FY20 and 1011734 from the Simons Foundation to D.C.C, and by Grant 290363 from the Simons Foundation to J.W.S. Z.R.C. was funded by an NSF GRFP fellowship (DGE 1762114) and by Grant 511570FY20. Z.R.T. is an NHFP postdoc (Grant HST-HF2-51471). J.W.S. is an Investigator of the Howard Hughes Medical Institute.

References

1. R. A. Black, M. C. Blosser, A Self-Assembled Aggregate Composed of a Fatty Acid Membrane and the Building Blocks of Biological Polymers Provides a First Step in the Emergence of Protocells. *Life* **6**, 33 (2016).

2. G. F. Joyce, J. W. Szostak, Protocells and RNA Self-Replication. *Cold Spring Harb Perspect Biol* **10**, a034801 (2018).

3. S. S. Mansy, *et al.*, Template-directed synthesis of a genetic polymer in a model protocell. *Nature* **454**, 122–125 (2008).

4. L. Jin, A. E. Engelhart, W. Zhang, K. Adamala, J. W. Szostak, Catalysis of Template-Directed Nonenzymatic RNA Copying by Iron(II). *J. Am. Chem. Soc.* **140**, 15016–15021 (2018).

5. J. Chen, *et al.*, Identification of the Catalytic Mg2+ Ion in the Hepatitis Delta Virus Ribozyme. *Biochemistry* **52**, 557–567 (2013).

6. P.-A. Monnard, C. L. Apel, A. Kanavarioti, D. W. Deamer, Influence of Ionic Inorganic Solutes on Self-Assembly and Polymerization Processes Related to Early Forms of Life: Implications for a Prebiotic Aqueous Medium. *Astrobiology* **2**, 139–152 (2002).

7. K. Adamala, J. W. Szostak, Nonenzymatic Template-Directed RNA Synthesis Inside Model Protocells. *Science* **342**, 1098–1100 (2013).

8. C. E. Cornell, *et al.*, Prebiotic amino acids bind to and stabilize prebiotic fatty acid membranes. *Proc. Natl. Acad. Sci USA* **116**, 17239–17244 (2019).

9. I. A. Chen, K. Salehi-Ashtiani, J. W. Szostak, RNA Catalysis in Model Protocell Vesicles. *J. Am. Chem. Soc.* **127**, 13213–13219 (2005).

10. E. Boros, M. Kolpakova, A review of the defining chemical properties of soda lakes and pans: An assessment on a large geographic scale of Eurasian inland saline surface waters. *PLOS ONE* **13**, e0202205 (2018).

11. J. K. Zorz, *et al.*, A shared core microbiome in soda lakes separated by large distances. *Nat Commun* **10**, 4230 (2019).

12. J. D. Toner, D. C. Catling, A carbonate-rich lake solution to the phosphate problem of the origin of life. *Proceedings of the National Academy of Sciences* **117**, 883–888 (2020).

13. J. D. Toner, D. C. Catling, Alkaline lake settings for concentrated prebiotic cyanide and the origin of life. *Geochimica et Cosmochimica Acta* **260**, 124–132 (2019).

14. S. Ranjan, Z. R. Todd, J. D. Sutherland, D. D. Sasselov, Sulfidic Anion Concentrations on Early Earth for Surficial Origins-of-Life Chemistry. *Astrobiology* **18**, 1023–1040 (2018).

15. B. H. Patel, C. Percivalle, D. J. Ritson, C. D. Duffy, J. D. Sutherland, Common origins of RNA, protein and lipid precursors in a cyanosulfidic protometabolism. *Nature Chem* **7**, 301–307 (2015).

16. J. Xu, *et al.*, Photochemical reductive homologation of hydrogen cyanide using sulfite and ferrocyanide. *Chem. Commun.* **54**, 5566–5569 (2018).

17. J. G. Lawless, G. U. Yuen, Quantification of monocarboxylic acids in the Murchison carbonaceous meteorite. *Nature* **282**, 396–398 (1979).

18. D. W. Nooner, J. Oro, "Synthesis of Fatty Acids by a Closed System Fischer-Tropsch Process" in *Hydrocarbon Synthesis from Carbon Monoxide and Hydrogen*, Advances in Chemistry., (American Chemical Society, 1979), pp. 159–171.

19. J. Criado-Reyes, B. M. Bizzarri, J. M. García-Ruiz, R. Saladino, E. Di Mauro, The role of borosilicate glass in Miller–Urey experiment. *Sci Rep* **11**, 21009 (2021).

20. Z. R. Cohen, *et al.*, Plausible Sources of Membrane-Forming Fatty Acids on the Early Earth: A Review of the Literature and an Estimation of Amounts. *ACS Earth Space Chem.* **7**, 11–27 (2023).

21. S. Haas, et. al.*In prep.*

22. S. Rajamani, *et al.*, Lipid-assisted Synthesis of RNA-like Polymers from Mononucleotides. *Orig Life Evol Biosph* **38**, 57–74 (2008).

23. J. P. Ferris, G. Ertem, Oligomerization of Ribonucleotides on Montmorillonite: Reaction of the 5'-Phosphorimidazolide of Adenosine. *Science* **257**, 1387–1389 (1992).

24. T. Walton, J. W. Szostak, A Highly Reactive Imidazolium-Bridged Dinucleotide Intermediate in Nonenzymatic RNA Primer Extension. *J. Am. Chem. Soc.* **138**, 11996–12002 (2016).

25. C. Giurgiu, *et al.*, Structure–Activity Relationships in Nonenzymatic Template-Directed RNA Synthesis. *Angewandte Chemie International Edition* **60**, 22925–22932 (2021).

26. R. Guth-Metzler, *et al.*, Goldilocks and RNA: where Mg2+ concentration is just right. *Nucleic Acids Research*, gkad124 (2023).

27. T. Wu, L. E. Orgel, Nonenzymic template-directed synthesis on hairpin oligonucleotides. 2. Templates containing cytidine and guanosine residues. *J. Am. Chem. Soc.* **114**, 5496–5501 (1992).

28. L. Zhou, D. Ding, J. W. Szostak, The virtual circular genome model for primordial RNA replication. *RNA* **27**, 1–11 (2021).

29. T. Walton, S. DasGupta, D. Duzdevich, S. S. Oh, J. W. Szostak, In vitro selection of ribozyme ligases that use prebiotically plausible 2-aminoimidazole–activated substrates. *Proceedings of the National Academy of Sciences* **117**, 5741–5748 (2020).

30. S. DasGupta, S. J. Zhang, M. P. Smela, J. W. Szostak, RNA-catalyzed RNA Ligation within Prebiotically Plausible Model Protocells. 2023.02.09.527907 (2023).

31. Z. R. Cohen, Caitlin. E. Cornell, D. C. Catling, R. A. Black, S. L. Keller, Prebiotic Protocell Membranes Retain Encapsulated Contents during Flocculation, and Phospholipids Preserve Encapsulation during Dehydration. *Langmuir* **38**, 1304–1310 (2022).

32. A. C. Fahrenbach, *et al.*, Common and Potentially Prebiotic Origin for Precursors of Nucleotide Synthesis and Activation. *J. Am. Chem. Soc.* **139**, 8780–8783 (2017).

33. S. J. Zhang, D. Duzdevich, D. Ding, J. W. Szostak, Freeze-thaw cycles enable a prebiotically plausible and continuous pathway from nucleotide activation to nonenzymatic RNA copying. *Proceedings of the National Academy of Sciences* **119**, e2116429119 (2022).

34. J. W. Szostak, The eightfold path to non-enzymatic RNA replication. *Journal of Systems Chemistry* **3**, 2 (2012).

35. D. K. O'Flaherty, *et al.*, Copying of Mixed-Sequence RNA Templates inside Model Protocells. *J. Am. Chem. Soc.* **140**, 5171–5178 (2018).

36. A. Khvorova, Y.-G. Kwak, M. Tamkun, I. Majerfeld, M. Yarus, RNAs that bind and change the permeability of phospholipid membranes. *Proceedings of the National Academy of Sciences* **96**, 10649–10654 (1999).

37. T. F. Zhu, J. W. Szostak, Coupled Growth and Division of Model Protocell Membranes. *J. Am. Chem. Soc.* **131**, 5705–5713 (2009).

38. R. A. Black, *et al.*, Nucleobases bind to and stabilize aggregates of a prebiotic amphiphile, providing a viable mechanism for the emergence of protocells. *Proc. Natl. Acad. Sci USA* **110**, 13272–13276 (2013).

39. D. Ding, L. Zhou, C. Giurgiu, J. W. Szostak, Kinetic explanations for the sequence biases observed in the nonenzymatic copying of RNA templates. *Nucleic Acids Research* **50**, 35–45 (2022).

40. C. Kao, S. Rüdisser, M. Zheng, A Simple and Efficient Method to Transcribe RNAs with Reduced 3' Heterogeneity. *Methods* **23**, 201–205 (2001).

Supplementary information

Section 1: Ionic composition of Last Chance Lake and Goodenough Lake

Table S1. Cation composition of Last Chance Lake and Goodenough Lake measured by inductively coupled plasma mass spectrometry

Ion name	**Concentration in Last Chance Lake (mM)**	**Concentration in Goodenough Lake (mM)**
Sodium	1824.2	711.4
Potassium	28.3	13.2
Monovalent cation total	1852.5	724.6
Magnesium	1.49	1.50
Calcium	0.09	< 0.01
Divalent cation total	1.58	1.50

Table S2. Anion composition of Last Chance Lake and Goodenough Lake

Ion name	**Concentration in Last Chance Lake (mM)**	**Concentration in Goodenough Lake (mM)**	**Analytical technique used**
Chloride	335.8	70.4	Ion chromatography
Nitrate	< 0.001	< 0.001	Spectrophotometry (1)
Phosphate	8.2	< 0.1	Spectrophotometry (2)
Sulfate	49.5	7.6	Ion chromatography
Carbonate & bicarbonate	898.8	156.3	Shimadzu total organic carbon/total nitrogen-VCSH

Table S3. pH of Last Chance Lake and Goodenough Lake

	Last Chance Lake	**Goodenough Lake**
pH	9.8	10.3

All data are reproduced from Haas et al. 2023 with permission from the authors (3).

All data are from water samples collected during November 2021.

Section 2: Non-enzymatic, RNA-templated RNA primer extension by 2-aminoimidazole activated ribonucleotides

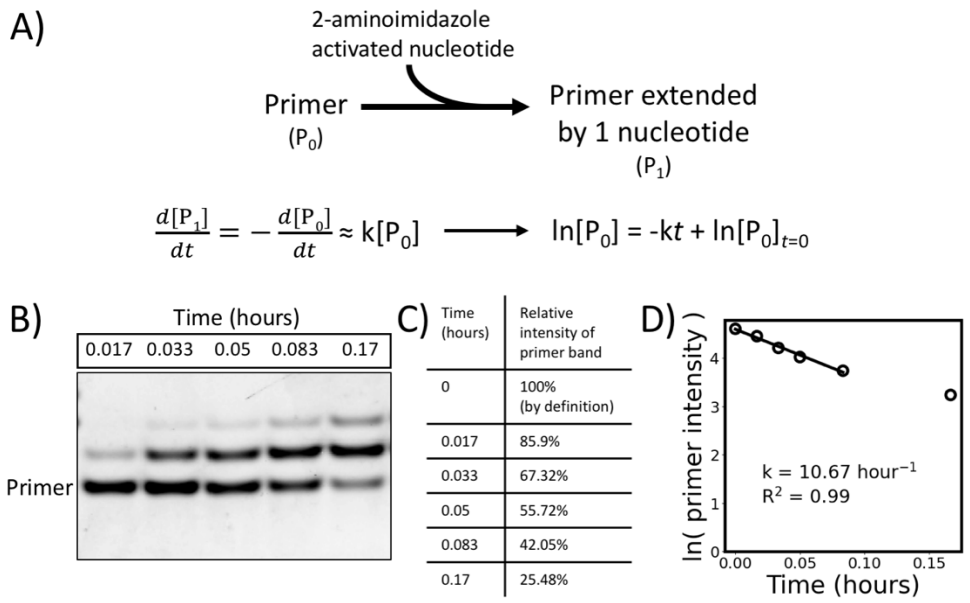

Fig. S1. Example calculation of the pseudo first-order rate constant for primer extension by the first nucleotide. A) When the concentration of 2-aminoimidazole activated nucleotides (20 mM) is in excess of the primer concentration (1 μM), the rate of production of primers that have been extended by 1 nucleotide is equal to the rate of consumption of unextended primer, and these rates depend approximately linearly on the concentration of unextended primer. The first-order integrated rate law can be used to estimate the rate constant, k. B) Example gel with labeled bands corresponding to the unextended primer. Bands corresponding to extended primers can be seen as well. These data are from 1 replicate experiment in artificial lake conditions from Fig. 1. C) Relative intensities of the unextended primer band can be quantified from the gel. By definition, none of the primer is extended at 0 hours. D) The negative slope of a plot of the natural logarithm of the unextended primer intensity vs time yields the pseudo first-order rate constant for primer extension by the first nucleotide.

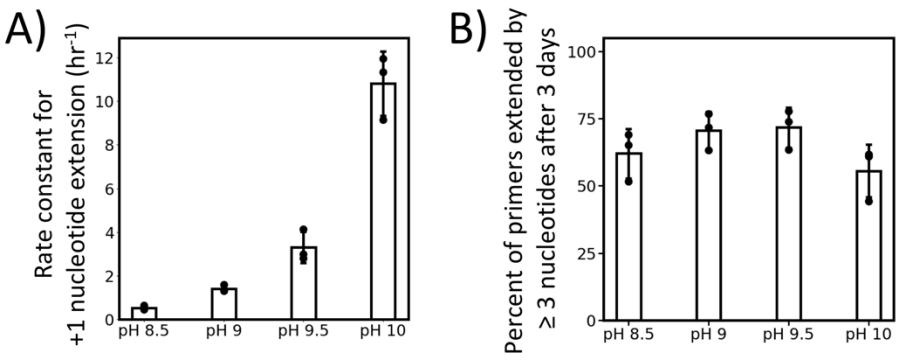

Fig. S2. In artificial lake water, A) pseudo first-order rate constants for primer extension increase with pH while B) the yield of extended primers after 3 days is largely unaffected by pH. All reactions contained 1 µM primer, 1.5 µM template, 20 mM nucleotide, 1 M NaCl, 1 mM $MgCl_2$, and 200 mM bis-tris-propane. Error bars correspond to the standard deviation from 3 independent experiments.

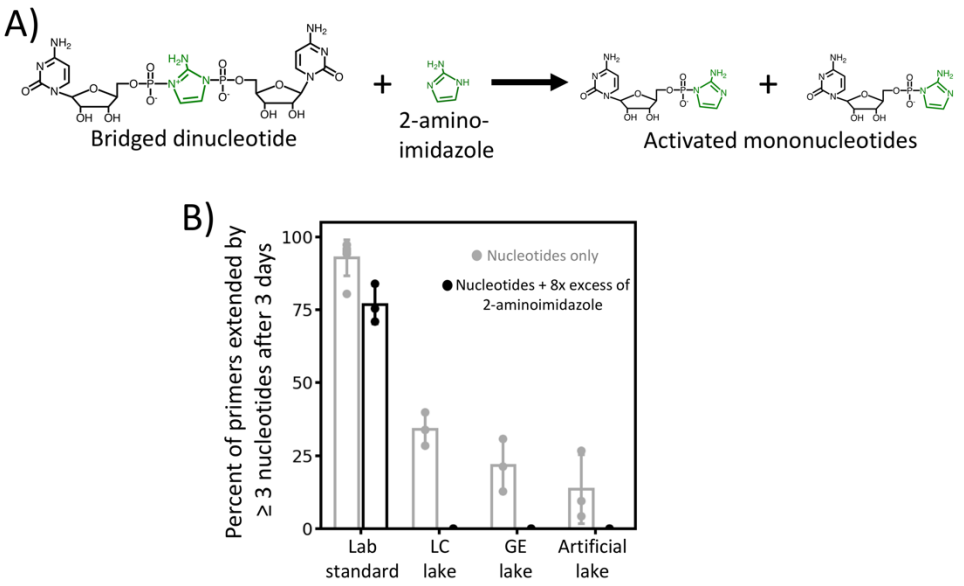

Fig. S3. Excess 2-aminoimidazole disrupts primer extension in lake water, suggesting that primer extension in lake water occurs via bridged dinucleotide intermediates. A) Excess 2-aminoimidazole disfavors formation of bridged dinucleotides. B) Comparison of primer extension in the presence or absence of excess 2-aminoimidazole. Data for "nucleotides only" are the same as in Fig. 3B, (20 mM nucleotide). Reactions with 8x excess of 2-aminoimidazole were performed similarly as described for "nucleotides only", except that 400 mM stock solutions of activated cytidine monophosphate ribonucleotides were resuspended in 3.2 M 2-aminoimidazole solution at pH 7, rather than ultrapure water. The final solution composition was 20 mM nucleotide, 160 mM 2-aminoimidazole, 1 µM primer, and 1.5 µM template. Standard lab conditions are 50 mM $MgCl_2$ and 200 mM bis-tris-propane at pH 8, and artificial lake water is 0.5 M Na_2CO_3, 1 mM $MgCl_2$, and 200 mM bis-tris-propane at pH 10. Error bars correspond to the standard deviation from 3 independent experiments, while the error bars in "nucleotides only" in lab standard conditions correspond to 6 independent experiments. LC is Last Chance Lake and GE is Goodenough Lake.

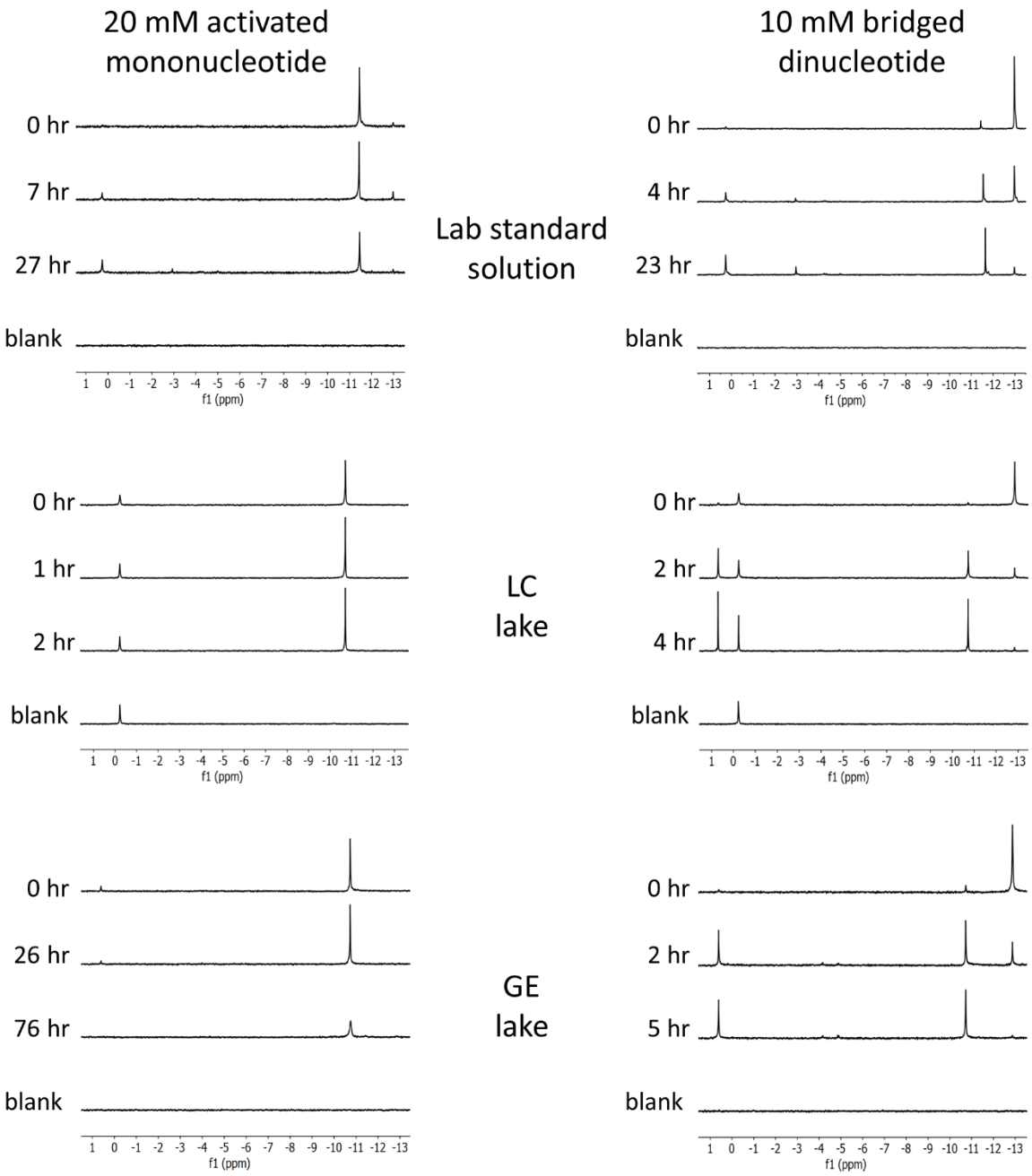

Fig. S4. ^{31}P NMR spectra of 2-aminoimidazole activated cytidine mononucleotide (-11.38 ppm) or bridged cytidine dinucleotide (-12.85 ppm). In standard lab conditions (50 mM $MgCl_2$ and 200 mM bis-tris-propane at pH 8), the bridged dinucleotide hydrolyzes slowly until it reaches a low equilibrium concentration after ~24 hours. In natural water from either Last Chance Lake (LC) or Goodenough Lake (GE), the activated mononucleotide is relatively stable throughout the experiment, whereas the bridged dinucleotide hydrolyzes rapidly within ~ 5 hours. For all samples, 10% D_2O was added to the solution before dissolving the solid mononucleotide or dinucleotide. Additional signals correspond to phosphate (-0.3 ppm) and cytidine monophosphate (0.28 ppm). ^{31}P spectra were acquired on a Varian Oxford AS-400 NMR spectrometer. Bridged cytidine dimers were prepared as described in Ding et al. 2022 (4).

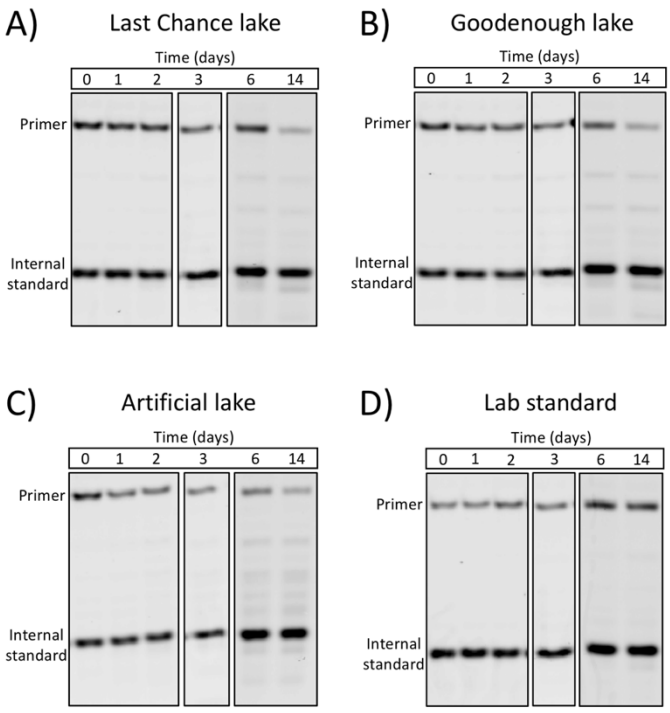

Fig. S5. In the absence of template RNA or activated nucleotides, the RNA primer is stable in lake water for at least 3 days. However, the primer begins to hydrolyze after 6 days in lake water. The primer is stable for 14 days in standard lab conditions. Standard lab conditions are 50 mM $MgCl_2$ and 200 mM bis-tris-propane at pH 8, and artificial lake water is 1 M NaCl, 1 mM $MgCl_2$, and 200 mM bis-tris-propane at pH 10.

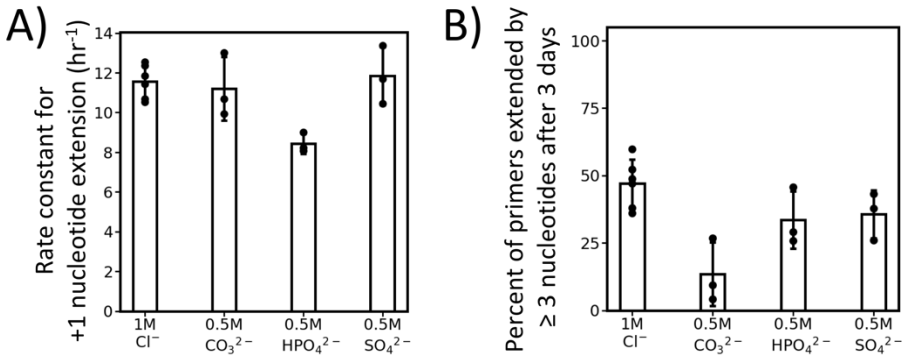

Fig. S6. In artificial lake water containing 1 M Na^+ and 1 mM Mg^{2+} at pH 10, A) the pseudo first-order rate constants for primer extension are similar regardless of whether chloride, carbonate, phosphate, or sulfate are used as anions. Data for "0.5 M CO_3^{2-}" are the same as in Figure 2C "Artificial Lake". B) The yield of extended primers after 3 days is lower when carbonate is used as the anion. Data for "0.5 M CO_3^{2-}" are the same as in Figure 3A "Artificial Lake, 20 mM initial nucleotide". All reactions contained 1 µM primer, 1.5 µM template, 20 mM nucleotide, and 200 mM bis-tris-propane. Error bars correspond to the standard deviation from 3 independent experiments, except for the error bars in the "1 M Cl^-" sample which correspond to 6 independent experiments.

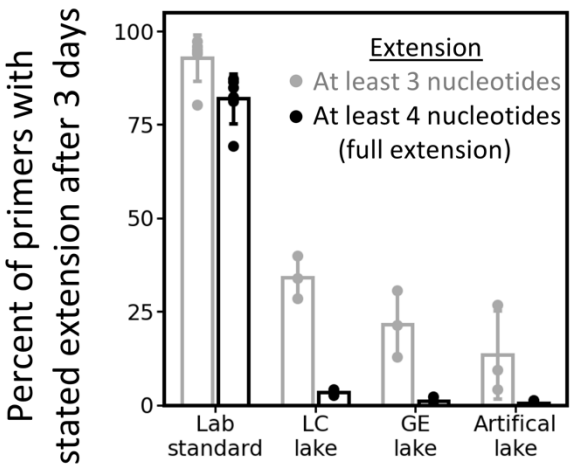

Fig. S7. The yield of fully extended RNA primers (+4 nucleotides) is low in carbonate lake water. All reactions contained 1 µM primer, 1.5 µM template, and 20 mM nucleotide. Standard lab conditions are 50 mM $MgCl_2$ and 200 mM bis-tris-propane at pH 8, and artificial lake water is 0.5 M Na_2CO_3, 1 mM $MgCl_2$, and 200 mM bis-tris-propane at pH 10. Error bars correspond to the standard deviation from 3 independent experiments, except for the error bars for the lab standard conditions which correspond to 6 independent experiments. LC is Last Chance Lake and GE is Goodenough Lake. Data for extension by at least 3 nucleotides are the same as in Figure 3A "20 mM initial nucleotide".

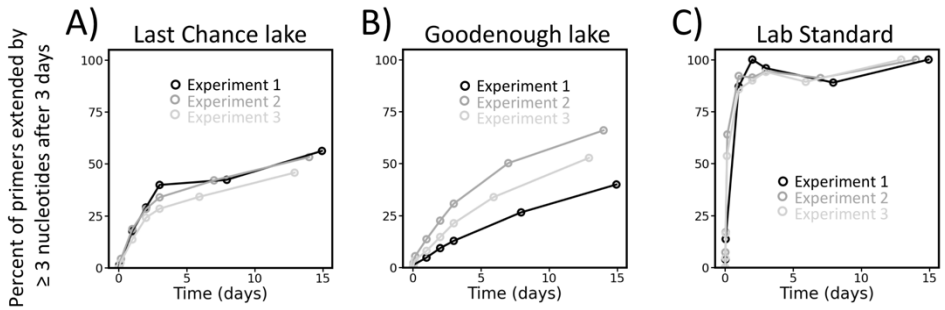

Fig. S8. The yield of RNA primers that have been extended by +3 nucleotides increases beyond 3 days. All reactions contained 1 μM primer, 1.5 μM template, and 20 mM nucleotide. Standard lab conditions are 50 mM $MgCl_2$ and 200 mM bis-tris-propane at pH 8.

Section 3: Activity of a ligase ribozyme

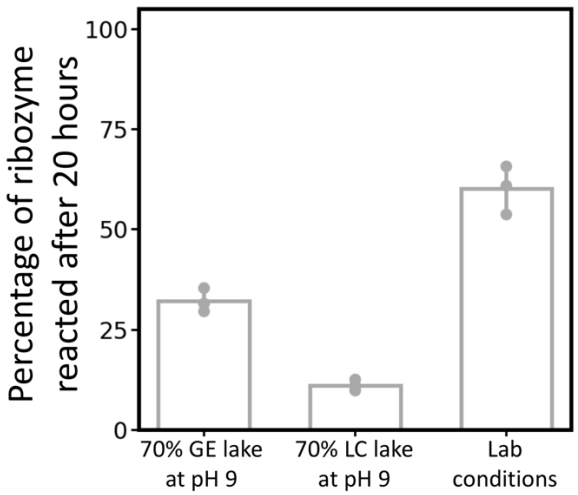

Fig. S9. The yield of reacted ribozyme after 20 hours in pH modified water from Goodenough lake (GE) or Last Chance lake (LC). Lab conditions are 0.362 M NaCl + 1.2 mM $MgCl_2$ + 242 mM bis-tris-propane at pH 8. The final solution volume was 5 µL, and the solution contained 1 µM ribozyme, 1.2 µM template, and 2 µM substrate. The error bars correspond to standard deviation from three independent experiments.

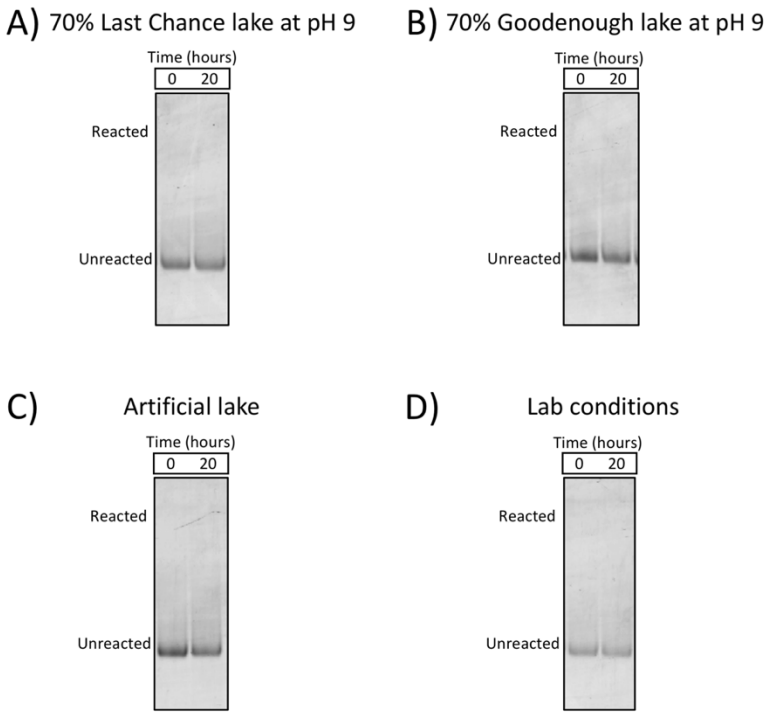

Fig. S10. In control reactions using an RNA construct with a completely randomized catalytic domain sequence instead of the ligase ribozyme, we do not observe ligation to the substrate. The reagent composition was otherwise identical to the ribozyme reactions described in the main text: the solution contained 1.2 µM template, 2 µM substrate, and 1 µM of the random 95 nucleotide RNA. Artificial lake conditions are 0.5 M Na_2CO_3 + 1 mM $MgCl_2$ + 200 mM bis-tris-propane at pH 9, and lab conditions are 0.362 M NaCl + 1.2 mM $MgCl_2$ + 242 mM bis-tris-propane at pH 8. The data for each solution are from a single experiment, and the results are consistent with two additional, independent replicate experiments.

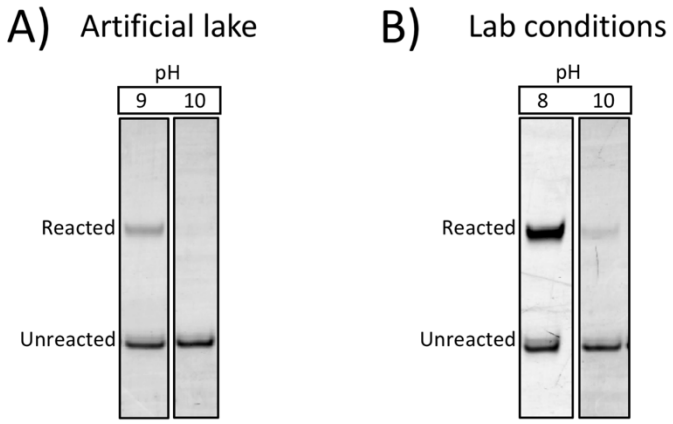

Fig. S11. Whether or not the salt composition mimics the natural lakes, ribozyme activity is higher when the pH is lowered below pH 10. A) In artificial lake conditions (0.5 M Na_2CO_3 + 1 mM $MgCl_2$ + 200 mM bis-tris-propane), more ribozyme has reacted after 20 hours in pH 9 solution than pH 10 solution. B) In lab conditions (0.362 M NaCl + 1.2 mM $MgCl_2$ + 242 mM bis-tris-propane), more ribozyme has reacted after 20 hours in pH 8 solution than pH 10 solution. The final solution volume was 5 µL, and the solution contained 1 µM ribozyme, 1.2 µM template, and 2 µM substrate.

Section 4: Encapsulation by prebiotic membranes

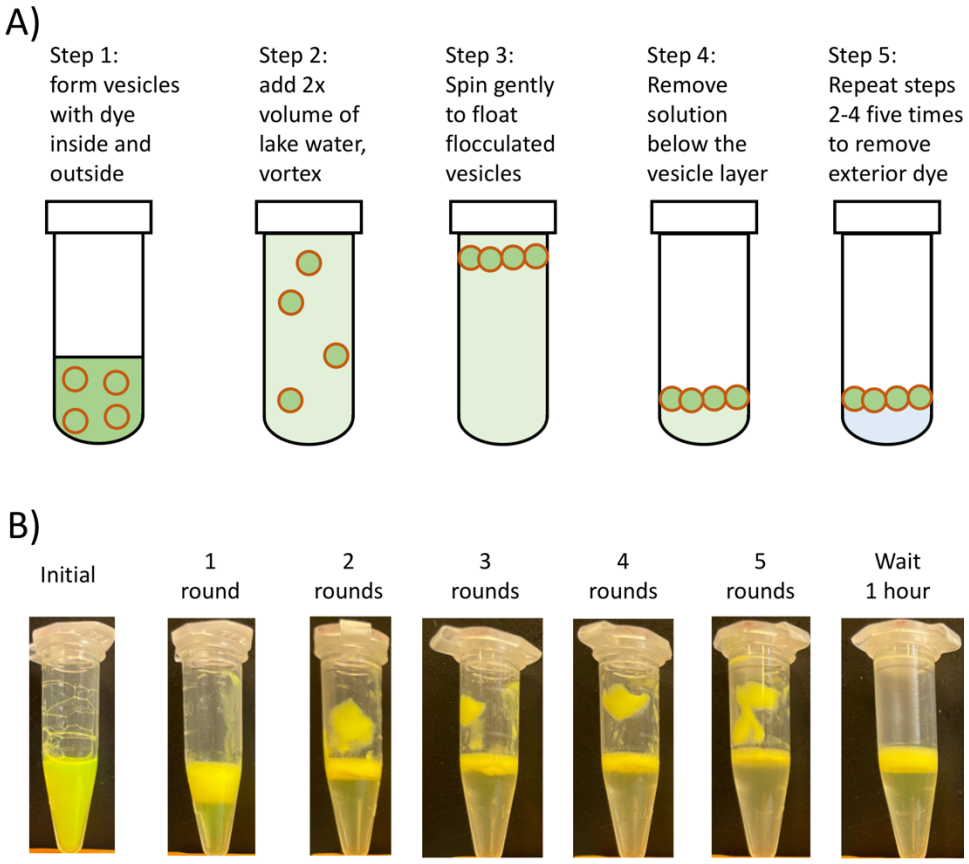

Fig. S12. A) Schematic of the process used to exchange the exterior solution around vesicles with lake water. B) Example of this process used to replace the exterior solution around vesicles with water from Last Chance lake. The initial vesicle sample is 112.5 mM decanoic acid + 112.5 mM decanol + 0.1 M $NaHCO_3$ + 0.1 mM carboxyfluorescein. After 5 rounds of solution replacement, the resulting layer of flocculated vesicles is stable for at least 1 hour.

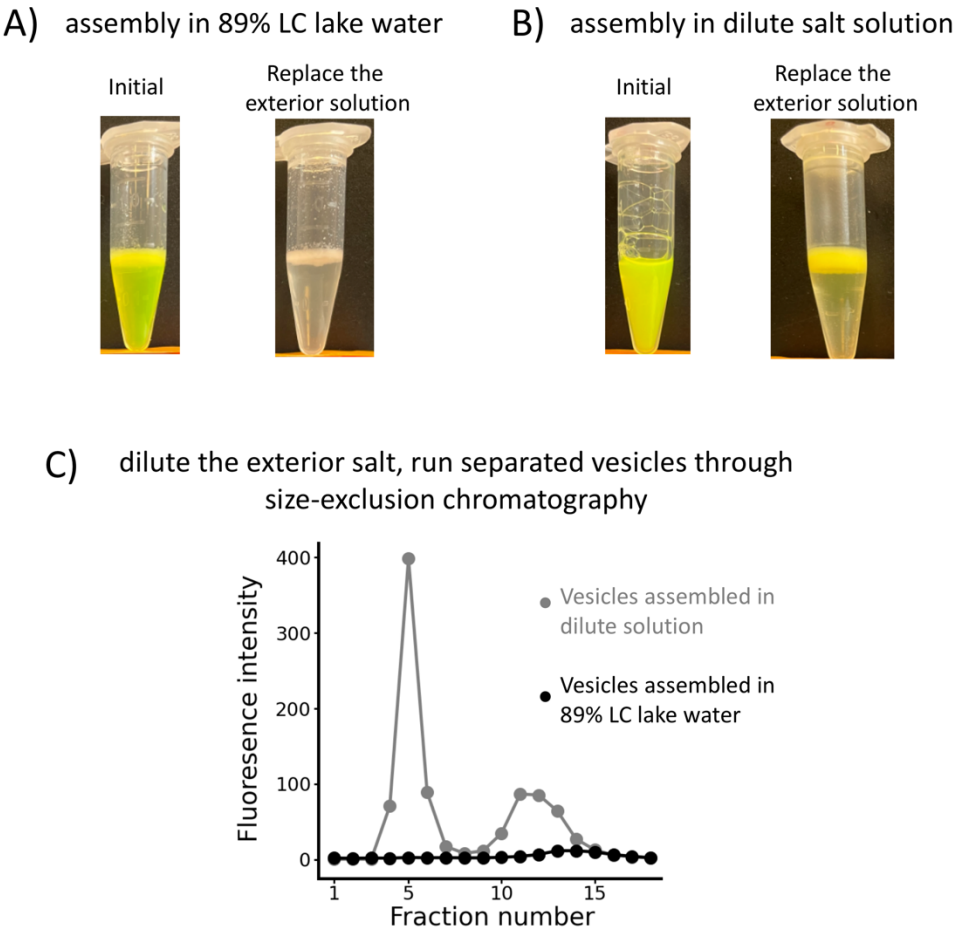

Fig. S13. Prebiotic amphiphiles do not assemble into vesicles in 89% water from the dry season of Last Chance lake (LC). A) When 112.5 mM decanoic acid + 112.5 mM decanol were allowed to assemble in 89% Last Chance lake water containing 0.1 mM carboxyflorescein, the amphiphiles immediately formed a floating layer. The solution below this layer was replaced with 100% Last Chance lake water as in Fig. S12. The amphiphile layer did not retain carboxyflorescein. B) As described in Fig. 4 of the main text, 112.5 mM decanoic acid + 112.5 mM decanol were allowed to assemble into vesicles in a dilute salt solution of 0.1 M NaHCO3 + 0.1 mM carboxyflorescein. After replacing the exterior solution with 100% Last Chance lake water as in Fig. S12, the vesicle layer did retain encapsulated carboxyflorescein. C) After 1 hour, both samples were subsequently diluted into a 56 mM decanoic acid + 0.1 M $NaHCO_3$, pH 10 solution. This diluted sample was eluted through a size-exclusion column. For the sample where amphiphiles were initially allowed to assemble in 89% Last Chance lake water, the chromatogram does not show an early-eluting peak, suggesting that very few vesicles contain carboxyflorescein. Meanwhile, there is an intense early-eluting peak of carboxyflorescein containing vesicles in the sample allowed to assemble in dilute salt solution. These data suggest that amphiphiles do not assemble into new vesicles in Last Chance lake water. Carboxyflorescein fluorescence was measured with excitation at 485 nm and emission at 520 nm. Data are from a single experiment, and they are consistent with an independent, replicate experiment.

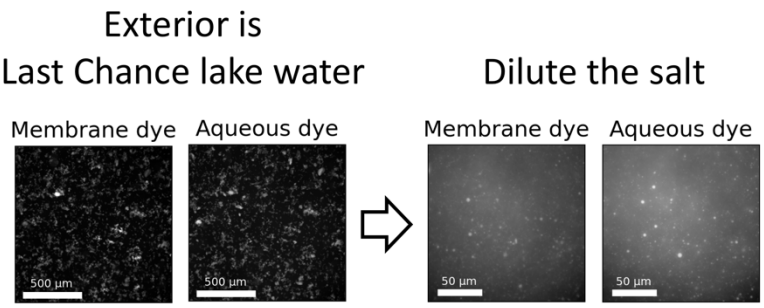

Fig. S14. Full field images of vesicles composed of 1:1 decanoic acid: decanol when the exterior solution is water from Last Chance lake, and after subsequent dilution into a 56 mM decanoic acid + 0.1 M $NaHCO_3$, pH 10 solution. Rhodamine 6G membrane dye was added immediately prior to imaging. Although these are not the same field shown in Fig. 5 of the main text, these images are also representative of the entire sample.

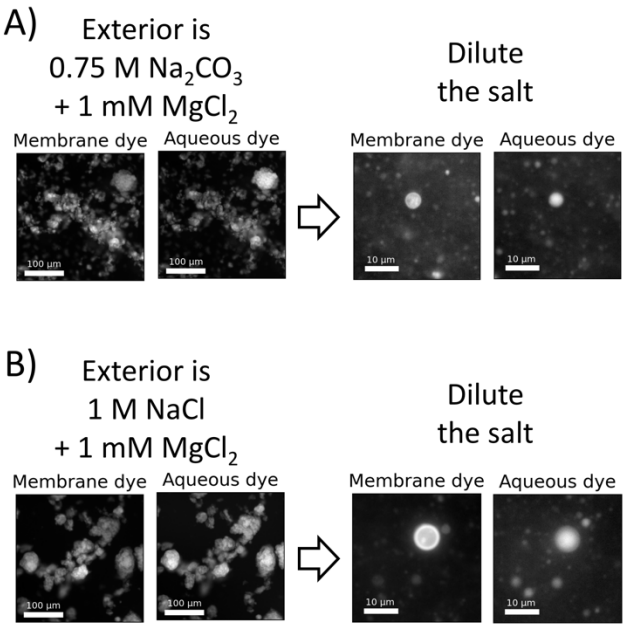

Fig. S15. Vesicles of 1:1 decanoic acid: decanol encapsulate aqueous carboxyflorescein dye for at least 1 hour when the exterior solution is artificial lake water at pH 10. Vesicles were initially assembled in a dilute salt solution of 0.1 M $NaHCO_3$ at pH 10 with 0.1 mM carboxyflorescein dye before the exterior solution was replaced with artificial lake water. Subsequent dilution into a 56 mM decanoic acid + 0.1 M $NaHCO_3$, pH 10 solution causes vesicles to separate from each other, and separated vesicles still retain encapsulated dye. Rhodamine 6G membrane dye was added immediately prior to imaging. Both sets of experiments were performed at pH 10, and 0.1 M $NaHCO_3$ was included to buffer pH in artificial lake water of 1 M NaCl + 1 mM $MgCl_2$.

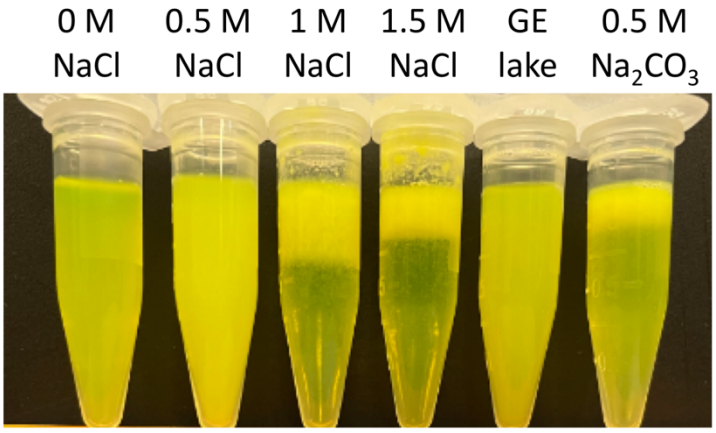

Fig. S16. Floatation of flocculated vesicles requires ~1 M unchelated Na^+. Because flocculated vesicles do not form a floating layer when the exterior solution is Goodenough lake (GE), we cannot determine whether vesicles retain dye. Similarly, not all vesicles float when the exterior solution is artificial lake water of 0.5 M Na_2CO_3 + 1 mM $MgCl_2$ at pH 10. All samples except natural Goodenough lake water contain 1 mM $MgCl_2$ at pH 10. NaCl solutions also contain 0.1 M $NaHCO_3$ buffer.

Section 5: SI References

1. J. D. H. Strickland, T. R. Parsons, A Practical Handbook of Seawater Analysis, 2nd edition. (1972).

2. L. I. Gordon, J. C. Jennings, A. A. Ross, J. M. Krest, A Suggested Protocol for Continuous Flow Automated Analysis of Seawater Nutrients (Phosphate, Nitrate, Nitrite and Silicic Acid) in the WOCE Hydrographic Program and the Joint Global Ocean Fluxes Study (1993).

3. S. Haas, et. al. *In prep.*

4. D. Ding, L. Zhou, C. Giurgiu, J. W. Szostak, Kinetic explanations for the sequence biases observed in the nonenzymatic copying of RNA templates. *Nucleic Acids Research* **50**, 35–45 (2022).

Conclusion

To better understand the origin of life, I have investigated the formation of key cell components such as membranes, peptides, and RNA in the early Earth environment. My research has advanced the hypothesis that all three of these cell components could have formed together within evaporating, carbonate lakes on the early Earth. Of course there are many important challenges that must be resolved before a complete scenario for the origin of life will come into focus. However, my research suggests that evaporating lakes may have been uniquely suited to enable the origin of life. Future research on the origin of life should test whether additional chemical processes can occur in evaporating lake conditions.

Appendix:

Surprising observations during size-exclusion chromatography with fatty acid vesicles

Main text

In order to prepare a sample of fatty acid vesicles that encapsulate an aqueous fluorescent dye, the amphiphiles are first allowed to assemble in a well-mixed solution of that dye so that the dye concentration inside the vesicles is equal to the dye concentration outside. Size-exclusion chromatography is a standard technique to separate unencapsulated dye from the vesicles. Because vesicles are relatively large (~1 μm) compared to many fluorescent dyes (< 10 nm), the vesicles elute quickly in the void volume, whereas unencapsulated dye molecules elute slowly after a circuitous passage through the chromatography resin. I have used this technique successfully with fatty acid vesicles in numerous experiments throughout chapters 2 & 3. However, I have also discovered some surprising challenges. Here, I will discuss these surprising observations in case they are useful to future researchers.

Section 1: quantifying fluoresence after size-exclusion chromatography fails a reasonable test

Many researchers collect size-exclusion chromatograms and use the integrated fluorescence intensity to estimate the percentage of dye that is encapsulated in vesicles (Fig. 1). This interpretation seems reasonable as long as fluorescence intensity is proportional to dye concentration, which can be verified by measuring fluorescence intensity across a range of dye concentrations. This approach is useful to estimate the leakage of dye from vesicles after some perturbation.

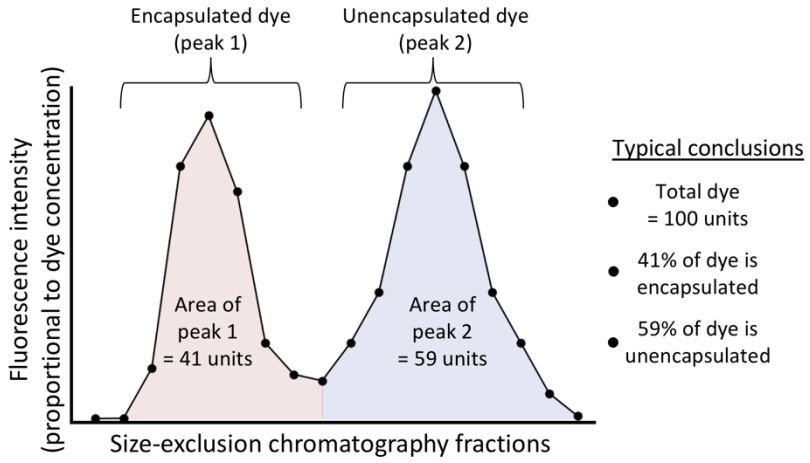

Figure 1: Typical interpretation of a size-exclusion chromatogram when fluorescence intensity is proportional to the dye concentration. By integrating the fluoresce in the early eluting peak, and normalizing by the total integrated fluorescence, researchers have attempted to estimate the percentage of dye molecules that are encapsulated.

If for some reason the vesicles do not elute through the column (e.g. the vesicles float above the resin due to flocculation in high salt solution), then the fluorescence from the encapsulated dye cannot be accurately measured. If it is desirable to estimate the percentage of dye molecules that are encapsulated, it seems reasonable to measure the fluorescence (and thus the number of moles) for only the unencapsulated dye, and to calculate the total moles of dye (encapsulated + unencapsulated) that are loaded into the column based on the fluorescence of the initial sample. Then, the percent of dye molecules that are encapsulated can be estimated using the following equations:

$$moles\ of\ encapsulated\ dye = (total\ moles\ loaded\ into\ column) - (unencapsulated\ moles) \quad (1)$$

$$\%\ encapsulated\ dye = \frac{moles\ of\ encapsulated\ dye}{(total\ moles\ loaded\ into\ column)} \quad (2)$$

To validate this approach, I asked a simple question with a sample of vesicles that does elute through a size-exclusion column: does the sum of the encapsulated and unencapsulated moles equal the number of moles that were loaded into the column (Fig. 2)? To test this, I made a sample of vesicles of 120 mM decanoic acid + 120 mM decanol with 0.1 mM carboxyflorescein in the interior and exterior solution. I also included 0.1 M $NaHCO_3$ to buffer the solution at pH 8.7. I showed that carboxyflorescein fluorescence is linearly dependent on carboxyflorescein concentration, and I measured the fluorescence intensity of the initial sample and all chromatography fractions. I calculated the number of moles of

carboxyflorescein in each sample, and I used these data to compare the number of moles inputted to the column with the total number of moles eluted from the column. My results are shown in Table 1.

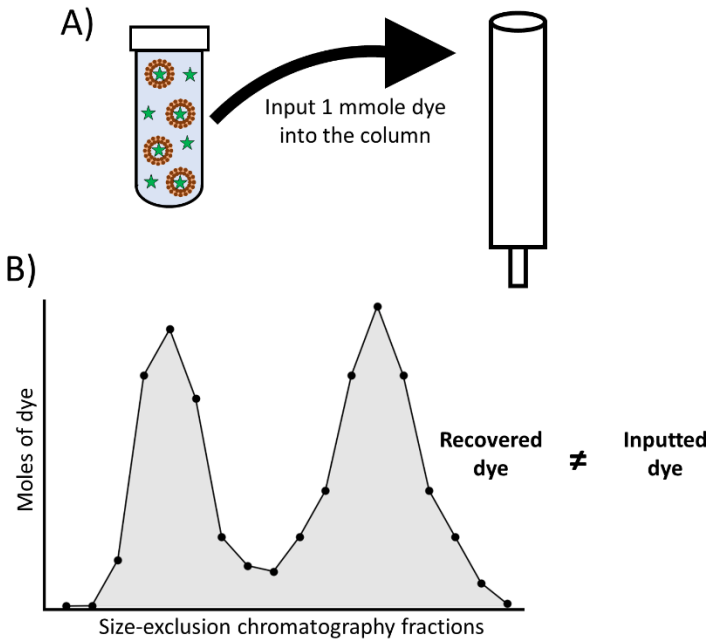

Figure 2: Quantitative interpretation of size-exclusion chromatography fails a simple test. In 3 trials, I could not recover all of the carboxyflorescein dye that was inputted to a size-exclusion chromatography run. Data for these experiments are shown in Figure 2.

Table 1: Results from three trials of size-exclusion chromatography to compare the inputted moles with recovered moles.

	Trial 1	Trial 2	Trial 3
Percent of carboxyflorescein recovered after size-exclusion chromatography	82% (low)	446% (nonphysical)	67.6% (low)

Surprisingly, I could not consistently account for all of the dye that I inputted into the size-exclusion column. In some cases, I recovered less dye than I inputted, and in other puzzling cases my data implied that I recovered more dye that I inputted. Although I only attempted this experiment 3 times, I concluded that my approach was insufficient to estimate the percent encapsulation of fluorescent dye. Perhaps the change to the amphiphile concentration before and after size-exclusion chromatography could alter the fluoresence measurements. In summary, these findings should make readers and future experimenters somewhat skeptical of any quantitative interpretation of size-exclusion chromatograms using carboxyflorescein.

Section 2: decanoic acid vesicles do not encapsulate self-quenched carboxyflorescein unless decanol is added to the membrane

Membrane permeability can be measured by encapsulating in vesicles a high enough concentration of dye so that the fluorescence is self-quenched. When dye molecules leak through the membrane into the exterior solution, the fluorescence of the sample increases. I have used this technique successfully in chapters 2 & 3 with membranes composed of fatty acid and fatty alcohol.

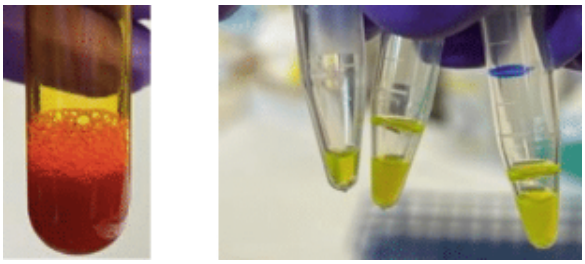

Figure 3: Decanoic acid vesicles do not maintain encapsulation of self-quenched carboxyflorescein after removal of exterior dye during size-exclusion chromatography. (Left) The initial vesicle sample is dark red because self-quenched carboxyflorescein (60 mM) is inside and outside of the vesicles. (Right) After size-exclusion chromatography, the early-eluting vesicle fractions retain encapsulated dye, but the dye concentration has fallen below the threshold for self-quenching.

I have also attempted this experiment twice with membranes composed only of 250 mM decanoic acid. I prepared a vesicle sample at pH 7 with a self-quenched concentration of carboxyflorescein (60 mM) in the interior and exterior solution. Although I was able to remove unencapsulated dye from the decanoic acid vesicles, the dye concentration inside the vesicles appeared

to have fallen below the self-quenching concentration (Fig 3). Somehow, the interior solution became diluted during the size-exclusion process. Decanoic acid membranes are highly permeable, so after removal of unencapsulated dye, water could have entered the vesicles to dilute the carboxyflorescein so that the interior and exterior osmolarities became the same. In the future, one possible adjustment to the protocol might be to maintain the size-exclusion running buffer at a higher osmolarity, so that the exterior dye can be removed and the interior dye can be maintained above the self-quenching concentration.

Section 3: vesicles of 1:1 decanoic acid: decanol give more reliable results with size-exclusion chromatography than vesicles of 2:1 decanoic acid: decanol.

Although I have had success removing unencapsulated dye from vesicles of 2:1 decanoic acid: decanol (chapters 2 & 3), size-exclusion chromatography occasionally fails with this membrane composition, meaning that I do not observe any vesicles eluting through the column. I have never encountered this problem with vesicles composed of 1:1 decanoic acid: decanol when I keep the total amphiphile concentration below 250 mM. I recommend using 125 mM decanoic acid + 125 mM decanol for all experiments that require encapsulation inside vesicles of prebiotically plausible amphiphiles.